DEVELOPMENT OF THE REGENERATIVE MAGNETIC REFRIGERATOR OPERATING BETWEEN 4.2 K AND 1.8 K

by

Sangkwon Jeong

B.S. Mech. Eng.,
Seoul National University, Seoul, Korea (1985)

M.S. Mech. Eng.,
Seoul National University, Seoul, Korea (1987)

Submitted to the Department of Mechanical Engineering
in Partial Fulfillment of the Requirements for the Degree of

DOCTOR OF PHILOSOPHY

at the

MASSACHUSETTS INSTITUTE OF TECHNOLOGY

May, 1992

Signature of Author_____
Department of Mechanical Engineering
May, 1992

Certified by_____
Joseph L. Smith, Jr.
Thesis Supervisor

Certified by_____
Yukikazu Iwasa
Thesis Supervisor

Accepted by_____
Ain A. Sonin, Chairman
Departmental Graduate Committee
Department of Mechanical Engineering

DEVELOPMENT OF THE REGENERATIVE MAGNETIC REFRIGERATOR OPERATING BETWEEN 4.2 K AND 1.8 K

by

Sangkwon Jeong

Submitted to the Department of Mechanical Engineering
on May 18, 1992 in Partial Fulfillment of the Requirements for the Degree of
Doctor of Philosophy in Mechanical Engineering

ABSTRACT

This thesis presents the design, computer simulation, construction, and the results from the successful operation of a prototype 100 mW tandem regenerative magnetic refrigerator in the temperature range 1.8 K~4.2 K. The inherent sources of irreversibility in regenerative magnetic refrigerators, *i.e.* helium entrainment, heat capacity imbalance between magnetic refrigerant and heat transport gas, and dead volume effect, have been minimized by the design optimization of the system components, performed with numerical analysis of the system. The magnetic system of the tandem refrigerator has two virtually identical units, each consisting of a GGG ($Gd_3Ga_5O_{12}$) magnetic core, a superconducting magnet, and a warm- and a cold-end heat exchanger. These components are united by a cryogenic displacer which shuttles 40-torr He^3 gas between the two units. A sub-atmospheric He^3 gas, rather than atmospheric He^4, was chosen as the heat transport medium chiefly to reduce the adverse effect of helium entrainment in the magnetic cores and to avoid undesirable superfluidity. Because of experimental difficulties, the prototype was operated with parameters that were different from those selected in the design phase. The experimental result shows that the net refrigeration rate was 12 mW at 1.8 K. The test also revealed about 40 % loss of performance by the magnetic core that contained crushed irregularly shaped granules of GGG compared to that achieved by the other magnetic core that contained about 70,000 GGG spheres, each 0.8 mm in diameter. The thesis concludes with design ideas for regenerative magnetic refrigerators that can reach warm-end temperatures up to 15 K and cover larger temperature span.

Thesis supervisor : Prof. Joseph L. Smith, Jr.
Title : Professor of Mechanical Engineering

Thesis supervisor : Prof. Yukikazu Iwasa
Title : Research Professor, Francis Bitter National Magnet Laboratory
Senior Research Engineer , Department of Mechanical Engineering

ACKNOWLEDGMENTS

The last four years at MIT was invaluable time in my life. I would like to thank Professor Joseph L. Smith, Jr. and Professor Iwasa for their support, as well as for their advice to the work presented in this thesis. It was always fun to weld with Professor Smith in the basement of building 41. He has taught me that there is no problem without solution. His endless idea helped me go through many obstacles. Professor Iwasa was kindly available to answer my questions about electronics and superconducting magnet. His experienced suggestion guided me to go to the right way. I also would like to thank my other committee member, Professor Lienhard for his advice. Through his class which I have taken at the first time in MIT, I learned how to handle engineering heat transfer problems without calculator. I wish to thank Sumitomo Heavy Industries and National Research Institute for Metals, Tsukuba Laboratory in Japan for their financial support.

My special thanks go to Dr. Numazawa. His help was essential for the final success in the experiment. We enjoyed doing experiments in the shaky, noisy, and dusty basement. I wish to thank other students and technicians at the Cryogenic Engineering Laboratory; Bob Gertsen and Mike Demaree for their assistance with machining and a helium leak detector, Don Anderson, Jerry Sullivan, and Louis Lamattina for prompt preparation of liquid helium and liquid nitrogen. I owe many things to people in Francis Bitter National Magnet Laboratory ; Mel Vestel for his assistance with constructing superconducting magnet, Ron Derocher for his kind explanation about preparing superjoint, David Johnson for his generous and versatile help, Larry Rubin for advice on temperature sensor calibration and power supply, David Lynch for repairing my troublesome power supply, Bruce Brandt for assistance with temperature sensor calibration work, and Paul Emery for helping me to prepare indium wire.

I would like to convey my special thanks to my host family, JoAnn and Fred for their parents-like everlasting warm welcome especially when I felt homesickness. Finally, I wish to thank my family. I am truly indebted to my parents and parents-in-law for their love, care, support, and constant advice. My deepest thanks and love go to my wife, Yeonhwa, for her patience, encouragement and indispensable help as an experiment assistant. She has never let me lose my confidence, managing to put up with me during the worst of times.

This thesis is dedicated to Yeonhwa who has spent many long lonely nights with our unborn child.

TABLE OF CONTENTS

NOMENCLATURE

A : Area

A_c : Cross-section area of GGG core

A_f : Average cross-section area of flow passage

A_H : Heat transfer surface area of flow passage

B : Magnetic flux density

B_m : Maximum magnetic field in the solenoid

C_H : Constant magnetic field specific heat

C_{Po} : Zero pressure specific heat

c : Specific heat

D_h : Hydraulic diameter

d : Diameter

E : Electric field

ΔE : Internal energy change

f : friction factor

G : Mass velocity $\left(= \frac{\dot{m}}{A} \right)$

H : Magnetic field intensity

h : Enthalpy

h : Heat transfer coefficient

I : Current

J : Current density

K : Permeability in porous media

k : Thermal conductivity

M : Mass

M : Magnetization

m : Mass

$\dot{m}$: Mass flow rate

Δm : Differential shuttle mass of helium

N_i : Mole numbers of i species

P : Pressure

P : A.C. loss

ΔP : Pressure drop

Pr : Prandtl number

Q_h : Rejection heat to warm reservoir

Q_{ref} : Refrigeration power

$\dot{Q}$: Heat transfer rate

q : Heat flux

R : Thermal resistance

R : Electrical resistance

Ra : Rayleigh number $\left(= \frac{K \rho_o \beta g \Delta T H}{\nu \alpha} \right)$

Re : Reynolds number $\left(= \frac{\rho \cdot D_h \cdot V}{\mu} \right)$

S : Entropy

S : Surface area

S_{gen} : Entropy

ΔS : Specific average entropy change

T : Temperature

T : Tesla (= 10,000 gauss)

T_m : Time for the magnetic field to rise to B_m

t : Time

t : Thickness

U : Internal energy

U : Overall heat transfer coefficient

V : Volume

$\overline{V}$: Average velocity of helium flow

ΔV : Differential core volume

α : Heat transfer area per unit length

α : Thermal diffusivity

β : Volume expansion coefficient

γ : Geometric factor in A.C. loss calculation

ε : Porosity

θ : Temperature difference

λ : Packing density of magnet

λ : Fraction of NbTi in superconducting wire

μ : Viscosity

μ_i : Chemical potential of i species

μ_o : Magnetic permeability of free space (= $4\pi \times 10^{-7}$ H/m)

ν : Kinematic viscosity

η : Cycle efficiency

ρ : Density

ρ : Electrical resistivity

σ : Heat capacity ratio in porous media

σ_θ : Hoop stress

τ : Cycle period

Subscripts

c : Magnetic core

c : Critical

c : Cold end of magnetic core

eff : Effective

GGG : GGG

h : Warm end of magnetic core

He : Helium

HX : Heat exchanger

m : Maximum

w : Wire

LIST OF FIGURES

LIST OF TABLES

I. INTRODUCTION

Magnetic refrigeration is a cooling method utilizing magneto-caloric effect of material. It has been used for over fifty years as a useful technique to obtain temperatures below 1 K. However, in the last ten years, the technology has also been developed for refrigeration applications at temperatures above 1 K, even at room temperature. While one mode of the magnetic refrigerator is an one-shot process type for approaching zero Kelvin, the other mode of a continuously operating magnetic refrigerator with reasonable refrigeration capacity has been in demand for engineering applications. Since the lower operating temperature of a vapor compression refrigerator is limited by the liquefaction temperature of the working fluid, a magnetic refrigerator takes a more important role at temperatures below 4.2 K, which is the boiling temperature of liquid helium at 1 atm.

The objective of this research is to design, construct and measure the performance of a prototype *regenerative magnetic refrigerator operating between 4.2 K and 1.8 K*. A refrigerator for this temperature range is frequently used to liquefy and maintain superfluid helium (He II), which is very useful for cooling sensors and other ultra-low temperature devices with its high heat transfer capability. The resolution of infrared sensors improves as their operating temperatures are decreased due to less back-current noise. Table 1-1 shows examples of He II cooled sensors for space applications (Hopkins et al., 1990). Because none of these systems carries a on-board He II refrigerator, the duration of their operating time is limited by their fluid capacity.

Table 1-1 Examples of He II cooled sensors for space applications.

System	Tank size (liters)	Reservoir temperature (K)	Vacuum shell temperatures (K)
XRS*	490	1.3	250
SAFIRE†	124	1.9	300

* X-Ray Spectrometer of the Advanced X-Ray Astrophysics Facility

† Spectroscopy of the Atmosphere using Far Infrared Emission instrument to be flown on the Earth Observing System

The magnetic refrigerator is reliable in two aspects : (1) virtually vibration-free and (2) relatively high thermodynamic efficiency even temperatures below ~20 K. Thus, provided that it can operate continuously, a large cryogen tank required in space application cited in Table 1-1 may be replaced by the magnetic refrigerator. However, one disadvantage is its relatively narrow working temperature span, *i.e.* the temperature difference between heat source and heat sink. This problem arises from the limitation of magneto-caloric effect inherent in magnetic materials. One way to overcome this deficiency is by applying Ericsson or Stirling magnetic cycles instead of single Carnot cycle. Therefore, the development of the regenerative machine should play a key role to increase the temperature span of magnetic refrigerator.

This thesis describes the *second generation* magnetic refrigerator developed in Cryogenic Engineering Laboratory of M.I.T. Although both devices use the same magnetic material, GGG ($Gd_3Ga_5O_{12}$: Gadolinium Gallium Garnet), the temperature range of present device is shifted to 4.2 K~1.8 K from the range 12 K~4.2 K in the previous device. Most components have been re-designed based on past experience.

The thesis is composed of the following parts: Chapter 2 contains designs of the major components ; Chapter 3 presents results of a computer simulation performed on the device; and Chapter 4 and Chapter 5 discuss experimental procedure and results. Chapter 6 concludes the thesis and Chapter 7 recommends the design for the next generation machine.

1.1 Magneto-thermodynamics

To describe how useful the magneto-caloric effect is for producing low-temperature, a thermodynamic energy relation of the system is first considered, including the term representing magnetic work.

$$dU = TdS - PdV + \Sigma\mu_i dN_i + \mu_o VHdM \qquad (1.1)$$

where μ_i is the chemical potential of i species and μ_o is the Magnetic permeability of free space ($= 4\pi \times 10^{-7}$ H/m).

With constant volume and in the absence of chemical reaction, Eq.1-1 reduces to:

$$dU = TdS + \mu_o VHdM \tag{1.2}$$

,where U is the internal energy, S is the entropy, H is the magnetic field, and M is the magnetization per unit volume.

Now, the entropy change of magnetic material can be expressed by two independent variables; T and H.

$$dS = \left(\frac{\partial S}{\partial T}\right)_H dT + \left(\frac{\partial S}{\partial H}\right)_T dH$$

$$= \frac{C_H}{T} dT + \mu_o V \left(\frac{\partial M}{\partial T}\right)_H dH \tag{1.3}$$

where the Maxwell relation $\left(\frac{\partial S}{\partial H}\right)_T = \mu_o V \left(\frac{\partial M}{\partial T}\right)_H$ is used.

From Eq.1.3, the *reversible adiabatic temperature change upon a magnetic field change* is derived as follows.

$$dT = -\frac{T}{C_H} \mu_o V \left(\frac{\partial M}{\partial T}\right)_H dH \tag{1.4}$$

As in Figure 1-1,which presents magnetization vs. temperature data of GGG, magnetization decreases at constant magnetic field as temperature increases. GGG is a typical paramagnetic material used in magnetic refrigeration and it is particularly effective at temperatures below 4.2 K. In the magnetic refrigerator, the temperature decreases when the material is demagnetized. The principle of magnetic refrigeration is based on this magneto-caloric effect. The unit of magnetization is actually A/m (ampere/meter). Figure 1-1 shows the volumetric magnetization of GGG which has a unit of $m^3/kg \cdot A/m$.

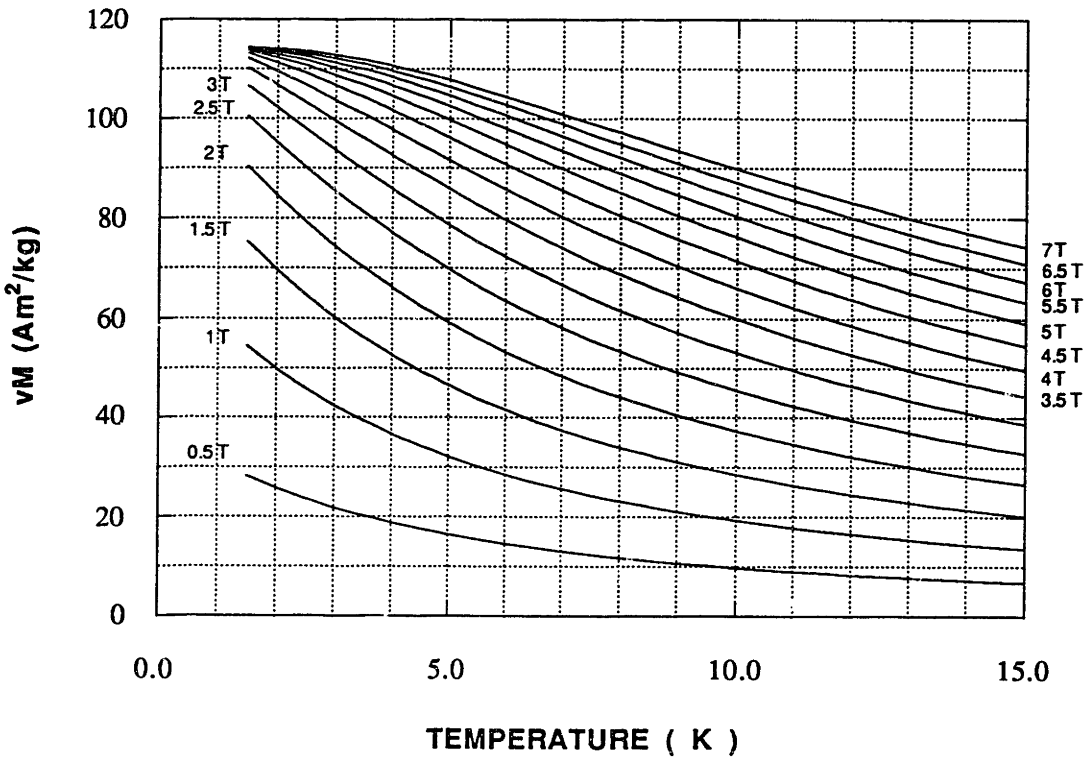

Fig.1-1 Magnetization vs. temperature at constant magnetic fields* for GGG ($Gd_3Ga_5O_{12}$; Gadolinium Gallium Garnet).

The magnetic refrigeration cycle is typically composed of four processes as shown in Figure 1-2, which illustrates two Carnot cycles, one based on vapor on the left and the other based on magnetic material on the right. Clearly the two cycles are in essence identical thermodynamically. Just as the working fluid in a vapor compression cycle undergoes a mechanical compression and expansion, so does the solid magnetic refrigerant magnetically. In other words, the magnetic cycle uses a solid magnetic refrigerant in place of the working fluid to achieve the cooling effect.

* Although the unit of magnetic field (H) in the SI unit is ampere/meter, the unit of magnetic induction (B), tesla is often used in most literature. This thesis, though realizing it is erroneous, nevertheless adopts the custom.

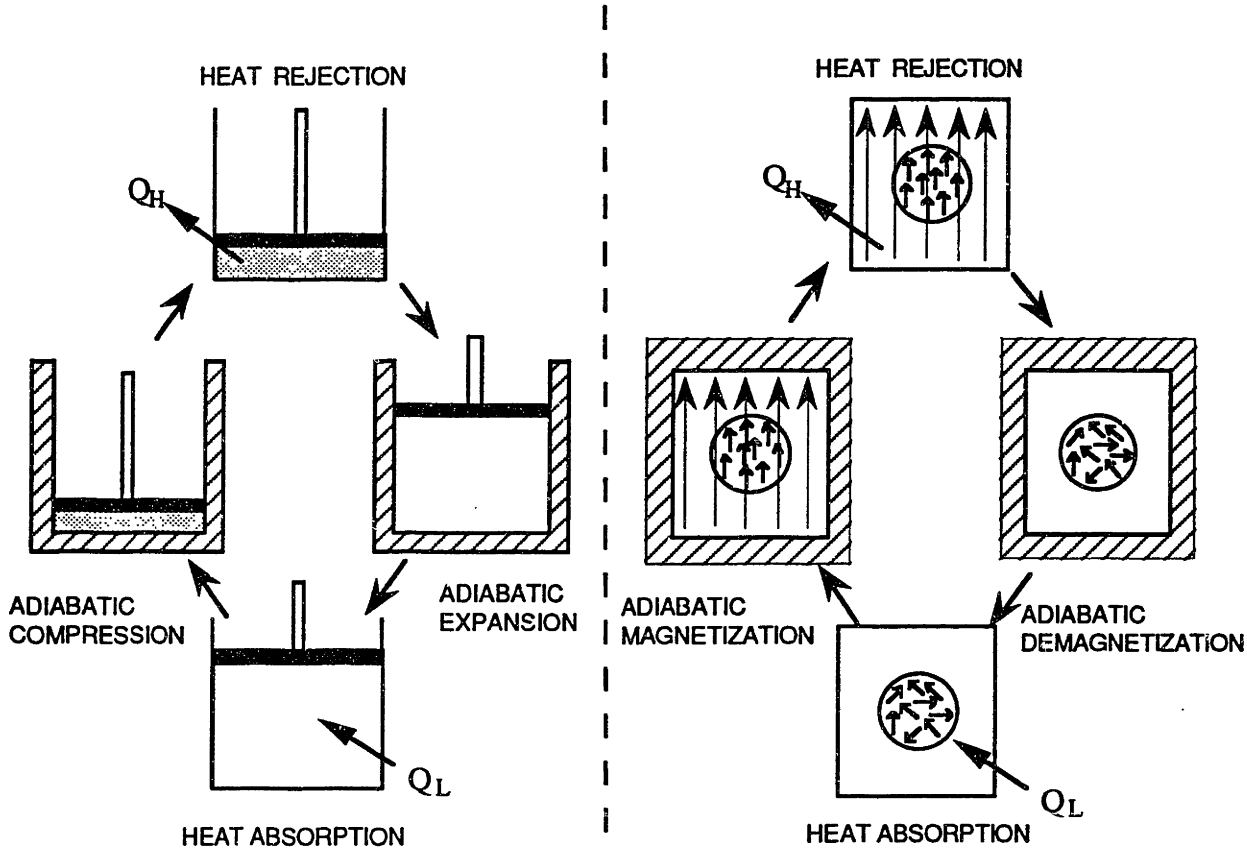

Fig.1-2 Comparison between vapor compression-expansion refrigeration and magnetic refrigeration cycle.

Table 1-2 summarizes the analogy between the vapor compression refrigeration cycle and the magnetic refrigeration cycle.

Table 1-2 Analogy between the vapor compression refrigeration cycle and the magnetic refrigeration cycle.

Vapor Compression Refrigeration Cycle	Magnetic Refrigeration Cycle
Pressure (P)	Magnetic field (H)
Volume (V)	Magnetic moment ($-\mu_o vM$)
Mechanical compressor	Magnetic compressor
Mechanical restriction of molecular motion	Magnetic restriction of magnetic moment

1.2 Historical development of magnetic refrigeration

The first important experimental demonstration of magnetic cooling was by W.F. Giauque, who in 1933 achieved temperatures below 1 K. P. Langevin, P. Weiss, and others also introduced the principle of magneto-caloric effect in their early research. Since 1933, many devices utilizing magneto-caloric effect of paramagnetism of electrons and nuclei have been developed to reach temperatures as low as 10^{-8} K.

While most early attempts to approach absolute zero Kelvin relied on 'one-shot' devices, there have been efforts notably since 1950, to develop continuously operating magnetic refrigerators, considered essential in most engineering application. Such magnetic refrigerators must have *a mechanism to transport heat from the magnetic refrigerant to the warm- and cold-end heat reservoirs.* Zimmerman *et al.* in 1962 used lead superconducting thermal valves as heat switches to control heat flow. In the superconducting state, the lead valves are "closed" and heat is passed; in the normal state, they are "open". These valves are magnetically activated. The disadvantage of this system is the narrow operating temperature range imposed by the valves and the loss of superconductivity at high heat fluxes, making such devices unsuitable for a large refrigeration capacity.

Mechanical contact switches have also been explored by Collins *et al.* (1953) and Numazawa (1990). Such a valve has an advantage in that there is virtually no heat leakage through it when the contact is broken. On the other hand, a serious disadvantage is energy dissipation associated with contact opening or closing. This energy dissipation is usually too large to be tolerated in the temperature region below 0.5 K. However, the mechanical valves in Numazawa's machine (1990) perform well in the warm-end side which is at above 8 K . Fulton *et al.* (1960) have investigated the use of liquid He^4 and liquid He^3 mixtures as thermal valves. With a vertical tube and copper blocks at both ends, a mixture with 0.5% He^3 shows a uni-directional conductivity in the downward direction. The heat pipe or thermosyphon has also been explored as a thermal switch by Nakagome (1984) and Hakuraku (1985).

The simplest magnetic refrigerator is a single Carnot type machine as shown in Figure 1-3. This single-cycle, shown in the left side, has been investigated by many researchers (Barclay *et al.*, 1985, Nakagome *et al.*, 1984, Hakuraku *et al.*, 1985, Numazawa *et al.*, 1990). However, the single Carnot cycle has some basic shortcomings. The magneto-

thermodynamic properties of most refrigerants make inherently it difficult to operate over a large temperature span with practical levels of magnetic field. Consequentially, the cascaded (regenerative) type, shown in the right side, is more appropriate than the single Carnot type for applications requiring large temperature spans (Van Geuns, 1966, Barclay et al., 1976, Taussig, 1986 *etc.*).

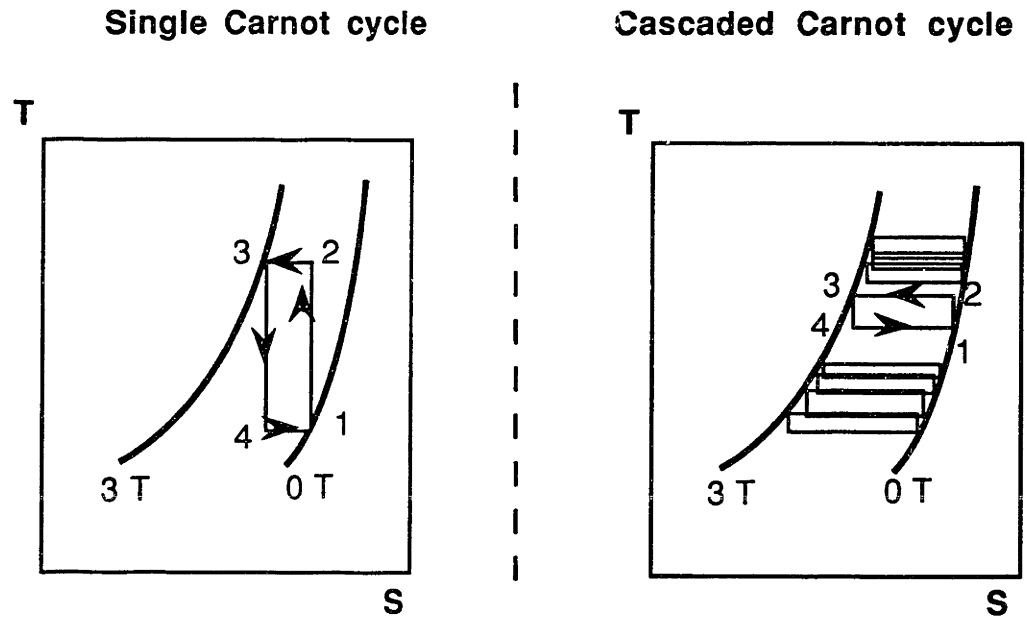

Fig.1-3 Single Carnot cycle vs. Cascaded Carnot cycle.

The cascaded Carnot cycle is composed of many independent single Carnot cycles. For the given magnetic field swing of 0 to 3 tesla, a magnetic refrigerant is efficiently utilized by the cascaded Carnot cycle. This kind of regenerative magnetic refrigerator was first attempted at M.I.T. by Taussig *et al.* (1986). The experimental apparatus used a GGG magnetic core. The heat was transported by 3-atm. supercritical helium. Its temperature range was between 4.2 K and 10 K. Even though the GGG core seemed to work well, the overall performance was degraded by many extraneous factors such as a large axial conduction loss, the helium entrainment, the dead volume effect.

From the next chapter, the development of the regenerative tandem magnetic refrigerator operating between 4.2 K and 1.8 K will be discussed.

ΔΕΣΙΓΝ

↓

ΣΙΜΥΛΑΤΙΟΝ

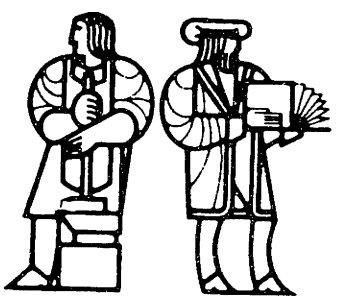

The research of 19th-century physicist and chemist Michael Faraday was the underpinning of motors, radio communication and many other modern advances. At the end of one of his lectures and experiments, a member of the audience said to the esteemed English scientist: "The behavior of the magnet and coil of wire was interesting, but of what possible use can it be?" Faraday answered politely, "Sir, of what use is a newborn baby?"
-from Issac Asimov's introduction to *The Greatest Adventure: Basic Research That Shapes Our Lives,* 1974

II. DESIGN

In this chapter, the design of each of the following major cryogenic components is discussed in detail: magnetic core; superconducting magnet; warm-end heat exchanger; cold-end heat exchanger; and displacer.

An ideal magnetic refrigeration cycle is composed of the following four processes: adiabatic magnetization; isothermal magnetization; adiabatic demagnetization; and isothermal demagnetization. In order to approach this ideal cycle, choosing a proper magnetic refrigerant is an important first step. Suitable materials characteristically have a large magneto-caloric effect near their magnetic phase transition temperatures. Table 2-1 shows magnetic materials that are potentially useful for refrigeration applications.

Table 2-1 Potential magnetic materials for a magnetic refrigerator.

No.	Substance	T_c* (K)	Characteristic	Reference
1	$Dy_3Ga_5O_{12}$ (DGG)	0.37	high thermal conductivity, good for Ericsson cycle (2 K ~ 12 K)	Hashimoto, 1986
2	$Gd_3Ga_5O_{12}$ (GGG)	0.85	high thermal conductivity, excellent magnetic refrigerant below 10 K	Barclay, 1982
3	$Gd_3Al_5O_{12}$ (GAG)		high thermal conductivity, difficult to make in the form of single crystal	Hashimoto, 1986
4	$Gd_3(Ga_{0.8}Al_{0.2})_5O_{12}$		solid solution of GAG and GGG	Hashimoto, 1986
5	$Gd_2(SO_4)_3$	< 1	lighter than GGG, good for temperatures below 1.8 K	Delpuech *et al.*, 1981
6	$Dy_2Ti_2O_7$	1.35	available in powder form, temperature range (4.2 K~20 K)	Flood, 1974
7	$HoPO_4$	1.39	RXO_4† family	Daudin *et al.*, 1981

* Phase transition temperature

† Rare earth material, X = V, As or P

Table 2-1 Potential magnetic materials for a magnetic refrigerator (continued).

No.	Substance	T_c^* (K)	Characteristic	Reference
8	$TmVO_4$	2.15	RXO_4† family, high thermal conductivity	Daudin *et al.*, 1981
9	$Dy_3Al_5O_{12}$ (DAG)	2.53	high thermal conductivity, better than GGG above 10 K	Li, 1986
10	$DyVO_4$	3.0	mixed with GGG in Ericsson type machine between 2 K and 20 K	Daudin *et al.*, 1982
11	$DyPO_4$	3.39	RXO_4† family	Daudin *et al.*, 1981
12	$TmAsO_4$	6.0	RXO_4† family, good material in the temperature range 5 to 10 K	Daudin *et al.*, 1981
13	ErN_{12}	6.7	promising material in the wide temperature range below 35 K	Tomokiyo *et al.*, 1986
14	$ErAl_2$	11.7	useful for compound material for Ericsson type machine above 15 K	Hashimoto *et al.*, 1987
15	$HoNi_2$	12.3	promising material in the wide temperature range below 35 K	Tomokiyo *et al.*, 1986
16	EuS	16.0	promising material in Ericsson type machine above 20 K	Hashimoto, 1986
17	$DyNi_2$	19.3	promising material in the wide temperature range below 35 K	Tomokiyo *et al.*, 1986
18	$HoAl_2$	26.8	useful compound material for Ericsson type machine above 15 K	Hashimoto *et al.*, 1987
19	$(Ho_{0.5}Dy_{0.5})Al_2$	46	useful compound material for Ericsson type machine above 15 K	Hashimoto *et al.*, 1987
20	$DyAl_2$	55.9	useful for Ericsson type machine between 20 K and 77 K	Hashimoto *et al.*, 1986
21	Ho_5Si_4	76	ferromagnetic rare-earth intermetallic compound	Brown, 1976

* Phase transition temperature

† Rare earth material, X = V, As or P

Table 2-1 Potential magnetic materials for a magnetic refrigerator (continued).

No.	Substance	T_c* (K)	Characteristic	Reference
22	$GdNi_2$	85	promising material in the wide temperature range below 35 K	Tomokiyo *et al.*, 1986
23	$(GdEr)_{0.5}Al_2$	96	compound of $GdAl_2$ and $Er_{0.5}Al_2$	Zimm *et al.*, 1984
24	Dy_5Si_4	140	ferromagnetic rare-earth intermetallic compound	Brown, 1976
25	$GdAl_2$	164	low hysterisis material	Zimm *et al.*, 1984
26	$GdAl_{1.9}Ni_{0.1}$	191	ferromagnetic rare-earth intermetallic compound	Brown, 1976
27	Gd_3In	213	ferromagnetic rare-earth intermetallic compound	Brown, 1976
28	Tb_5Si_4	225	ferromagnetic rare-earth intermetallic compound	Brown, 1976
29	Gd_3Al_2	287	ferromagnetic rare-earth intermetallic compound	Hashimoto *et al.*, 1981
30	Gd	293	useful for room temperature heat pump	Brown, 1976
31	MnP	298	magnetic material for room temperature heat pump	Hashimoto *et al.*, 1981
32	Gd_5Si_4	336	magnetic material for room temperature heat pump	Hashimoto *et al.*, 1981

In the operating temperature range between 4.2 K and 1.8 K, GGG ($Gd_3Ga_5O_{12}$; Gadolinium Gallium Garnet) has excellent properties of magneto-caloric effect and thermal conductivity. GGG is a paramagnetic material in the rare earth family with a density of 7.14 g/cm^3. Due to its high thermal conductivity, single crystal GGG is preferred in the magnetic refrigerator rather than polycrystalline GGG. The magneto-thermodynamic properties of GGG are shown in Figure 2-1 in terms of temperature-magnetic field-entropy relation.

* Phase transition temperature

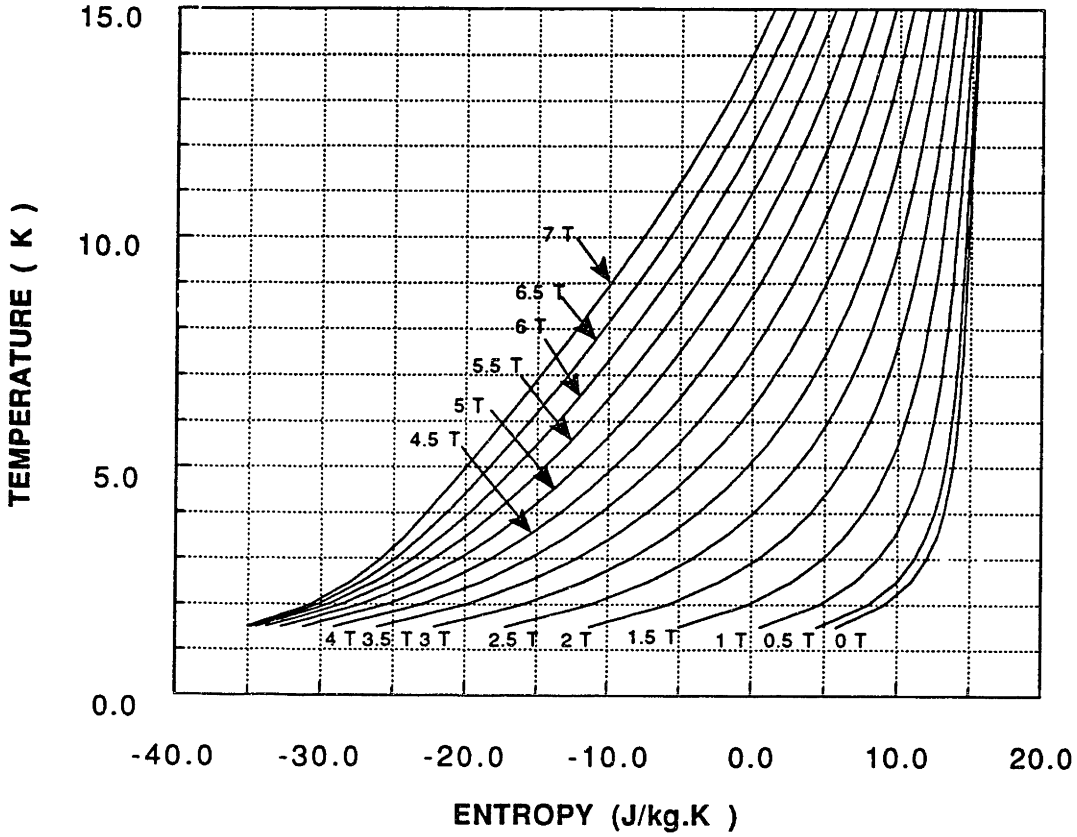

Fig.2-1 Temperature - entropy diagram of GGG ($Gd_3Ga_5O_{12}$; Gadolinium Gallium Garnet). [Note that as discussed in the footnote of p.16, magnetic field is given in the unit of magnetic induction.]

One of the major features introduced in the new second-generation magnetic refrigerator is a tandem mode. Figure 2-2 shows the schematic diagram of the tandem magnetic refrigerator.

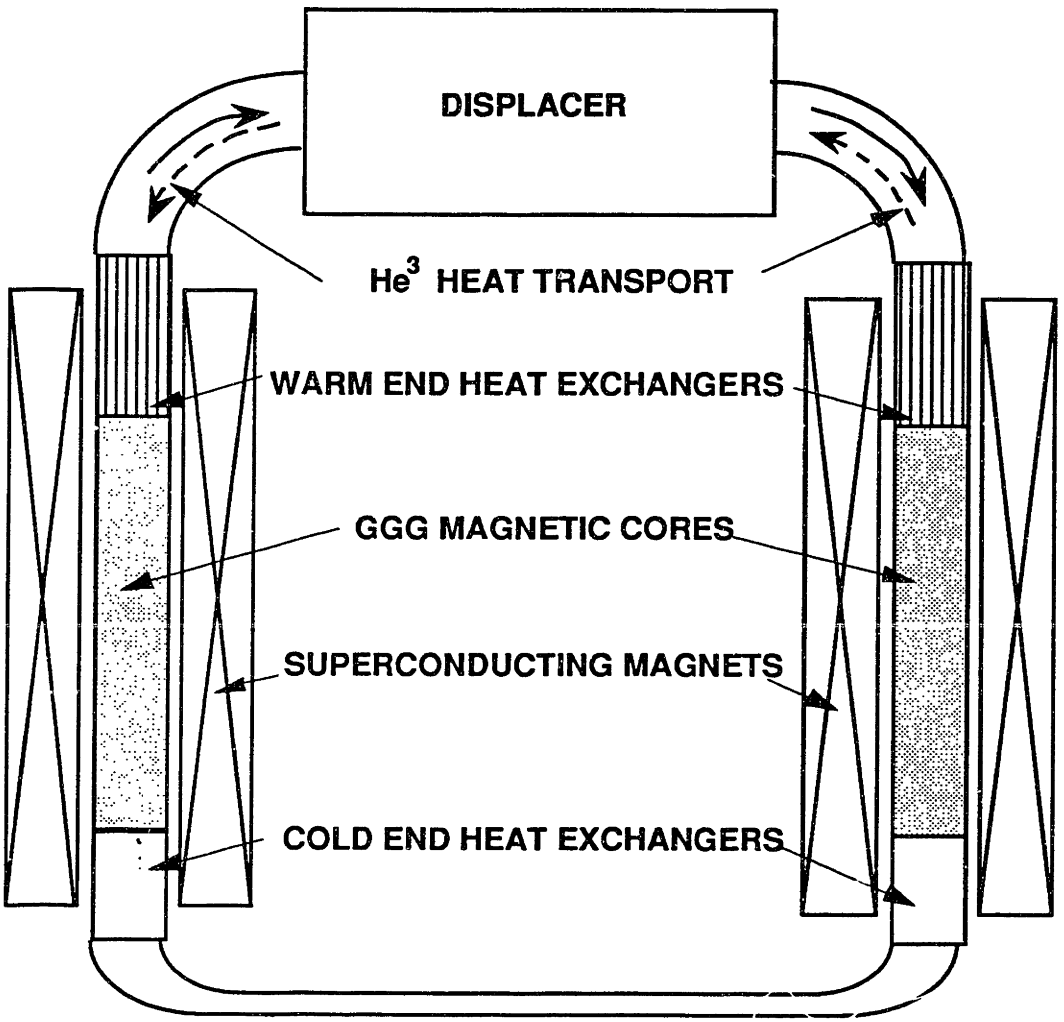

Fig.2-2 Schematic diagram of the second-generation magnetic refrigerator built at MIT.

The two magnetic systems, each consisting of a GGG magnetic core, a superconducting magnet, and a warm- and a cold-end heat exchanger are connected by a displacer. The displacer is a constant-pressure actuator for moving the heat transport medium (sub-atmospheric He^3 gas) through the two magnetic systems.

The advantages of tandem system are as follows:

* Doubling of refrigeration cycle frequency (2 refrigeration cycles / period).
* Simplified displacer mechanism.
* Potential simplification in magnet energization.

Each magnetic core to be energized up to 3 tesla by a superconducting coil, is composed of many (~ 70,000) GGG spheres, each 0.8 mm in diameter. As a heat transport medium between the magnetic refrigerant and the heat exchangers, a 40-torr He^3 gas has been selected. It reduces the adverse effect of helium entrainment and to avoid the undesirable superfluidity which will occur if the ordinary helium were used. Since this magnetic refrigerator works regeneratively, it is important to maintain the temperature gradient in the core along its axial direction. Selection of 40-torr He^3 gas as a heat transport medium is discussed in detail in the next section.

The system design minimizes the dead volume between the active magnetic core and the heat exchanger; one at the 1.8 K cold-end and the other at the 4.2 K warm-end. To minimize the power requirements for each superconducting magnet, an innovative idea that incorporates a persistent-current mode operation is used. The design value of refrigeration capacity is 100 mW at 1.8 K.

2.1 Magnetic Core

To achieve the characteristics of a cascaded Carnot cycle introduced in the earlier section, the magnetic core configuration must be designed so that the axial heat conduction is small compared with refrigeration capacity. Such a design requirement is possible by forming the magnetic core with many small magnetic particles as a packed bed (Figure 2-3). The axial conduction of a packed bed of GGG particles can be estimated by using an experimental correlation of McAdams (1954). With the following physical properties of the GGG core,

$$k_{gas} \cong 0.013 \text{ W/m·K} \quad (\text{He}^3 \text{ at } 3 \text{ K})$$
$$k_{solid} \cong 94 \text{ W/m·K} \quad (\text{GGG at } 3 \text{ K})$$
$$\varepsilon \cong 0.38 \quad (\text{porosity of packed bed})$$

the effective thermal conductivity is calculated to be 0.2 W/m·K. Therefore, the axial conduction over the entire core, 93 mm long, is given:

$$q_{AX.} = k_{eff} A \cdot \frac{\Delta T}{\Delta x}$$
$$= 0.2 \times \frac{\pi}{4} \cdot (20.4 \times 10^{-3})^2 \times \frac{4.2 - 1.8}{93 \times 10^{-3}}$$
$$= 1.7 \times 10^{-3} \text{ W}$$
$$= 1.7 \text{ mW} \qquad (2.1)$$

This value is considered negligible compared to the refrigeration capacity.

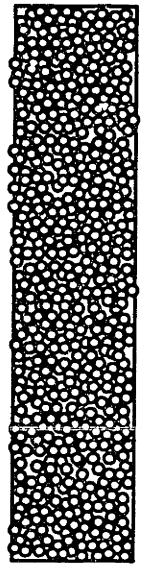

Fig.2-3 Schematic diagram of the GGG magnetic core containing ~70,000 GGG spheres, each 0.8 mm in diameter.

2.1.1 Heat transport medium

Choosing a proper heat transport medium is one of the most important design requirements in developing magnetic refrigerators because the heat transport medium should serve as a moving regenerator associated with the magnetic refrigerant. In the temperature range below 4.2 K, there are several possible heat transport media, each with advantages and disadvantages, as summarized in Table 2-2. Among those listed in Table 2-2, sub-atmospheric He^3 is selected as the most suitable transfer medium. He^3 at 0.053 atm. (40 torr) shows neither superfluid transition nor liquid-vapor phase change during the magnetic refrigerator operation.

Table 2-2 Candidates for heat transport medium for regenerative magnetic refrigerator.

Species	Working pressure	State	Reasons	Problems
He^4	0.007 atm.	vapor	To avoid two phase operation	too big displacer volume
He^4	1 atm.	liquid (superfluid)	To avoid big displacer volumes	large axial conduction due to superfluidity
He^4	3 atm.	supercritical	To avoid a big displacer volume and phase change	large mass of entrained helium
He^3	> 1.15 atm.	supercritical	To avoid superfluidity	large mass of entrained helium
He^3	0.053 atm.	vapor	To avoid liquid-vapor phase change and to keep the displacer volume small	expensive ($ 90/STP liter)

He^3, a stable isotope of He^4, is only about 0.1 ppm of natural helium but can be obtained readily as a by-product of nuclear reactions (Van Sciver, 1986). The physical behavior of low-temperature He^3 is fundamentally quite different from that of the common isotope because of its different quantum statistics. An atom of He^4 has zero nuclear spin and therefore obeys Bose-Einstein statistics. Consequently, at temperatures below 0.5 K, liquid He^4 is effectively in its quantum mechanical ground state (so-called *Bose condensation*). Very few phonons are excited and liquid He^4 therefore is thermodynamically inert. The lighter isotope He^3 has a nuclear spin of 1/2 and thus obeys Fermi-Dirac statistics. It does not exhibit Bose condensation and behaves very differently. The superfluid λ-transition of He^3 is not observed until the temperature is below 2.6 mK, which is about three orders of magnitude lower than the corresponding T_λ for He^4. Another very important property of He^3 is that it has a higher vapor pressure than He^4 at given temperatures as shown in Table 2-3.

Table 2-3 Comparison of vapor pressures of He^3 and He^4 at selected temperatures.

T (K)	P_{sat} (He^3) (mm Hg)	P_{sat} (He^4) (mm Hg)
0	-	-
0.6	0.544	2.81×10^{-4}
1.2	20.163	0.625
1.8	102.516	12.466
2.4	288.613	63.304
3.0	617.907	182.073
3.6	-	400.471
4.2	-	749.328

To proceed further in design, the calculation of the thermodynamic properties of He^3 is required. From the P-v-T equation of Sydoriak *et al.*(1964) and the zero pressure specific heat, the enthalpy of superheated vapor of He^3 can be calculated.

$$P v = R T\left(1 + \frac{B(T)}{v} + \frac{C(T)}{v^2}\right) \tag{2.2}$$

where $B(T) = 4.942 - \frac{270.986}{T}$ (cm^3 / mol)

$C(T) = \frac{2866}{\sqrt{T}}$ (cm^6 / mol)

$$h = h_o(2.0\ \mathrm{K}) + \int_{2.0}^{T}\left(\frac{\partial h}{\partial T}\right)_P dT + \int_{o}^{P}\left(\frac{\partial h}{\partial P}\right)_T dP$$

$$= h_o(2.0\ \mathrm{K}) + C_{PO}(T - 2.0) + \int_{o}^{P}\left(v - T\left(\frac{\partial v}{\partial T}\right)_P\right) dP \tag{2.3}$$

where h_o (2.0 K) is taken as 0 as a reference enthalpy value.

The required refrigeration capacity at 1.8 K determines the first estimate for the amount of He^3 gas needed. During the down-flow demagnetization process (which is equivalent to

the isothermal demagnetization process in an ideal Carnot cycle), the cold 1.5 K helium is assumed to be produced and warmed up to 1.8 K, absorbing heat from cooling load.

$$\dot{Q}_{ref.} \times \tau = m_{He} \times [h\,(1.8\ \mathrm{K}) - h\,(1.5\ \mathrm{K})] \tag{2.4}$$

where τ is cycle period and m_{He} is the shuttling mass of helium . From Eq. 2.4,

$$m_{He} = \frac{\dot{Q}_{ref.} \times \tau}{[h\,(1.8\ \mathrm{K}) - h\,(1.5\ \mathrm{K})]} \tag{2.5}$$

2.1.2 Determination of GGG parameter

GGG amount

For the required refrigeration capacity, the least amount of GGG needed can be estimated using an entropy balance for the down flow demagnetization process (Figure 2-4).

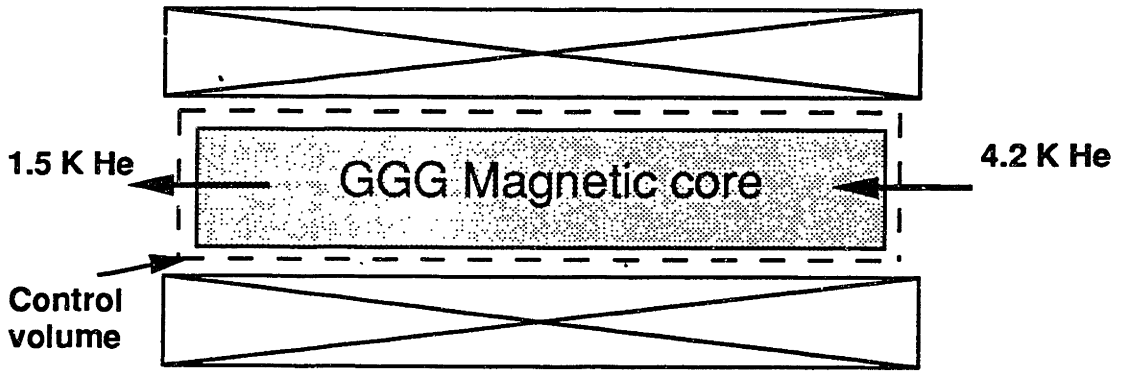

Fig.2-4 Entropy balance of the magnetic refrigerator.

$$m_{GGG} \times \Delta\bar{S}_{GGG} = m_{He}\ [S_{He}(4.2\ \mathrm{K}) - S_{He}(1.5\ \mathrm{K})] + \Delta S_{gen}$$

$$m_{GGG} > \frac{m_{He}\,[S_{He}(4.2\ \mathrm{K}) - S_{He}(1.5\ \mathrm{K})]}{\Delta \bar{S}_{GGG}} \qquad (2.6)$$

where $\Delta \bar{S}_{GGG}$ is the specific average entropy change of GGG during the demagnetization-flow process and ΔS_{gen} is the accompanied entropy generation.

Core configuration

As mentioned earlier, the magnetic core is of a packed bed type composed of many tiny GGG spheres. In this configuration, one advantage is a small axial conduction loss due to the high thermal contact resistance between GGG spheres. The other advantage of the packed bed core is its large area-to-volume ratio, which results in a small temperature differences between GGG and heat transport medium. On the other hand, one disadvantage is the high porosity of the core, especially if randomly packed. The porosity defined as the ratio of the helium volume to the total core volume, is directly related to the amount of helium entrained in the core. During the adiabatic magnetization or demagnetization process, the entrained helium flows out of or into the core due to the density change, even though the displacer does not move. Especially at the cold-end part, the expanded warm helium may deteriorate the total refrigeration capacity. This helium entrainment problem or helium exhalation effect can be alleviated by using low pressure (or low density) helium gas as heat transport medium.

The core diameter and length have been determined through consideration of commercially available stainless steel tube sizes and random packing porosity. The core size has been checked again in the section of heat exchanger design to assure that the magnetic core, the warm-end heat exchanger, and the cold-end heat exchanger can be assembled into a single tube.

GGG sphere size

The GGG particle size has been optimized to minimize entropy generation during the flow processes. In calculating entropy generation of the magnetic core, the radial temperature variation is assumed to be negligible compared with the axial temperature variation, because of the thermal contact resistance between the GGG spheres. As shown in Figure 2-5, the energy balance for helium is,

$$\dot{m}\frac{dh}{dx} = \dot{Q} \tag{2.7}$$

where $\dot{Q}$ is the rate of heat transfer between the helium gas and GGG per unit core length ; it is generated due to the magneto-caloric effect of GGG.

The axial conduction loss and the heat leak through the stainless steel core tube are neglected in this analysis.

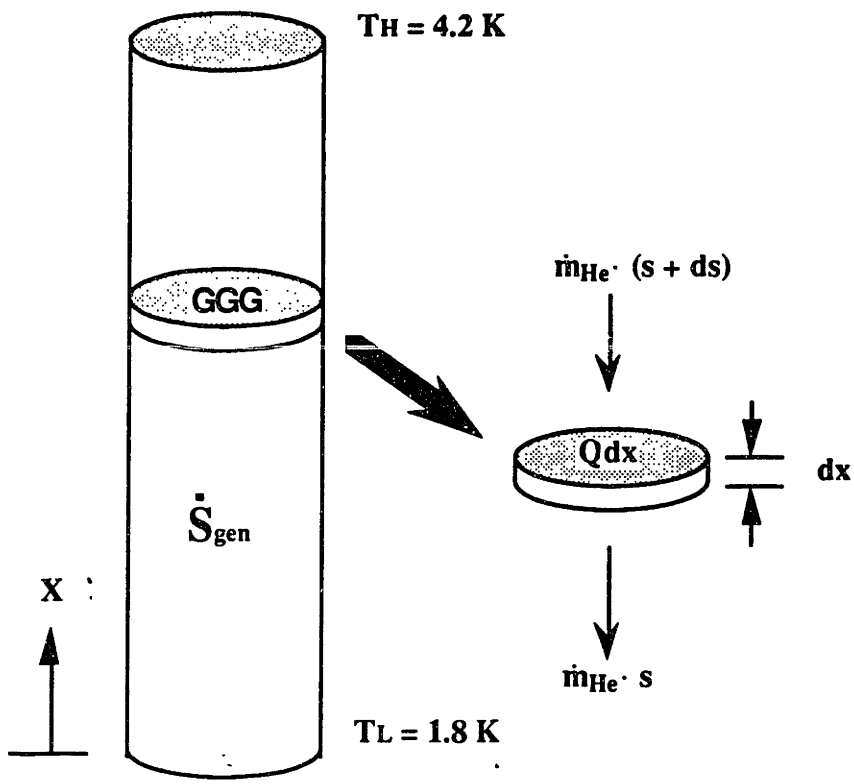

Fig. 2-5 Differential section of the magnetic core

The entropy balance for helium is as follows.

$$\dot{m}\frac{ds}{dx} = \frac{\dot{Q}}{T + \Delta T} + \frac{d\dot{s}_{gen}}{dx} \tag{2.8}$$

where ΔT is the small temperature difference between GGG and helium.

From the thermodynamic relation;

$$Tds = dh - vdP \tag{2.9}$$

the following equation can be obtained.

$$\frac{ds}{dx} = \frac{1}{T}\frac{dh}{dx} - \frac{1}{\rho \cdot T}\frac{dP}{dx} \tag{2.10}$$

Now, the entropy generation rate, $\frac{d\dot{s}_{gen}}{dx}$, can be expressed with two terms : (1) that due to the finite temperature difference in the heat transfer and (2) that due to the pressure drop.

$$\frac{d\dot{s}_{gen}}{dx} = \dot{Q}\left(\frac{1}{T} - \frac{1}{T + \Delta T}\right) - \frac{\dot{m}}{\rho \cdot T}\frac{dP}{dx} \tag{2.11}$$

Since the rate of heat transfer for differential segment is as follows,

$$\dot{Q} = h\alpha\Delta T = T\overline{\Delta\dot{S}_{GGG}}\,\rho_{GGG}(1 - \varepsilon)A_c \tag{2.12}$$

where A_c is the cross-section area of GGG core,

$\overline{\Delta\dot{S}_{GGG}}$ is the specific entropy change rate of GGG due to magnetic field change at constant temperature, T.

α is the heat transfer area per unit length which can be expressed in terms of GGG particle diameter, d_p, and porosity, ε, for the packed bed core.

$$\alpha = \frac{6A_c(1 - \varepsilon)}{d_p} \tag{2.13}$$

Therefore,

$$\frac{d\dot{s}_{gen}}{dx} = \frac{\dot{Q}^2}{h\alpha T^2} - \frac{\dot{m}}{\rho T}\frac{dP}{dx}$$

$$= \frac{\overline{\Delta \dot{S}_{GGG}}^2 \rho_{GGG}^2 (1-\varepsilon)^2 A_c^2}{h \cdot \alpha} - \frac{\dot{m}}{\rho \cdot T} \frac{dP}{dx} \tag{2.14}$$

The heat transfer coefficient and pressure drop relation for this analysis are assumed as those values of infinite random stacked sphere matrix (Kays and London, 1962).

$$h = 0.23(Re)^{-0.3}(Pr)^{-2/3} G C_p \tag{2.15}$$

$$\frac{dP}{dx} = -\frac{2fG^2}{\rho_{He} D_h} \tag{2.16}$$

where G is the mass velocity and C_p is the specific heat. The hydraulic diameter, D_h, is related to the GGG particle diameter, d_p, as follows (Smith, 1966):

$$\begin{aligned} D_h &= \frac{4A_f L}{A_H} \\ &= \frac{2\varepsilon}{3(1-\varepsilon)} d_P \end{aligned} \tag{2.17}$$

where A_H and A_f are respectively the total heat transfer surface area and the average cross-sectional area of the flow passage and L is the core length. Substituting equations (2.13 and 2.15 ~ 2-.17) into Equation (2-14) gives the entropy generation rate in terms of d_p.

$$\begin{aligned} \frac{d\dot{s}_{gen}}{dx} = \left(\frac{2}{3}\right)^{0.3} & \frac{\overline{\Delta \dot{S}_{GGG}}^2 \rho_{GGG}^2 A_c^{1.7}}{6 \times 0.23 \dot{m}^{0.7}} \frac{\varepsilon (1-\varepsilon)^{0.7} Pr^{2/3}}{\mu^{0.3} C_p} d_p^{1.3} \\ & + \frac{3f}{\rho_{He}^2 T} \frac{\dot{m}^3 (1-\varepsilon)}{\varepsilon^3 A_c} \frac{1}{d_P} \end{aligned} \tag{2.18}$$

As shown in Figure 2-6, the entropy generation during the demagnetization-flow process is a function of sphere diameter. In consideration of manufacturing capability, a diameter of 0.8 mm was selected for the size of GGG spheres.

The flow inside the packed-bed magnetic core is laminar with an average Reynolds number of about 120. The calculated total pressure drop along the two cores is 420 Pa, which is about 10 % of the working pressure.

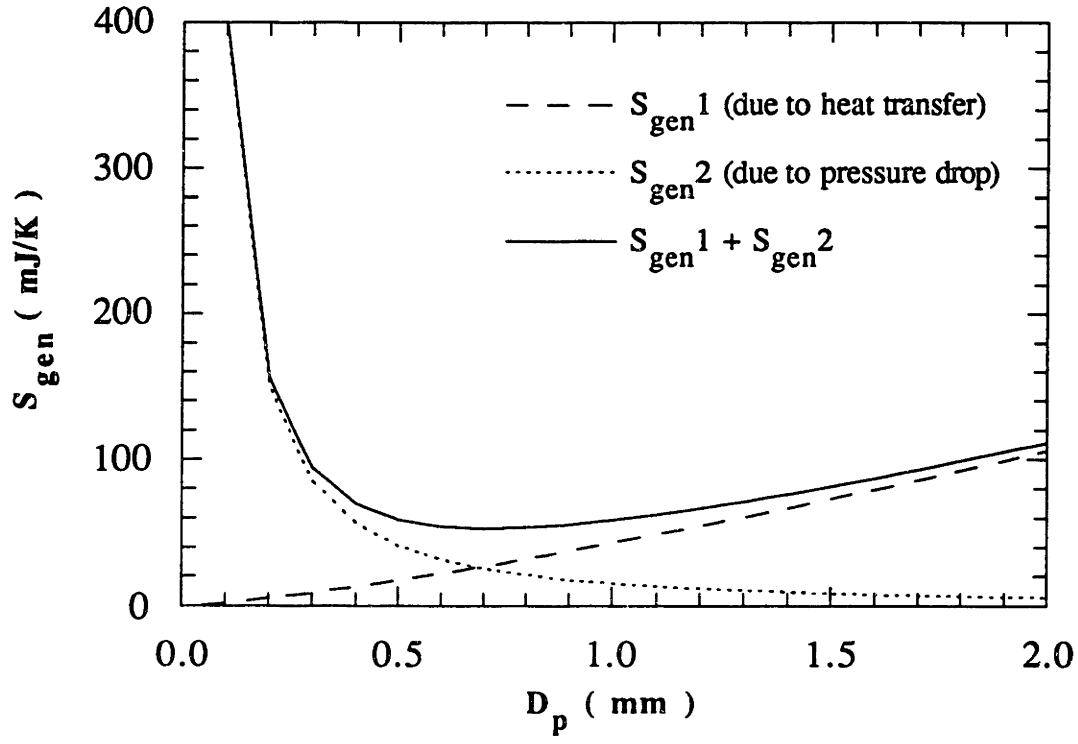

Fig.2-6 Entropy generation in the magnetic core.

Table 2-4 summarizes the important design parameters for each magnetic core.

Table 2-4 Magnetic core specifications.

---- Material : GGG ($Gd_3Ga_5O_{12}$) ---

No.	Parameter	Value	Description
1	D_c	20.4 mm	core diameter
2	L_c	93 mm	core length
3	V_c	30.5 cc	core volume
4	ε	0.38	porosity of randomly packed core
5	m_{GGG}	135 g	total mass of GGG in the core
7	d_h	0.33 mm	hydraulic diameter of packed bed core
8	A_f	124 mm^2	total flow area through the core

Table 2-4 Magnetic core specifications (continued).

No.	Parameter	Value	Description
9	ρ_{He^3}	0.653 kg/m^3	He^3 density at 3.0 K and 40 torr
10	m_{He^3}	7.5x10^{-3} g	mass of He^3 in core voids at 3.0 K
11	$\overline{V}$	0.67 m/sec	average He^3 velocity in the core
12	$\dot{m}$	0.054 g/sec	He^3 mass flow rate of He^3
13	Re	120	average Reynolds number in the core
14	$\bar{f}$	1.1	average friction factor in the core
15	h	224 W/m^2·K	average heat transfer coefficient in the core
16	ΔP	420 Pa	pressure drop in the core during the flow cycle
17	A_H	1418 cm^2	total heat transfer area of the core
18	k_{eff}	0.2 W/m·K	effective axial thermal conductivity of the core
19	$Q_{axial\text{-}c}$	1.7 mW	axial conduction loss of the core
20	$Q_{axial\text{-}s.s.}$	0.18 mW	axial conduction loss of stainless steel core tube
21	Bi	0.002	Biot number of the core configuration

2.2 Superconducting magnet

The superconducting magnet acts as an electrical dual compressor-expander in the magnetic refrigerator. It produces high enough magnetic field change to permit the magnetic refrigerant to reject or absorb heat.

2.2.1 Magnet configuration

Figure 2-8 shows a schematic diagram of one of the two superconducting magnets for the magnetic refrigerator.

Each magnet has a pair of secondary-notch coils to enhance field uniformity over the entire length of the core. Figure 2-9 shows the computed field profiles along the magnet axis. Even though the SI unit for magnetic field intensity is A/m rather than tesla, $\mu_o H$ instead of H is actually plotted in this picture. Another addition in each superconducting magnet system is an inverse coil, which reduces A.C. losses in the warm-end heat exchanger by producing an opposing field that tends to cancel some portion of the magnetic field of the primary coil and the secondary coils at the heat exchanger region.

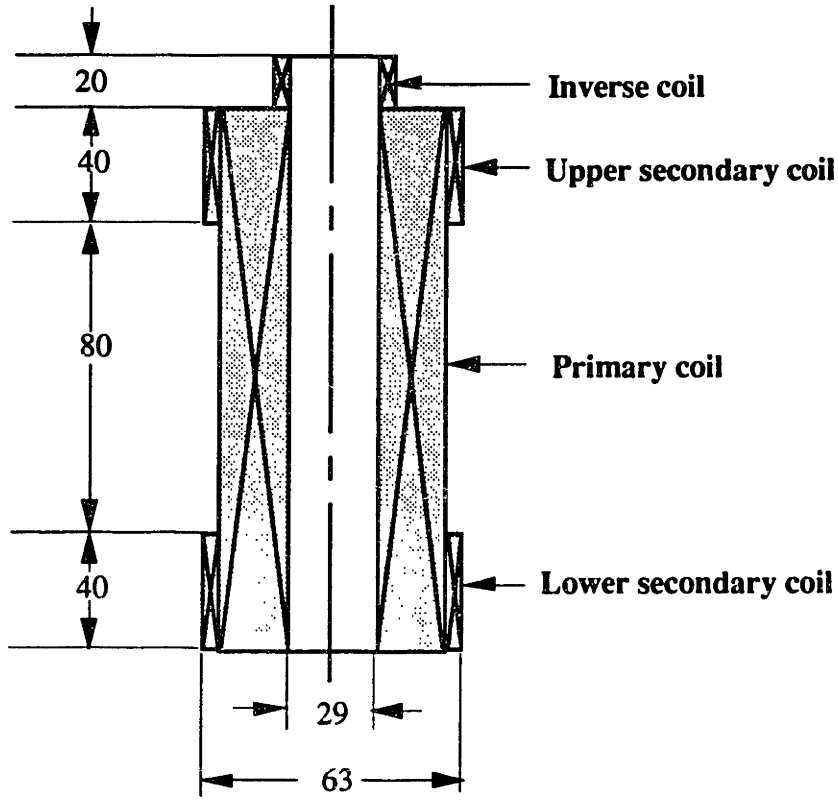

Fig.2-7 Schematic diagram of one of the two superconducting magnets in the magnetic refrigerator (units in mm).

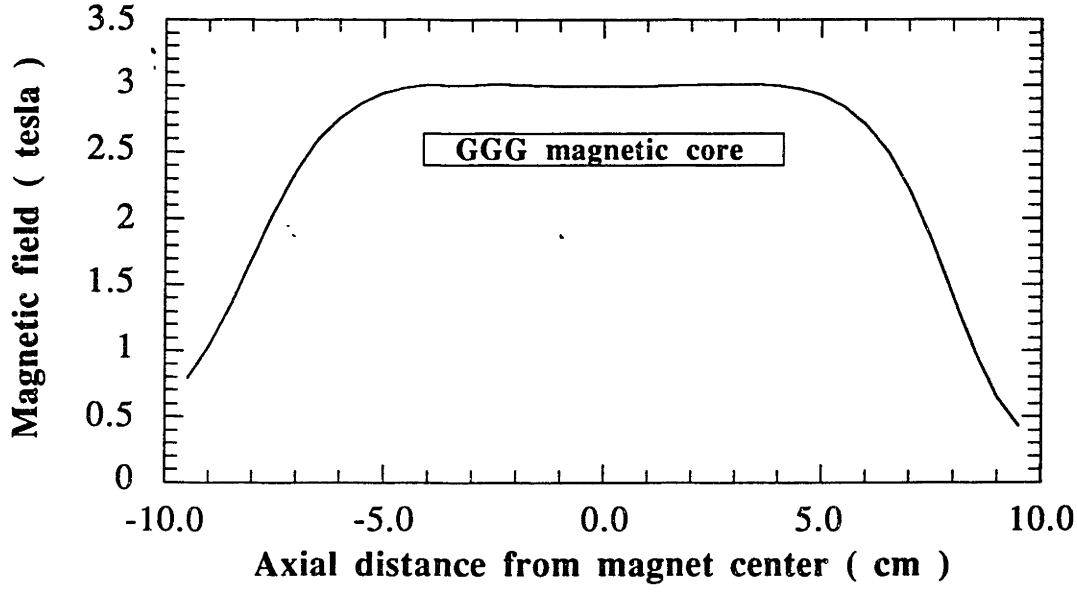

Fig.2-8 Calculated magnetic field of the superconducting magnet.

By using a thin superconducting wire, the A.C. losses of the magnet, itself, is reduced and the low-operating current generally makes magnet energization less demanding.

2.2.2 Power supply scheme of tandem magnets

The magnetic refrigerator is designed to operate in a tandem mode. In other words, while one magnetic unit is being magnetized, the other one is being demagnetized: magnetic field variations are 180° out of phase with respect to each other.

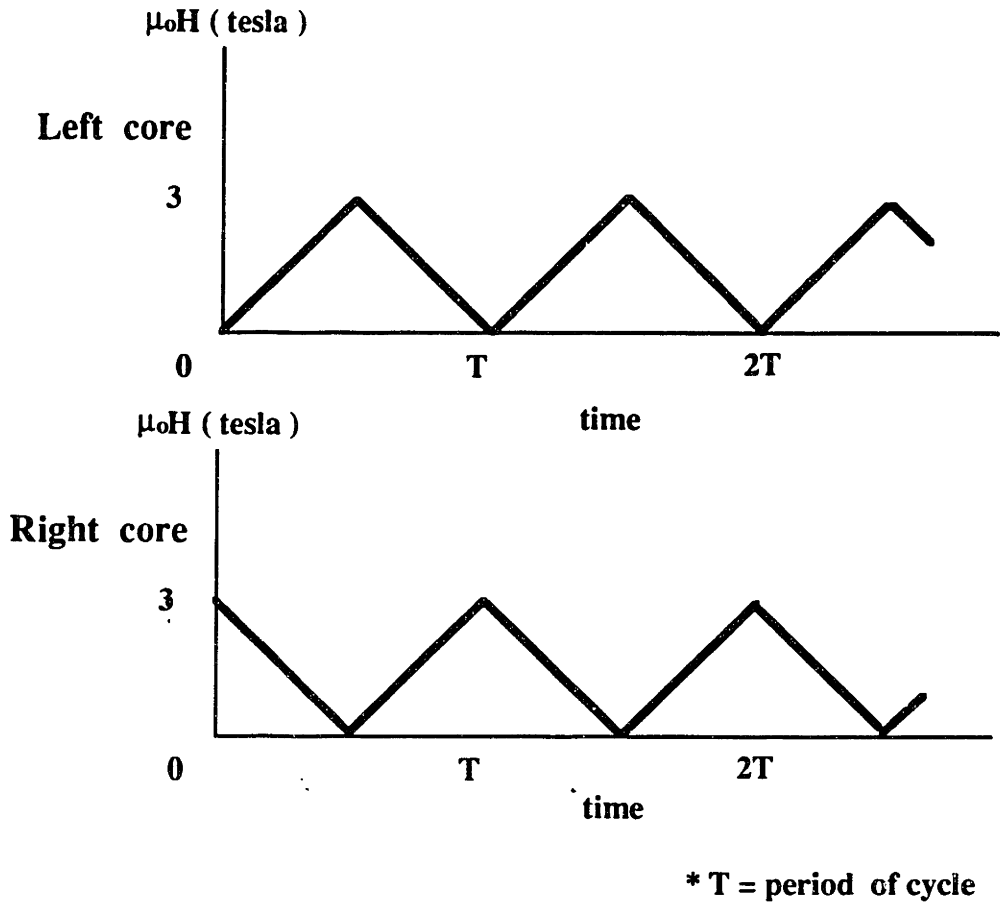

Fig.2-9 Field vs. time variations for the two magnets in the tandem refrigerator.

The required time-dependent magnetic field variations with time is as shown in Figure 2-9 when operating in ramp mode. In refrigeration, power loss is a premium and it must be kept minimum, even from the magnet charging system. In addition to achieve time-dependent magnetic field variation, the system must handle reactive power flow, which when it is large, adds complexities to the power supply. For these reasons - to minimize

power dissipation and reactive power flow - an innovative charging arrangement, described below, has been adopted.

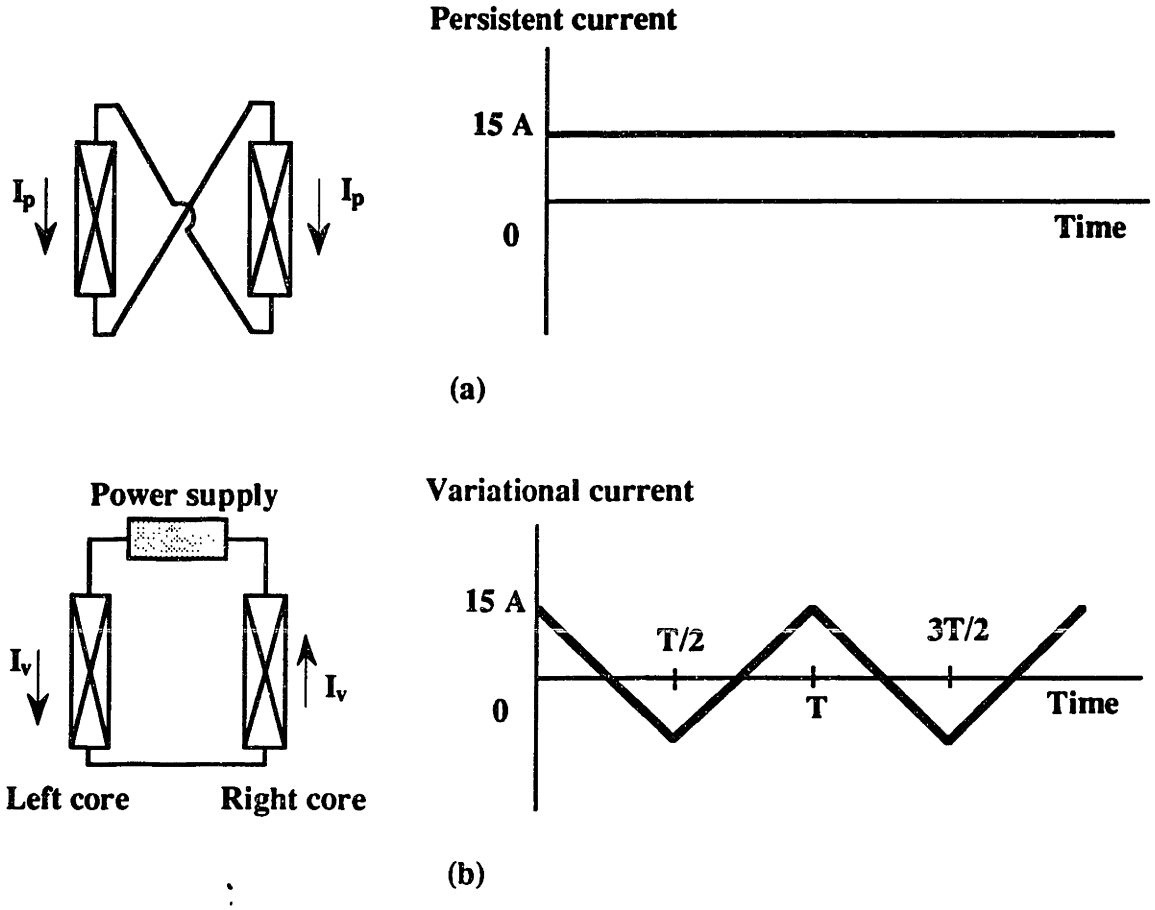

Fig.2-10 Magnet charging arrangement adopted in the tandem system. (a) Persistent-current mode coil energization (b) Variational-current mode coil energization

The tandem magnetic energization is to be incorporated to reduce such loss. In order to facilitate this new charging arrangement, each magnet consists of two separate coils; one for the persistent-current mode operation and the other for the variational-current mode. Each mode coil is again composed of a primary coil, a secondary coil, and an inverse coil with one wire. Figure 2-10 illustrates the charging arrangement schematically and by means of current vs. time plots for the two coils. The self inductance of each variational-current mode coil is about 1.8 H, which is only 25% of the total inductance of each unit. Because of this reduction in inductance in the variational-current mode coil, the reactive power requirement is reduced by a factor of 4. As shown in Figure 2-10, the persistent-

current mode coils which are connected in series, are energized up to 15 A, which contributes 1.5 tesla all the time for both GGG magnetic cores. The variational-current mode coils in the two units, connected in series, are energized by a single bipolar power supply. The direction of this field in each coil is arranged to be added to the persistent field in one core and subtracted to the persistent field in the other core.

In order for this persistent-variational mode concept to work, each pair coil in the two magnets must be identical. The persistent-current coil and the variational-current coil are actually wound together by juxtaposing them in a magnet winding machine. The measured mutual inductance between the persistent and variational coils is 1.0, which confirms that they are well coupled. Table 2-5 lists parameters of the two identical magnets. Appendix A discusses further the details of the superconducting magnet construction.

Table 2-5 Superconducting magnet specifications.

Parameter	Magnet #1	Magnet #2	Description
B_{max}	3 Tesla	3 Tesla	maximum magnetic field (without GGG)
I_{op}	15 A	15 A	operating current of the magnetic refrigerator
D_{SC}	25.4 mm	25.4 mm	bore diameter
a_1	15.88 mm	15.875 mm	inside radius of solenoid winding
a_P	29.25 mm	29.63 mm	outside radius of primary coil
b_P	160 mm	159.5 mm	axial length of primary coil
N_P	26284	26206	No. of total turns (2 x 13142)
NL_P	47	47	No. of winding layers
l_P	3726 m	3746 m	total length of primary coil
J_P	18423 A/cm^2	17917 A/cm^2	overall current density of primary coil
λ_P	0.84	0.84	computed packing density of primary coil

Table 2-5 Superconducting magnet specifications (continued).

Parameter	Magnet #1	Magnet #2	Description
$a_{u.s2}$	31.5 mm	31.5 mm	outside radius of upper-half secondary coil
$b_{u.s}$	40 mm	39.5 mm	axial length of upper-half secondary coil
$N_{u.s}$	826	812	No. of total turns (2 x 413)
$NL_{u.s}$	6	6	No. of winding layers
l_s	158 m	156 m	total length of upper-half secondary coil
$J_{u.s}$	13767 A/cm^2	16490 A/cm^2	overall current density of upper-half secondary coil
$\lambda_{u.s}$	0.94	0.81	computed packing density of upper-half secondary coil
$a_{l.s2}$	31.5 mm	31.5 mm	outside radius of lower-half secondary coil
$b_{l.s}$	40 mm	39.5 mm	axial length of lower-half secondary coil
$N_{l.s}$	826	814	No. of total turns (2 x 413)
$NL_{l.s}$	6	6	No. of winding layers
l_s	158 m	156 m	total length of lower-half secondary coil
$J_{l.s}$	13767 A/cm^2	16530 A/cm^2	overall current density of lower-half secondary coil
$\lambda_{l.s}$	0.94	0.81	computed packing density of lower-half secondary coil
$a_{I.2}$	19.0 mm	19.6 mm	outside radius of inverse coil
b_I	20 mm	20.5 mm	axial length of inverse coil
N_I	858	858	No. of total turns (2 x 429)
NL_I	13	13	No. of winding layers
l_I	94 m	96 m	total length of inverse coil
J_I	20592 A/cm^2	16854 A/cm^2	overall current density of inverse coil
λ_I	0.94	0.76	computed packing density of inverse coil
L	1.8 H	1.8 H	self inductance of persistent or variational coil
$Q_{A.C.}$	8 J/cycle	8 J/cycle	A.C. loss

2.3 Warm-end heat exchanger

The warm-end heat exchanger is to release the thermal energy of the magnetized GGG into the 4.2-K Liquid helium reservoir to permit continuous operation of the magnetic refrigerator.

The outer diameter of the heat exchanger has been determined to fit the magnetic core tube. This design consideration reflects an effort to locate the heat exchanger as close to the GGG core as possible in order to minimize dead volume. The large dead volume between the active magnetic core and the two end heat exchangers was considered one of the main deteriorating factors in the performance of the first-generation machine developed at M.I.T. However, if the heat exchanger is close to the magnetic core, it is exposed to a changing magnetic field of the superconducting magnet. Thus, an important design objective for the heat exchanger is to minimize A.C. losses, whose resultant heat generation puts an additional load on the heat exchanger. This problem is even more critical for the cold-end heat exchanger.

Figure 2-11 is a schematic diagram of the warm-end heat exchanger. The asteroid fin type is selected to minimize A.C. losses caused by large axial magnetic field variation. Since the electrical resistivity of copper increases as its purity decreases at low temperatures, a block of low purity ETP (Electrolytic Tough Pitch, RRR-30) copper is machined by EDM (Electric Discharge Machine) to form the warm-end heat exchanger. The detailed A.C. loss calculation is presented in Appendix B.

The warm-end heat exchanger has a liquid helium filled cavity at its center to keep its fins at 4.2 K. The diameter of inside cavity, D_i, has been selected to maximize overall thermal performance of the heat exchanger. Figure 2-12 shows an equivalent thermal resistance circuit. Figure 2-13 shows thermal resistance and the overall heat transfer coefficient calculation vs. cavity diameter plots. In the figures, h_i is the heat transfer coefficient of boiling liquid helium (~2000 $W/m^2 \cdot K$) and h_o is the forced convection heat transfer coefficient for He^3 side.

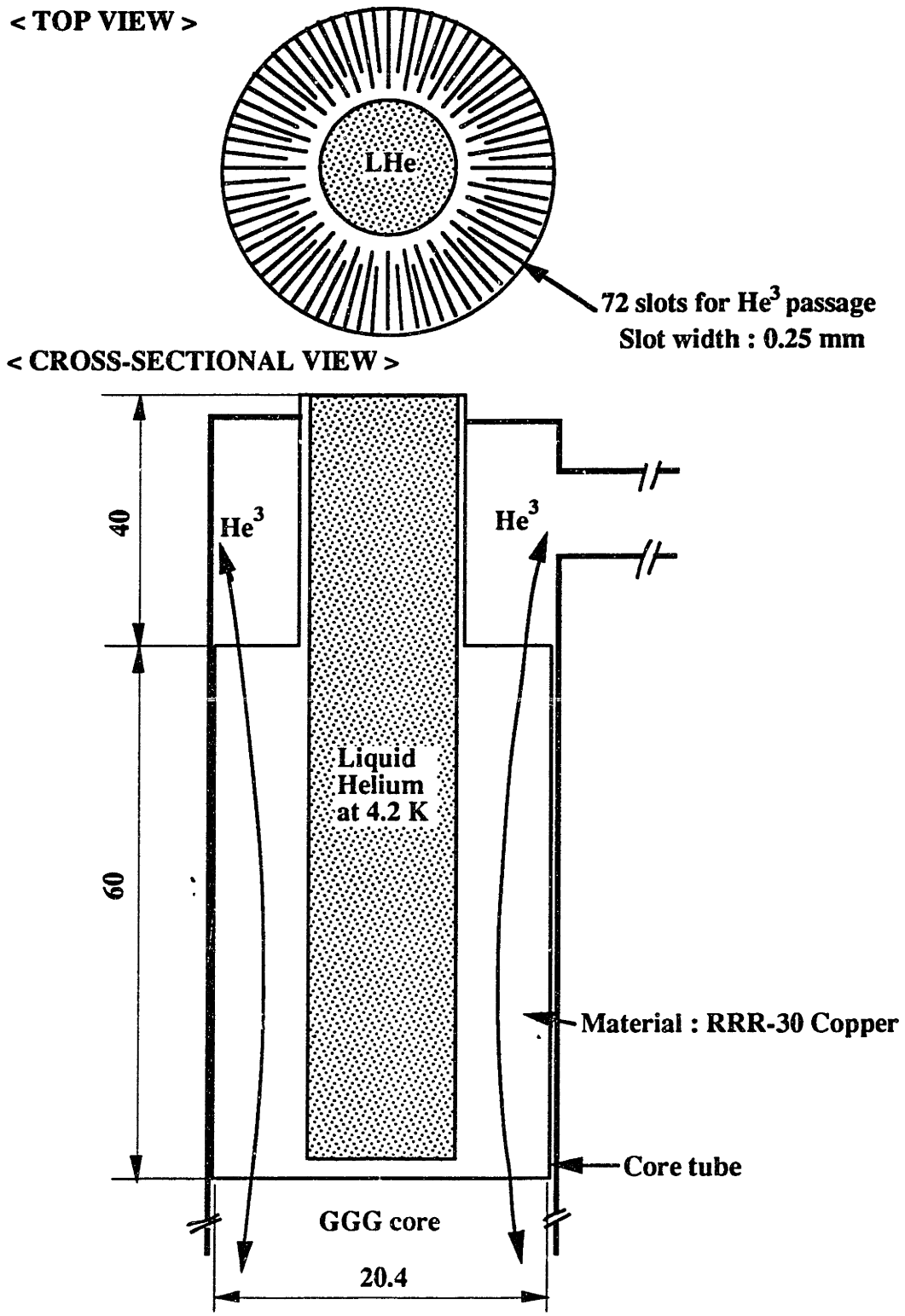

Fig.2-11 Schematic diagram of the warm-end heat exchanger (dimensions in mm).

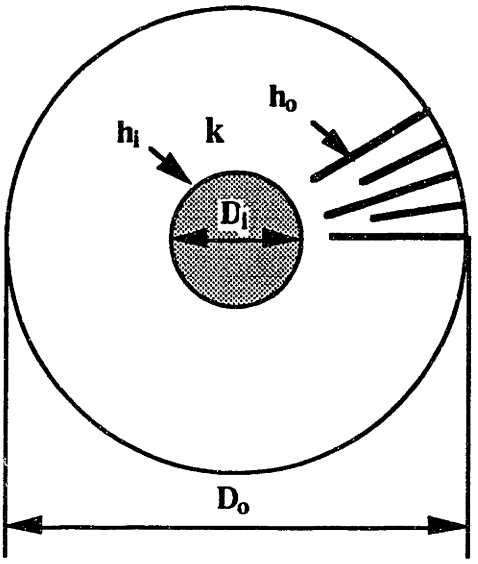

* Depth : L

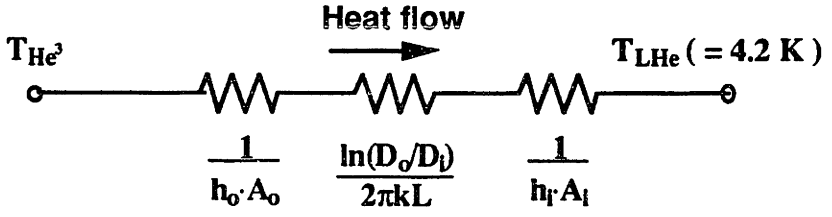

$$\therefore \quad U_o A_o = \left(\frac{1}{h_o A_o} + \frac{ln(D_o/D_i)}{2\pi kL} + \frac{1}{h_i A_i} \right)^{-1}$$

Fig.2-12 Thermal resistance circuit in the warm-end heat exchanger.

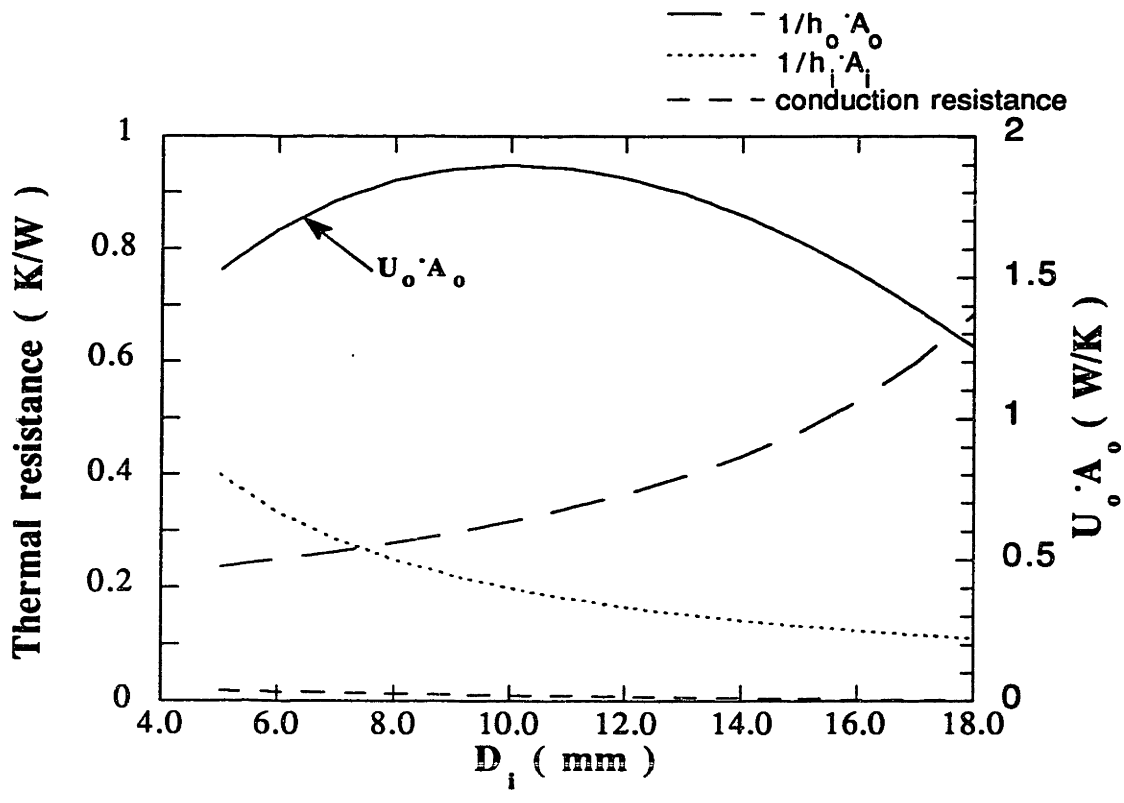

Fig.2-13 Overall heat transfer coefficient calculation of the warm-end heat exchanger.

The design parameters of the warm end heat exchanger are summarized in Table 2-6.

Table 2-6 Warm-end heat exchanger specifications.

---- Material : Electrolytic tough pitch copper (RRR-30) ---

No.	Parameter	Value	Description
1	D_{HXo}	20.4 mm	outer diameter of the heat exchanger
2	D_{HXi}	10 mm	optimum inner diameter of the heat exchanger
3	L_{WHX}	60 mm	height of the heat exchanger
4	L_{slot1}	4.5 mm	radial length of longer slot
5	$L_{slot\ 2}$	3.5 mm	radial length of shorter slot
6	t	0.25 mm	He^3 passage gap width
7	P_{Gap}	594 mm	total perimeter of He^3 passage gap
8	D_h	0.5 mm	hydraulic diameter

Table 2-6 Warm-end heat exchanger specifications (continued).

No.	Parameter	Value	Description
9	A_f	72 mm^2	flow area
10	ρ_{He}	0.395 kg/m^3	average He^3 density in the heat exchanger
11	$\overline{V}$	1.9 m/sec	average flow velocity in the heat exchanger
12	$\dot{m}$	0.054 g/sec	mass flow rate of He^3
13	Re	288	average Reynolds number in the heat exchanger
14	$\bar{f}$	0.08	friction factor at laminar region (= 23/Re)
15	ΔP	28 Pa	pressure drop in the heat exchanger
16	x_{entry}	7.2 mm	entry length ($\frac{x/D_h}{Re} = 0.05$)
17	Nu	6.7	average Nusselt number in the heat exchanger
18	k_{He}	0.01 W/m·K	thermal conductivity of He^3
19	h_o	173 W/m^2·K	heat transfer coefficient for He^3 side
20	A_i	1571 mm^2	heat transfer area for He^4 side
21	A_0	29700 mm^2	heat transfer area for He^3 side
22	k_{HX}	200 W/m·K	thermal conductivity of copper (RRR-30) at 4.2 K
23	ρ_{Cu}	5x10^{-10} Ω·m	electrical resistivity of copper (RRR-30) at 4.2 K
24	$(UA)_o$	1.74 W/K	overall heat transfer coefficient
25	Q_h	546 mW	heat transfer rate of the heat exchanger
26	$Q_{A.C.}$	2.1 mW	A.C. losses of the heat exchanger
27	$\Delta L/L$	0.33	thermal expansion coefficient of copper at 4.2 K
28	NTU	3.8	$\frac{U_o A_o}{\dot{m} Cp}$
29	ε	0.98	heat exchanger efficiency (= 1 - e^{-NTU})

2.4 Cold-end heat exchanger

The cold-end heat exchanger is principally designed to measure the refrigeration capacity at 1.8 K in this study. Figure 2-14 is a schematic diagram of the cold-end heat exchanger.

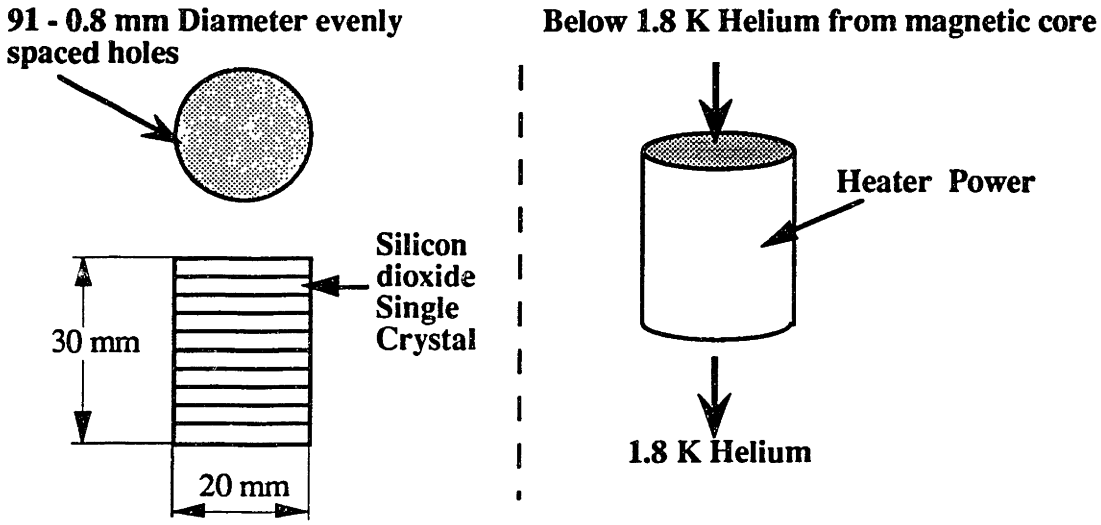

Fig.2-14 Schematic diagram of the cold-end heat exchanger.

As discussed in the warm-end heat exchanger design, A.C. loss is a major concern of the cold-end heat exchanger design. In order to minimize this eddy-current heat generation, a single crystal (SiO_2 ; Quartz) is used as the heat exchanger material. Single crystal SiO_2 has a high thermal conductivity at low temperatures (20 W/m·K at 1.8 K), even though it is a well-known dielectric material. The heat exchanger is composed of 10 disks, each 3 mm thick and with 91 0.8-mm diameter holes in it. The evenly spaced holes are aligned disk to disk. During the flow-demagnetization process, the cold helium coming out of the magnetic core bottom is warmed to 1.8 K in the heat exchanger by the temperature controlled heater attached to the heat exchanger. This kapton heater is bonded to the outside diameter of the silicon dioxide disks to make good thermal contact. The heater input power simulates thermal load and is equivalent to the refrigeration capacity at 1.8 K. Appendix C describes in detail the temperature controller for the cold-end heat exchanger. Table 2-7 summarizes the design parameters of the cold-end heat exchanger.

Table 2-7 Cold-end heat exchanger specifications.

---- Material : Quartz (SiO_2 single crystal) ---

No.	Parameter	Value	Description
1	D_{HXo}	18.6 mm	outer diameter of the heat exchanger
2	L_{HX}	30 mm	total height of the heat exchanger (Each disk height is 3 mm.)
3	d_{hole}	0.8 mm	diameter of 91 holes for He^3 passage
4	A_f	45.7 mm^2	total flow area
5	ρ_{He}	1.25 kg/m^3	average He^3 density in the heat exchanger
6	$\overline{V}$	0.94 m/sec	average flow velocity in the heat exchanger
7	$\dot{m}$	0.054 g/sec	mass flow rate of He^3
8	Re	855	average Reynolds number in the heat exchanger
9	$\bar{f}$	0.019	friction factor at laminar region (=16/Re)
10	ΔP	< 1 Pa	pressure drop in the heat exchanger
11	x_{entry}	34 mm	entry length ($\frac{x/D_h}{Re} = 0.05$)
12	Nu	3.66	average Nusselt number in the heat exchanger
13	k_{He}	0.01 W/m·K	thermal conductivity of He^3
14	h_i	46 $W/m^2 \cdot K$	heat transfer coefficient
15	A_o	6861 mm^2	heat transfer area for He^3 side
16	ΔT_{max}	0.03 K	radial temperature difference across the heat exchanger
17	k_{HX}	20 W/m·K	thermal conductivity of SiO_2 at 1.8 K
18	$(UA)_o$	0.28 W/K	overall heat transfer coefficient
19	Q_h	50 mW	heat transfer rate of the heat exchanger
20	$Q_{A.C.}$	negligible	almost electric non-conductor
21	$\Delta L/L$	0.25	thermal expansion coefficient of SiO_2 at 1.8 K
22	ε	0.54	heat exchanger efficiency

2.5 Displacer

The heat transport medium, He^3 gas, at 40 torr, is to be displaced through the magnetic cores by a piston-type displacer shown in Figure 2-15.

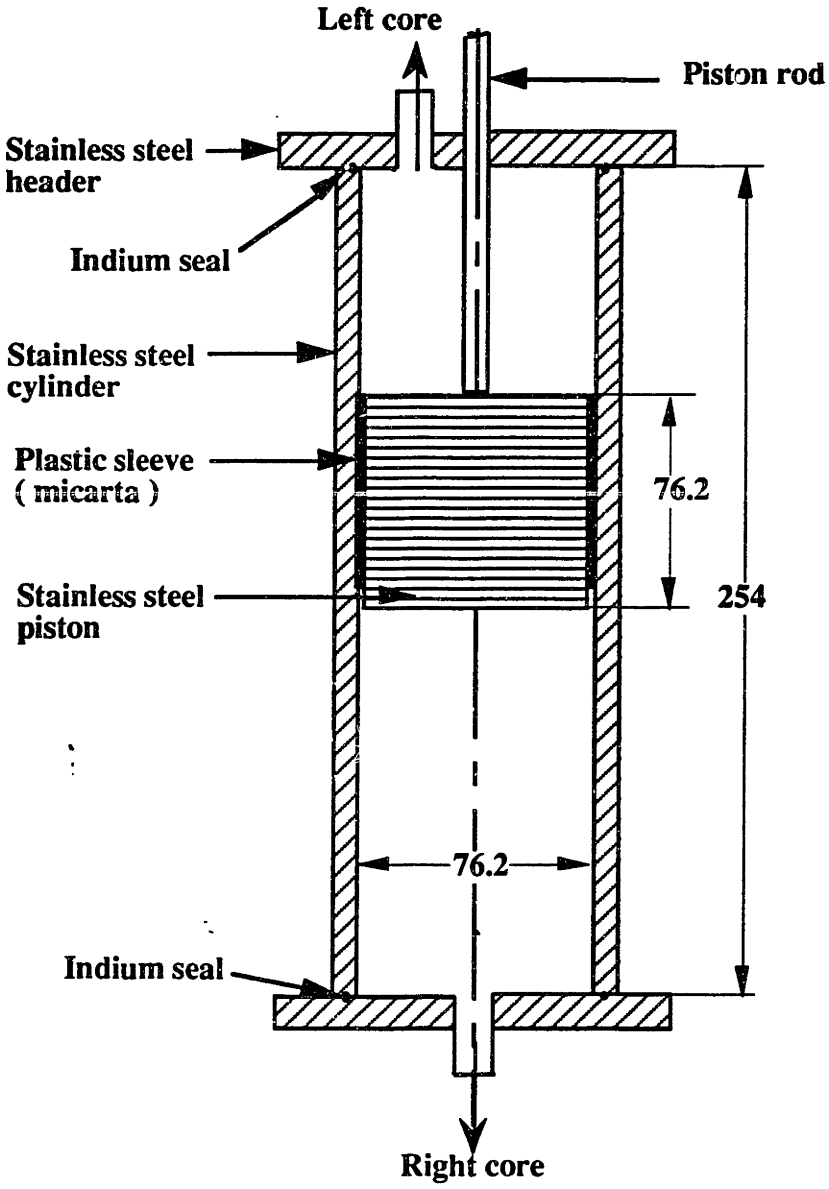

Fig.2-15 Schematic diagram of the displacer (dimensions in mm).

It is composed of a stainless steel piston covered by thin phenolic sleeve, which is accurately fitted to the stainless steel cylinder. The purpose of using phenolic as sleeve

material is to prevent galling between the piston and the cylinder. In addition, it has a thermal expansion coefficient similar to that of stainless steel. Clearance between piston and cylinder is maintained at about 0.025 ~ 0.05 mm (1 or 2 mils). The displacer is located between the two tandem magnetic cores and submerged in liquid helium.

An indium wire is used for the demountable seal in the displacer assembly at 4.2 K. The reasons for choosing indium as a cryogenic demountable sealing material for this application are (1) it has a low vapor pressure and (2) it is very malleable even at liquid helium temperature. The groove design of this plastic seal is different from that of ordinary elastic rubber O-rings. An indium wire should overfill the groove completely and produce a uniform hydrostatic pressure to give good sealing. Sixteen bolts around the seal generates a uniform pressing force on the indium wire in the displacer end cap header seal assembly. Figure 2-16 shows the shapes of indium wire before and after deformation.

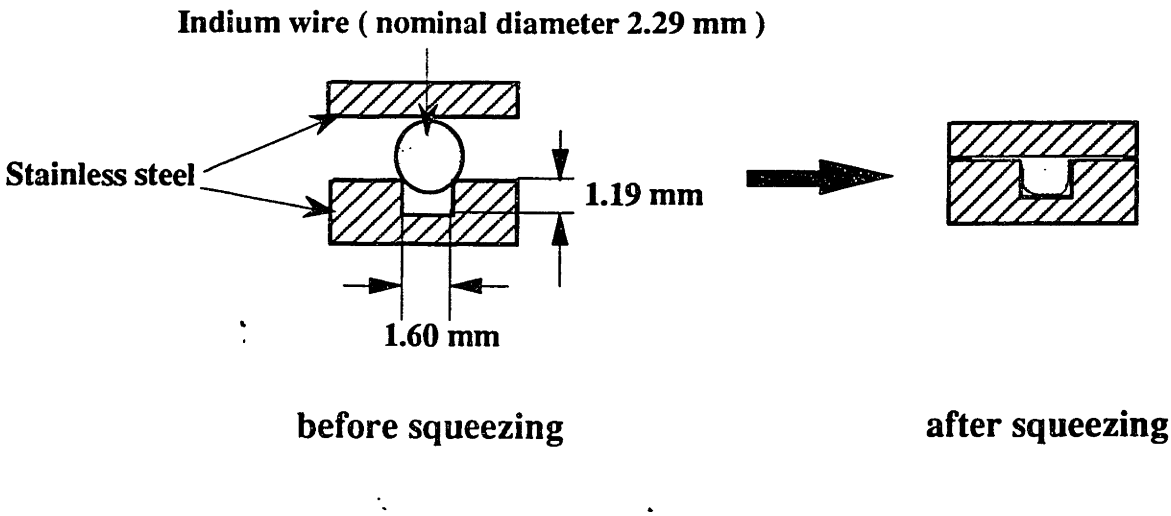

Fig.2-16 Cross-section of cryogenic indium sealing.

Since the indium wire is prepared by warm extrusion of an indium stock through the 1.5875-mm diameter hole, the wire diameter is bigger than the hole diameter due to swelling. The wire is laid out in a circle the diameter of the groove and the two free ends which are cut off at a 10^{o} angle are placed together closely in order to eliminate a leakage through that gap.

Table 2-8 summarizes the design parameters of the displacer.

Table 2-8 He^3 displacer specifications.

---- Material : Stainless steel 304 ---

No.	Parameter	Value	Description
1	V_D	585 cm^3	displaced volume for helium transfer
2	D_P	76.15 mm	diameter of the piston
3	L_P	63.5 mm	length of the piston
4	D_{Ci}	76.2 mm	inner diameter of the cylinder
5	D_{Co}	95.25 mm	outer diameter of the cylinder
6	S_P	128 mm	stroke of the piston
7	L_C	254 mm	length of the cylinder
8	P	0.053 atm.	operating pressure (~40 torr)
9	ΔP	420 Pa	estimated pressure difference between top and bottom of piston during flow process

2.6 Summary

This chapter discussed the designs of the major cryogenic components for the tandem regenerative magnetic refrigerator. Each component is designed to fulfill its maximum capability within the given design constraints. In summary, the following are the key design concepts.

(1) Overall system characteristics --> **tandem** regenerative magnetic refrigerator with **minimal dead volume**

(2) Magnetic core ----------> randomly **packed GGG spheres** for **small axial conduction loss**

(3) Heat transport medium ----------> sub-atmospheric **He^3** (40 torr) for **no phase transition** in core and minimal helium entrainment

(4) Superconducting magnet -------> **persistent-current** mode and **variational-current** mode coils to minimize power dissipation and reactive power flow

(5) Warm-end heat exchanger ------> **axial plate fin** type copper heat exchanger to reduce A.C. losses

(6) Cold-end heat exchanger --------> **SiO_2 single crystal** heat exchanger without A.C. losses

(7) Displacer ----------> **piston-cylinder** type cryogenic leak-tight displacer

The next chapter describes the numerical simulation work for predicting the performance of the magnetic refrigerator designed in this chapter.

III. SIMULATION

This chapter discusses the magnetic refrigerator model that predicts the overall system performance.

The computer program simulates the behavior of tandem magnetic cores during four cycle processes: adiabatic magnetization; flow magnetization; adiabatic demagnetization; and flow demagnetization. By assuming the initial temperature of the entire core to be 4.2 K, the transient as well as the cyclic steady state temperature profiles of the core can be obtained The computer program is listed in Appendix G.2.

3.1 Assumptions

(1) The warm-end heat sink temperature is constant at 4.2 K. This means that the warm-end heat exchanger has a sufficiently large capability to keep the helium flow temperature at 4.2 K. The cold end does not have such a restriction. Because the real experimental system utilizes a temperature controlled heater to keep the helium flow temperature at 1.8 K in the cold end heat exchanger, the helium temperature flowing from the cold end reservoir can be greater than or equal to 1.8 K, but not lower than 1.8 K.

(2) The axial conduction loss in the magnetic core is zero. The thermal contact resistance of packed bed core is very high at low pressure and low temperature, such that conduction losses are small in comparison with the refrigeration power. For example, in Table 2-4, the actual axial heat conduction in one core is 2 mW, while the designed refrigeration capacity is 50 mW.

(3) Heat transfer between the magnetic core and its surroundings is zero. This condition is approximated with a vacuum insulation between the core and the liquid helium that surrounds it. Heat transfer occurs only between GGG and He^3 transport gas.

(4) Dead volume between the magnetic core's warm-end and the displacer is zero. Consequentially, the induced inhalation or exhalation of entrained helium, due to density change in the core during the adiabatic processes, is only allowed through the cold-end boundary.

(5) The operating pressure is constant. The pressure drop in the system during the flow processes is assumed zero. This assumption is justified because the pressure drop across both magnetic cores is less than 10% of operating pressure as shown in Table 2-4.

(6) Both magnetic cores are composed of 0.8 mm diameter GGG spheres. In the actual system, one of the cores is filled with crushed irregularly shaped bits of GGG.

(7) The heat transfer coefficient correlation for packed bed cores is valid for the entire range of Reynolds numbers. The flow process correlation is used for adiabatic processes, because density induced flow may occur. The adiabatic process heat transfer coefficient is much smaller than that of flow process. Typically the following calculated heat transfer coefficients are used.

$$h_{adiabatic\ process} \sim 1\ W/m^2 \cdot K$$
$$h_{flow\ process} \sim 200\ W/m^2 \cdot K$$

3.2 Modeling

This section describes how the discretization energy equations are developed for GGG and helium. The two state variables to be solved for are the GGG and helium temperatures. The input parameters of the simulation program are also specified.

3.2.1 Energy equations

The temperature of GGG and the temperature of helium in each differential section of core are solved for at each time step. From the energy diagram, Figure 3-1, during the incremental time step, the following two energy equations can be obtained.

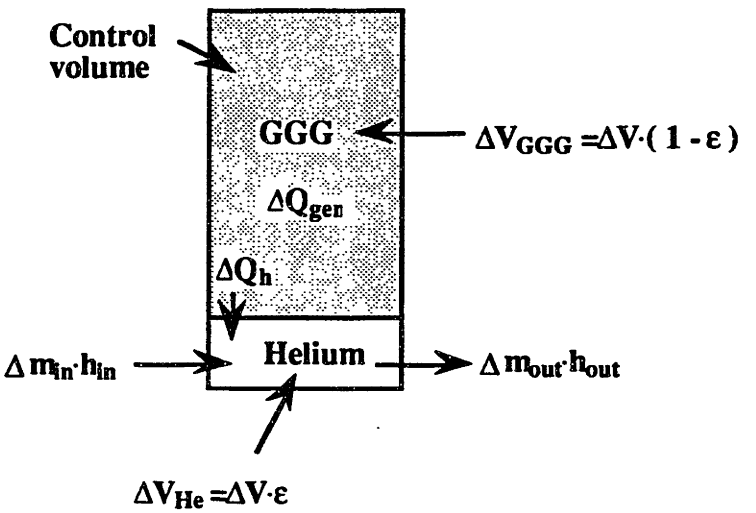

Fig.3-1 Control volume for differential section of core.

For helium

$$\Delta U_{He} = \Delta Q_h + \Delta m_{in} H_{in} - \Delta m_{out} H_{out} \tag{3.1}$$

For GGG

$$\Delta U_{GGG} = \Delta Q_{gen} - \Delta Q_h \tag{3.2}$$

Each term in Eq.3.1 and Eq.3.2 can be described as follows. In this formulation, T is the temperature of helium, T_g is the temperature of GGG, the subscript 1 refers to the former time step which is known, and the subscript 2 refers to the present time step which is unknown. The flow temperatures in the control surface are evaluated at the present time step's temperature.

The internal energy change of the entrained helium is calculated as the following.

$$\begin{aligned}\Delta U_{He} &= \varepsilon\Delta V(\rho_2 u_2 - \rho_1 u_1) \\ &= \varepsilon\Delta V[\rho_2(h_2 - \frac{P}{\rho_2}) - \rho_1(h_1 - \frac{P}{\rho_1})] \\ &= \varepsilon\Delta V(\rho_2 h_2 - \rho_1 h_1)\end{aligned} \tag{3.3}$$

where ε is the porosity of core and ΔV is the volume of the differential segment.

The heat transfer between GGG and helium is,

$$\Delta Q_h = h\Delta A_h \Delta t(T_g - T) \tag{3.4}$$

where h is the heat transfer coefficient determined by flow parameters, ΔA_h is the heat transfer area of GGG.

Consideration of the effect of density change on entrained helium gives the following enthalpy flux change.

$$\Delta m_{out}h_{out} - \Delta m_{in}h_{in} = [\Delta m_{in} + \varepsilon\Delta V(\rho_1 - \rho_2)]h_{out} - \Delta m_{in}h_{in} \tag{3.5}$$

Now, the internal energy change of GGG can be calculated in terms of constant magnetic field specific heat, C_H and its temperature difference.

$$\Delta U_{GGG} = T\Delta S + \mu_o VH\Delta M$$

$$= T\left[\left(\frac{\partial S}{\partial T}\right)_H \Delta T + \left(\frac{\partial S}{\partial H}\right)_T \Delta H\right] + \mu_o VH\Delta M$$

$$= (1 - \varepsilon)\Delta V \rho_{GGG}\overline{T_g}\left[\left(\frac{\partial S}{\partial T_g}\right)_{H=\overline{H}} (T_{g2} - T_{g1}) + \left(\frac{\partial S}{\partial H}\right)_{T=\overline{T_g}} \Delta H\right] + \mu_o VH\Delta M \tag{3.6}$$

where $\overline{T_g} = (T_{g2} + T_{g1})/2$ and $\overline{H} = (H_1 + H_2)/2$.

The heat generation of differential segment comes from magneto-caloric effect of GGG.

$$\Delta Q_{gen} = \mu_o V H \Delta M \tag{3.7}$$

where ΔH is the incremental magnetic field change.

If Eqs. (3.3) ~ (3.7) are substituted for Eqs.(3.1) and (3.2), since the temperatures of former time step and upstream are known, there are only two unknown variables : T_2 and T_{g2} in Eqs. (3.1) and (3.2).

3.2.2 Programming

The simulation program solves the discretization energy equations with the thermodynamic properties of GGG and He^3. The program is divided into four principal processes during one cycle. During each process, the system energy equations are solved for in a finite-difference, time-stepping method. Figure 3-2 is helpful to understand how the simulation program runs. When the energy balance equation is solved, the density-driven helium displacement during adiabatic process is also checked. Since the displacer is connected to the warm end of core, the net helium displacement should occur only through the cold-end boundary. If the net flow constraint is not satisfied, the energy equation is solved again with a new helium shuttle mass input at the cold-end.

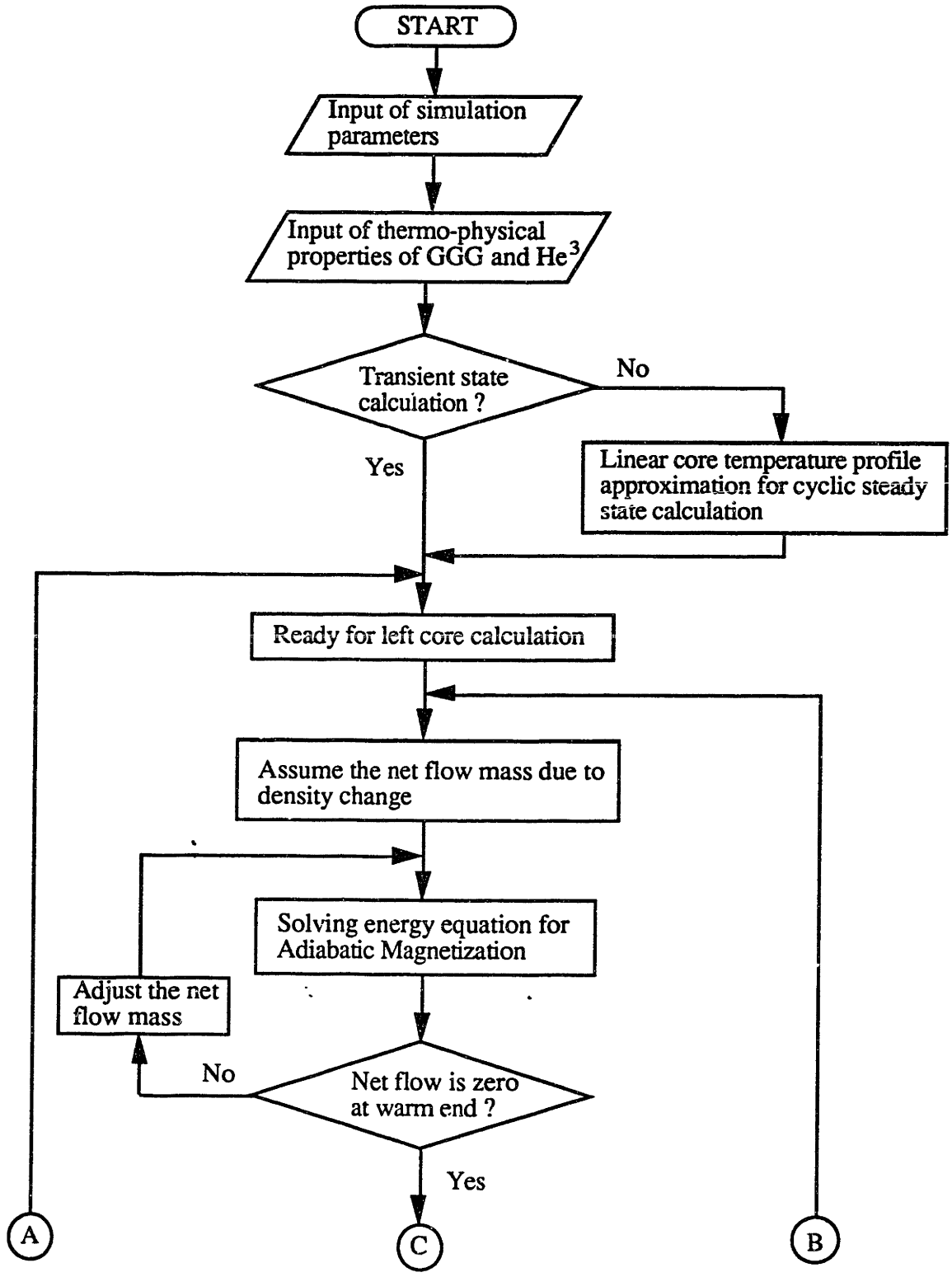

Ⓐ,Ⓑ,Ⓒ continue to next page.

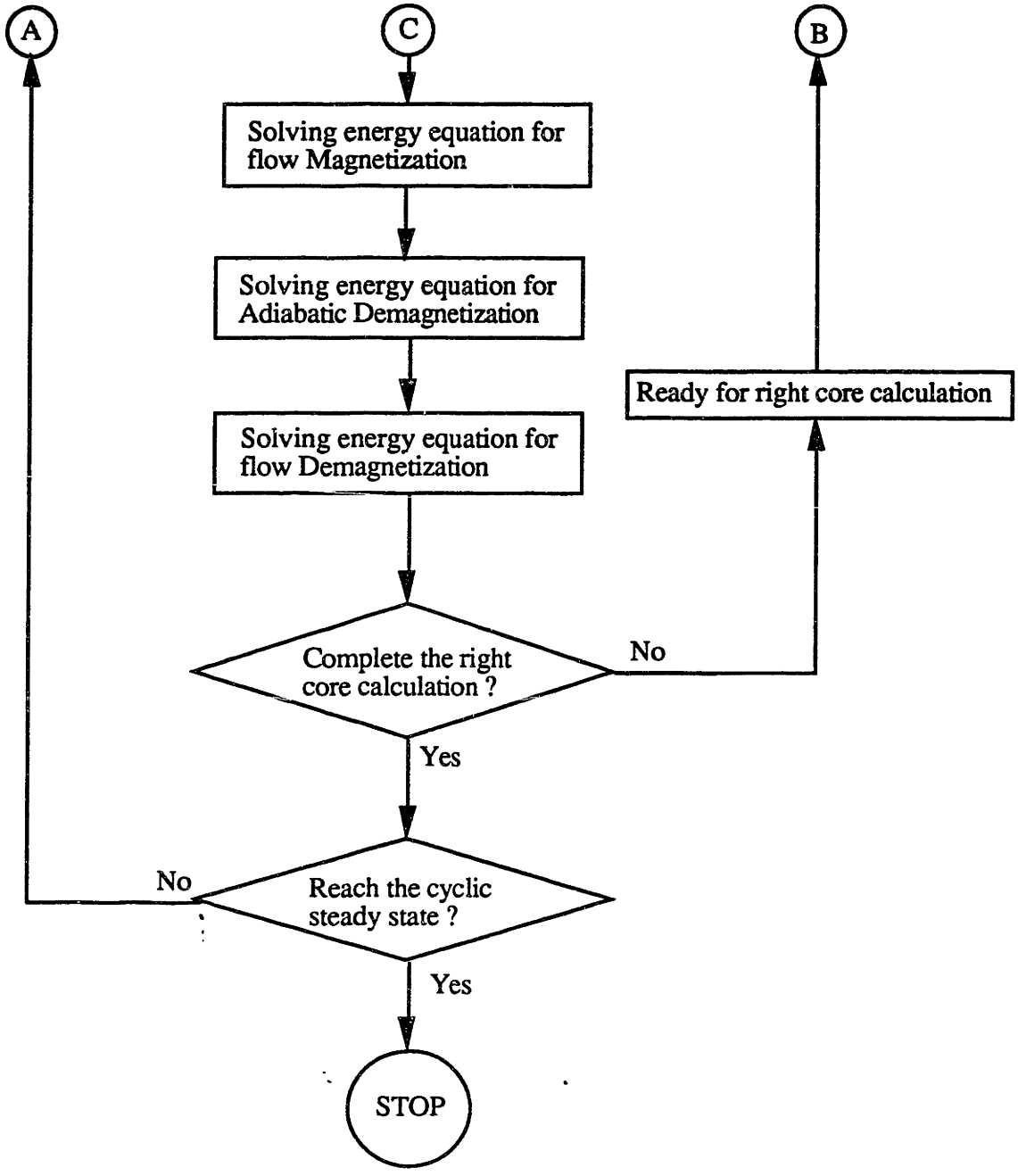

Fig.3-2 Flow chart of the computer simulation program.

3.2.3 Input parameters

Since the magnetic refrigerant and heat transport medium are predetermined, the most important input parameters are the temperature and magnetic field swing range. Other input parameters are the magnetic core's physical dimensions and porosity. The following text is the typical input file contents of the simulation program.

'Enter number of complete cycles desired'	5
'Number for temperature input file or 0 '	0
'Initial temp. of linear Tcold_end & Twarm_end'	1.8 4.2
'Number of segments '	20
'Enter 1 for starting from 4.2 K everywhere'	0
'Enter the operating pressure (atm.) bet. 0.02 and 0.06'	0.053
'Enter the temperature of the warm reservoir'	4.2
'Enter the temperature of the cold reservoir'	1.8
'Initial field for the cold and warm ends in adia. mag.'	0.0 0.0
'Final field for the cold and warm ends in adia. mag.'	0.5 0.5
'Period during adia. mag. (sec)'	1.0
'Number of field steps in adia. mag.'	4
'Total forced helium flow during adia. mag.'	0.00
'Final field for the cold and warm ends in flow mag.'	3.0 3.0
'Period during flow mag.'	5.0
'Number of field steps in flow ma.'	8
'Total forced helium flow during flow mag.'	0.27
'Final field for the cold and warm ends in adia. demag.'	2.5 2.5
'Period during adia. demag.'	1.0
'Number of field steps in adia. demag.'	4
'Total forced helium flow during adia. demag.'	0.00
'Final field for the cold and warm ends in flow demag.'	0.0 0.0
'Period during flow demag.'	5.0
'Number of field steps in flow demag.'	8
'Total forced helium flow during flow demag.'	0.27
'Enter 1 for plotting or 0 for non-plotting '	0

3.3 Thermodynamic properties of GGG and He^3

In order to analyze the thermodynamic cycles of GGG in the core and also calculate temperature profiles of both GGG and He^3, their thermodynamic properties must be known. For GGG, Gallagher (1986) developed an empirical magnetization function. With this magnetization function and the zero specific heat relation, the entropy function of GGG can be obtained with two independent variables : T (temperature) and H (magnetic field).

$$S(T,H) = S_o + \int_{T_o}^{T} \left(\frac{\partial S}{\partial T}\right)_H dT + \int_0^H \left(\frac{\partial S}{\partial H}\right)_T d(H)$$

$$= S_o + \int_{T_o}^{T} \frac{C_{H=0}(T)}{T} dT + \int_0^{\mu_o H} v\left[\left(\frac{\partial M}{\partial T}\right)_H\right]_T d(\mu_o H) \qquad (3.8)$$

Figure 2-1 is the graphical representation of Eq.3.8 with the reference entropy set to 0 at 0 tesla and 1 K. As shown in Figure 2-1, temperature-entropy diagram of GGG, the magneto-caloric effect is not significant from 0 to 0.5 tesla. Therefore, the magnet does not have to be fully discharged in the magnetic cycle. Stopping at 0.5 tesla rather than discharging to 0 tesla does not make a significant difference in terms of magneto-caloric effect. When the magnetic refrigerator operates as a tandem system with persistent- and variational-current coils, the maximum value of variational-current can be reduced by increasing the value of persistent-current without changing the maximum total field.

The thermophysical properties of He^3 are not as well known as those of He^4. However, since the operating pressure is 40 torr and the temperature range is about 1.8 K to 4.2 K, He^3 exists only as superheated vapor state. As described in section 2.1, the P-v-T equation and the zero specific heat relation are used to calculate enthalpy and entropy of He^3. The other transport properties of He^3 such as thermal conductivity and viscosity are obtained from Gibbons (1967).

In the magnetic core of the tandem magnetic refrigerator, GGG is the magnetic refrigerant and He^3 is a *moving regenerative material.* This fact can be also verified by comparing the heat capacity of two materials. Debye's T^3 law states that the specific heat of a solid is proportional to the third power of temperature. The specific heat of GGG decreases with temperature except around the phase transition temperature (~ 0.85 K). On the other hand, helium gas (either He^4 or He^3) has high specific heat at cryogenic temperature. In the temperature range of 4.2 K and 1.8 K, the specific heat of GGG is on the order of 10 J/kg·K, and He^3 is 7000 J/kg·K. Since the mass of refrigerant (GGG) is 135 g and the shuttle mass of regenerator (He^3) is 0.27 g, the total heat capacity of He^3 (= 1.9 J/K) is greater than that of GGG (= 1.35 J/K), which again confirms the right choice of relative mass of two materials.

The computer program list in Appendix G.2 is used for generating thermodynamic properties of GGG and He^3. The output of He^3 program is an input data file of the main simulation program.

3.4 Results and discussion

This section presents the results of the tandem magnetic refrigerator simulation for various input parameters.

First, Figures 3-3 ~ 3-6 show the evolution of the helium temperature profile as magnetic field is increased from zero to 3 T and back to zero. These cyclic steady-state temperature profiles are obtained after five cycle periods. The input file is given in section 3.2. GGG's temperature is also calculated. Its temperature profile history is almost the same as that of helium due to the large heat transfer area. '*Non-dimensional length*' in these figures denotes the normalized distance from the cold-end side in the magnetic core; *i.e.*, 0.0 is the cold-end at 1.8 K and 1.0 is the warm-end at 4.2 K. There are several curves according to the different magnetic field values. Note again that it is given in the unit of magnetic induction. For this simulation, the total cycle period is 12 seconds: 1 second for the adiabatic magnetization process; 5 seconds for the flow magnetization process; 1 second for adiabatic demagnetization process; and 5 seconds for flow demagnetization process. In this simulation, the temperature below 1.8 K at the cold-end during the flow demagnetization ensures the positive refrigeration power.

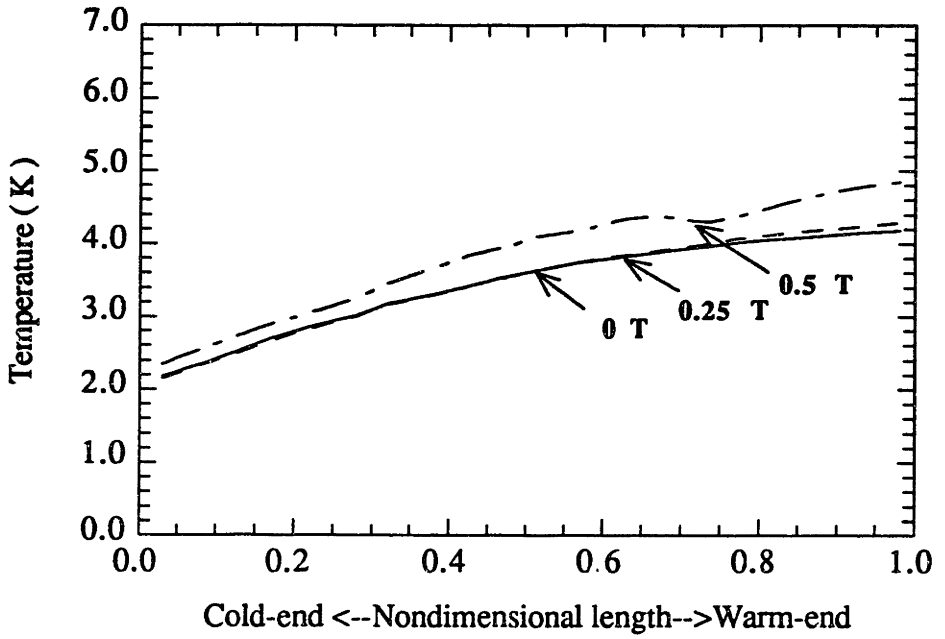

Fig.3-3 Helium temperature profile during adiabatic magnetization process.

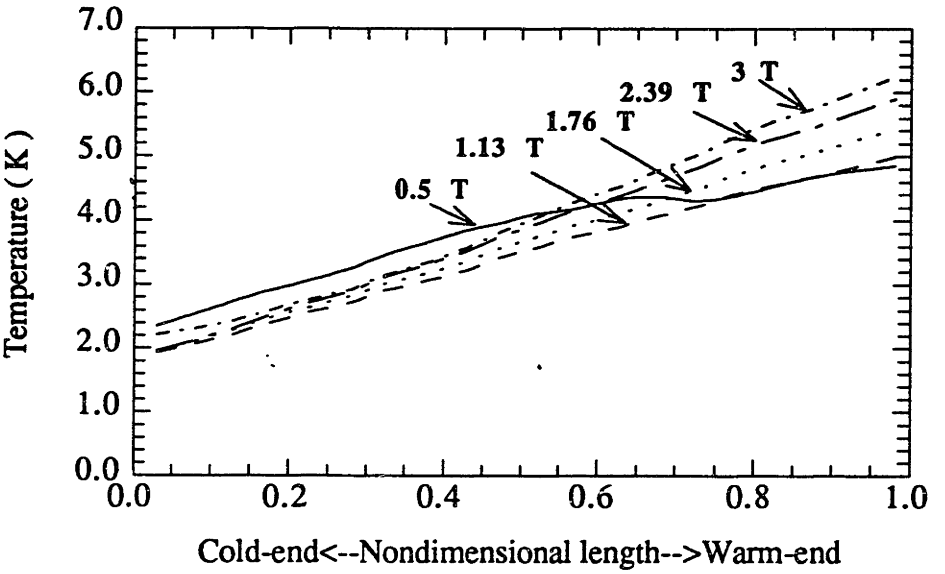

Fig.3-4 Helium temperature profile during flow magnetization process

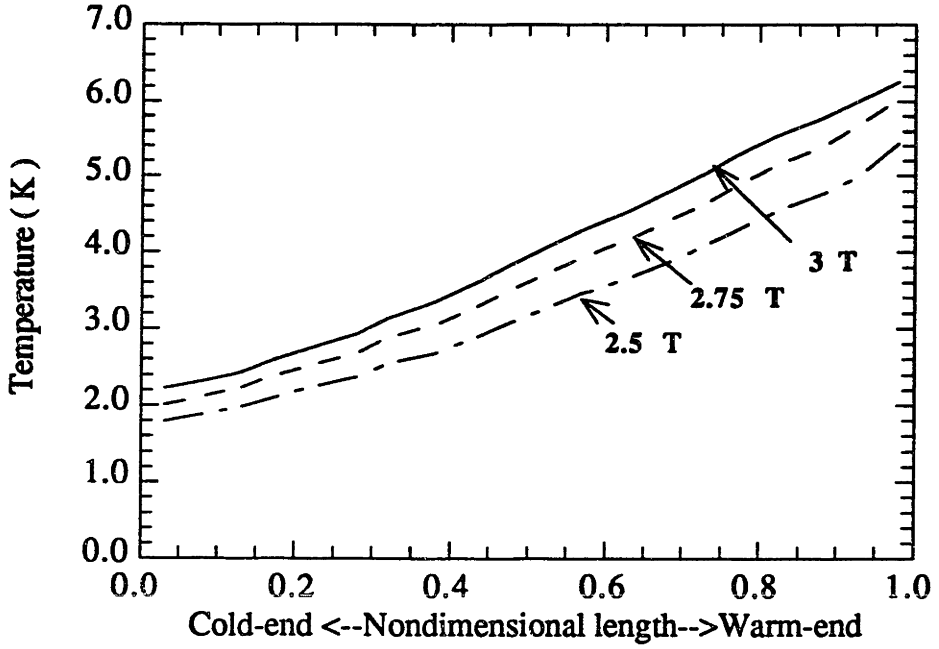

Fig.3-5 Helium temperature profile during adiabatic demagnetization process.

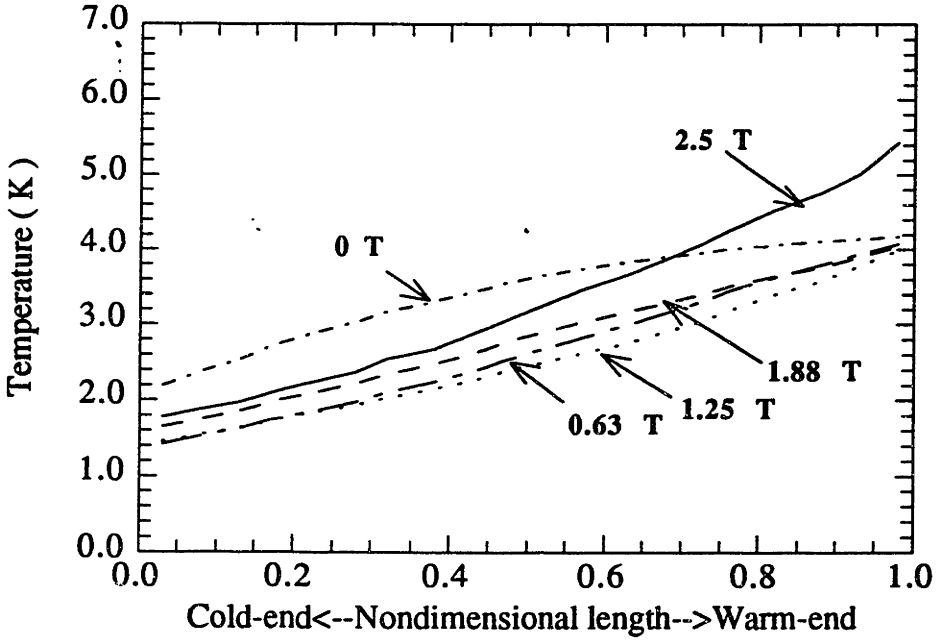

Fig.3-6 Helium temperature profile during flow demagnetization process.

From the analysis in this chapter, it is expected that the refrigeration capacity of the designed tandem magnetic refrigerator would be 70 mW or 70 % of the designed value. In this case, the Carnot efficiency of the tandem magnetic refrigerator, defined below, is calculated as 25 %.

$$\eta_{Carnot} = \frac{\left(\frac{Q_c}{W}\right)_{actual}}{\left(\frac{Q_c}{W}\right)_{Carnot}} = \frac{\frac{Q_c}{Q_h - Q_c}}{\frac{T_c}{T_h - T_c}}$$

There are several reasons why the actual magnetic cycle deviates from the ideal cycle. The first and the most important reason is the *heat capacity imbalance between GGG and the helium flow.* The *uniform* magnetic field energization and de-energization of a magnetic refrigerant at different temperature ranges inevitably generates an irreversible loss due to the heat capacity imbalance between the magnetic refrigerant and the heat transport medium.

The other source of inherent irreversible losses of the regenerative magnetic refrigerator is the *helium entrainment effect.* During the adiabatic process, the entrained helium is subject to temperature rise or fall by GGG, which results in helium exhalation or inhalation in the magnetic core. This breathing effect of the porous core is considered in the simulation of adiabatic processes. The breathing phenomenon of the core is also observed in the experiment.

The resultant temperature-entropy cycle diagram of the GGG in the core, shown in Figure 3-7, demonstrates the non-ideal characteristics of the regenerative magnetic refrigeration. The typical four magnetic cycles of GGG at different locations in the core are drawn by temperature calculation result.

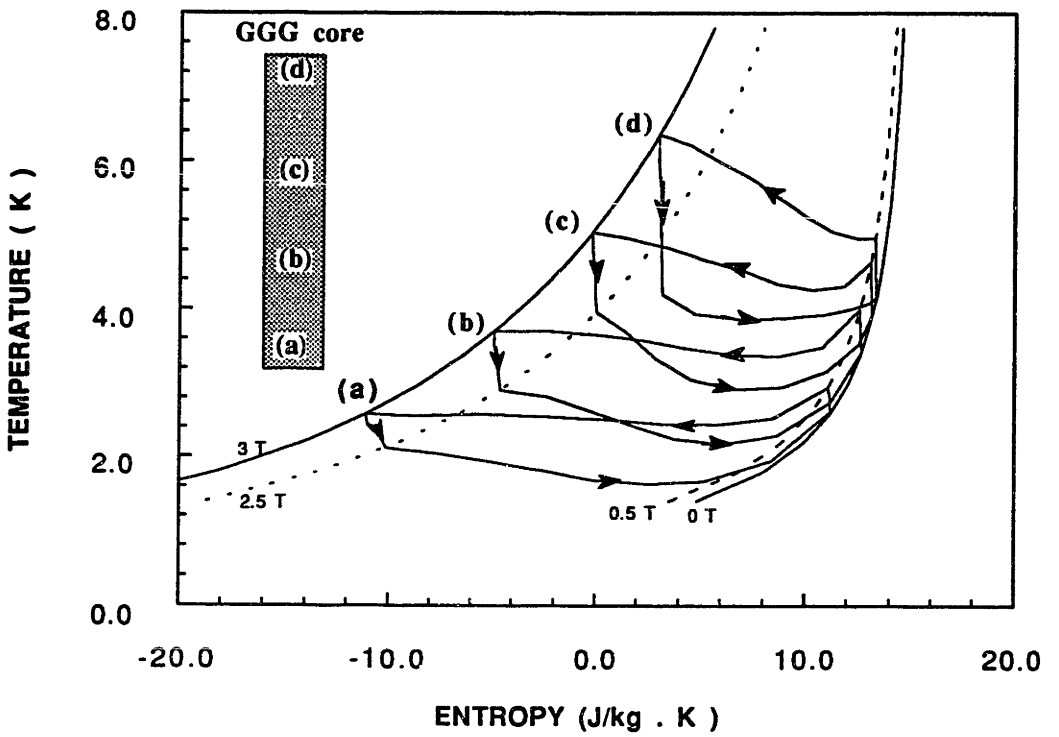

Fig.3-7 Simulated cycle diagrams at four different GGG segments.

In way to reduce the field-flow imbalance effect: there are at least three possible methodologies:

(1) Magnetic field modification along the core axis.
(2) Core diameter variation, keeping the field profile along the axis uniform.
(3) Magnetic refrigerant substitution along the core axis.

The first method is to construct the magnet so that the magnetic field swing can be adjusted along the core axial position. The applied magnetic field should be functions of space as well as of time to make the cycles in Figure 3-7 close to the ideal cascaded Carnot cycles. However, this method is very difficult in that the superconducting magnet construction and its operation is too complex.

The second method is to make the magnetic core diameter vary along the axis. It can be realized if the heat capacity of the heat transport medium is not changing rapidly with a

temperature. The large specific heat difference at different temperature levels may result in a significant core diameter variation, which can be impractical in the assembly of the magnetic core and superconducting magnet. The magnet still must provide a uniform field profile along the axis.

The third method is to vary the magnetic material composition along the axis to approach ideal cycle behavior. This method is more practical than the other two methods if such magnetic materials are available. One way of material variation is mixing two or more magnetic materials with a certain composition so that their magneto-caloric effects at different temperatures will complement each other. Here, the mixing of the magnetic materials must be mechanical not chemical. As described in Table 2-1, there are many candidates, each effective over a different temperature ranges. Hashimoto *et al.* (1987) have demonstrated that a complex ferromagnetic material, for instance, $(ErAl_2)_{0.312}(HoAl_2)_{0.198}(Ho_{0.5}Dy_{0.5}Al_2)_{0.490}$ has the most favorable characteristics for an ideal Ericsson cycle above 15 K. The packed bed configuration consisting of tiny spheres makes it easy to vary the magnetic refrigerant composition along the core axis. This idea is explained in more detail in the section 7.1.

(1) Porosity effect

The porosity effect on the regenerative packed bed core is strongly related to the entrained helium problem. The entrained helium with a large specific heat at low temperature is an irreversibility source during adiabatic magnetization and demagnetization processes. Figure 3-8 shows a plot of calculated refrigeration power vs. porosity. As porosity increases , system performance is degraded by increased helium entrainment effect. The porosity of the designed GGG core is 0.38.

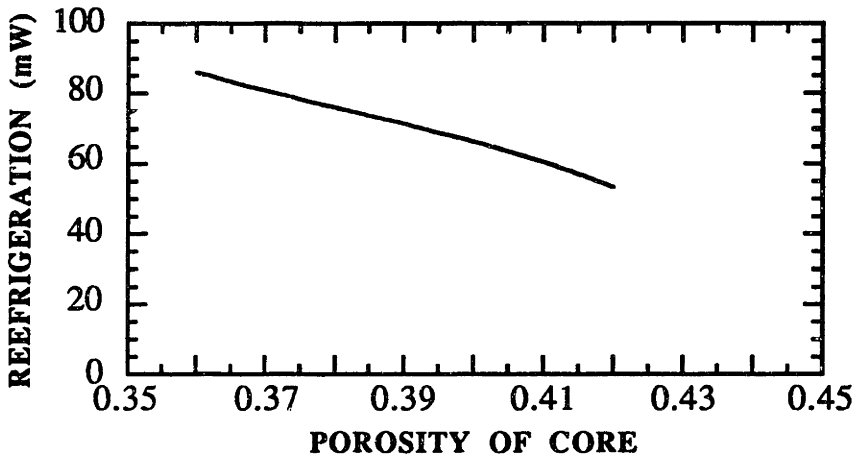

Fig.3-8 Porosity effect on refrigeration power.

(2) Cold-end temperature

The designed cold-end temperature is 1.8 K. Figure 3-9 is a plot of calculated refrigeration power vs. cold-end temperature for the same warm-end temperature of 4.2 K. This result agrees with an expected trend of refrigeration systems. The refrigeration power decreases as the load temperature is decreased.

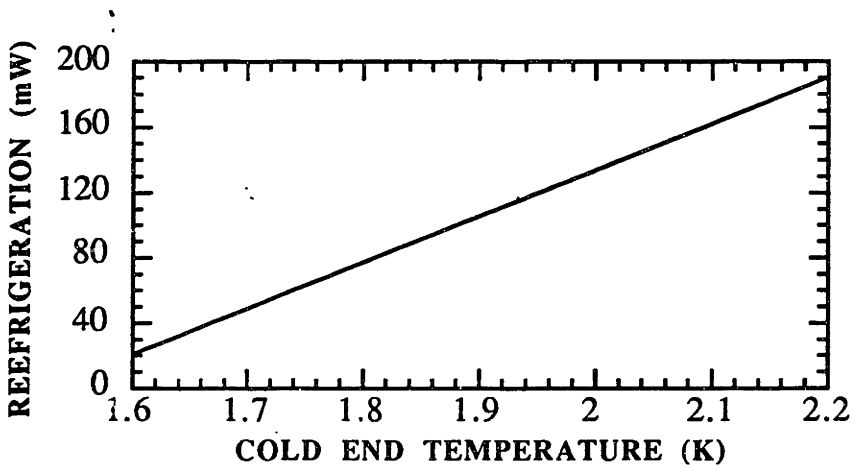

Fig.3-9 Cooling load temperature effect on refrigeration power.

(3) Operating pressure of heat transport medium

The operating pressure of the heat transport medium, He^3 is an input parameter. The system pressure is kept low to prevent any phase transition. This study considers pressure effect for operating pressures below 40 torr.

In the actual experiment, the displaced volume of heat transport medium is determined by the stroke and cross-sectional area of the displacer. For a given displacer volume, lowering the operating pressure lowers the amount of helium shuttle mass. The change of shuttle mass affects relative magnitudes between the overall magneto-caloric effect of the GGG core and the heat capacity of the shuttled helium.

Figure 3-10 is a simulation result of refrigeration vs. operating pressure. If the pressure is too low or the shuttle mass too small, the magnetic work term is larger than the helium convection term. The helium, cooled by the demagnetized GGG during the flow demagnetization process, cannot reach the cold-end efficiently, resulting in loss of refrigeration. On the other hand, if the pressure is too high or the shuttle mass too large, the convection of helium dominates the magneto-caloric effect of GGG. As a result, the down-flow helium cannot be completely cooled by GGG during the flow demagnetization process. The refrigeration capacity consequentially drops with operating pressure as shown in Figure 3-10.

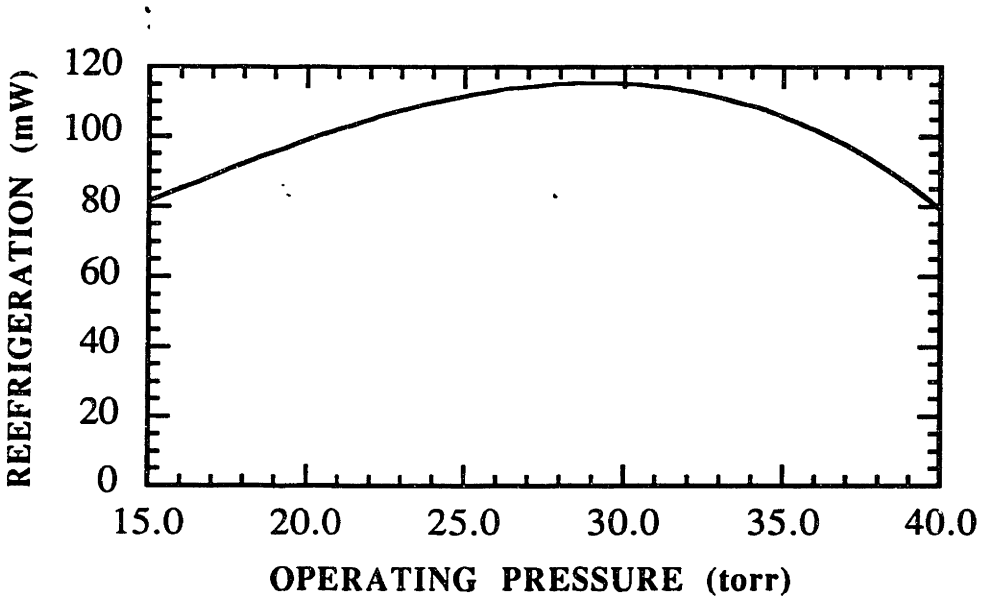

Fig.3-10 Operating pressure effect of He^3 on refrigeration power.

3.5 Summary

This chapter explained predictions by a computer simulation program of the overall system performance for the tandem magnetic refrigerator.

With some basic assumptions, the discretization energy equations for the differential control volume containing GGG and He^3 are solved. The successive iterations through the entire core volume at different time steps produce the cyclic steady-state temperature profiles of GGG and He^3. Even though the empirical heat transfer coefficient relation is used to calculate temperature difference between GGG and He^3, their temperature profiles are almost the same due to the large heat transfer area of the GGG core configuration. From the temperature calculations, the inherent irreversibility sources (the magnetic field-helium flow heat capacity imbalance and the helium entrainment effect) are discussed. The refrigeration capacity at the cooling load temperature can also be estimated by the enthalpy flux calculation. Changing the input parameters shows qualitatively correct simulation results, which validates the simulation program as a design tool.

The next chapter describes the construction of the experimental apparatus, experimental procedure, and test results.

ΕΞΠΕΡΙΜΕΝΤ

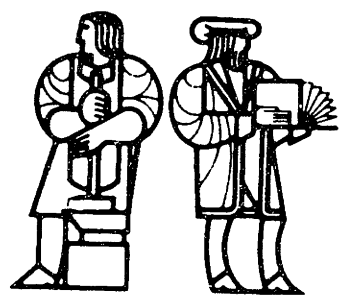

The ability to analyze a problem involves a combination of inherent insight and experience. The former, unfortunately, cannot be learned, but depends on the individual. However, the latter is of equal importance, and can be gained with patient study.

- from V.S. Arpaci's *Conduction heat transfer,* 1966

IV. EXPERIMENT

This chapter presents and discusses the experimental results of a prototype tandem magnetic refrigerator. Section 4.1 describes how the experimental apparatus was assembled for its successful operation. In section 4.2, three important preliminary tests are discussed: tandem superconducting magnet test, heat transport medium circulation test, and He^3-charcoal adsorption test. After performing these preliminary tests successfully, the main tandem magnetic refrigerator test was performed. Section 4.3 summarizes the experimental data and results.

4.1 Experimental apparatus

The tandem magnetic refrigerator can be divided into three subsystems: 4.2 K cryogenic assembly, step motor assembly at room temperature, and He^3 recycling system.

4.1.1 Cryogenic part

In the assembly of the cryogenic part, a main requirement is to minimize liquid helium consumption by effective thermal insulation, As shown in Figure 4-1, the main key components of the magnetic refrigerator are inserted into a double-vacuum jacket cryostat. All 4.2-K parts are compactly assembled and located at the bottom of the cryostat to minimize heat loss. The convection shields as well as radiation shields, shown in Figure 4-1, are also used to keep the boil-off rate small. It takes about 40 liters of liquid helium to prepare for an experimental session which usually lasts about 5 hours.

As stated in Chapter II, each cold-end heat exchanger consists of single crystal SiO_2 disks. The whole assembly is wrapped by a 0.25 mm thick Minco kapton thermo-foil heater. Figure 4-2 shows one of the two cold-end heat exchanger assemblies. To keep the GGG particles within each core volume and prevent them from falling down into the cold-end heat exchanger, a layer of 30 x 30 stainless steel mesh is placed between the core bottom and the cold-end heat exchanger top by welding the mesh to stainless steel core tube. The core space is then filled with GGG particles. A SYSTRON vibrator is used during filling to increase the packing density. Afterwards, the warm-end heat exchanger is placed snugly at the top to minimize dead volume.

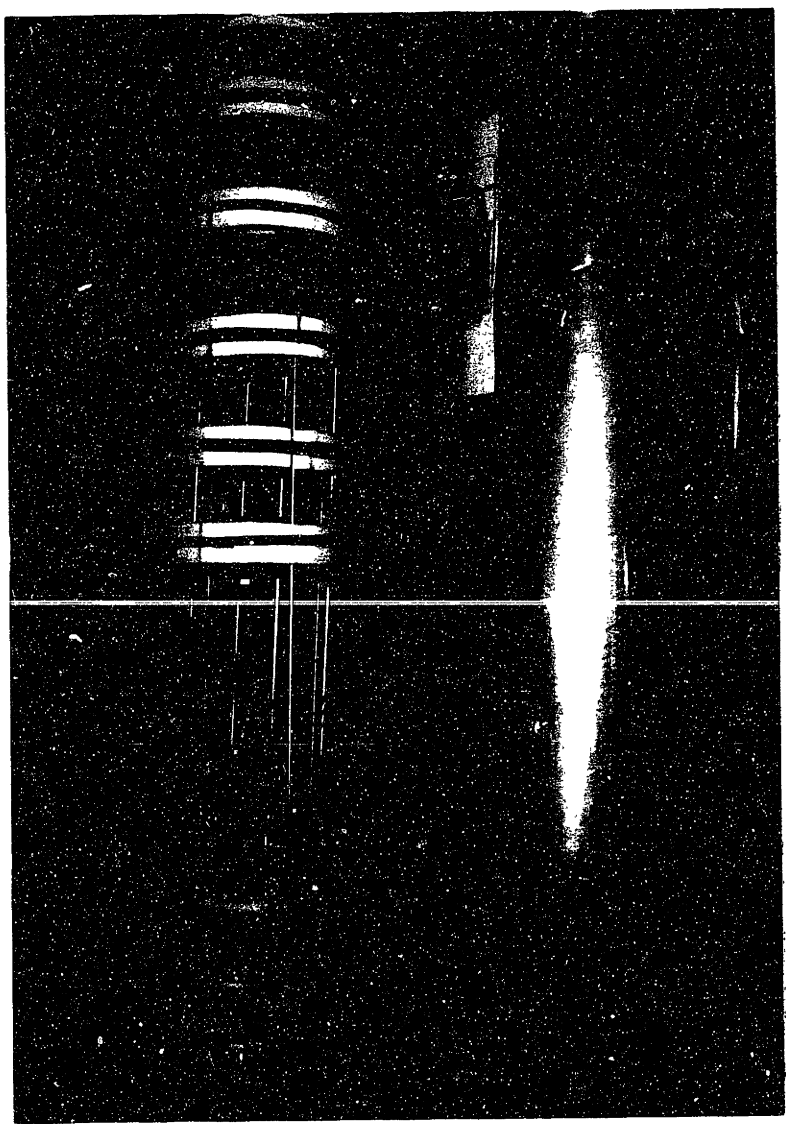

Fig. 4-1 4.2 K part assembly and its cryostat, which in the liquid helium section is 1.5 m long.

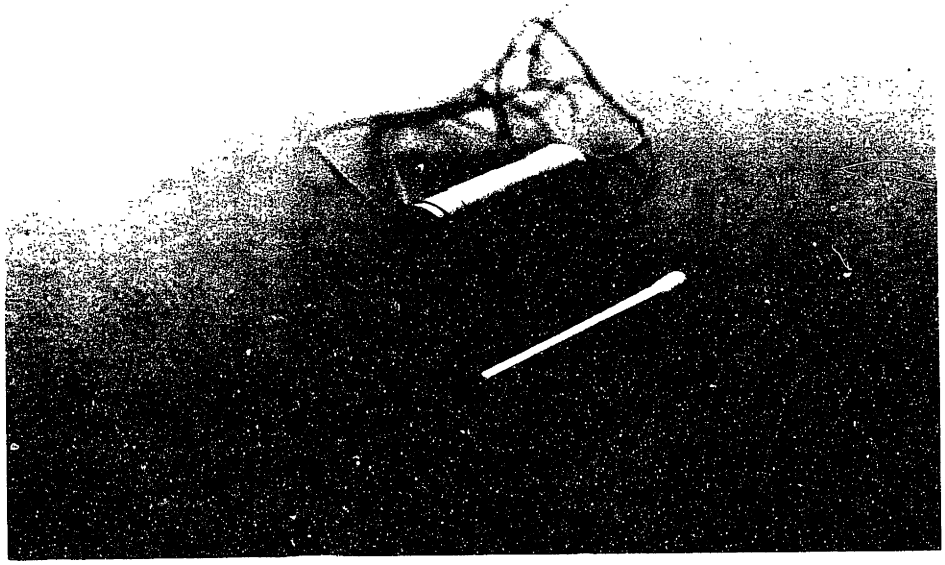

Fig. 4-2 One of the cold-end heat exchangers. The orange wires are for the heater foil wrapped around the heat exchanger.

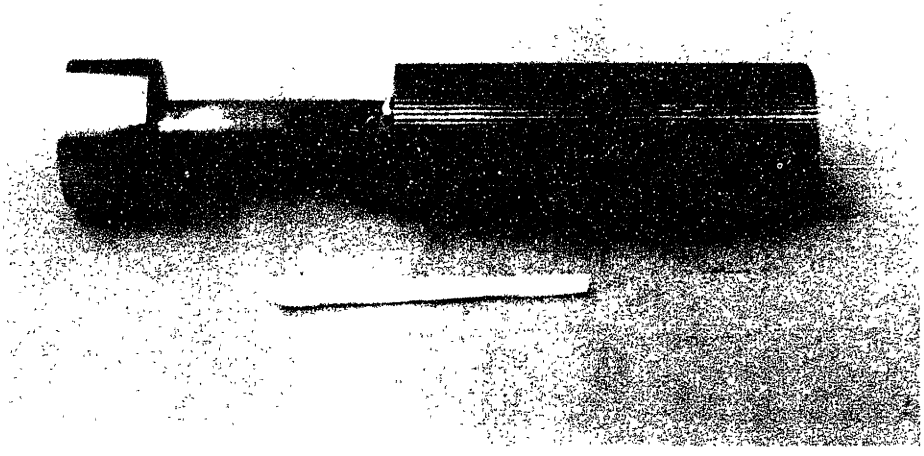

Fig. 4-3 Warm-end heat exchanger brazed to the stainless steel header.

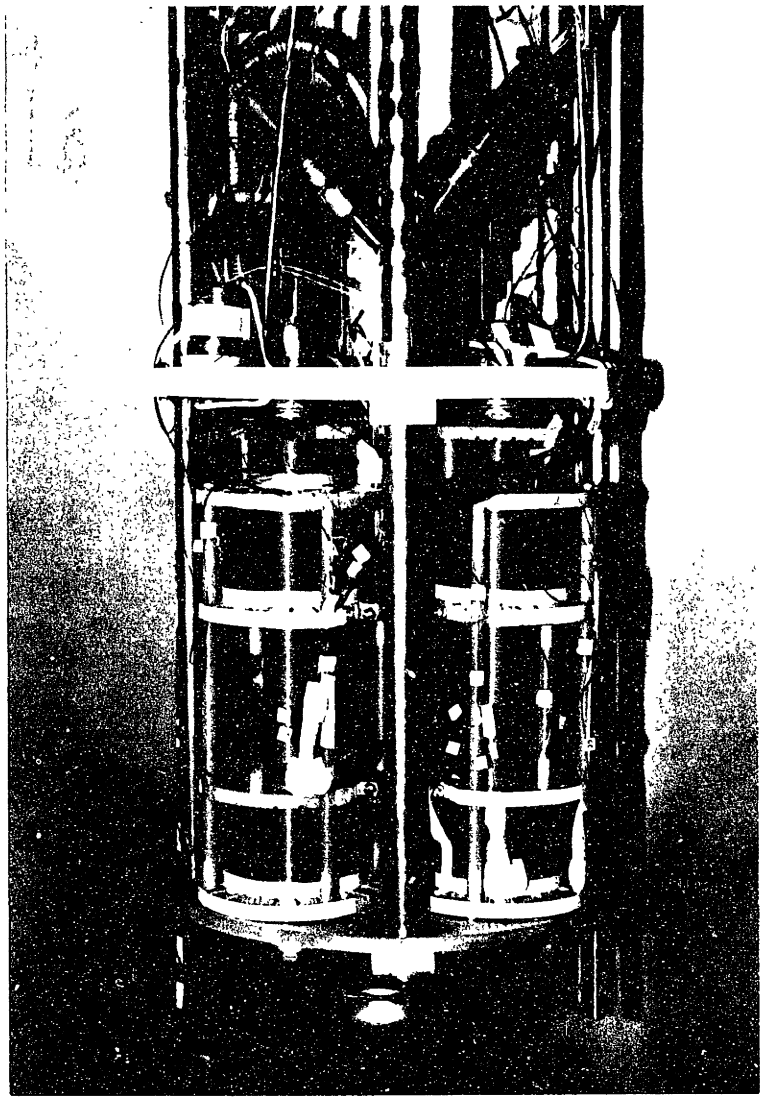

Fig. 4-4 Front view of the 4.2-K cryogenic part assembly, showing two magnetic units.

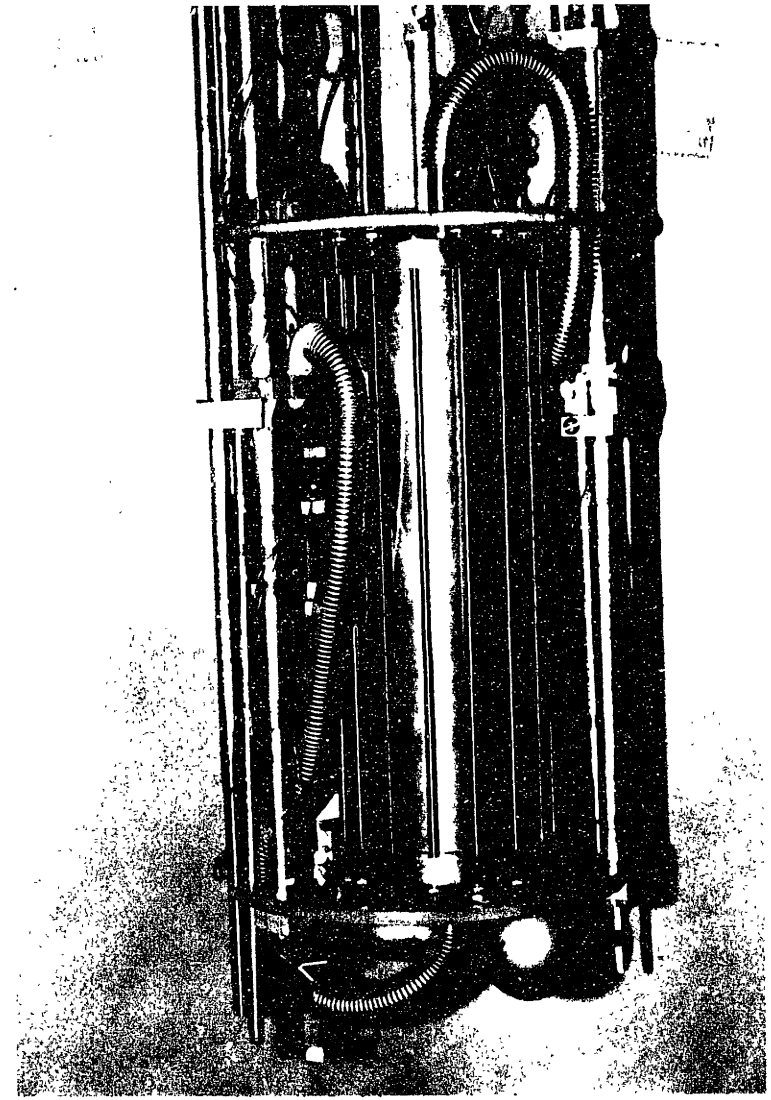

Fig. 4-5 Back view of the 4.2-K cryogenic part assembly, showing the displacer and the charcoal container.

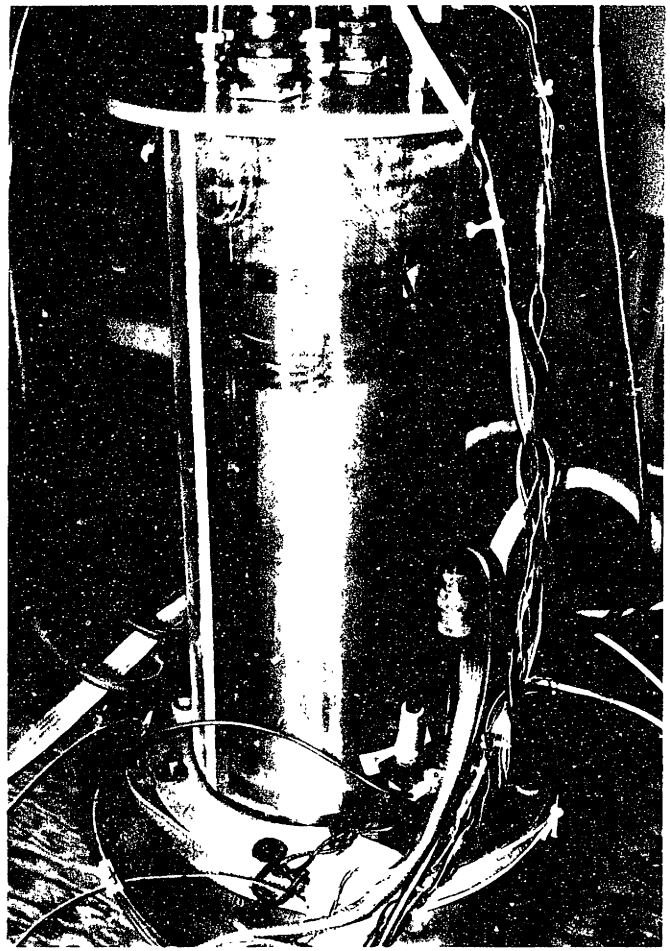

Fig. 4-6 Room temperature part assembly, located at the cryostat top. The step motor is seen at the upper portion through the Pyrex tube.

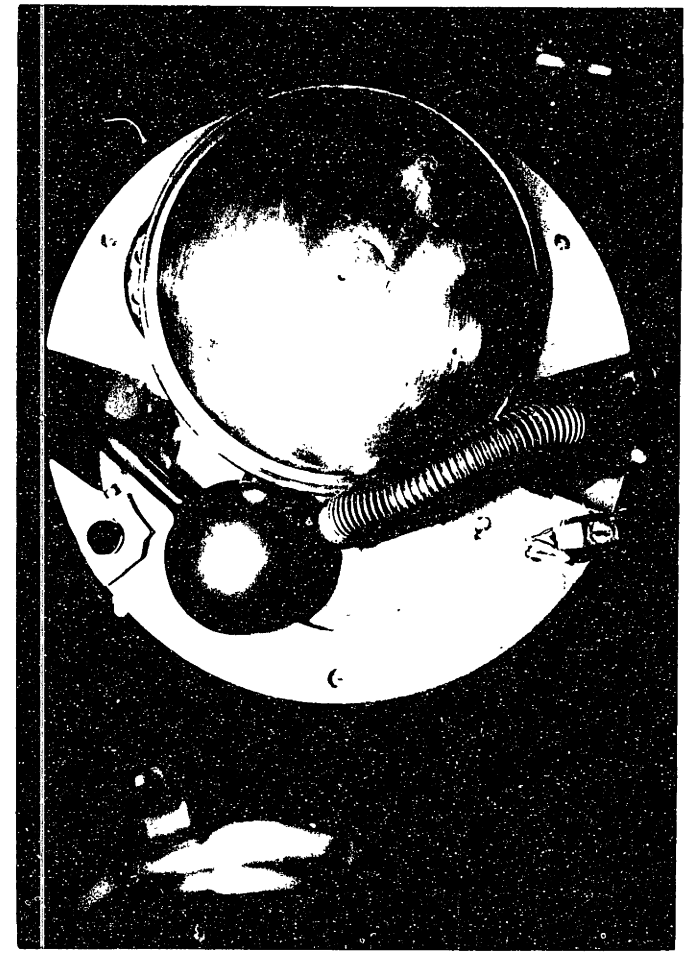

Fig. 4-7 Bottom view of the 4.2-K cryogenic part assembly, showing the charcoal helium adsorber and the vacuum jacket.

The left side magnetic core (referring to Figure 4-4) is filled with about 70,000 GGG spheres, each of 0.8 mm in diameter. However, the right side core is filled with irregular GGG granules which pass through #18 mesh (opening size 1 mm) but do not pass through #25 mesh (opening size 0.71 mm). One consisting of uniform spheres and the other consisting of irregular shaped granules, is another interesting aspect of research. Table 4-1 summarizes the comparison of two magnetic cores.

Table 4-1 Comparison of two magnetic cores in the tandem magnetic refrigerator.

	Left side core	Right side core
Particle shape	ø 0.8 mm sphere	granule (18 to 25 mesh)
Mass	135 g	132 g
Porosity	0.38	0.40
Adiabatic demagnetization from 1.5 tesla and 4.2 K	1.88 K	1.89 K

Connection of the copper warm-end heat exchanger to the stainless steel core tube is through a stainless steel header which is first brazed to the copper warm-end heat exchanger. The header and core tube are welded together later, after the other part of core unit is assembled. Figure 4-3 shows the warm-end heat exchanger brazed to its header. The connection between each magnetic core unit and the displacer is through a 12.7 mm diameter flexible stainless steel tube.

Since the bottom part of the core is colder than liquid helium, it must be thermally isolated from the 4.2-K bath. The 9.53 mm diameter stainless steel linkage connecting the two cores is protected by a semi-spherical stainless steel vacuum jacket. Before the vacuum jacket is welded, the inside part including the linkage was verified to be leak tight.

Figure 4-4 shows a front view of the cryogenic part assembly, very carefully assembled to fit into the cryostat. Figure 4-5, a back view of the system, shows the displacer assembly with the flexible lines connecting to the core assemblies. The spherical vessel underneath the displacer is a charcoal container. Section 4.1.3 discusses this charcoal He^3 recycling system in detail. Figure 4-7 is the bottom view of the 4.2-K cryogenic part assembly,

showing the charcoal He^3 adsorber sphere and the vacuum-protected space that contains He^3 heat transport linkage between the two units.

4.1.2 Step motor assembly

A step motor, located above the cryostat top, provides the stroke motion (125 mm) of the displacer. It is linked to the displacer, about 1.5 m below, by a stainless steel tube. Since it is virtually impossible to have a movable leak-tight linkage between the displacer piston and the step motor, the whole assembly, including the motor, is contained in a leak-tight assembly filled with He^3. The Pyrex tube (7 mm thick), seen in Figure 4-6, is a part of this container. The tube is sealed at both ends by O-rings with aluminum plates. The linear motion of the displacer rod is monitored by a 10-turn potentiometer, also placed in the He^3 space.

Since the step motor has to run inside a vacuum, there is not enough cooling media for the motor. To prevent the motor from overheating, which may result in large outgassing rates or breakdown, a copper chill with copper tube are wrapped around the motor through which cooling water of 12 ^{o}C is forced to circulate by a water pump through the test.

Figure 4-6 shows the room temperature part, the upper portion of which is the step motor. The bottom aluminum flange is exposed to a flow of cold cryogen vapor boiling when liquid nitrogen or liquid helium is charged into the cryostat. Two G-10 plates and a 120 V-200 W-Thermolyne band heater wrapped around the flange are used to keep the O-ring from freezing.

4.1.3 He^3 recycling system

For the heat transport medium, 10 liters (STP) of 99.8 % He^3 gas was purchased from E.G.&G Mound Applied Technologies. A relatively high cost of He^3 ($89.70/liter at STP) means that a closed recycling system must be used. An estimated total quantity of He^3 contained in the experimental assembly is about 5 liters (4.7 liters in the 4.2-K part, 0.3 liters in the 300-K part). In order to keep the He^3 gas free of contamination, a charcoal adsorber was constructed. In general, the amount of helium adsorbed by charcoal depends strongly on both temperature and pressure. However, if charcoal is cooled by liquid helium, a large amount of helium is adsorbed over a wide pressure range (even below 10 mtorr).

Figure 4-7 again shows a bottom view of the cryogenic assembly. The stainless steel sphere contains about 39 g of charcoal which can potentially adsorb about 63 liters of helium gas at standard conditions. (Helvensteijn, 1990). The charcoal used in this experiment is the carbon sample type PE and Mesh 12 x 30 from Barnebey&Sutcliffe Corp. The charcoal adsorber collects virtually all of the He^3 gas from the refrigerator space at the conclusion of a test. Since the charcoal is located at the bottom of the cryostat, it remains at 4.2 K even after the end of the test until the liquid helium in the cryostat boils away. Typically the suction time of the charcoal adsorber is approximately one day, enough for complete adsorption. Eventually when the charcoal warms up, the He^3 is released into another 5-liter container. In order to repeat this recycling operation, the He^3 piping line is prepared with several packless-type bellows valves. Figure 4-8 presents the plumbing used for the He^3 recycling system.

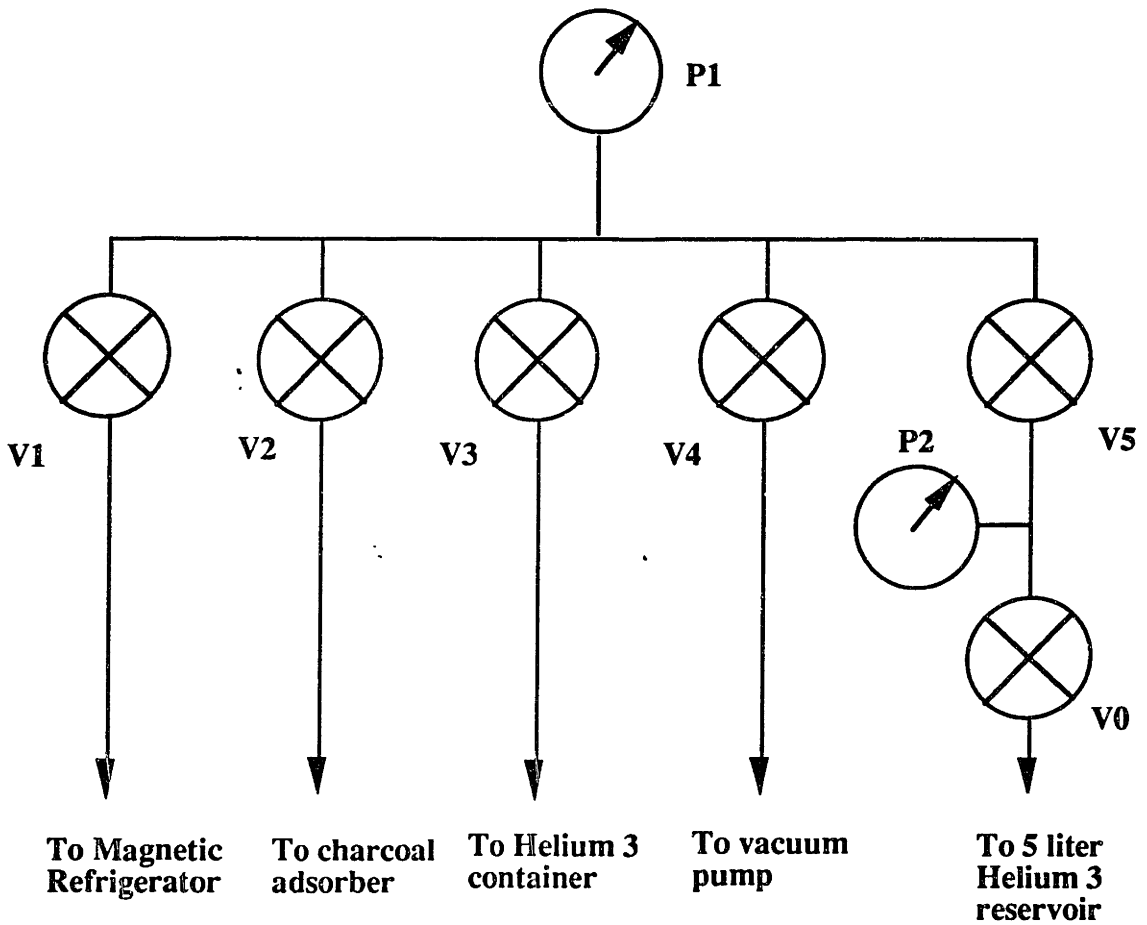

Fig. 4-8 He^3 piping system.

The pressure gauge P1 is a Varian 801 thermocouple vacuum gauge which accurately measures down to 1 mtorr. Since P2 should also measure the positive pressure (above the atmospheric pressure), the Bourdon type mechanical pressure gauge is employed.

During the initial purging process, valves V0, V1, V2, V3, V4, and V5 are opened to remove contaminants (residual gas and moisture). For the initial charging of He^3 and cool-down process, V2, V4, and V5 are closed. When the desirable amount of helium gas is charged in the magnetic system, V1 and V3 are closed. At the conclusion of magnetic refrigeration experiment, the He^3 gas is transferred from the working space into the charcoal adsorbent by opening V1 and V2. During this adsorption period, the pressure in the system will change from 40 torr to less than 10 mtorr, which means that most of the helium gas in the magnetic system is adsorbed by the charcoal. As the charcoal temperature increases over 10 K, V1 is closed and V5 is opened to keep the pressure in the charcoal container from building-up. When the system is completely warmed up to room temperature, a majority of the He^3 gas is transferred into the 5-liter He^3 reservoir, approximately at a pressure of 680 torr. V5 and V0 may now be closed.

At the beginning of subsequent experiment, valves V1 and V4 are opened to purge the He^3 space and then, after closing V4 when the desirable vacuum level (~10 mtorr) is reached, V1, V5, and V0 are opened to charge the magnetic refrigerator. After pressure equilibrium is obtained in the magnetic refrigerator, V5 is closed and V3 is slightly opened to make up He^3.

4.1.4 Cool-down characteristic

This section discusses the cool-down characteristic of the system assembly during the experimental preparation procedure.

Vacuum

Before the system is cooled, the vacuum insulation jacket of the system is pumped down below 10 mtorr to remove all contaminants. The liquid helium transfer line and two independent vacuum jackets of the cryostat have already been pumped down beforehand and it is not necessary to evacuate them again.

Liquid nitrogen precooling

Cooling the experimental apparatus to 77 K is done by filling liquid nitrogen into the cryostat. Also the liquid nitrogen jacket of the cryostat is simultaneously filled with liquid nitrogen. Precooling the system by liquid nitrogen must be done slowly and patiently so that thermal strain can transpire without damaging any joints within the assembly.

First, the system is charged with He^3 gas (about 40 torr). Cold nitrogen gas is then introduced into the cryostat. This precooling process can be monitored by four temperature sensors, located at the bottom of the cryostat, at the bottom of the magnetic refrigeration system, at the top of the superconducting magnet, and at the top of the magnetic refrigeration system respectively, using the program PRECOOL.BAS listed in Appendix G.1. Another useful precooling process monitor is to read the resistance of variational mode coils of superconducting magnets. The resistance changes from 2.1 kΩ at room temperature to approximately 253 Ω at 77 K.

The whole cryogenic part is submerged in liquid nitrogen overnight to cool it to 77 K. During this period, a caution must be exercised not to operate the displacer, because the inner piston cools down more slowly than the outer cylinder. The cumulative thermal shrinkage of stainless steel from 300 K to 77 K is large enough that the differential contraction will lock the piston in the cylinder so that any operation may damage the displacer mechanism. Liquid nitrogen precooling continues until all four monitoring temperature sensors indicate about 77 K; Submerging the system in liquid nitrogen overnight is usually sufficient to cool the system to 77 K completely. Leaving the system more than one day under this condition is undesirable because some moisture or air may be trapped in the cryostat.

Purging nitrogen

When the whole cryogenic part is completely cooled by liquid nitrogen (usually this is true after overnight precooling), the purging procedure starts. Liquid nitrogen is pumped out of the cryostat by pressurizing it with nitrogen gas. The nitrogen gas is fed through the vent line of cryostat and then liquid nitrogen flows out the liquid charging line. This pumping-out procedure does not remove all nitrogen from the cryostat. It is important that any residual nitrogen, liquid and gas should be expelled, which can be achieved by forcing the warm helium gas into the system. The importance of removing nitrogen from the

cryostat before liquid helium transfer, cannot be overemphasized. This can be double checked by analyzing the vent gas composition while the warm helium gas is being introduced into the cryostat (*e.g.* checking the speed of sound change in the vent gas or making a balloon with the vent gas and comparing its density with pure helium balloon). If any nitrogen is in the cryostat when liquid helium is transferred, solid nitrogen is easily formed at 63.2 K. The high heat capacity of solid nitrogen makes successful liquid helium charging almost impossible. During this purging process, the resistance of the superconducting coil increases by about 8 Ω.

Liquid helium charging

Transfer of liquid helium immediately follows the nitrogen purging to avoid introducing any contaminants into the system. Figure 4-9 shows a typical set of temperature traces and liquid helium level during the helium transfer process. The liquid helium supply dewar pressure is maintained at about 6.9 kPa (1 psi.) to maintain a continuous, quiet, and safe helium transfer. Especially during the initial transfer process, helium flow oscillations typically occur due to liquid helium abruptly boiling when it hits on the hot system inside the cryostat. About 25 liters of liquid helium is consumed to cool the cryogenic part to 4.2 K. This 4.2 K cooling is done slowly, lasting for about 50 minutes to prevent any thermal-shock induced damage, even though most thermal strain is transpired at the conclusion of liquid nitrogen precooling.

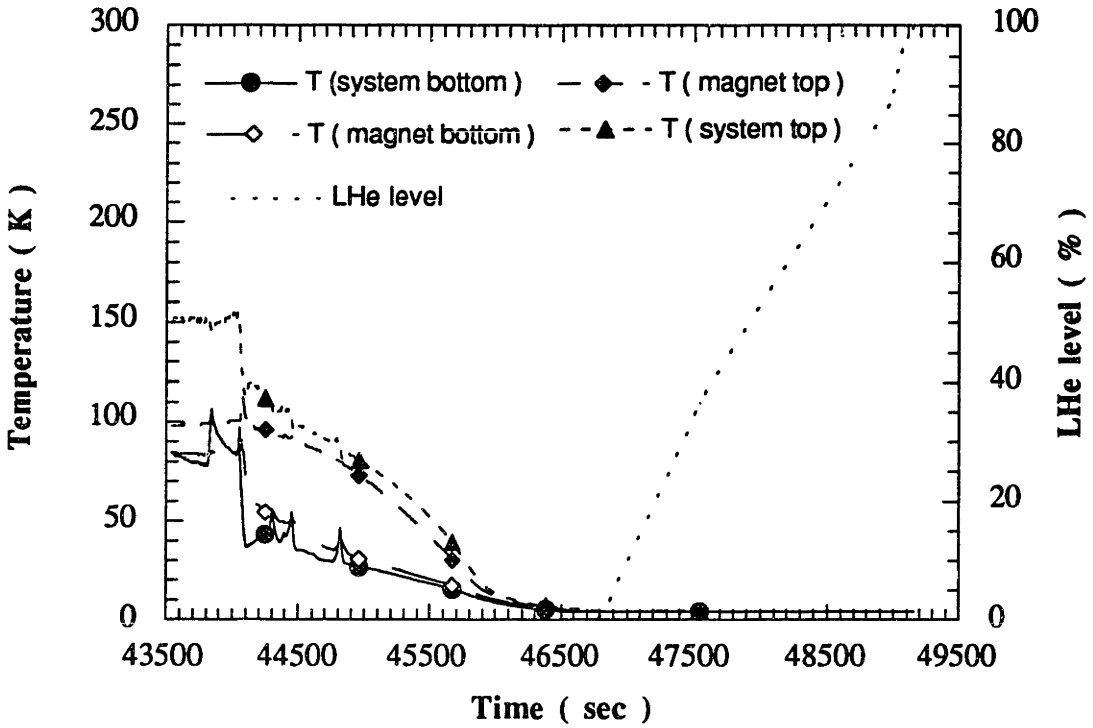

Fig. 4-9 Liquid helium charging.

When the liquid helium level reaches 100 % in a level indicator, equivalently a height of 750 mm from the cryostat bottom, the liquid volume in the cryostat is estimated at 15 liters. The experiment can be performed until the liquid helium level comes down to 60 %. Due to the careful thermal design of the system and good vacuum insulation of the cryostat, the cool-down characteristic is very satisfactory and the experimental session can last over 5 hours without liquid helium refill.

4.2 Preliminary tests

Before the main tandem magnetic refrigeration experiment, three major preliminary tests were performed to ascertain that each component work properly.

4.2.1 Tandem superconducting magnet test

The tandem magnets require a special magnet configuration and power supply scheme. This section discusses the experimental data from the operation of the tandem superconducting magnets. To energize the variational-current coils, KEPCO BOP-36-12 power supply was used in the current-control mode. Usually, a bipolar operational power supply does not work very well with a highly inductive load such as a super conducting magnet (which, in the case of this study, has a total inductance of 3.6 H.). Therefore, special attention has to be paid in selecting the power supply. Otherwise a high-power resistor should be connected in series with the magnet to change the impedance characteristics of the load.

At first, a Techron 7570 power supply was tried. However, its d.c. load characteristic did not provide a desirable output for a highly inductive load. At a low voltage with a high current, this power supply showed a problem. One of the power transistors in the power supply is overheated. After several preliminary tests with the Techron power supply, it was concluded that this power supply was unsuitable for energizing the tandem magnets.

The next choice was a KEPCO 400 W BOP series power supply; KEPCO BOP-36-12M. The KEPCO BOP series have a different four-quadrant d.c. load feature; they can also be stabilized by adding a capacitor in the output current amplifier when a highly inductive load is connected. Figure 4-10 shows current, voltage, and field traces when the variational-current coils were charged during a power supply test. The current is varied with a maximum amplitude of 12 A in a ramp mode. The cycle period is 24 seconds

Persistent current charging

After confirming the performance of the power supply for charging the magnets, the persistent-current charging test was performed. Charging the persistent-current coils is more complex than a simple ramping test.

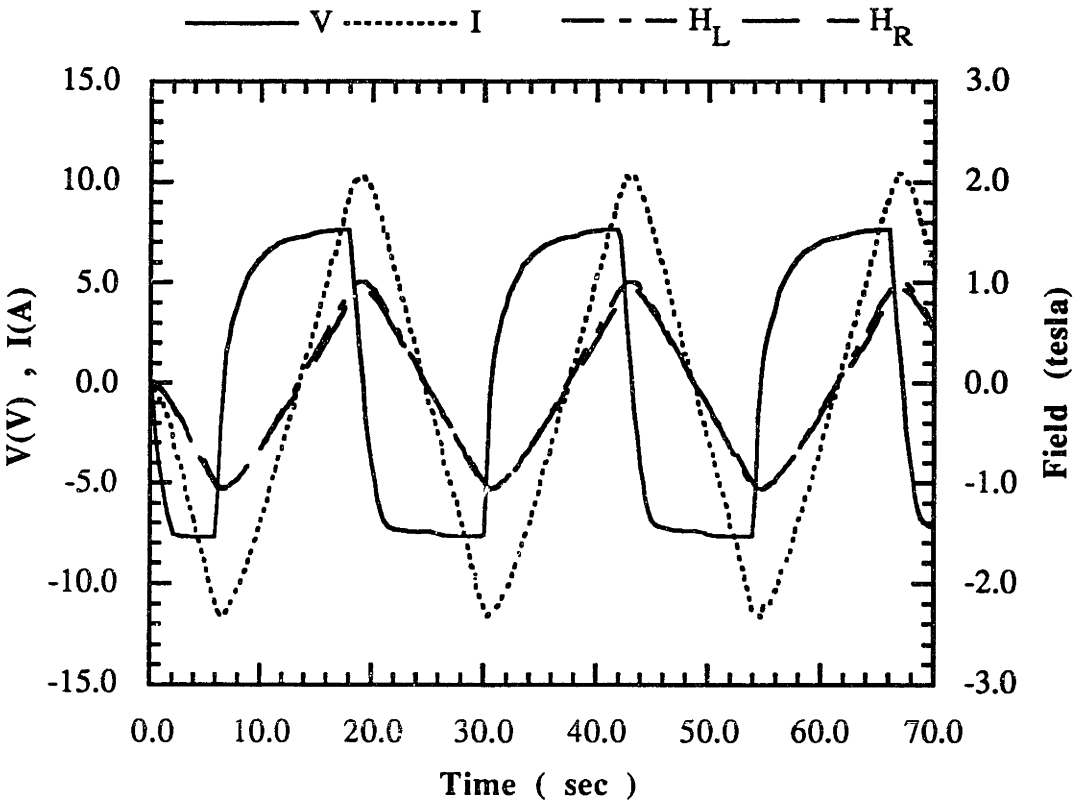

Fig. 4-10 Magnet system charging test. (Trace V is the applied voltage, trace I is the current, trace H_L is the field of the left core and trace H_R is the field of the right core.)

To charge the persistent current, the following procedure is used. Refer to Figure A-4 given in Appendix A.

(1) The persistent switch heater is turned on and kept the switch wire resistive to force the current through the magnet.

(2) A small voltage (typically 1 V) is applied to the magnet so that the current gradually increases towards an operating level. This step takes about 3 minutes. (See Figure 4-11 for traces taken during a charge-up of the persistent-current coils.)

(3) When the current reaches the operating level and remain constant, the persistent switch heater is turned off, making the switch to be superconducting. Since the persistent

switch has a thermal inertia, it takes about 20 ~ 30 seconds to cool to 4.2 K and become superconducting.

(4) The power supply current level is reduced slowly to zero, leaving a persistent current loop charged at the operating current of the coils.

(5) Once the current returns zero, the power supply can be disconnected. The constant persistent current can be monitored by a Hall probe magnetic field sensor.

As shown in Figure 4-11, the two coils are charged to a current of 18 A, corresponding to a central axial field of 1.8 T in the magnet. The axial field directions of the two coils are opposed from each core. Each will add or subtract 1.8 T from a field generated by its respective variational-current coil.

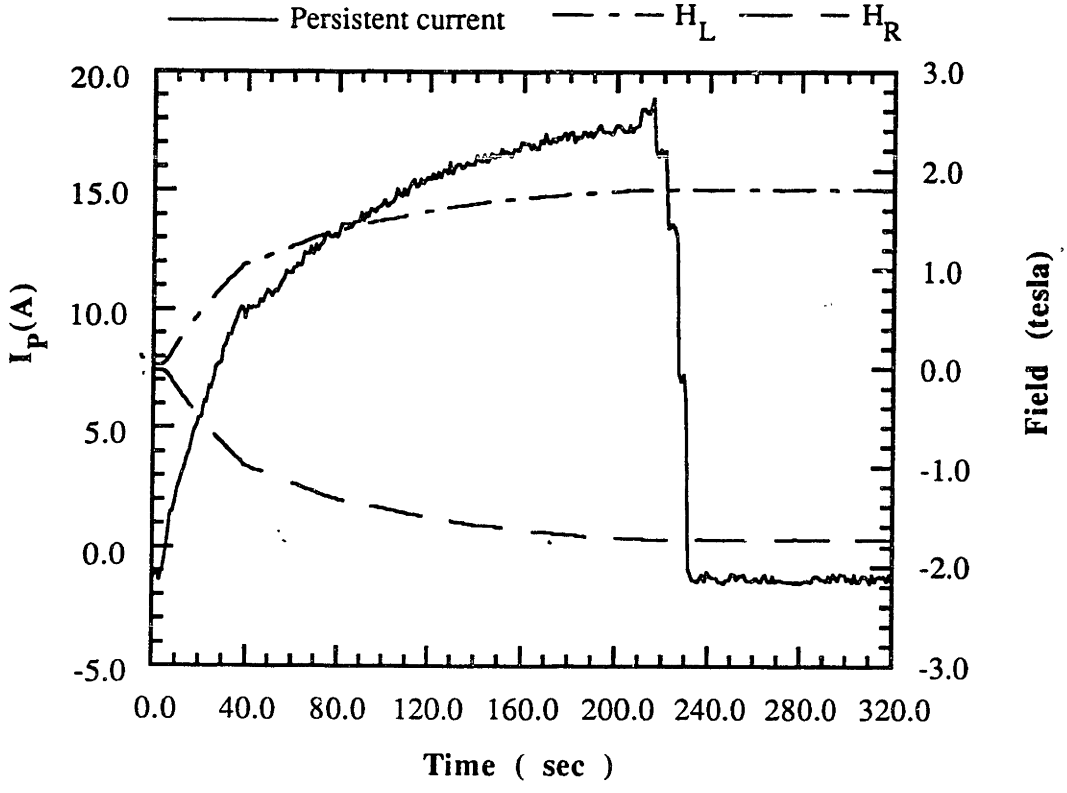

Fig. 4-11 Persistent current charging test (18 A). (Trace H_L is the field of the left core and trace H_R is the field of the right core.)

Tandem energization

Figure 4-12 shows the test results when the variational-current were charged together with the persistent current coils energized to 18 A. Note that as the total central field in one core increases while it decreases in the other core. A sinusoidal current excitation was also tried on the variational-current coils. Figure 4-13 shows resultant traces. Even though the persistent circuit for the persistent-current coils was found not to be absolutely persistent, a resultant current decay in the coils was so small that it does not affect refrigeration test.

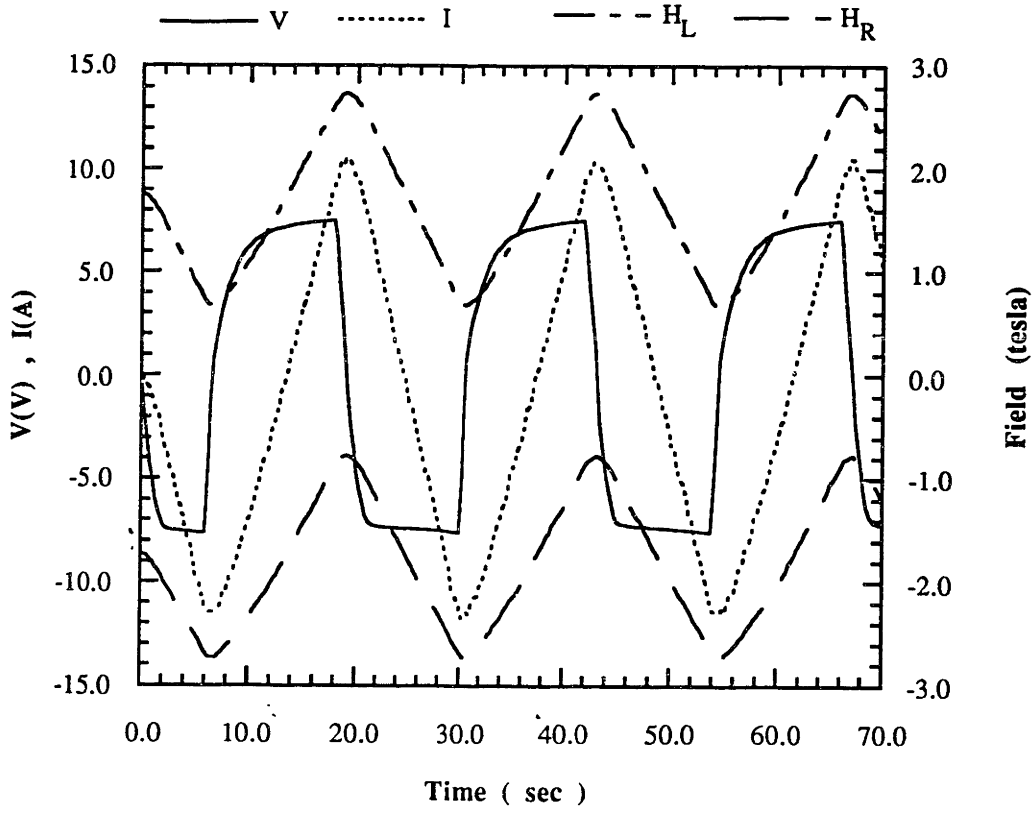

Fig. 4-12 Tandem magnet energization test in ramp mode. (Trace V is the applied voltage, trace I is the current, trace H_L is the field of the left core and trace H_R is the field of the right core.)

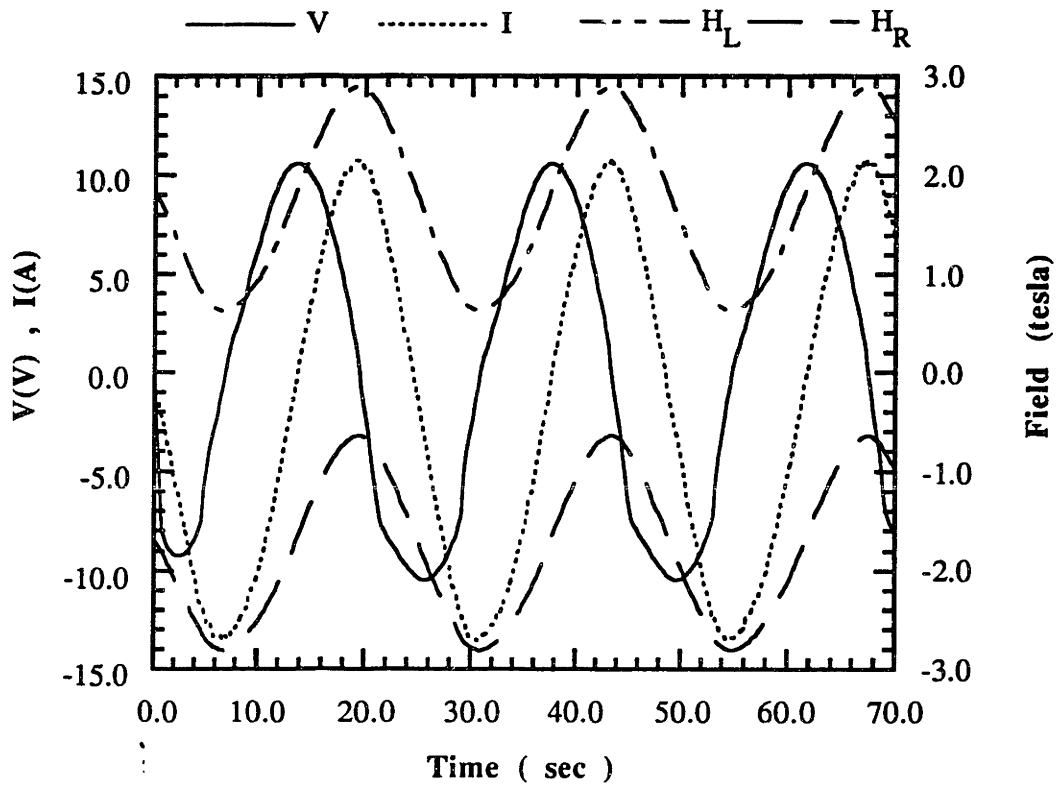

Fig. 4-13 Tandem magnet energization test in sine wave mode. (Trace V is the applied voltage, trace I is the current, trace H_L is the field of the left core and trace H_R is the field of the right core.)

4.2.2 Heat transport medium circulation test

The purpose of this preliminary test was to check the displacer operation at 4.2 K and estimate pressure drop across each magnetic core. The displacer drive mechanism encased in a 40-torr space was tested when the cryogenic part was at 300 K, at 77 K, and at 4.2 K. Figure 4-14 presents signal traces when He^3 gas was circulated through the system by the displacer. The helium gas temperature influences the pressure variations in each magnetic core. The observed differences in pressures at 300 K, at 77 K, and at 4.2 K can be explained by the temperature dependence of the gas viscosity. Since the viscosity decreases as the temperature goes down from 300 K to 77 K and to 4.2 K, the pressure fluctuation is also suppressed. The pressure drop estimation of 420 Pa (3.15 torr) presented in section 2.1.2, agrees quite well with that indicated by the pressure traces for operation at 4.2 K.

In general, the dynamic pressure measurement via a capillary tube involves errors from the so-called (Karam, 1973, and Benedict, 1984) " *transmission line effect* " : (1) delay, (2) attenuation (decrease in amplitude of a propagating step), (3) dispersion (such as smoothing or distortion of the leading edge of a step pressure input). However, the relative amplitude of pressure fluctuation with respect to the working pressure is very small at 4.2 K (less than 10 %) so that this effect can be ignored.

This preliminary displacer test showed that there would be no significant pressure difference due to flow in the magnetic core for operation at 4.2 K.

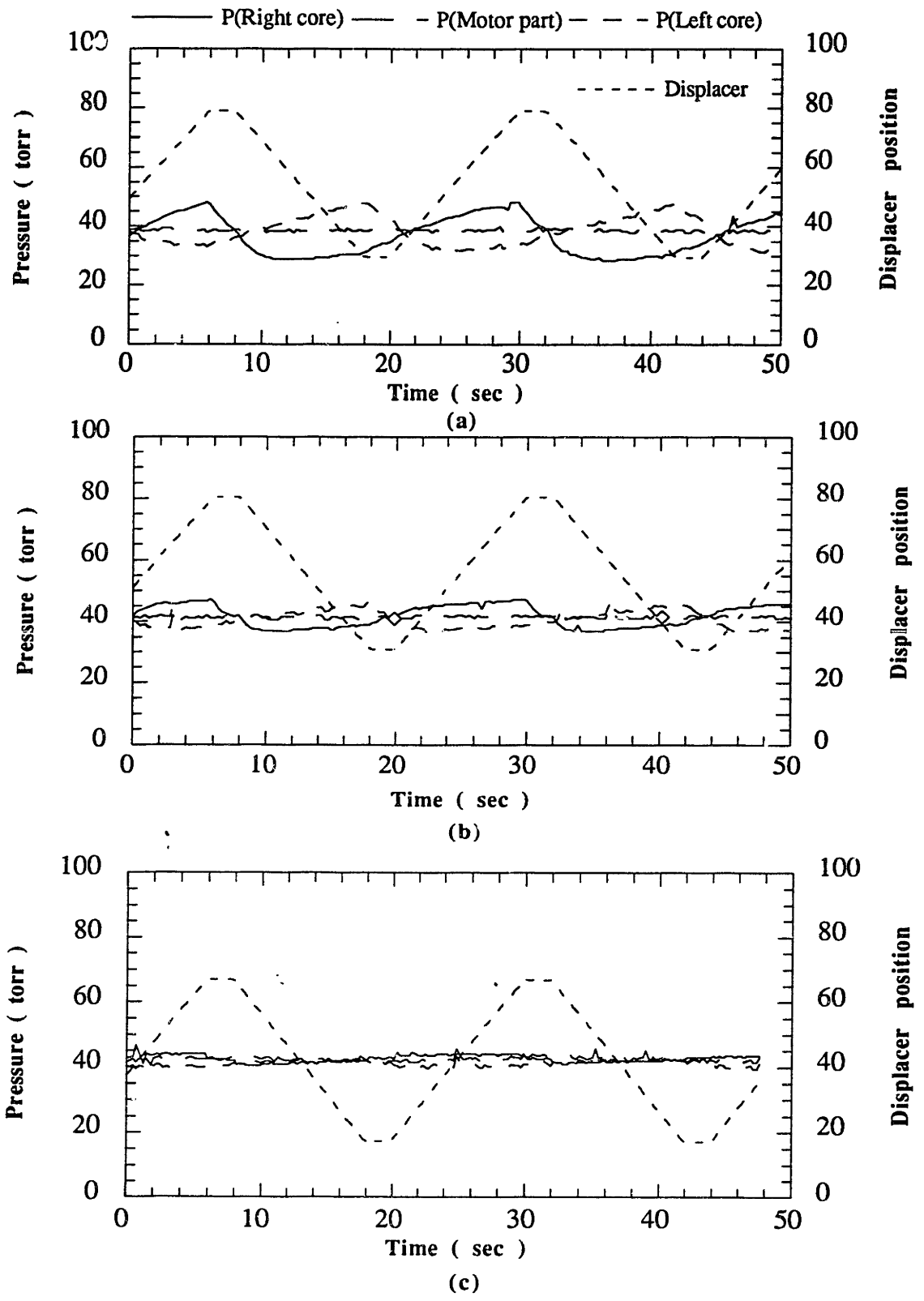

Fig. 4-14 Pressure variations in the displacer test . (a) 300 K (b) 77 K (c) 4.2 K.

4.2.3 He^3-charcoal adsorption test

This section presents a further discussion on the experimental data of He^3-charcoal adsorption test.

It is known that one gram of charcoal (or activated carbon) adsorbs about 0.1 g of He^4 gas at 4.2 K (Helvensteijn, 1990). Even though Helvensteijn's value is for He^4 gas and it depends also on pressure, 39 g of charcoal in the He^3-recycling system is considered more than enough to adsorb 0.6 g of He^3, the amount used to transport heat in the system. As the charcoal container is located at the lowest level in the cryostat, it will stay at 4.2 K for a long time even after the main experiment is ended. Figure 4-15 (a) shows typical experimental data of the He^3-charcoal recycling process. The He^3 pressure in the experimental unit was 46 torr when the valve to the charcoal container was opened. It took about 25 hours for most of the He^3 gas in the system to be adsorbed into the charcoal. The final pressure of the system was below 10 mtorr, which means more than 99.9 % of the initial He^3 gas was completely contained in the charcoal space.

The long adsorption process taken in this experimental data can be explained by the following qualitative reasonings.

(1) The flow passage between the He^3 working space (or the main magnetic refrigerator space) and the charcoal container is very small. This restricts the flow causing a slow pumping speed of charcoal.

(2) The flow passage runs through the room temperature piping system as shown in Figure 4-8. In other words, He^3 gas which stayed at 4.2 K in the cryogenic part, is warmed up as it passes through the room temperature valves, and then must be cooled down to 4.2 K in the charcoal container. Since the specific heat of charcoal at 4.2 K is very small (about 0.16 J/kg·K), it may be easily warmed up by the adsorbed helium gas. Also this warm-up phenomenon is enhanced by the heat of adsorption, which is about order of 1700 J/mole (Chan, 1981). The amount of He^3 to be adsorbed in charcoal is 0.61 g, which may involve 350 J of heat. If the charcoal is warmed up by warm incoming helium gas and by the heat of adsorption, it needs time to become cool again, since the amount of helium adsorbed by the charcoal depends strongly on temperature.

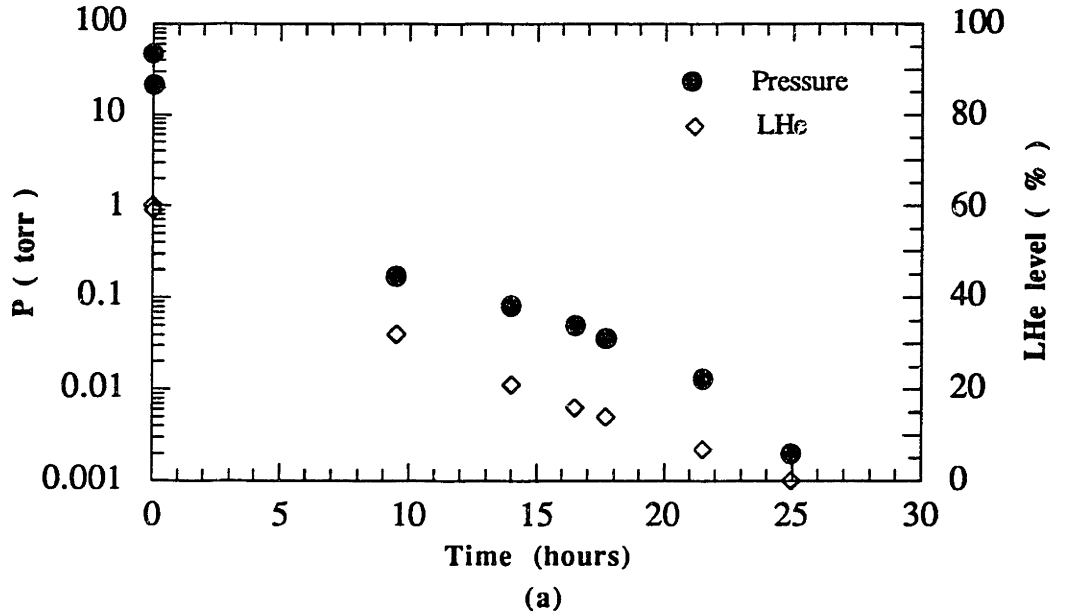

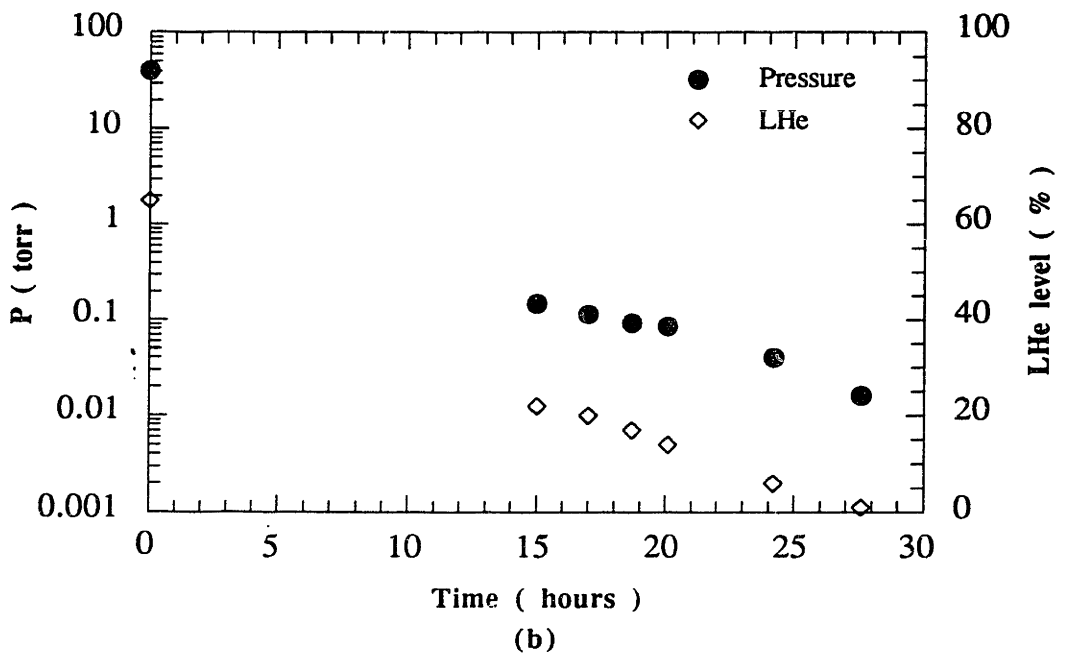

Fig. 4-15 Charcoal adsorption test. (a) He^3 (b) He^4

Since the thermal conductivity of charcoal at 4.2 K is very small (~0.04 W/m·K), the effective thermal diffusivity of the inside of the charcoal container is almost the same as that of helium gas at 4.2 K (McAdams, 1954, and Bejan, 1984).

$$\alpha_{eff} = \frac{k_{eff}}{(\rho C_p)_f}$$

$$\approx \frac{0.02}{0.462 \times 6991}$$

$$= 6.2 \times 10^{-6} \text{ m}^2/\text{sec} \qquad (4.1)$$

This low thermal diffusivity retards cooling the inside of charcoal, which at the same time is warmed by the incoming helium gas.

(3) The physical adsorption rate of gas molecule itself can be slow. The number of molecules incident on unit area is given by Roth (1978).

$$\frac{dn_a}{dt} = 3.15 \times 10^{22} \left[\frac{P}{(MT)^{1/2}}\right] f \text{ molecules/cm}^2\text{sec} \qquad (4.2)$$

where P is the pressure (torr), M is the molecular weight (g/mole), T is the temperature (K), f is the sticking coefficient.

Eq.4.2 states that the adsorption rate decreases as pressure decreases or molecular weight increases. The charcoal adsorption period in Figure 4-15 (a) can be divided into two parts; above 80 mtorr region and below 80 mtorr region, according to the convex and concave characteristic of experimental data.

During the early adsorption period, which is above 80 mtorr region or first 17 hours, the adsorption rate is governed by the mechanism (2). The warmed charcoal itself retards the overall process time. About 99 % of helium gas is adsorbed into charcoal during this period.

After 17 hours, since most helium gas is already adsorbed, the adsorption rate is now controlled by the mechanisms (1) and (3); small pumping speed associated with small flow passage and the slow collision rate of molecules (Eq. 4.2). The experimental data of He^4 as shown in Figure 4-15 (b), indicates that it takes a longer time to adsorb He^4 than He^3. This result can also be explained by the first and third mechanisms.

4.3 Active magnetic refrigeration test

The main tandem magnetic refrigerator was tested in a continuous mode after successful completion of the above preliminary tests. This test is a synchronous combination of the two tests described in section 4.2.1 and 4.2.2. This section describes the experimental procedure and a typical set of experimental data.

4.3.1 Experimental procedure

The cooldown procedure including liquid helium charging is same as the preliminary test case. When the liquid helium level meter reaches 100 %, the persistent-current is charged according to the procedure described in section 4.2.2. During the persistent-current charging process, both GGG magnetic cores are magnetized and the displacer motion is utilized to cool the core to 4.2 K. When it is confirmed that the persistent-current produces a uniform magnetic field and both core temperatures are all at 4.2 K, the tandem magnetic refrigerator operation starts. The computer program MAIN.BAS is used to synchronize the magnetic field swing with the displacer motion while the experimental data are collected every 0.4 sec. The program explanation and a listing are given in Appendix G.

An important variable experimental parameter is the cycle period. Even though the machine was designed to run with a cycle time of 12 seconds, a cycle time of 24 seconds was used because of the power supply used to power the magnets. There are two mechanisms to change the cycle time in the real experiment. One is the power supply and the other is the step motor. The electrical load for the power supply and the mechanical load for the step motor are alleviated when the cycle period is doubled.

There was another significant modification in the experiment. Due to the limited capacity of the KEPCO bipolar power supply, the maximum amplitude of variational current was limited to less than 7.5 A. Since the power supply shows erratic characteristics for highly inductive loads ($\approx$ 3.6 H), a capacitor of 11.1 μF was attached across the current amplifier module, and a 1.6-Ω resistor was connected in series with the magnets to stabilize the power supply. The persistent current was first charged up to 14 A and a 7.5-A amplitude variational current was superimposed to generate a field swing of 0.6 ~ 2.3 tesla.

4.3.2 Data analysis

The experimental data collected by MAIN.BAS during the operation are : 12 magnetic core temperatures, 2 magnetic field measurements, 3 pressures, the voltage and current for each variational coil, and displacer position. The data collection is done at every 0.4-seconds.

Figures 4-16 (a), (b) show typical temperature traces for the left and right cores. For the first 140 seconds, they show the transient characteristic, after which the cyclic steady-state is reached. The cycle time is 24 seconds. Since the persistent-current already exists at the initial state, during the first half cycle, the left core is magnetized while the right core is demagnetized. The actual locations of these 6 temperature sensors in each core are as shown in Figure F-1, Appendix F. From the experimental data, it is deduced that sensor T2 in the left core (Figure 4-16 a) is actually placed a little bit higher than the intended location during the assembly.

The overall temperature data show that the cor ıuous operation of the tandem magnetic refrigerator is possible. The lowest no-load temperature obtained in the continuous operation is 1.50 K, achieved at the core bottom.

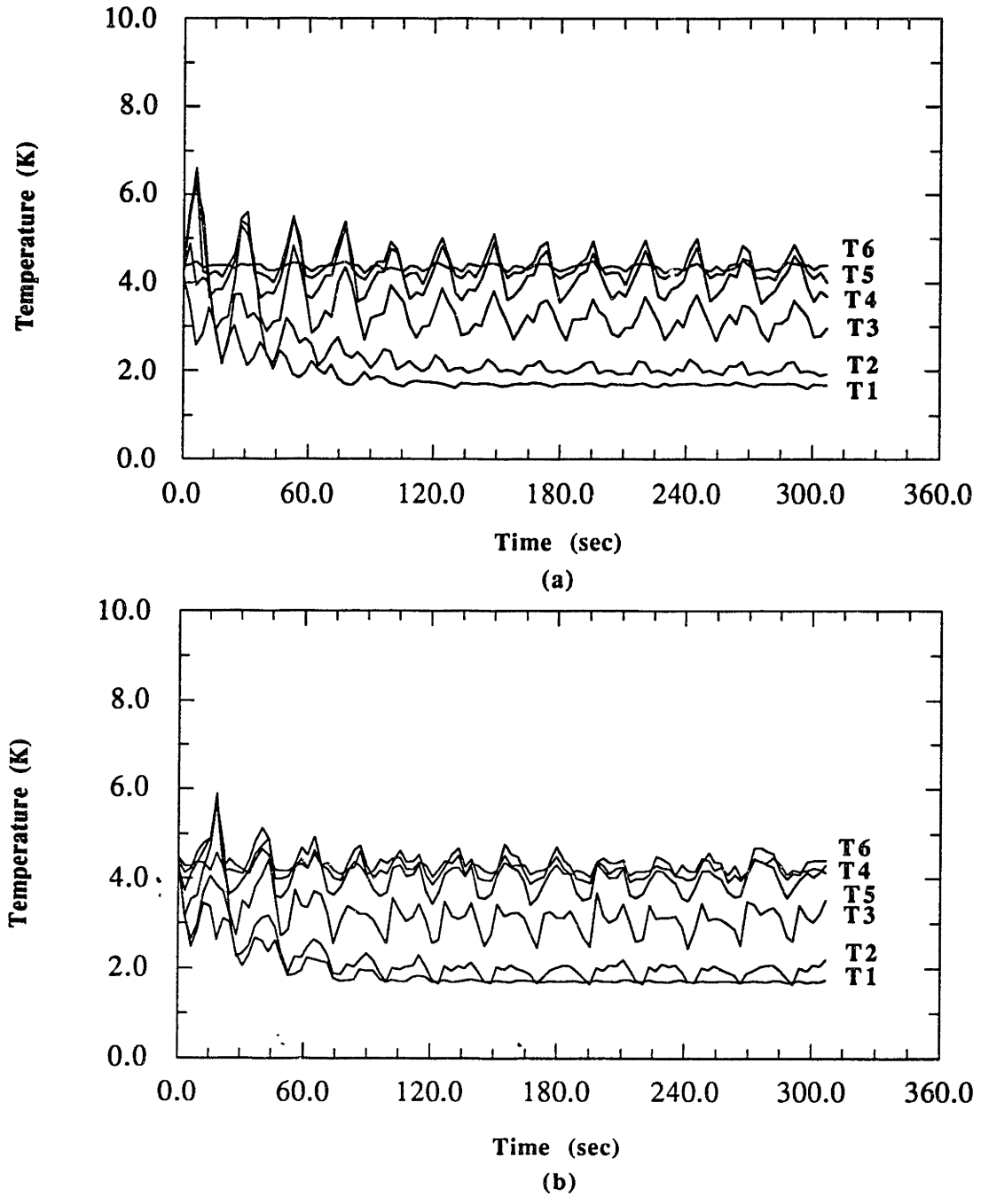

Fig. 4-16 Temperature data of the tandem magnetic refrigeration.
(a) Left core (b) Right core

The trace T6 demonstrates that each warm-end heat exchanger works well to cool the warm helium to 4.2 K. However, T6 in the right core (Figure 4-16 b) shows a little fluctuation around 4.2 K. This may be caused by the channeling effect in the warm-end heat exchanger, because there is a channel in the heat exchanger to let the instrumentation wires pass through. Some helium gas can flow through this slot rather than through the uniform heat exchanger flow channels. In spite of this small leakage of helium gas flow, the overall efficiency of each heat exchanger appears satisfactory.

In order to present the cyclic steady-state temperature profiles more clearly, Figure 4-17, which includes field and displacer traces, is prepared. The field traces clearly show that the two magnetic cores operate 180° out of phase; when the left core is magnetized, the right core is demagnetized, and vice versa. It is noticeable that the temperature peaks (T2, T3, T4, T5) during one cycle, occur before the magnetic field maximum or minimum is reached in one core. This shows that each magnetic core is cooled by the up-flow helium during flow-magnetization process and warmed by the down-flow helium during the flow-demagnetization process. In other words, the up-flow helium is warmed by the magnetized GGG and the down-flow helium is cooled by the demagnetized GGG. Finally, the cold helium, below 1.8 K, is produced at the bottom of each magnetic core.

Each cold-end heat exchanger supplies a controlled load at 1.8 K to measure the refrigeration power. In the case of Figure 4-17, the measured combined refrigeration power from the two magnetic cores is 12.2 mW. Chapter V. discusses more about the refrigeration power of the tandem magnetic refrigerator.

Figure 4-18 shows a typical axial temperature profile of each core right after the magnetic refrigerator operation is stopped. The effective thermal conductivity of the core depends on those of the packed GGG spheres and He^3, both of which decrease as temperature goes down. The fact that the temperature gradient in the warm-end side is lower than that in the cold-end side implies that the axial conduction is constant along the core. This result shows that the vacuum jacket around the core is good, indicating virtually no heat leak to the 4.2-K helium bath. While the axial temperature gradient in each warm-end heat exchanger is small due to high thermal conductivity of copper, each cold-end heat exchanger has a slightly large axial temperature gradient. This is because it is made of ten separate SiO_2 disks, each 3 mm thick. The radial temperature uniformity of the cold end heat exchanger is again assured by the analysis presented in Appendix D.

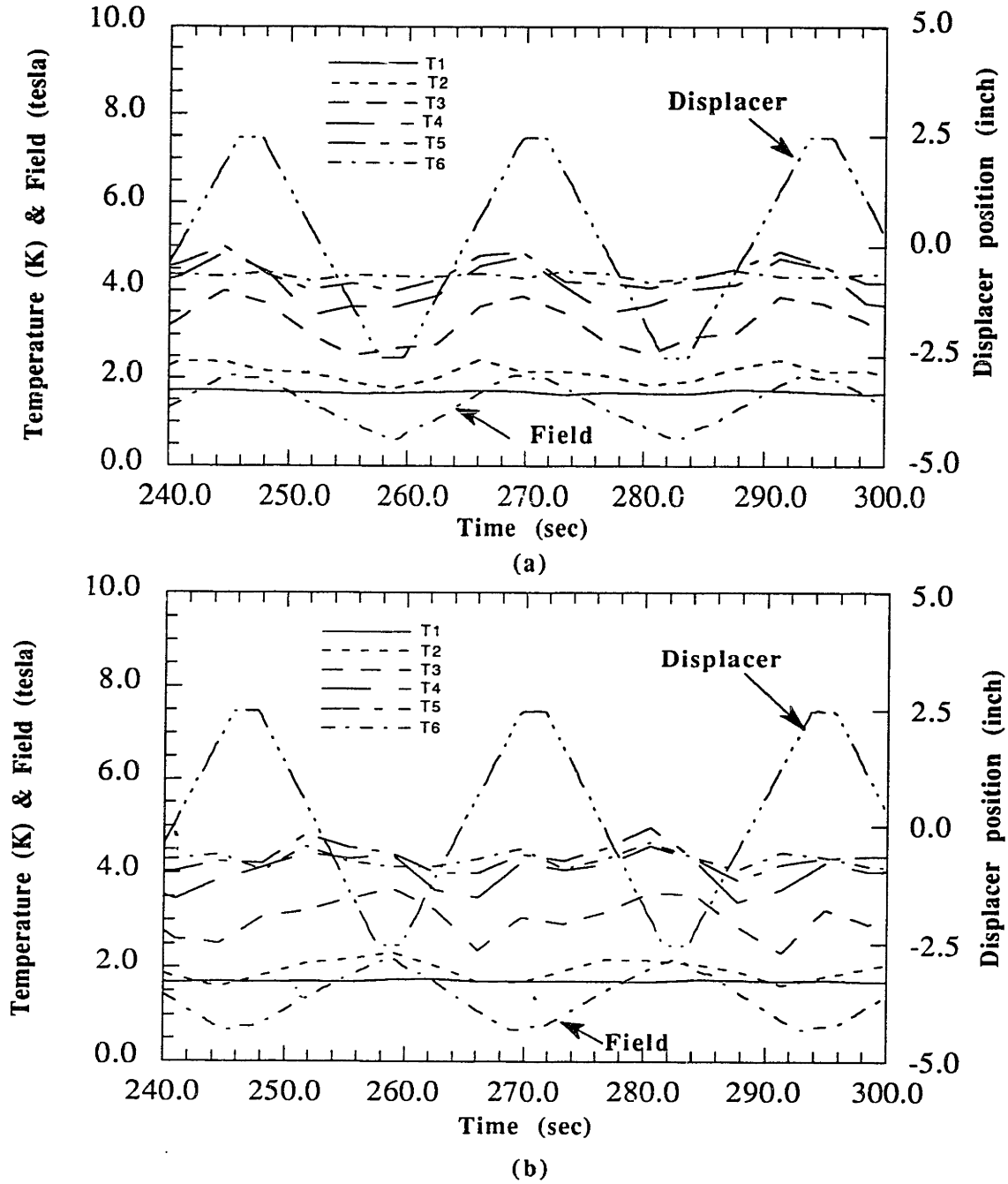

Fig. 4-17 Cyclic steady state temperature data of the tandem magnetic refrigeration. (a) Left core (b) Right core

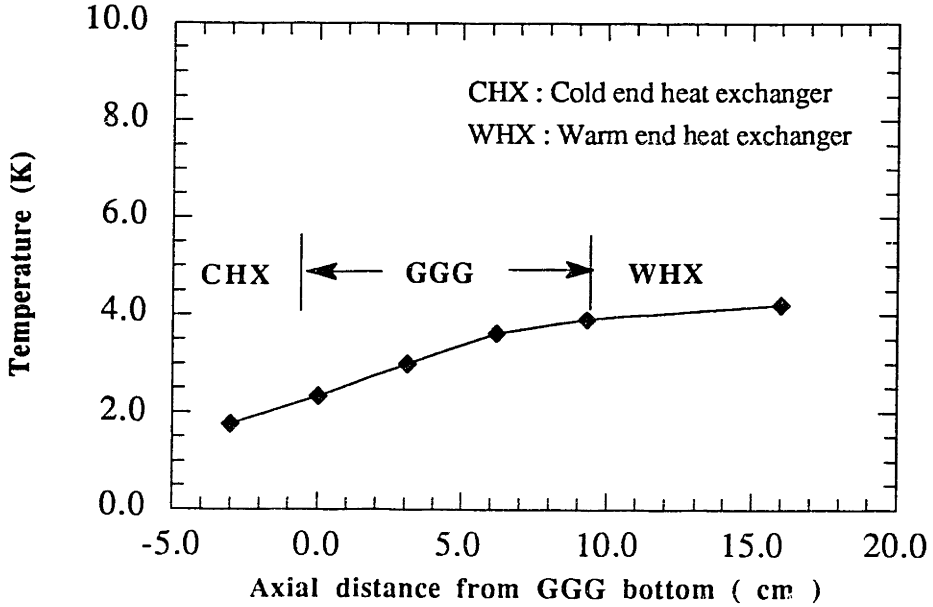

(a)

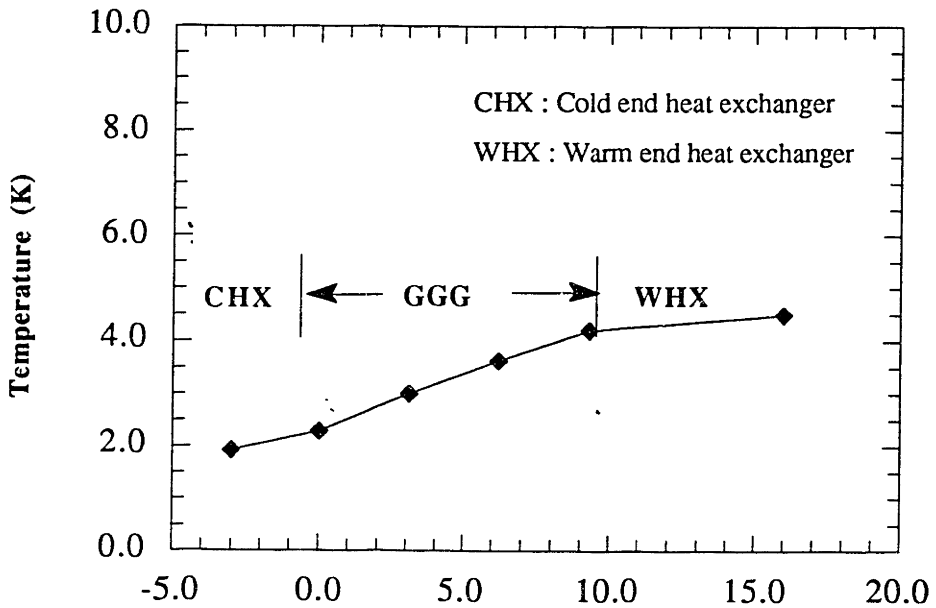

(b)

Fig. 4-18 Typical temperature gradient of the tandem magnetic refrigerator.
(a) Left core (b) Right core

V. RESULTS AND DISCUSSION

The experiment with the tandem magnetic refrigerator demonstrated successful operation over the temperature range 4.2 K~1.8 K. The maximum refrigeration power obtained at 1.8 K was 12.2 mW, for the values of the experimental parameters selected. This chapter describes the experimental results in detail and the problems encountered in the experiment.

Experimental parameters

The experimental parameters used in the test were slightly different from those selected in the design and used for computer simulation. Table 5-1 summarizes both sets of parameters and reasons for the differences.

Table 5-1 Differences between design and experimental parameters.

Parameter	Design	Experiment	Comments
Amount of GGG in the left core	135 g	135.1 g	38 % porosity
Amount of GGG in the right core	135 g	132 g	Larger porosity (40%) due to irregular granules
Minimum magnetic field	0 tesla	0.6 tesla	Persistent current adjustment
Maximum magnetic field	3.0 tesla	2.3 tesla	Power supply limit
Cycle time	12 seconds	24 seconds	Power supply limit
Refrigeration	100 mW	12.2 mW	Discussed in the main text

Even though the measured refrigeration power is 12.2 mW at 1.8 K, which is much smaller than a design value of 100 mW, it is consistent when changes in two important parameters (cycle time and magnetic field swing range) are taken into consideration.

Doubling the cycle period reduces the refrigeration power by a factor of half and also the shrunk magnetic field swing range (between 0.6 tesla and 2.3 tesla rather than 0 tesla and 3.0 tesla) must result in the small refrigeration power. The simulation program result with the experimental input parameters actually predicted 6 mW at 1.8 K, which is even smaller than the experimental result. The discrepancy of the refrigeration power values between the simulation and the experiment occurs due to the error of the thermodynamic property calculations of GGG and He^3, the heat transfer coefficient correlation, the estimation of the helium shuttle mass, the input magnetic field variation values for the program, and extra numerical errors. Nevertheless, the simulation program is no doubt useful to predict the system performance reasonably.

Shuttle mass of helium

The shuttle mass of helium is an important system parameter which affects the overall refrigeration performance. Three different charging pressures of helium were tested; 34 torr, 40 torr, and 46 torr. Each pressure results in equivalently 0.23 g, 0.27 g, and 0.31 g of the shuttle mass of helium. Figures 5-1 and 5-2 are the temperature traces for the operating pressure of 34 torr and 46 torr. Even though these temperature data are similar to those of Figure 4-16, which is for the case of 40 torr, it is found that there is an optimum shuttle mass of helium to maximize the magneto-caloric effect of a given amount of GGG. The resulting refrigeration power values for 34 torr, 40 torr, and 46 torr case are respectively 7.4 mW, 12.2 mW, and 4.6 mW. The shuttle mass effect on refrigeration power was already predicted by the computer simulation in Chapter III. Initially, the refrigeration power increases as the helium mass is increased to 0.27 g, but it decreases as the helium mass is further increased to 0.31 g. The optimum shuttle mass of He^3 in this experiment was found to be almost 0.27 g.

Magnetic field

The magnet is energized with the power supply in current-control mode. After several preliminary magnet tests, it was concluded that a small resistance connected in series with the magnet was required to stabilize the bipolar power supply. Even with this method, due to the reduced current capability of the power supply, the maximum variational current was limited to 7.5 A in the main test. As a result, the magnetic field swing in the experiment is reduced as shown in Table 5-1. However, the tests, preliminary and main, clearly demonstrated that the tandem superconducting magnets can be operated with 180 ° phase difference with a single power supply.

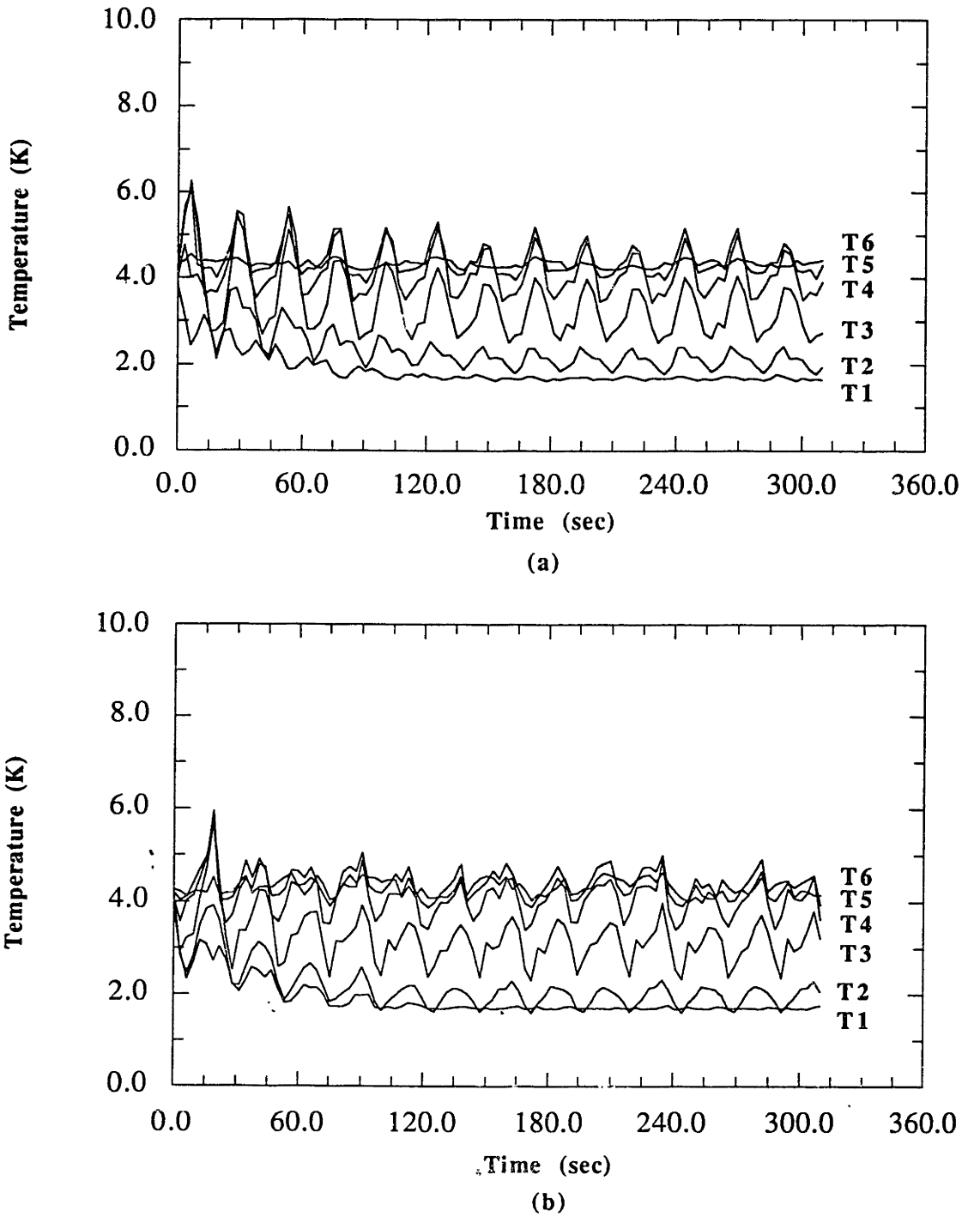

Fig. 5-1 Temperature data of He^3 inside the magnetic core at 34 Torr.
(a) Left core (b) Right core.

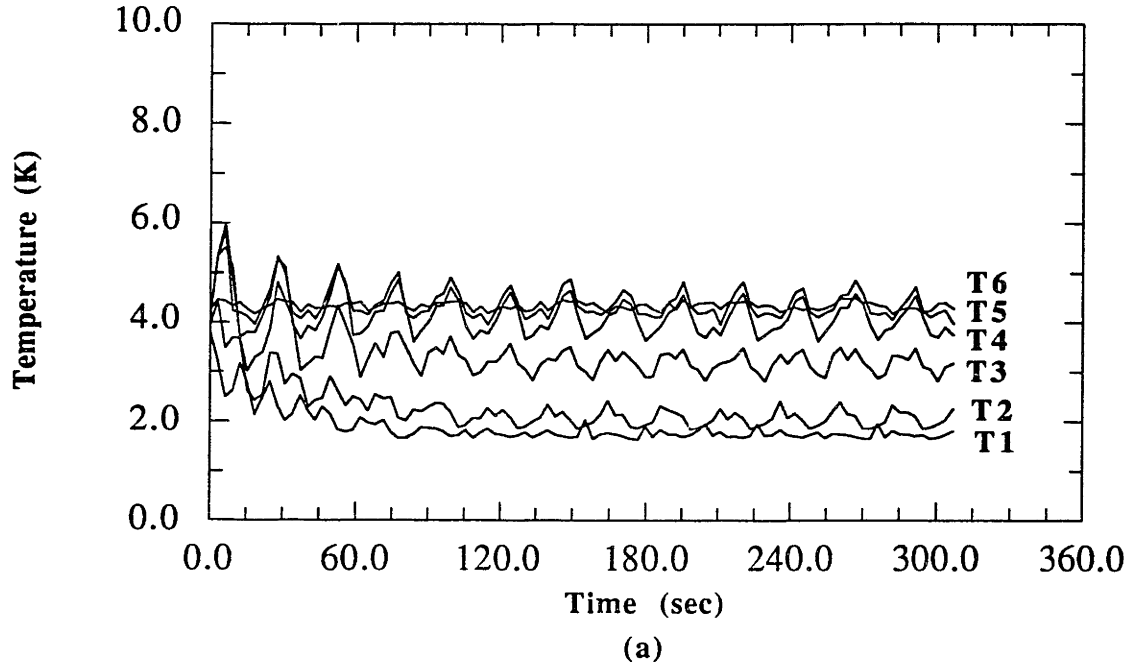

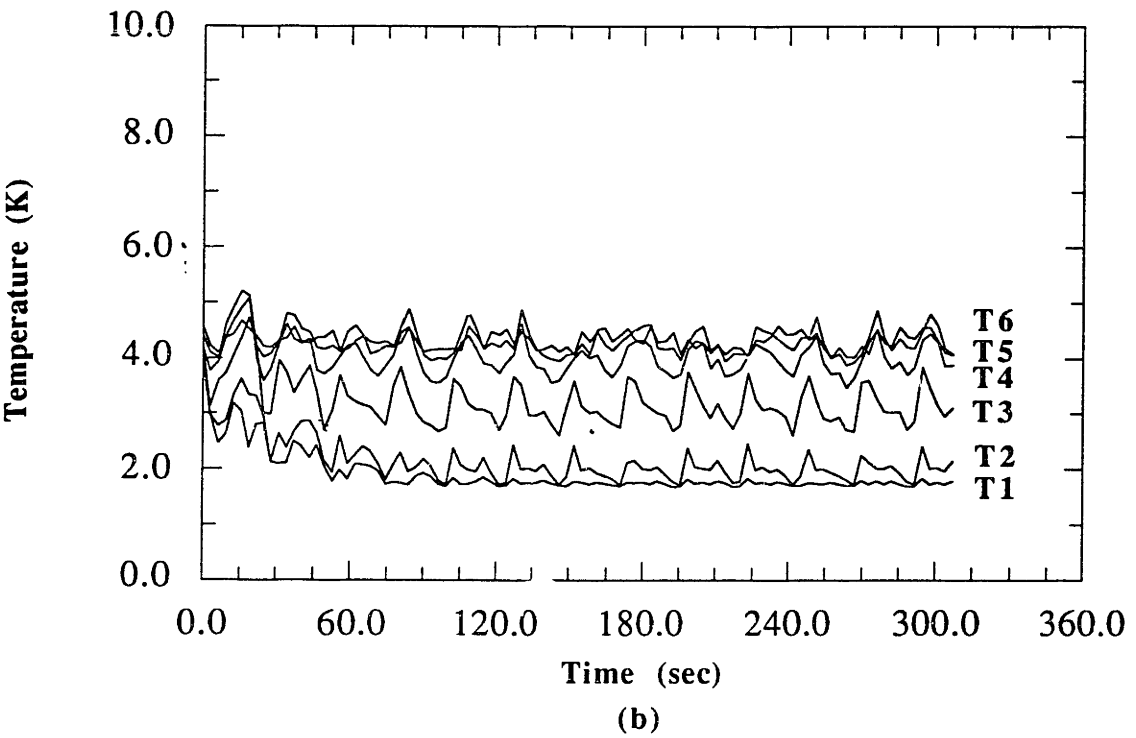

Fig. 5-2 Temperature data of He^3 inside the magnetic core at 46 Torr.
(a) Left core (b) Right core.

Thermodynamic efficiency

In order to calculate the thermodynamic efficiency of the magnetic refrigerator, the enthalpy flux method is used to estimate the rejection of heat to the 4.2 K reservoir.

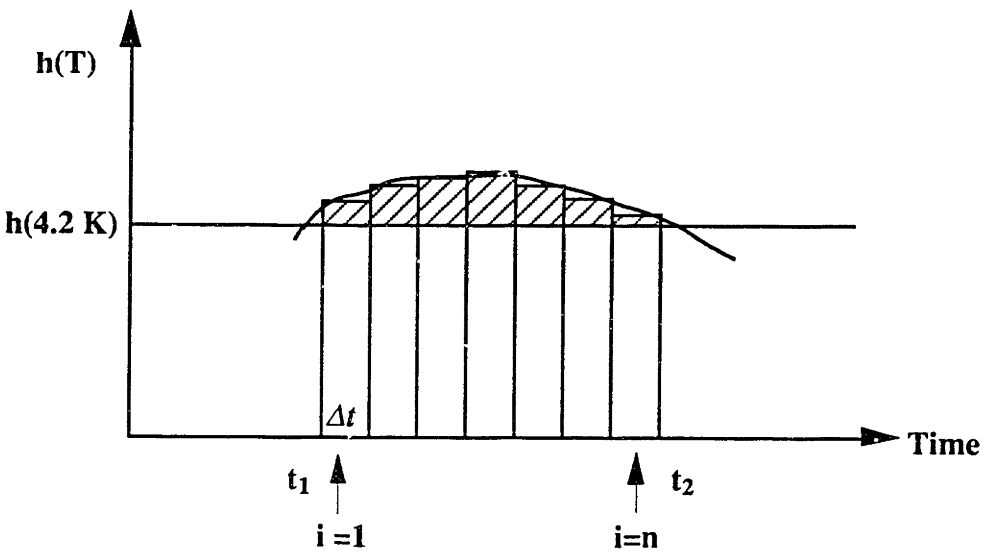

$$Q_h \approx \Delta m \times \sum_{i=1}^{n} [h_i(T) - h(4.2K)]$$

$$\approx \frac{\Delta m}{\Delta t} \cdot \int_{t_1}^{t_2} [h_i(T) - h(4.2K)]dt$$

Fig. 5-3 Enthalpy flux method to estimate the rejection heat to 4.2 K reservoir.

Figure 5-3 is the enthalpy trace of the experiment during flow magnetization process. The rejection heat to 4.2 K warm reservoir, Q_h, can be calculated by time integration of enthalpy difference during this process. Δm is an incremental mass of helium entering the warm-end heat exchanger over a time increment.

According to the temperature data of Figure 4-17,

$$Q_h = \frac{0.27\ \text{g}}{10\ \text{sec}} \times 27.9\ \text{J/g·sec}$$

$$= 0.75\ \text{J} \qquad (5.1)$$

Since the total cycle time is 24 seconds,

$$\eta_{carnot} = \frac{\frac{Q_c}{Q_h - Q_c}}{\frac{T_c}{T_h - T_c}} = \frac{24 \times 12.2\times10^{-3}}{\frac{2\times0.75 - 24 \times 12.2\times10^{-3}}{1.8}}{4.2 - 1.8}$$

$$= 0.24 \qquad (5.2)$$

It has a good agreement with the simulation result which is 25 % as shown in section 3.4. Note that this efficiency does not account for losses in the superconducting magnets.

Contamination of helium 3 space

The contamination of He^3 is a serious problem in the operation of the tandem magnetic refrigerator. If the system is heavily contaminated with any other gas than helium, the displacer cannot be operated because of the frozen contaminants in the small clearance (~ 0.03 mm) between the piston and cylinder wall. Therefore special attention was paid to eliminating leaks and evacuating the He^3 space for a long time. The final pressure of the He^3-space obtained after several days of pump-out was less than 5 mtorr. However, when the vacuum pump was stopped, the pressure at room temperature rose to about 20 mtorr after 10 minutes due to outgassing. Since the operating pressure of He^3 was about 40 torr, the He^3 space was virtually filled with 99.95 % of He^3 gas.

In order to reduce the outgassing rate, it is necessary to keep the step motor in the vacuum enclosure, from overheating. The outgassing rate of the step motor increases significantly with temperature. The cooling of the motor with cold water was thus indispensable and very effective.

Sphere vs. granule

Basically, the left magnetic core is composed of uniform 0.8 mm diameter GGG spheres, while the right core is filled with 18x25 mesh crushed GGG (Table 4-1). The difference of packing density results in a different amount of active magnetic refrigerant in the two core volumes. The performance of less packed magnetic core is expected to produce less refrigeration power than the packed one. The temperature data of the left and right core are

quite similar. There is no significant defect in the right core which contains irregular crushed GGG granules. However, the actual measurement of refrigeration power at 1.8 K shows that the irregular packed bed core generates only about 60 % of refrigeration generated by the uniform sphere core. Actually, the manufacturing cost difference between GGG sphere and crushed GGG is very large. About 70,000 GGG spheres were used to fill the left side core which costs about $20,000. On the other hand, for the right side core, GGG chunk was just crushed and filtered by the author. In consideration of its economical cost effectiveness, the crushed GGG is considered still very useful in many applications.

Experimental problems

Due to the cryogenic temperature, vacuum, and superconducting magnet operation, there have been many technical problems encountered before the successful experiment. Table 5-2 briefly summarizes those problems and remedies. Since these problems may also occur in other cryogenic fields, the following list should be helpful for those who design and construct similar cryogenic devices in the future.

Table 5-2 Experimental problem list and the solutions in constructing the tandem magnetic refrigerator.

No.	Problems	Remedies
1	Vacuum leakage at the joint between the core tube and the vacuum jacket	Stycast 2850FT is applied and penetrated.
2	Indium sealing for displacer at 4.2 K	A little oversized indium wire is better to fill the grove completely.
3	Vacuum pumping line leakage	Check the joints and resolder a weak joint.
4	Low vacuum pumping speed of He^3 space	Parallel connection of vacuum pumps.
5	Step motor outgassing	Bake out and evacuate for a long time (~5 days).
6	Crack in the cryogenic weld-mount hermetic connector	Replace it by welding again. Copper chill is absolutely necessary not to overheat the welding object.

Table 5-2 Experimental problem list and the solutions in constructing the tandem magnetic refrigerator (continued).

No.	Problems	Remedies
7	Cooling channel of step motor vacuum feed-thru	Make it flexible.
8	Warm end heat exchanger instrumentation wire passage	Use thermo-shrinkable tube to protect the sensor wire.
9	Super-joint and normal-joint in superconducting magnet	Test them separately before the main experiment.
10	Highly inductive load for bipolar power supply	Series connection of a resistor with magnet.
11	Making a small tolerance between phenolic shell and cylinder	Use a grinder in a lathe and avoid the measurement error by matching to a real counter part.
12	Air diffusion through the acrylic tube	Use glass instead of acrylic tube.
13	Off-roundness of Pyrex glass tube	Re-machine the metal part which contacts glass.
14	Noise problem in digital motor control circuit	Attach a small capacitor (~ 0.47 μF) across high and low terminals of each chip.
15	Noise problem in data acquisition	Use a shield wire and low pass filter in the amplifier.

VI. CONCLUSION

The thesis covers the design of a regenerative tandem magnetic refrigerator, the construction of a prototype and the experimental demonstration and measurement. The objective of this research was to develop a 1.8-K refrigerator by incorporating many innovative design concepts, which are: 1) the adoption of a tandem-mode operation, 2) use of He^3 as a heat transport medium, 3) GGG packed bed core (both spheres and crushed granules), 4) step motor operation in a vacuum enclosure, and 5) a combination of persistent- and variational-mode operation for the magnetic system.

Most importantly, the tandem magnetic refrigerator worked in a continuous mode, producing a maximum refrigeration power at 1.8 K of 12.2 mW with heat rejection at 4.2 K. The thermodynamic efficiency of the system is about 24 %, which is in good agreement with the simulation result. The simulation results were useful to verify important design parameters chosen for a prototype.

The key to developing a successful regenerative magnetic refrigerator is to minimize the following system irreversibilities by selection of optimum design parameters.

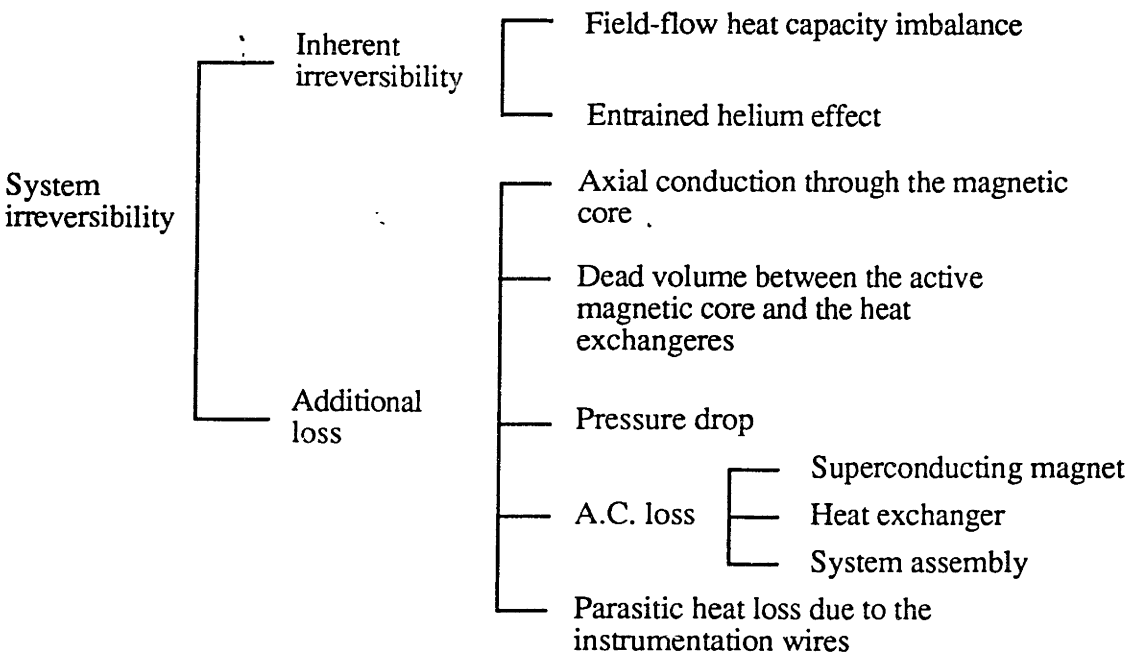

VII. NEW IDEA FOR NEXT DEVELOPMENT

This thesis shows that the tandem magnetic refrigerator that was designed operates successfully in the temperature range between 4.2 K and 1.8 K. However, increasing the temperature span of continuous magnetic refrigerators remains a challenge. As the possible improvements, two magnetic refrigerators of the next generation are discussed in this chapter.

7.1 Mixed magnetic refrigerant

The mixed magnetic refrigerant idea comes from the generic similarity between the magnetic refrigeration and the vapor compression refrigeration (Maytal, 1990 and Berntsson, 1985). The basic goal of the mixed magnetic refrigeration is to achieve a relatively uniform magneto-caloric effect over a broader temperature ranges. Since the magnetic entropy change of the material is large near its transition temperature, mixing two or more magnetic materials is a viable way to improve regenerative magnetic refrigerators.

Hashimoto *et al.* (1987) explore possibility of using complex magnetic materials as the magnetic refrigerant in an Ericsson magnetic refrigerator. Above 15 K, the ferromagnetic materials are attractive due to their high phase change temperatures. According to the theoretical results, the complex ferromagnetic refrigerant is suitable between 15 K and 30 K.

In the temperature range around 4.2 K, there is no doubt that GGG is the best magnetic refrigerant. However, since the magneto-caloric effect of GGG decreases as the temperature goes up above 10 K, other magnetic materials may have larger magneto-caloric effects than GGG. One of the promising substitutes for GGG is DAG ($Dy_3Al_5O_{12}$; Dysprosium Aluminum Garnet). Figure 7-1 shows the entropy-temperature diagrams of both GGG and DAG.

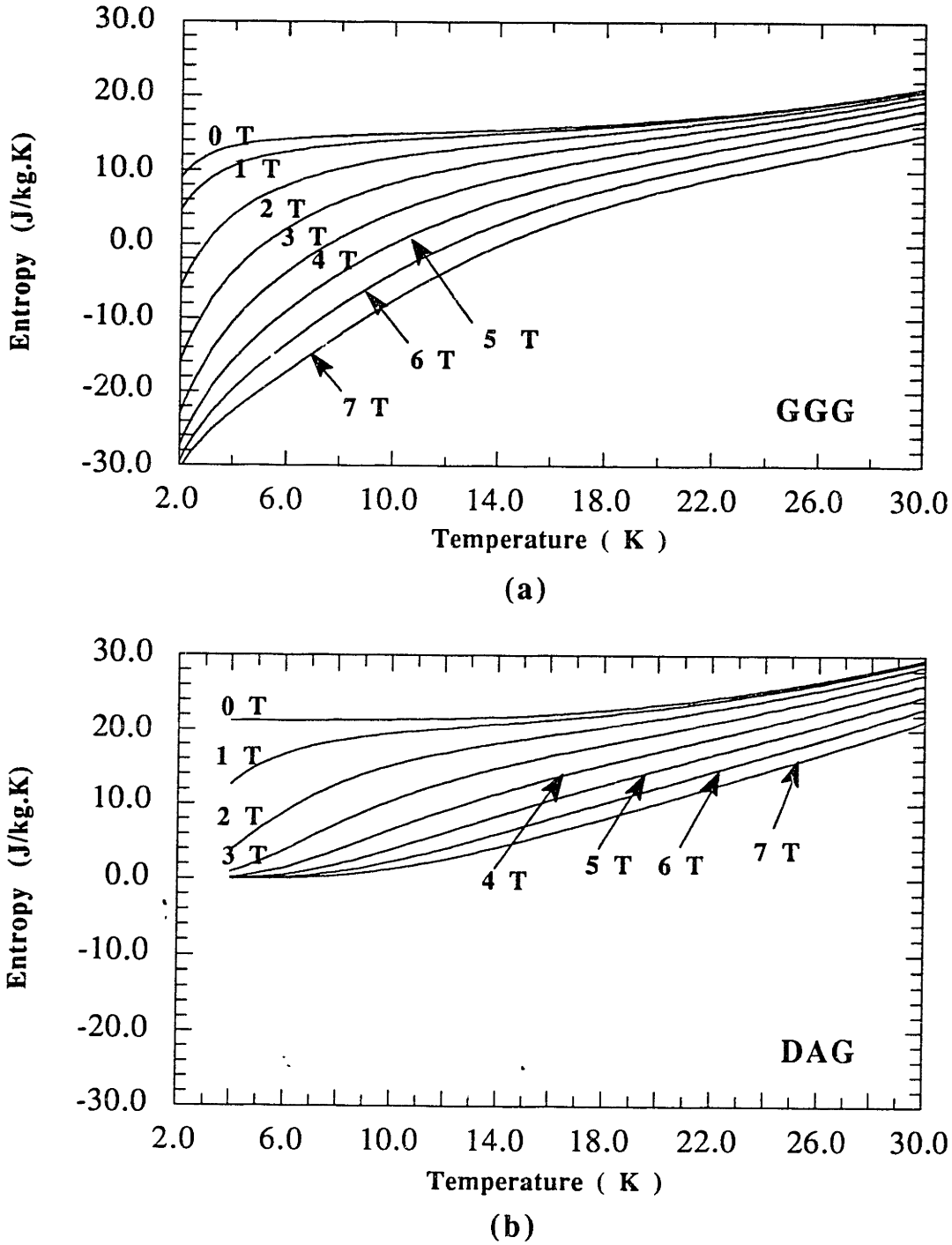

Fig.7-1 Entropy diagrams of GGG and DAG. (a) GGG (b) DAG.

If a regenerative magnetic refrigerator is to operate at 15 K at its warm end, it is desirable to use a mixed refrigerant of GGG and DAG The packed bed type magnetic core, which is

the current GGG core of the tandem magnetic refrigerator, can easily adopt the mixing characteristic. Figure 7-2 shows a suggested material distribution for a regenerative magnetic refrigerator operating between 1.8 K and 15 K. A gradual composition change of the packed bed core, from purely GGG to purely DAG along the temperature coordinate, avoids an abrupt step transition.

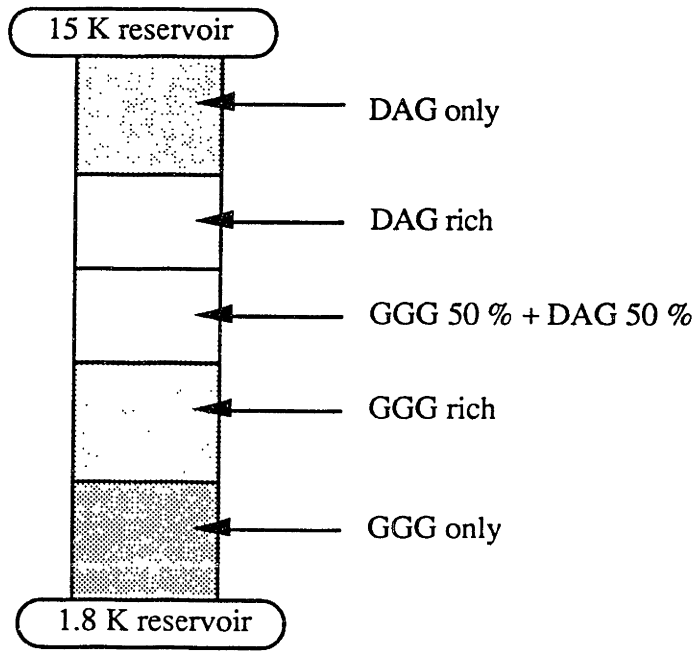

Fig.7-2 GGG to DAG transition in the regenerative magnetic core.

The exact composition variation needs more analysis through computer simulation. The heat capacity balance between the mixed magnetic refrigerant and heat transport medium is still the key to the successful operation of the system.

7.2 Combination with G-M cryocooler

Since the magnetic refrigerator generally works well in low temperature ranges (< 4.2 K) with a small temperature span, it needs an additional cooling mechanism for its warm end reservoir. A reliable Gifford-McMahon cryocooler is one practical way. This cascade connection is called " *the external combination* " of the magnetic refrigerator with a gas refrigerator. On the other hand, " *the internal combination* " between magnetic and gas refrigerator is possible. Figure 7-3 is the conceptual design of such a device operating between 300 K and 1.8 K.

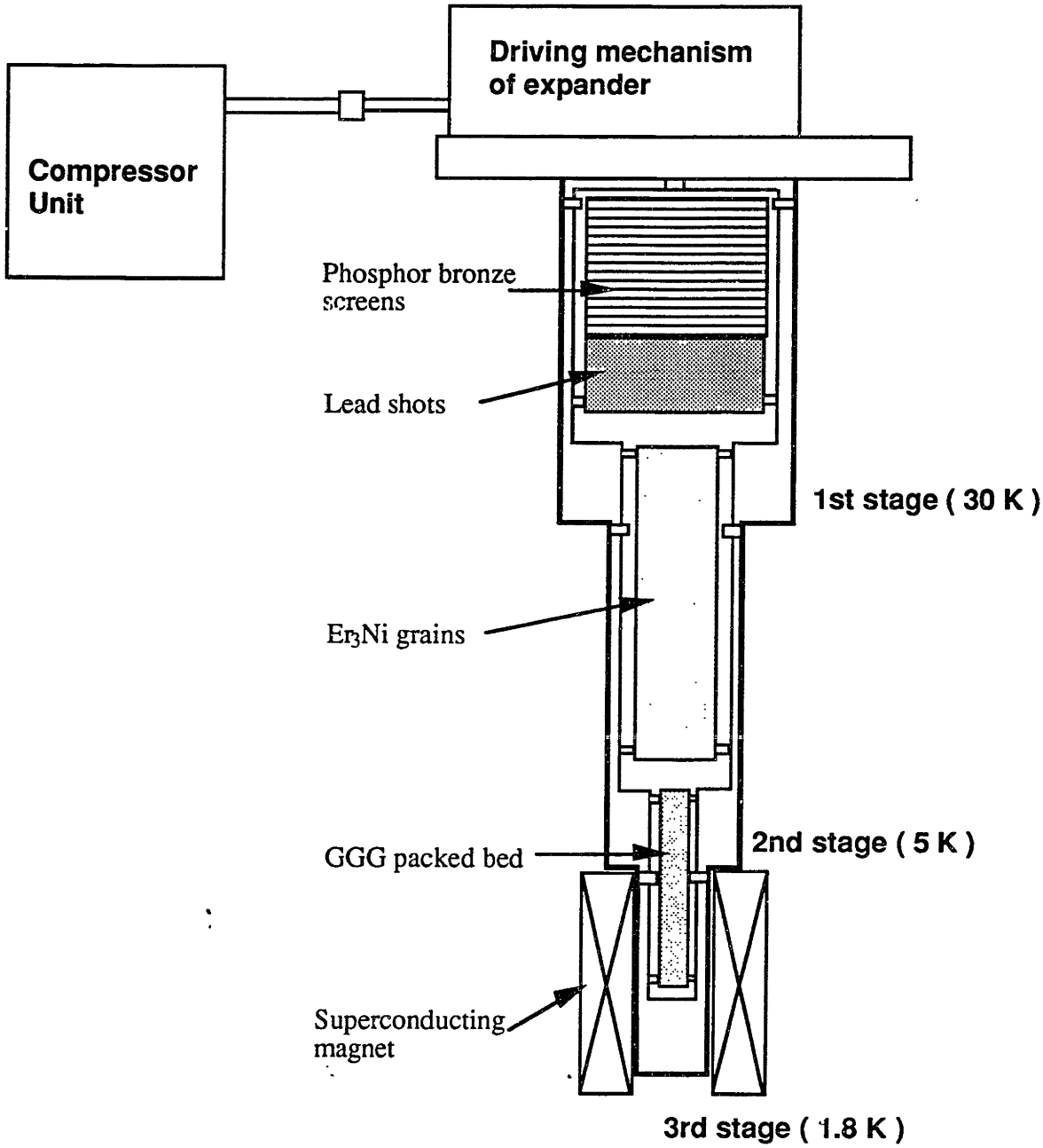

Fig.7-3 Schematic of magnetic G-M cryocooler.

This idea comes from the attractiveness of using a magnetic material as a regenerator material for G-M cryocoolers. It is reported that some magnetic materials such as Er_3Ni, GdRh, and ErRh have higher volumetric specific heat than that of lead, which is a usual regenerator material (Takashi et al., 1990).

Since the specific heat of a typical magnetic material shows a high peak near its transition temperature and can be varied by applied magnetic field, it is possible to use GGG as a low temperature magnetic regenerator in the last stage of a G-M cryocooler . As shown in Figure 7-3, each stage has a different regenerator material. The magnetic field in the third stage enhances the regenerator characteristic of GGG.

This operation of the magnetic G-M cryocooler is as the followings.

Process 1-2

With the displacer at the bottom of the cylinder, the inlet valve is opened and the pressure within the upper expansion space and the regenerator is increased from a low pressure P1 to a high pressure P2. GGG is adiabatically demagnetized from a high field H1 to a medium field H2.

Process 2-3

With the inlet valve still open and the exhaust valve closed, the displacer is moved to the top of the cylinder. This action moves the gas which was originally in the upper expansion space down through the regenerator to the lower expansion space. During this process, GGG is continuously demagnetized to 0 tesla. This magnetic process is equivalent to the flow demagnetization process. Since the gas is cooled as it passes through the regenerator, it will decrease in volume so that gas will be drawn in through the inlet valve during this process to maintain a constant pressure within the system.

Process 3-4

With the displacer at the top of the cylinder, the inlet valve is closed and the exhaust valve is opened, thus allowing the gas within the lower expansion space to expand to the initial pressure P1. This causes the gas in the lower expansion space to drop to a low temperature. GGG is magnetized up to a medium field H2. The exhaust gas takes thermal energy of magnetized GGG out of the system.

Process 4-1

With the exhaust valve still open, the displacer is moved to the bottom of the cylinder. This action moves the gas up through the regenerator to the upper expansion space. GGG is continuously magnetized up to a high field H1, which is equivalent to the flow

magnetization process. During this process, the warm magnetized GGG is cooled by the up-flow gas and the low pressure gas is compressed again, returning to process 1-2.

There are some practical problems in this combined refrigerator.

- Gas (typically helium) entrainment effect in the third regenerator at high pressure.
- Fast charging and discharging the magnet for synchronization with the cycle frequency of G-M cycle, which is typically about 0.5 Hz.
- Liquefaction in the bottom of the system , unless He^3 gas is used for the working medium.
- Large force to move GGG inside the strong magnetic field.

In this chapter, two advanced ideas of regenerative magnetic refrigerators are briefly discussed. These ideas, even though not obviously practical, should be applicable for next-generation magnetic refrigerator of the future.

REFERENCES

Barclay, J.A., 1986, "Magnetic Refrigeration : A Review of a Developing Technology," *Advances in Cryogenic Engineering*, Plenum Press, New York, Vol.32, pp.719-731.

Barclay, J.A., Stewart, W.F., Overton, W.C., and Candler, R.J., 1985, "Experimental Results on a Low-Temperature Magnetic Refrigerator," *Advances in Cryogenic Engineering*, Plenum Press, New York, Vol.31, pp.743-752.

Barclay, J.A. and Steyert, W.A., 1982, "Materials for magnetic refrigeration between 2 K and 20 K," *Cryogenics*, Vol.22, pp.73-80.

Bejan, A., 1984, *Convection heat transfer*, John Wiley & Sons, Inc., New York, pp.343-416.

Benedict, R.P., 1984, *Fundementals of temperature pressure, and flow measurements*, 3rd ed. John wiley & Sons, pp.375-391.

Berntsson, K.M. and Berntsson, T., 1985, "Large heat pumps with nonazeotropic mixtures as working fluids - some results from computer simulations," *Proceedings of the meetings of refrigeration science and technology.*, pp.31-39.

Brown, G.V., 1976, "Magnetic heat pumping near room temperature," *J. Appl. Phys.*, Vol.47, No. 8, pp.3673-3680.

Chan, C.K., 1981, "Cryogenic refrigeration using a low temperature heat source," *Cryogenics*, Plenum press, pp.391-399.

Cheng, P., 1978, "Heat transfer in geothermal systems," *Advances in Heat transfer*, Vol.14, pp.1-105.

Cogswell, F.J., Smith,Jr., J.L., and Iwasa, Y., 1988, "Regenerative Magnetic Refrigeration over the Temperature Range of 4.2 K to 15 K," *Proceedings of the Fifth International Cryocoolers Conference*, pp.81-90.

Collins, S.C., and Zimmerman, F.J., 1953, "Cyclic Adiabatic Demagnetization," *Phys. Rev.*, Vol.90, pp.991-992.

Daudin, B., Lacaze, A.A., and Salce, B., 1982, "$DyVO_4$-$Gd_3Ga_5O_{12}$: A composite material to achieve magnetic refrigeration using a cycle with internal heat transfer," *Cryogenics*, Vol.22, pp.439-450.

Daudin, B., Lagnier, R., and Salce, B., 1981, "Thermal properties of rare earth vanadates and arsenates with a view to magnetic refrigeration applications," *Journal of Magnetism and Magnetic Materials*, Vol.25, pp.197-200.

Delpuech, C., Berangerk, R., Bon Mardion, G., Claudet, G., and Lacaze, A.A., 1981, "Double acting reciprocating magnetic refrigerator: first experiments," *Cryogenics*, Vol.21, pp.579-584.

Flood, D.J., 1974, "Magnetization and magnetic entropy of $Dy_2Ti_2O_7$," *J. Appl. Phys.*, Vol.45, No. 9, pp.4041-4044.

Gallagher, G.R., 1986, "Analysis of a Magnetically Active Regenerator," M.S.Thesis, Dept. of Mech. Eng., Massachusetts Institute of Technology, Cambridge, MA.

Gibbons, R.M. and Nathan, D.I., 1967,"Thermodynamic data of Helium-3," *Technical report AFML-TR-67-175.*

Hakuraku, Y. and Ogata, H., 1985, "A Static Magnetic Refrigerator for Superfluid Helium with New Heat Switches and a Superconducting Pulse Coil," *Japanese Journal of Applied Physics*, Vol.24, No.11, pp.1538-1547.

Hashimoto, T., Kuzuhara, T., Sahashi, M., Inomata, K., Tomokiyo, A., and Yayama, H., 1987, "New application of complex magnetic materials to the magnetic refrigerant in an Ericsson magnetic refrigerator," *J. Appl. Phys.*, Vol.62, No. 9, pp.3873-3878.

Hashimoto, T., 1986, "Recent Investigation on Refrigerants for Magnetic Refrigerators," *Advances in Cryogenic Engineering*, Plenum Press, New York, Vol.32, pp.261-270.

Hashimoto, T., Matsumoto, K., Kurihara, T., Numazawa, T., Tomokiyo, A., Yayama, H., Goto, T., Todo, S., and Sahashi, M, 1986, "Investigations on the possibility of the RAl_2 system as a refrigerant in an Ericsson type magnetic refrigerator," *Advances in Cryogenic Engineering*, Plenum Press, New York, Vol.32, pp.279-286.

Hakuraku, R., and Ogata, H., 1985, "A static magnetic refrigerator for superfluid helium with new heat switches and a superconducting pulse coil," *Japanese Journal of Applied Physics,* Vol.24, No.11, pp.1538-1547.

Haus, H.A., and Melcher, J.R., 1989, *Electromagnetic fields and energy*, Prentice-Hall.

Helvensteijn, B.P.M., Kashani, A., and Wilcox, R.A., 1990, "Activated carbon test assembly," *Proceedings of the Sixth International Cryocoolers Conference*, Vol.II, pp.103-113.

Hildebrand, F.B., 1976, *Advanced calculus for applications,* 2nd ed., Prentice-Hall, Inc., pp.141-151.

Hopkins, R.A., Lee, J.H., Oonk, R.L., Miller, C.D., and Nieczkoski, S.J., 1990, "Long-life time stored cryogen systems using refrigerators to reduce parasitic heat input," *Proceedings of the Sixth International Cryocoolers Conference*, Vol.II, pp.153-171.

Jeong, . and Smith, D., 1990, *Allen-Bradley 47 Ω 1/8 W resistor calibration for temperature sensors between 4.2 K and 1.5 K*, Progress Report, M.I.T.

Karam Jr., J.T., and Leonard, R.G., 1973, "A simple yet theoretically based time domain model for fluid transmission line systems," *Trans. ASME, J. Fluid engineering*, pp.498-504.

Kays, W.M., and London, A.L., 1964, *Compact heat exchangers*, 2nd ed., McGraw-Hill, Inc., New York, pp.131-132.

Kittel, P., 1990, "Eddy current heating in magnetic refrigerators," *Advances in Cryogenic Engineering*, Plenum Press, New York, Vol.35, pp.1141-1148.

Matsumoto, K., Ito, T., and Hashimoto, T., 1986, "An Ericsson magnetic refrigerator for low temperature," *Advances in Cryogenic Engineering*, Plenum Press, New York, Vol.32, pp.743-750.

Maytal, B., Van Sciver, S.W., and McMahon, P.D., 1990, "Thermodynamic analysis of mixed fluid Joule-Thomson cryocoolers," *Proceedings of the Sixth International Cryocoolers Conference*, Vol.II, pp.111-135.

McAdams, W.H., 1954, *Heat transmission*, 3rd ed, McGraw-Hill, New York.

Li, R., Numazawa, T., Hashimoto, T., Tomokiyo, A., Goto, T., and Todo, S., 1986, "Magnetic and thermal properties of $Dy_3Al_5O_{12}$," *Advances in Cryogenic Engineering*, Plenum Press, New York, Vol.32, pp.287-294.

Nakagome, H., Tanji, N., Horigami, O., Ogiwara, H., Numazawa, T., Watanabe, Y., and Hashimoto, T., 1984, "The Helium Magnetic Refrigerator I. : Development and Experimental Results," *Advances in Cryogenic Engineering*, Plenum Press, New York, Vol.29, pp.581-587.

Rohsenow, W.M., Hartnett, J.P., and Ganic, E.N., 1985, *Handbook of heat transfer applications*, 2nd ed., Chapter 11.

Roth, A., 1978, *Vacuum technology*, North-Holland Publishing company, New York, pp.170-183.

Sample, H.H., and Neuringer, L.J., 1974, "Low temperature thermometry in high magnetic fields. IV. Allen - Bradley carbon resistors (0.5 - 4.2 K)," *Rev. Sci. Instrum.*, Vol.45, No.11, pp.1389-1391.

Smith Jr., J.L., 1966, "The presentation of heat-transfer and friction factor data for heat exchanger design," *ASME 66-WA/HT-59*.

Sydoriak, S.G., Roberts, T.R., and Sherman, R.H., 1964, "The 1962 He^3 Scale of Temperatures, II. Derivation," *Journal of Research of the NBS-A*, Vol.68A, No.6, pp.559-565.

Takashi, I., Nagao, M., and Yoshimura, H., 1990, "Two-stage Gifford-McMachon cycle cryocooler operating at about 2 K," *Proceedings of the sixth International Cryocoolers Conference*, Vol.II, pp.25-36.

Taussig, C.P., Gallagher, G.R., Smith,Jr., J.L.,and Iwasa, Y., 1986, "Magnetic Refrigeration Based on magnetically Active Regeneration," *Proceedings of the Fourth International Cryocoolers Conference*, pp.79-88.

Tomokiyo, A., Yayama, H., Wakabayashi, H., Kuzuhara, T., Hashimoto, T., Sahashi, M., and Inomata, K., 1986, "Specific heat and entropy of RNi_2 (R : Rare earth heavy metals) in magnetic field," *Advances in Cryogenic Engineering*, Plenum Press, New York, Vol.32, pp.295-301.

Van Sciver, S.W., 1986, *Helium cryogenics*, Plenum Press, pp.335-347.

Wilson, M.N., 1983, *Superconducting magnets*, Clarendon Press, Oxford.

Zimm, C.B., Barclay, J.A., and Johanson, W.R., 1984, "Low hysteresis materials for magnetic refrigeration : $Gd_{1-x}Er_xAl_2$," *J. Appl. Phys.*, Vol.55, No. 6, pp.2609-2610.

Zimmerman, J.E., McNutt, J.D., and Bohm, H.V., 1962, "A magnetic refrigerator employing superconducting solenoids," *Cryogenics*, Vol.2. No.3, pp.153-159.

Appendix A. Construction of the superconducting magnet

This appendix describes the procedure for constructing two tandem superconducting magnets used in the regenerative magnetic refrigerator.

A.1 Design constraints

The design of the superconducting magnet is constrained by the geometric compatibility as well as the electric requirements.

- Maximum magnetic field : 3 tesla
- Maximum operating current : 15 A
- Magnet bore size : 2.86 cm (1.125 inch)
- Uniform magnetic field region length at center : 10 cm
- Outer diameter of the magnet : 8.4 cm

The most important electrical design constraint is the low input current; the magnet should be able to produce 3 tesla over all of the magnetic core with only 15 A. The primary purpose for keeping the low current is to use a moderate size bipolar power supply. The other important constraint is the size of the system assembly, which has to fit in a cryostat. Figure 4-1. shows the compactness of the system assembly.

A.2 Field design

The design concept of this superconducting solenoid magnet is to provide uniform magnetic field over the entire magnetic core region and to reduce the edge field as much as possible. In given design constraints, the dimensions of primary coil, secondary coil, and inverse coil are determined iteratively by using "SOLDESIGN", a numerical software written exclusively for solenoid design in the Francis Bitter National Magnet Laboratory of MIT.

After an appropriate superconducting wire is selected, which will be discussed in the next section, the detailed field, inductance, and force calculations are performed. Figures A-1 ~ A-3 show the field calculation results when the magnet is energized with 15 A.

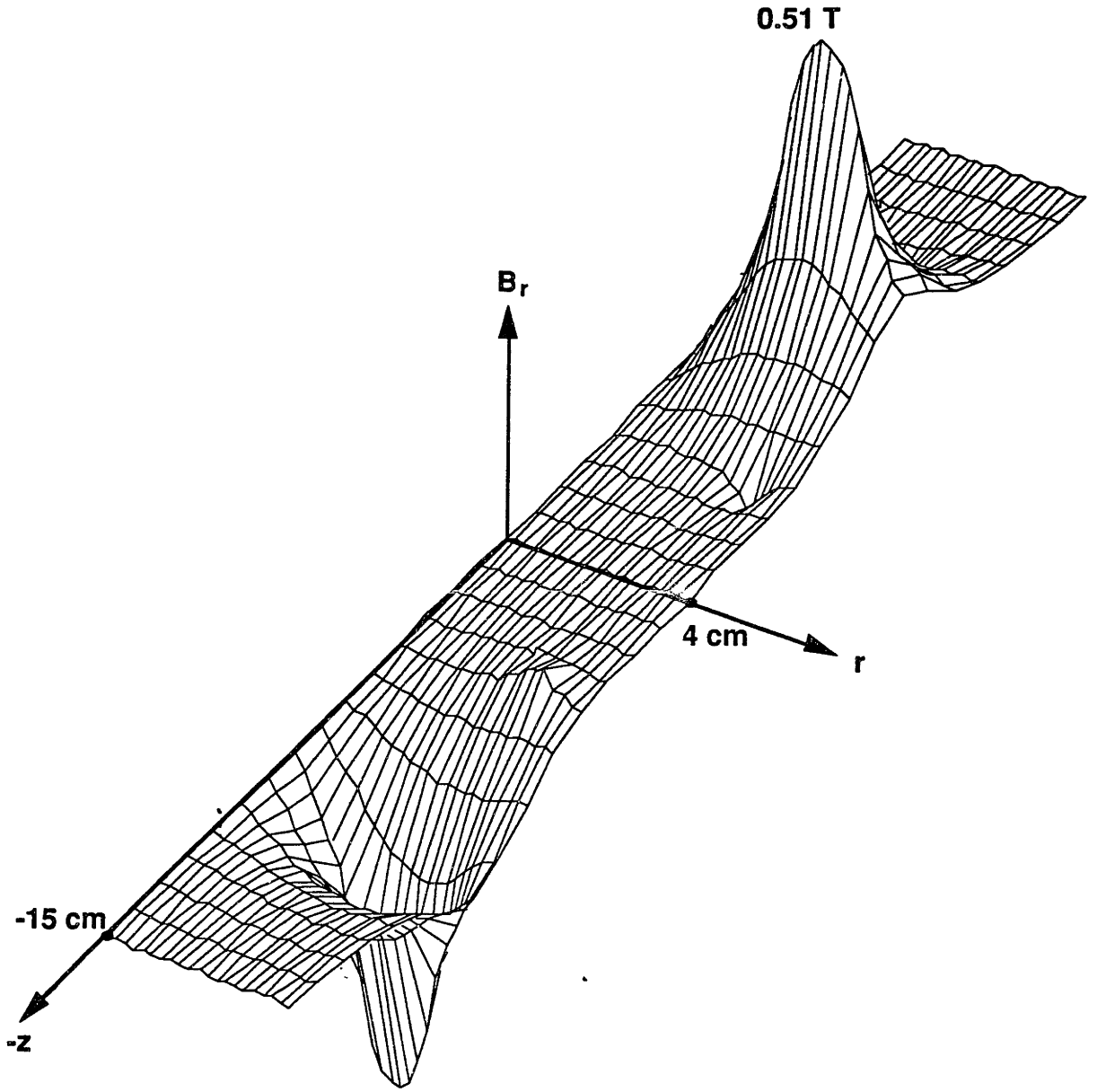

Fig. A-1 Radial component of the magnetic field calculation.

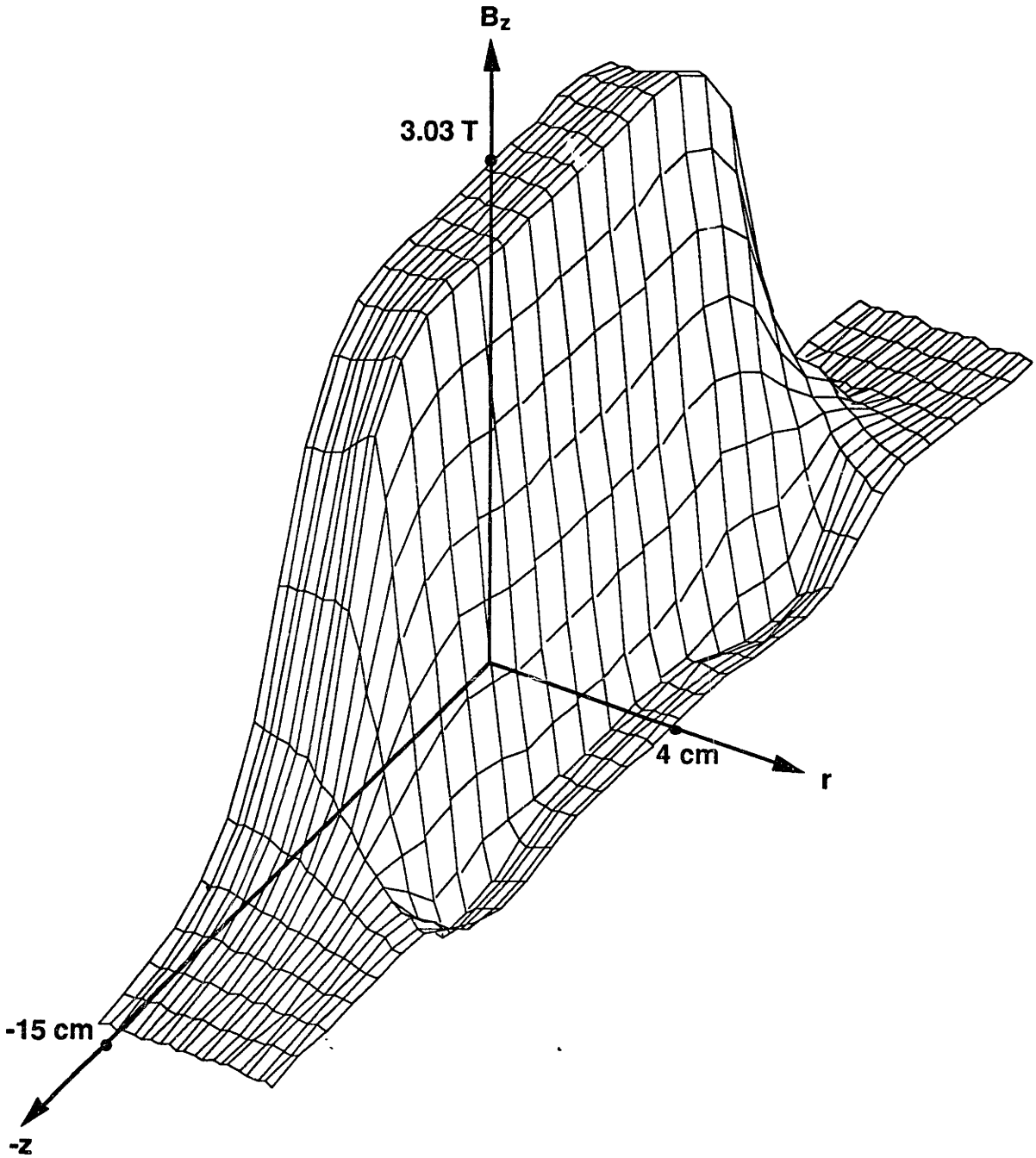

Fig. A-2 Axial component of the magnetic field calculation.

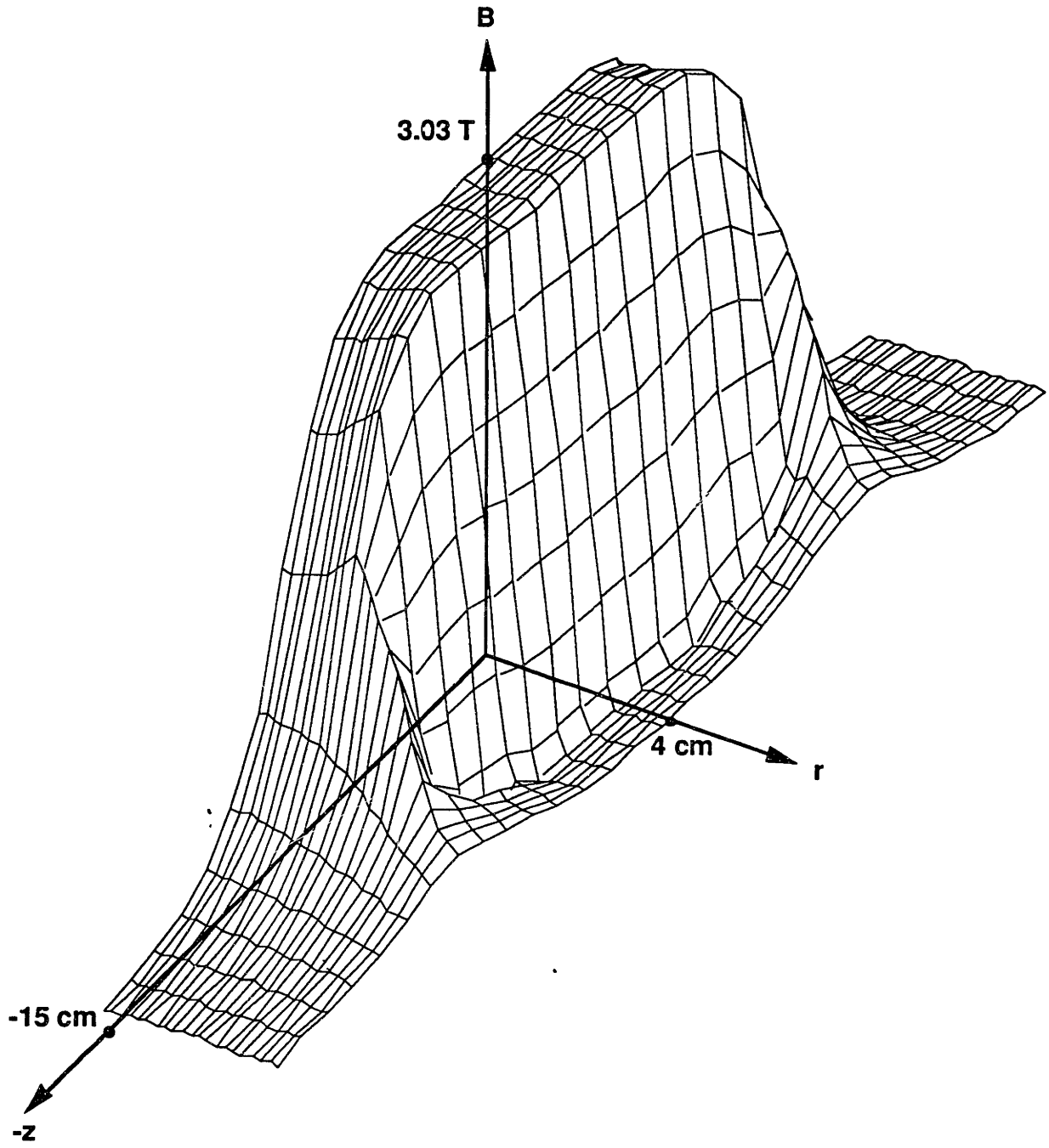

Fig. A-3 Total magnetic field calculation.

The magnet center is at r = 0 and z = 0, the total magnetic field in the magnetic core region $(0 \leq r \leq 1.1$ cm and -4.6 cm $\leq z \leq 4.6$ cm$)$ is quite uniform with the value of 3.0 ± 0.04 tesla.

A.3 Magnet coil winding

Winding the magnet coil is one of the most important works in construction of the magnetic refrigerator. Among commercially available superconducting wires, 54S33 wire from Supercon Inc. was chosen for the winding. It consists of 54 individual superconducting filaments embedded in a copper matrix. The superconducting alloy is T48: niobium and 48 % titanium. The copper:superconductor ratio is 2:1. The individual T48 filaments are 17 μm diameter. The superconducting wire diameter including formvar insulation (0.015 mm thick) is 0.28 mm. Each superconducting wire layer is also separated by several 0.05 mm thick and 6.35 mm wide mylar tapes. As shown in Figure A.4, these axial directional mylar tape layers provide cooling channels for liquid helium, which maintain all parts of the magnet at 4.2 K.

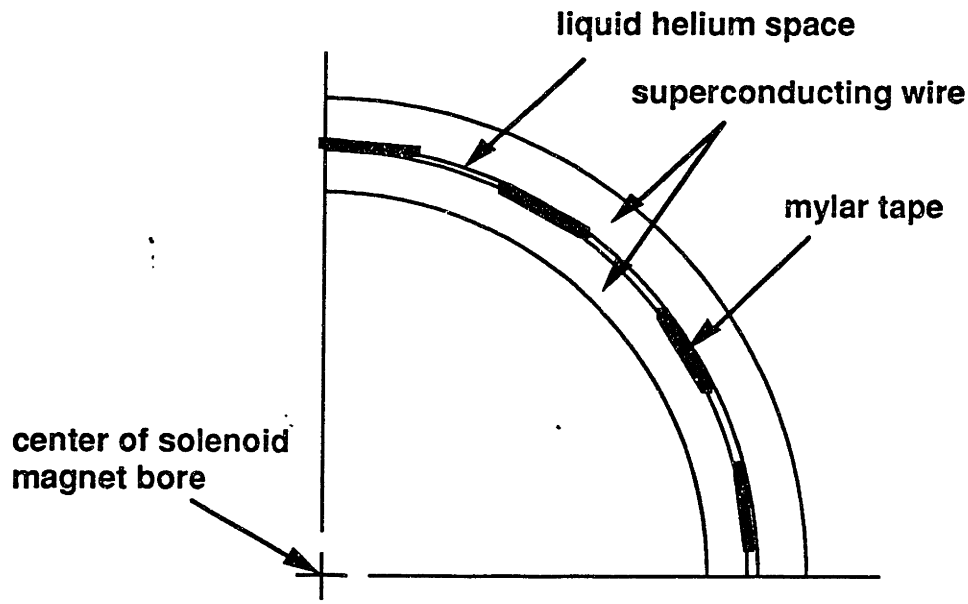

Fig. A-4 Liquid helium cooling channel in the superconducting magnet.

The magnet spool and structure is built with G-10 (Glass fiber reinforced plastic). In order to get a good liquid helium flow passage, both ends of the spool are drilled with 36 evenly spaced 6.35 mm diameter holes.

The winding configuration is analyzed for thermal stability. For a good cryogenic stabilized magnet, the local heat generation flux in the magnet should be smaller than the critical boiling heat flux of liquid helium. For the estimated A.C. loss value for one magnet of about 8 J/cycle, which will be described in detail in the section A.4, the average heat flux is,

$$\begin{aligned} \bar{q} &= \frac{\text{A.C.losses / Cycle period}}{\text{Surface area of superconducting wire}} \\ &\approx \frac{8/12}{\pi \times (0.28 \times 10^{-3}) \times (4136)} \\ &= 0.18 \ \text{W/m}^2 \\ &= 1.8 \times 10^{-5} \ \text{W/cm}^2 \end{aligned} \tag{A.1}$$

Even though only half of the area of the superconducting wire is assumed to be exposed directly to liquid helium, this heat flux value is much smaller than the critical boiling heat flux of liquid helium ($\approx 0.5 \sim 1$ W/cm^2). Thus, the cooling requirement is sufficiently satisfied for thermal stability.

The hoop stress in thin superconducting wire resulting from the magnetic force may cause a structural problem. By assuming that each coil turn acts independently without influencing its neighbors, the hoop stress can be calculated easily (Wilson, 1983). Within the winding of a solenoid, the variation of axial field with radius may usually be approximated to a fair accuracy by a linear fall-off from B_a at the inner radius a to B_b at the outer radius b, *i.e.*

$$B = \frac{(b - r)B_a + (r - a)B_b}{(b - a)} = \frac{(\alpha - \varepsilon)B_a + (r - 1)B_b}{(\alpha - 1)} \tag{A.2}$$

where $\varepsilon = r/a$ and $\alpha = b/a$.

For the special case of an infinite solenoid, $B_b = 0$ and $B_a = \mu_o J(b-a)$ so that

$$\sigma_\theta = B J r = \frac{B_a^2 (\alpha-\varepsilon)\varepsilon}{\mu_0 (\alpha-1)^2} \tag{A.3}$$

The maximum hoop stress, occurring when $\varepsilon = \frac{\alpha}{2}$, is ;

$$(\sigma_\theta)_{max} = \frac{B_a^2 \quad \alpha^2}{2\mu_0 2(\alpha-1)^2} \tag{A.4}$$

With the real design values for the magnet;

$a = 15.9\ mm$
$b = 31.1\ mm$
$\alpha = b/a = 31.1/15.9 = 1.96$
$J = 18423$ A/cm^2

The maximum hoop stress is calculated as follows,

$$\begin{aligned}
(\sigma_\theta)_{max} &= \frac{B_a^2 \quad \alpha^2}{2\mu_0 2(\alpha-1)^2} \\
&= \frac{[\mu_0 J(b-a)]^2 \quad \alpha^2}{2\mu_0 \quad 2(\alpha-1)^2} \\
&= \frac{\left[4\pi\times10^{-7}\times18423\times10^4\times(31.1-15.9)\times10^{-3}\right]^2}{2\cdot4\pi\times10^{-7}} \cdot \frac{(1.96)^2}{2(1.96-1)^2} \\
&= 1.03 \times 10^7 \text{ N/m}^2 \\
&= 10.3 \text{ MPa}
\end{aligned} \tag{A.5}$$

This value is much smaller than the reasonable working maximum allowable stress, for NbTi composite which is 500 MPa. Therefore the applied hoop stress is within the design requirement.

A.4 A.C. losses

A.C. losses are resistive losses occurring in the magnet due to A.C. fields. The changing magnetic field generates an e.m.f. within the superconductor which locally drives the current density beyond its critical value.

The primary A.C. loss is due to hysteresis, which is independent of the cycle time. The secondary loss is due to eddy current loss associated with the current coupling phenomena in superconductor-normal conductor geometry. This eddy current loss, unlike hysteresis loss, depends on the cycle time.

For the large ratio of the maximum field to the penetration field, the hysteresis loss can be estimated by the following formula. (Wilson, 1983)

$$Q_h = \frac{8}{3\pi} a J_{C0} B_0 \left\{ \frac{B_m + B_0}{B_m} \ln\left(\frac{B_m + B_0}{B_0}\right) - 1 \right\}, \qquad \text{(A.6)}$$

where B_m is the maximum magnetic field, J_{C0} and B_0 are constants in high field superconductor model of Kim and Anderson, *i.e.*, $J_c(B) = \frac{J_{C0} B_0}{(B + B_0)}$, a is the filament radius.

For the designed superconducting magnet,

$$Q_h = \frac{8}{3\pi} \cdot 8.5 \times 10^{-6} \cdot 2.0 \times 10^{10} \cdot 0.71 \cdot \left\{ \frac{3.0 + 0.71}{3.0} \cdot \ln\left(\frac{3.0 + 0.71}{0.71}\right) - 1 \right\}$$

$$= 107104 \text{ J/cycle·m}^{-3} \qquad \text{(A.7)}$$

In this calculation, it is assumed that the magnet is composed of single coil and the field varies linearly over the winding, *i.e.*, each field interval between zero and the maximum amplitude B_m occupies an equal volume of winding.

Since the total superconductor volume is,

$$\lambda V = 0.33 \times \frac{\pi}{4} \times (d_w)^2 \times l_w$$

$$= 0.33 \times \frac{\pi}{4} \times \left(0.25 \times 10^{-3}\right)^2 \times 4136$$

$$= 6.7 \times 10^{-5} \text{ m}^3, \qquad \text{(A.8)}$$

where λ is the fraction of NbTi in the magnet wire. The resultant hysteresis loss for one magnet is,

$$Q_h \lambda V = 107104 \times 6.7 \times 10^{-5}$$

$$= 7.2 \text{ J/cycle.} \qquad \text{(A.9)}$$

The superconducting wire is usually manufactured in the form of filamentary composites and the filaments in such composites are coupled together by changing fields. The extra losses associated with this coupling current are eddy current losses, which depend on the cycle time. To reduce this coupling effect, the filamentary superconducting composites are always twisted. For the case of uniform field changing rate where the time T_m for the field to rise to B_m is long compared with the characteristic time τ. The eddy current loss per unit volume per cycle is calculated as follows (Wilson, 1983),

$$Q_e = \frac{B_{ml}^2 \delta \tau}{2\mu_0 T_m} \tag{A.10}$$

where B_{ml} is the averaged local field amplitude, and $\tau = \frac{\mu_0}{2\rho_e}\left(\frac{L}{2\pi}\right)^2$; the natural time constant of the eddy current system. L is the twist pitch of the superconducting filaments, $\rho_e = \rho_m \frac{1+\lambda}{1-\lambda}$; the effective resistivity of the matrix, and ρ_m is the matrix resistivity.

For the designed magnet, the effective resistivity is,

$$\begin{aligned} \rho_e &= \rho_m \frac{1+\lambda}{1-\lambda} \\ &= 3\times 10^{-10} \times \frac{1+0.33}{1-0.33} \\ &= 6.0\times 10^{-10}\ \Omega.\text{m} \end{aligned} \tag{A.11}$$

Therefore, the natural time constant is

$$\begin{aligned} \tau &= \frac{\mu_0}{2\rho_e}\left(\frac{L}{2\pi}\right)^2 \\ &= \frac{4\pi\times 10^{-7}}{2\times 6.0\times 10^{-10}}\left(\frac{12.7\times 10^{-3}}{2\pi}\right)^2 \\ &= 0.0043 \text{ sec.} \end{aligned} \tag{A.12}$$

$$\therefore\ Q_e = \frac{B_{ml}^2}{2\mu_0} \cdot \frac{8\tau}{T_m}$$

$$= \frac{\frac{1}{3}\times(3.0)^2}{2\times 4\pi\times 10^{-7}} \cdot \frac{8\times 0.0043}{6}$$

$$= 6860 \text{ J/cycle}\cdot\text{m}^3. \qquad \text{(A.13)}$$

The resultant eddy current loss for one magnet is,

$$Q_e\lambda V = 6860\times 6.7\times 10^{-5}$$

$$= 0.46 \text{ J/cycle.} \qquad \text{(A.14)}$$

According to the above analysis, the total A.C. losses of the designed magnet is about 7.7 J/cycle. Since the hysteresis is the primary cause of the A.C. loss, using a thin superconducting filament composite wire such as 5 μm in diameter which is commercially available in magnet wire, can greatly reduce the total A.C. losses.

Besides the A.C. losses, there are another two parasitic heat losses in superconducting magnet operation; Joule heating loss and axial conduction loss which occur in current leads. Even though the current lead wire size could be optimized according to the magnet operation condition (Wilson, 1984), 9.5 mm diameter vapor-cooled current leads were used just for their availabilities. As a result, Joule heating loss is negligible (order of 1 mW), but the conduction loss (about 0.5 mW) is comparable to the A.C. losses of the magnet when it is operated with the cycle period of 12 seconds.

A.5 Persistent-current loop construction

Theoretically if the superconducting magnet operates in d.c. mode, it requires no energy to maintain the constant magnetic field. The external power supply is only needed to raise or lower the operating current. In general, when a magnet is intended for long time operation at a steady field, there are advantages in using a superconducting persistent-current switch to capture a persistent-current in a magnet.

Persistent-current switch

As shown in Figure A-5, the magnet is shorted by a superconducting switch wire which may be driven normal by a heater so that the magnet current may be raised or lowered. When the desired current is reached, the heater power is turned off, allowing the persistent-current switch wire to become superconducting. It is then possible to disconnect the external power supply to let the persistent-current loop produce the steady magnetic field.

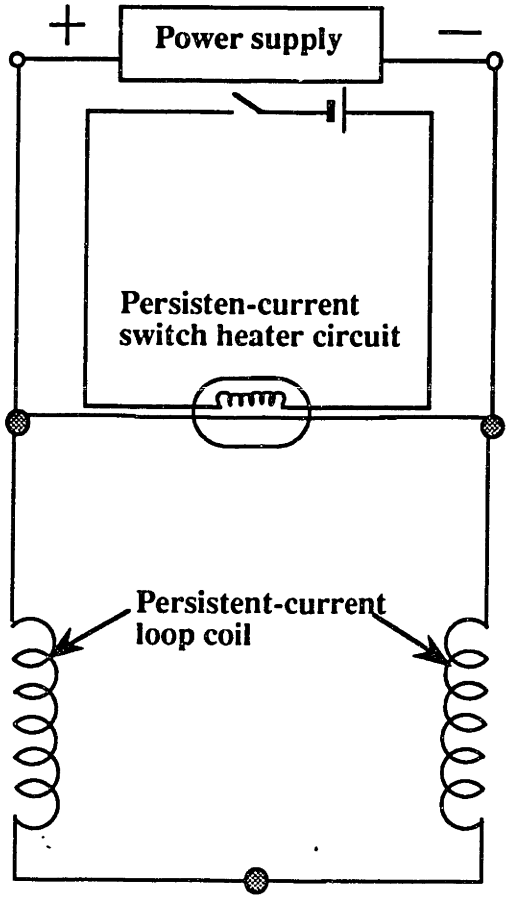

Fig. A-5 Persistent-current loop and switch.

The persistent-current switch is made by winding a heater wire and a superconducting switch wire non-inductively on the same phenolic spool. The superconducting wire used for the persistent-current switch has a copper-nickel matrix. The persistent-current switch should have a high electrical resistivity when it is on and also a moderate thermal insulation to reduce the boil-off rate of liquid helium when in the normally conducting mode. Manganin wire is used for the heater wire since it is insensitive to magnetic field. The

persistent-current switch is generally located in the weak magnetic field region to reduce any possibility of field induced quenching.

Superjoint

The superjoint means, in general, the resistanceless connection between two superconducting wires. This joint is indispensable in constructing the persistent-current loop of the superconducting magnet. If the superjoint has a resistance then the magnet energy will be dissipated across the joint resistance resulting in no persistent-current. In the persistent-current loop of the tandem magnets, two superjoints are made to connect the magnet wire and the switch wire, and one superjoint between two tandem magnet wires.

In order to obtain good electrical contact between superconducting filaments of two separate superconducting wires, the following procedure is performed carefully.

(1) First, the extra-long two superconducting wires are prepared. (If the joint is turned out to be resistive, it has to be cut and tried again.)
(2) The formvar insulation layer is stripped from the wire by knife or sand paper.
(3) The copper or copper-nickel matrix is etched away by nitric acid and rinsed by warm water.
(4) The right size of hole is drilled in OFHC (Oxygen Free High Purity Copper) ferrule. (Figure A-6) The hole size is determined so that two bare superconductors and extra NbTi filler can snugly slide in.
(5) Before the superconductors are put into the ferrule, they must be cleaned by mixed hydrofluoric and nitric acid solution, water, methanol, and acetone sequentially. For small filaments, it is important not to keep them in strong acid excessively. As soon as the bubbles start to form, the filaments should be taken out of the acid.
(6) Two superconducting wires (which are usually multi-filament wires) and NbTi filler are positioned in OFHC ferrule. (Figure A-6)
(7) A Nicopress crimp tool is used to squeeze the middle of ferrule to the round shape with the diameter of 4 mm. After crimping, a bare copper braid wire is wrapped over the stripped portion of the superconducting wires around at one end of the ferrule for soldering. The other end of the ferrule is just trimmed and filed smoothly.
(8) Both ends are soldered to add additional structural strength.
(9) The superjoint is usually covered by porous Silica fiber cloth for electrical insulation thus allowing liquid helium to penetrate in to the conductor.

(10) It is necessary to test the superjoint in liquid helium before the main magnet experiment. If a joint is resistive, it should be cut and made again.

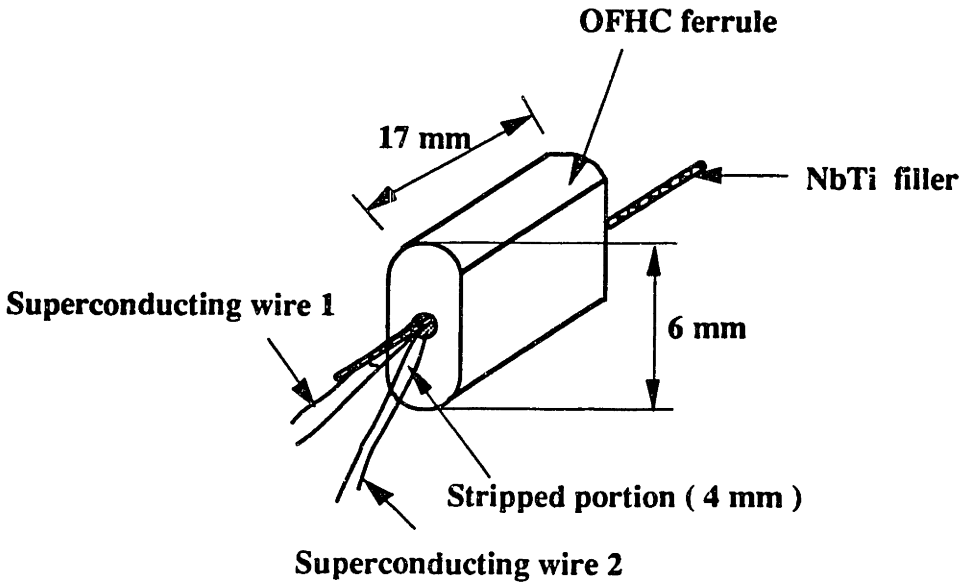

Fig. A-6 Superjoint construction for NbTi wires.

Appendix B. A.C. loss calculations

A.C. loss or eddy current heating can be a significant source of parasitic heating in low temperature devices. This heat is the result of the dissipation of eddy currents induced by changing magnetic fields (A.C. loss). This appendix describes the A.C. losses in the He^3 space, which may degrade the system performance.

In general, the power, P, dissipated by a current, I, flowing in a loop of resistance R is given by $P = I^2R$. Within a small volume element the incremental power is $dP = j^2\rho dV$; where $j = I/dA_x$, $\rho = RdA_x/dl$, $dV = dA_x dl$, A_x and l are, respectively, the cross-sectional area and length of the loop. The current generated by a changing magnetic field is given by,

$$IR = \int_l E \cdot dl = -\frac{d}{dt}\int_S B \cdot dA_l, \qquad (B.1)$$

where the first integral is of the induced electrical field, E, and is taken around the path (loop) l that the current follows (Figure B-1).

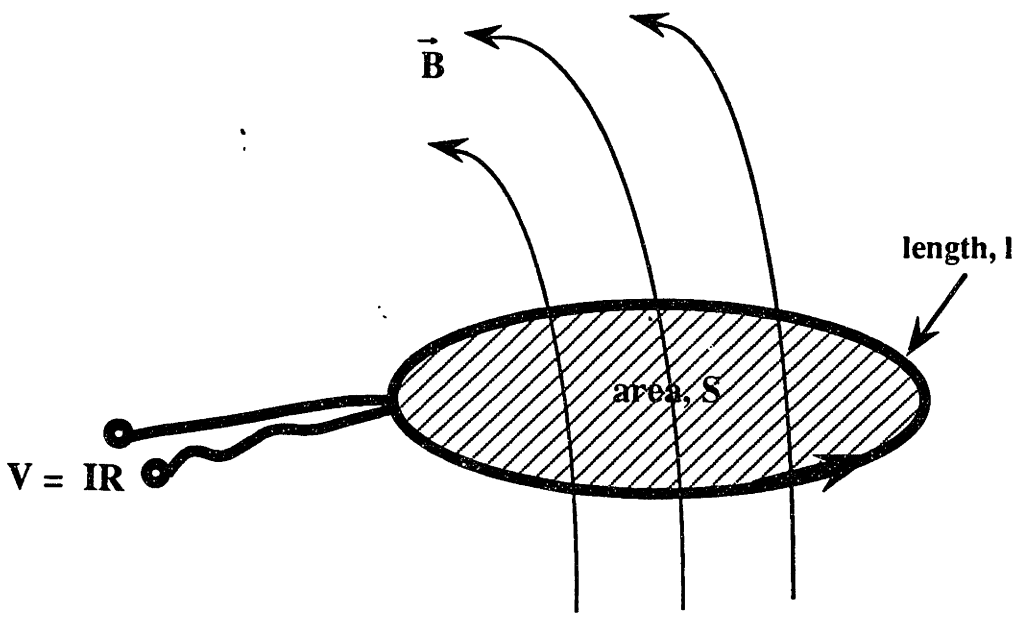

Fig.B-1 Eddy current generation by changing magnetic flux.

A_l is the area enclosed by the loop and the second integral is over the magnitude and direction over the surface, S, enclosed by l. Usually, it is assumed that dB/dt is uniform in magnitude and direction over the entire volume of interest. In order to check the validity of this assumption, the magnetic diffusion penetration depth is compared to the geometric scale of the system. The penetration depth for usual copper is,

$$\delta = \sqrt{\frac{2}{\omega\mu\sigma_o}}$$

$$= \sqrt{\frac{2}{\frac{2\pi}{12}\times 4\pi\times 10^{-7}\times 0.2\times 10^{10}}}$$

$$= 0.039 \text{ m}$$

$$= 39 \text{ mm},$$

where ω is the frequency of the changing field μ is the permeability of the material, and σ_o is the electrical resistivity.

Since this penetration depth is bigger than the thickness of the geometric dimension in this chapter, the changing field fully penetrates. Also, E, l, and I are taken to lie in the plane perpendicular to dB/dt. Under these conditions IR = -dB/dt A_l or $j\rho$ = -dB/dt A_l/l where R is taken to be the resistance over the path l, j is the current density, and ρ is the resistivity. The power dissipated in an incremental volume is then;

$$dP = \frac{(dB/dt)^2 A_l^2 dV}{\rho l^2} = \frac{(dB/dt)^2}{\rho} \gamma A_l^2 dV, \qquad \text{(B.2)}$$

where $\gamma = A_l/l^2$. For circles $\gamma = 1/4\pi$.
Again, this relation applies only when the field variation fully penetrates the conductor.

B.1 Warm-end heat exchanger

The A.C. loss of the warm-end heat exchanger can be calculated as the sum of the A.C. losses occurring in 2 parts ; inner cylinder and bottom solid copper disk.

A.C. loss of inner cylinder part

This calculation can be approximated by that of a thin cylindrical shell that is subject to field that is constant in the axial direction (Kittel, 1990).

$$Q_1 = \int_0^h \int_0^{2\pi} \int_{r_o - w}^{r_o} \frac{(dB/dt)^2}{\rho}\left(\frac{\pi r^2}{2\pi r}\right)^2 r dr d\phi dz \qquad \text{(B.3)}$$
$$= \frac{(dB/dt)^2}{32\rho}\frac{8}{\pi}(\pi r_o^2)(2\pi r_o w h)$$

where r_o, w, h are the radius, thickness and height of the inner cylinder part respectively. Assuming the electrical resistivity of ETP (Electrolytic Tough Pitch) RRR-30 copper as 5×10^{-10} Ω·m,

$$Q_1 = \frac{\left(\frac{1.68}{6}\right)^2}{32\times5\times10^{-10}}\cdot\frac{8}{\pi}\cdot(\pi\cdot(5.7\times10^{-3})^2)\cdot(2\pi\cdot5.7\times10^{-3}\cdot0.7\times10^{-3}\cdot60\times10^{-3})$$
$$= 1.92\times10^{-3}\ \text{W} \quad \text{or} \quad 1.92\ \text{mW} \qquad \text{(B.4)}$$

A.C. loss of solid copper disk part at the heat exchanger bottom

Similarly, for field that is uniform through the thickness,

$$Q_2 = \int_0^h \int_0^{2\pi} \int_0^{r_o} \frac{(dB/dt)^2}{\rho}\left(\frac{\pi r^2}{2\pi r}\right)^2 r dr d\phi dz$$
$$= \frac{(dB/dt)^2}{32\rho}\frac{4}{\pi}(\pi r_o^2)(\pi r_o^2 h)$$
$$= \frac{\left(\frac{3.0}{6}\right)^2}{32\times5\times10^{-10}}\cdot\frac{4}{\pi}\cdot\pi\cdot(5.7\times10^{-3})^2)\pi\cdot(5.7\times10^{-3})^2\cdot(1\times10^{-3})$$
$$= 2.07\times10^{-4}\ \text{W} \quad \text{or} \quad 0.21\ \text{mW} \qquad \text{(B.5)}$$

This calculation is also based on the assumption of full penetration. Since the A.C. loss due to radial field variation is very small compared to that of axial field variation, the total

A.C. losses in the warm end heat exchanger can be estimated less than 3 mW. This is negligible in comparison to the rejection heat at the warm end heat exchanger.

B.2 Cold-end heat exchanger

As described in the design part of Chapter II., single crystal SiO_2 is actually non-conductor with the electrical resistivity of higher than 10^{17} Ω·m (Haus, 1989). Consequently the eddy current heat generation in the cold-end heat exchanger is virtually zero.

B.3 Magnetic core tube

The magnetic core housing is constructed from a thin 304 stainless steel tube. Since the penetration depth for stainless steel is 1.35 m, which is much larger than the thickness of the core tube, the full penetration calculation is again performed to estimate A.C. loss. With the electrical resistivity of stainless steel of 6×10^{-7} Ω·m at 4.2 K,

$$Q_3 = \frac{\left(\frac{3.0}{6}\right)^2}{32\times6\times10^{-7}} \cdot \frac{8}{\pi} \cdot \pi \cdot (22.2\times10^{-3})^2) \cdot 2\pi \cdot (22.2\times10^{-3} \cdot 0.78\times10^{-3} \cdot 183\times10^{-3})$$

$$= 1.02\times10^{-3} \text{ W} \quad \text{or} \quad 1.02 \text{ mW} \qquad \text{(B.6)}$$

This A.C. loss in the core tube is also negligible in comparison to the refrigeration power per core of 50 mW.

Appendix C. Cold-end heat exchanger temperature controller

This appendix is a detailed description of the temperature controller circuit of the cold-end heat exchanger discussed in section 2.4. Figure C-1 is the schematic diagram of the circuit.

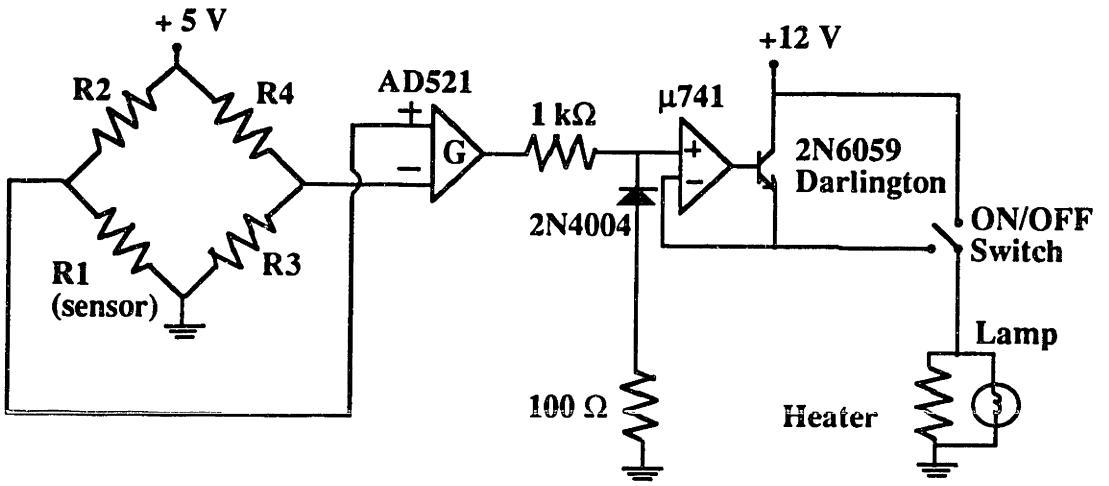

R2 = 498 kΩ
R3 = 1588 Ω
R4 = 498 kΩ

Fig. C-1 Cold-end heat exchanger temperature controlled heater.

The controller circuit has three modes: manual off, automatic heater control, and manual on. R1 is the actual temperature sensor T1, which is located at the bottom of the cold-end heat exchanger. R2, R3, and R4 form a resistance bridge to supply approximately 10 μA for the temperature sensor and provide the differential voltage input for the AD521 instrumentation amplifier. Since this differential voltage is approximately proportional to the cold helium's temperature deviation from the 1.8 K balance condition, this controller circuit is a proportional controller with negative feedback. If the temperature T1 is higher than 1.8 K, the heater power is turned off. The voltage and current measurement of the heater can estimate the refrigeration capacity. Both magnetic cores are independently equipped with the same separate controller unit.

Appendix. D Radial temperature non-uniformity at cold-end heat exchanger

The cold-end heat exchanger which is made of SiO_2 single crystal is wrapped by a Minco thermofoil kapton heater to simulate the actual refrigeration load condition. The heater current is feed-back controlled to keep the temperature of out-going helium flow at 1.8 K in the heat exchanger.

Even though SiO_2 single crystal is a good material for the heat exchanger at low temperature because of its high thermal conductivity and virtually zero eddy current parasitic heating, the radial temperature non-uniformity has to be checked to insure successful operation. The thermal conductivity of SiO_2 single crystal at 1.8 K is about 20 W/m·K while its maximum value is about 1000 W/m·K at 10 K.

In order to calculate the radial temperature distribution, 1-D fin analysis is used. The cold-end heat exchanger with 91 holes is approximated as a semi-porous material with porosity 0.17 (Figure D-1).

The quasi-steady state heat conduction equation for the above small element is as follows:

$$-k\frac{dT}{dr}(r2\pi r)L = \left(-k\frac{dT}{dr} - k\frac{d^2T}{dr^2}dr\right)(r+dr)\,2\pi rL + h(T-T_\infty)A_{conv.} \qquad (D.1)$$

where $A_{conv.} = \pi \cdot d_h \cdot n \cdot L$,
T_∞ is the temperature of helium,
d_h is the diameter of the helium passage hole,
n is the number of holes in the small element,
L is the thickness of the small element.

Since the porosity $\varepsilon = \dfrac{\frac{\pi}{4}d_h^2 n}{(r2\pi r)dr} = 0.17$ in the heat exchanger cross-section is,

< THICKNESS : L >

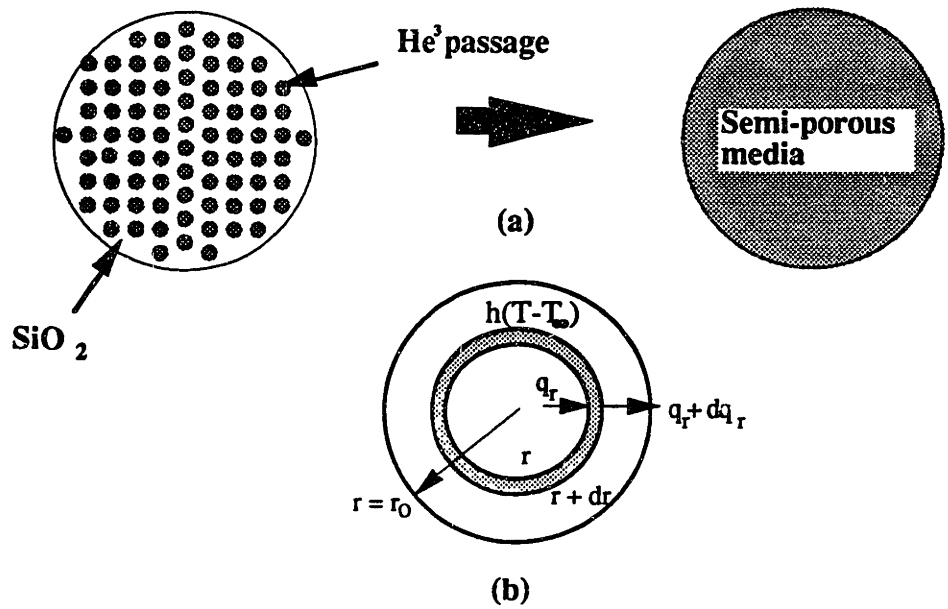

Fig. D-1 Heat transfer in the cold-end heat exchanger. (a) Semi-porous media approximation (b) Heat transfer relation in the small element.

$$A_{conv.} = \pi d_h L \frac{\varepsilon r 2\pi r dr}{\frac{\pi}{4} d_h^2} = 4\varepsilon \frac{L}{d_h} r\, 2\pi r dr \qquad \text{(D.2)}$$

and also by letting $\theta = T - T_\infty$ in equation (d.1),

$$r\frac{d^2\theta}{dr^2} + \frac{d\theta}{dr} - r\left(\frac{h}{k_{eff}} \frac{4\varepsilon}{d_h}\right) \theta = 0 \qquad \text{(D.3)}$$

or

$$x^2 \frac{d^2\theta}{dx^2} + x\frac{d\theta}{dr} - x^2\, \theta = 0 \qquad \text{(D.4)}$$

where $x = \sqrt{\frac{h\ 4\ \varepsilon}{k_{eff}\, d_h}}\, r$.

This is *the modified Bessel function of the first kind of order 0* (Hildebrand, 1976). With the following boundary conditions,

$$\theta = \textit{finite at } x = 0$$

$$q_w = k\left(\frac{d\theta}{dx}\right)_{x=x_o}\sqrt{\frac{h}{k_{eff}}\frac{4\varepsilon}{d_h}} \quad at\ x = x_o \tag{D.5}$$

where q_w is the heat flux from the heater and

k_{eff} is the effective thermal conductivity of SiO_2 single crystal in the heat exchanger.

The approximate solution is

$$\theta = C_1 \cdot I_0(x). \tag{D.6}$$

$$where\ I_0 = \sum_{k=0}^{\infty} \frac{\left(\frac{x}{2}\right)^{2k}}{(k!)^2}.$$

Now, with the real physical values,

$$h = Nu\frac{k_{He}}{d_h} = 3.66 \times \frac{0.011}{0.8\times10^{-3}} = 50.3 \ \text{W/m}^2\cdot\text{K}$$

$$k_{eff} = k_{SiO_2} \times (1 - \varepsilon) + k_{He} \times \varepsilon = 16.6 \ \text{W/m}\cdot\text{K}$$

$$x_o = \sqrt{\frac{h}{k_{eff}}\frac{4\varepsilon}{d_h}}\, r_o = 0.472 \ \text{m}$$

$$q_w = \frac{\dot{Q}_{ref}}{\pi D_{HX} L} = \frac{0.05}{\pi \times 0.0186 \times 0.03} = 28.5 \ \text{W/m}^2$$

and using the approximation of Bessel function solution,

$$\theta = C_1\left(1 + \frac{x^2}{4} + \frac{x^4}{64} + \cdots\right) \cong C_1\left(1 + \frac{x^2}{4} + \frac{x^4}{64}\right) \tag{D.7}$$

C_1 is determined by the following boundary condition.

$$q_w = k_{eff}\left(\frac{d\theta}{dx}\right)_{x=x_o}\sqrt{\frac{h}{k_{eff}}\frac{4\varepsilon}{d_h}} = k_{eff}\sqrt{\frac{h}{k_{eff}}\frac{4\varepsilon}{d_h}}\, C_1\left(\frac{2x_o}{4} + \frac{4x_o^3}{64}\right) \tag{D.8}$$

$$\therefore C_1 = 0.14$$

Therefore the temperature distribution in the radial direction can be expressed as:

$$\theta = T - T_\infty \cong 0.14\left(1 + \frac{x^2}{4} + \frac{x^4}{64}\right) \tag{D.9}$$

where $x = \sqrt{\frac{h}{k_{eff}} \frac{4\varepsilon}{d_h}}\ r = 50.4\, r$

Through the above analysis, it is confirmed that the radial temperature variation of the cold end heat exchanger is less than 0.01 K ($\Delta T_{max} \cong 0.14 \left(\frac{x_o^2}{4} + \frac{x_o^4}{64} \right) = 0.01\ K$). Therefore, the SiO_2 cold-end heat exchanger can be considered as an isothermal block.

Appendix. E Time constants of cooling the magnetic refrigerator

The cool-down process is divided into two steps; one from room temperature to 77 K by liquid nitrogen and the other from 77 K to 4.2 K by liquid helium. Since the former step is usually done overnight before the experiment day, the cooling time constant consideration is not so critical. On the other hand, during the latter cooling process, it is important to understand how fast the system is cooled. This appendix describes the two longest cooling time constants of the experimental apparatus: one for the GGG magnetic core and the other for the displacer piston.

GGG magnetic core

As it is described in section 4.1.1, the magnetic core tube is vacuum insulated. The schematic diagram of the GGG magnetic core is shown in Figure E-1.

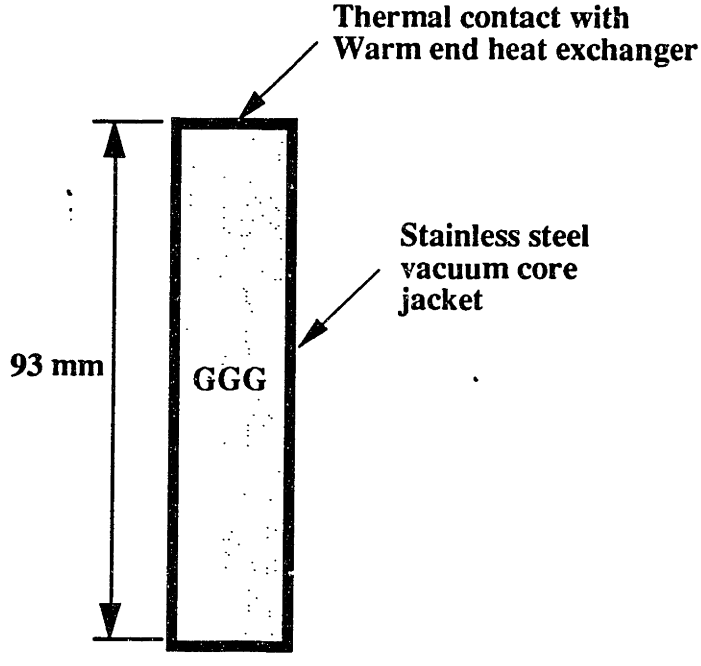

Fig. E-1 Schematic diagram of the GGG magnetic core.

Since the core has thermal contact with liquid helium via the warm-end heat exchanger, the cool-down process can be modeled as the cooling porous media enclosure with the cold top wall. In order to determine what is the dominant heat transfer mechanism in this case, the Rayleigh number of porous media is calculated (Rohsenow, 1985).

$$Ra = \frac{K\rho_o\beta g(T_0 - T_1)H}{\nu\alpha} \qquad \text{(E.1)}$$

, where K is the permeability $\left(\approx \frac{d^2\,\varepsilon^3}{(1-\varepsilon)^2}\right)$

d is the particle diameter

ε is the porosity

H is the height of the porous media.

Using the physical properties of He^3 at 40 K and 40 torr,

ρ = 0.0487 kg/m^3

β = 1/T = 1/40 1/K

$$\nu = \frac{\mu}{\rho} = \frac{5\times10^{-6}}{0.0487} = 1.03\times10^{-4}\ \text{m}^2/\text{sec}$$

$$\alpha = \frac{k}{\rho C_P} = \frac{0.048}{0.0487\times6900} = 1.42\times10^{-4}\ \text{m}^2/\text{sec}$$

$$K \approx \frac{d^2\,\varepsilon^3}{(1-\varepsilon)^2} = \frac{(0.8\times10^{-3})^2\times(0.38)^3}{(1-0.38)^2} = 9.15\times10^{-8}\ \text{m}^2$$

$H = 0.093$ m

$$Ra = \frac{9.15\times10^{-8}\times0.0487\times\frac{1}{40}\times9.8\times(77-4.2)\times0.093}{1.03\times10^{-4}\times1.42\times10^{-4}} = 0.5$$

This Rayleigh number is much smaller than the critical Rayleigh number, Ra* ($= 4\pi^2$, Rohsenow, 1985). Therefore, it is considered that the natural convection does not occur in the early cool-down process. The thermal conduction is the dominant heat transfer mechanism.

The effective thermal conductivity of the magnetic core is estimated with the physical properties of He^3 and GGG in the temperature range of 77 K and 4.2 K. According to the experimental correlation of McAdams (1954), the effective thermal conductivity of the core is about ten times that of He^3 at 40 K (i.e. $k_{eff} = 0.46$ W/m·K).

The energy equation of two-dimensional porous media is ,

$$\sigma\frac{\partial T}{\partial t} + u\frac{\partial T}{\partial x} + v\frac{\partial T}{\partial y} = \alpha_{eff}\left(\frac{\partial^2 T}{\partial x^2} + \frac{\partial^2 T}{\partial y^2}\right), \qquad \text{(E.2)}$$

where σ is the heat capacity ratio defined as below. Because the thermal inertia of the medium depends on the inertias of the solid and the fluid (Cheng, 1978),

$$\sigma \equiv \frac{\varepsilon\,(\rho C_p)_f + (\,1 - \varepsilon\,)\,(\rho C)_s}{(\rho C_p)_f} \qquad \text{(E.3)}$$

α_{eff} is the effective thermal diffusivity of the medium $\left(\equiv \frac{k_{eff}}{(\rho C_p)}\right)$. Ignoring the convection term in the above energy equation, the thermal inertia and heat conduction are balanced each other.

$$\sigma\frac{\Delta T}{\tau} \sim \alpha_{eff}\frac{\Delta T}{x_p^2}$$

or

$$\tau \sim \frac{\sigma}{\alpha_{eff}}\, x_p^2, \qquad \text{(E.4)}$$

where x_p is the growing thermal conduction penetration depth into the porous media. With the actual physical properties of the core,

$$\sigma \equiv \frac{\varepsilon\,(\rho C_p)_f + (\,1 - \varepsilon\,)\,(\rho C)_s}{(\rho C_p)_f}$$

$$= \frac{0.38\cdot(0.0487\times 6900) + (\,1 - 0.38\,)\cdot(7140\times 30)}{(0.0487\times 6900)}$$

$$= 396$$

and also,

$$\alpha_{eff} = \frac{k_{eff}}{(\rho C_p)_f} = \frac{0.46}{0.0487 \times 6900}$$

$$= 0.0014 \ \text{m}^2/\text{sec}$$

Taking the core length as the penetration depth,

$$\tau \sim \frac{396}{0.0014} \times (0.093)^2$$

$$= 2500 \ \text{sec}$$

Therefore, for the core to be cooed by conduction only, it would take about 3 hours (~ 4 τ). However, as the temperature goes down, actually the natural convection will occur, because the Rayleigh number becomes large with the following relation.

$$Ra = \frac{K \rho_o \beta g \Delta T H}{\nu \alpha} \sim \frac{\rho \frac{1}{T} T}{\frac{1}{\rho} \frac{1}{\rho}} \sim \frac{1}{T^3} \qquad \text{(E.5)}$$

It is obvious that there is a natural convection flow inside the magnetic core near at 4.2 K. Therefore, the actual cooling time constant of the magnetic core must be shorter than 3 hours, which is also in good agreement with the experimental result. If the axial conduction of the stainless steel core jacket and radiation heat transfer are also included, the cooling time constant can be estimated as 1 or 2 hours.

Displacer piston

As shown in Figure E-2 (a), the piston is floating inside the cylinder filled with helium gas. Figure E-2 (b) is the schematic diagram of thermal resistance circuit during cool-down process.

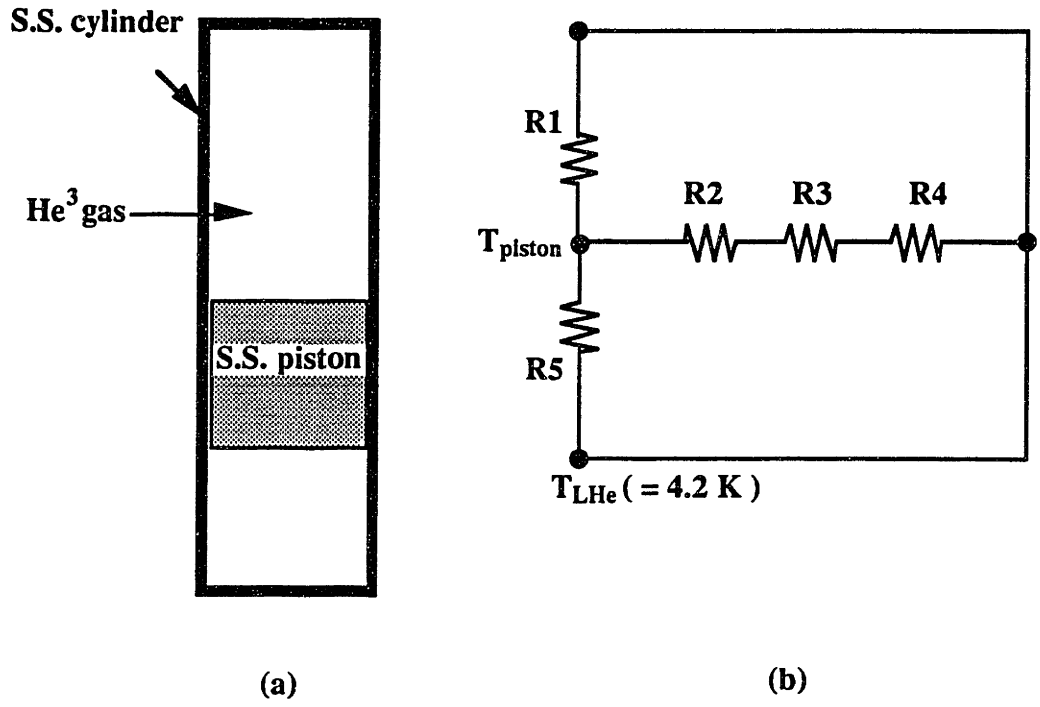

Fig. E-2 Displacer unit modeling. (a) Schematic diagram of the displacer assembly (b) Thermal resistance circuit of the displacer piston cool-down with liquid helium.

In Figure E-2 , each thermal resistance can be expressed as the following.

$R1 = \frac{1}{h_{NC} A_{top}}$: Natural convection heat transfer

$R2 = \frac{t_{ph}}{k_{ph} A_{side}}$: Thermal conduction in phenolic on the piston

$R3 = \frac{t_{He}}{k_{He} A_{side}}$: Thermal conduction in helium gap between piston and cylinder

$R4 = \frac{t_{s.s}}{k_{s.s} A_{side}}$: Thermal conduction in stainless steel cylinder

$R5 = \frac{t_{bottom}}{k_{He} A_{bottom}}$: Thermal conduction through the bottom of piston in helium gas,

where h_{NC} is the heat transfer coefficient of natural convection in enclosure. k_{ph}, k_{He}, and $k_{S.S}$ are respectively thermal conductivity of phenolic, helium gas, and stainless steel. t_{ph}, t_{He}, $t_{s.s}$ and t_{bottom} also respectively denote conduction layer thickness of phenolic, helium gap between piston and cylinder, stainless steel, and bottom helium space.

It is evident by intuition that the conduction heat transfer around the piston wall is dominant. The total thermal resistance calculation result is 0.34 k/W. By the lumped heat capacity equation,

$$q = \frac{T - T_{\infty}}{\Sigma R} = c \rho v \frac{dT}{dt}, \qquad \text{(E.6)}$$

where q is the total heat transfer from the piston, T_{∞} is the liquid helium temperature, ΣR is the total thermal resistance, c , ρ, v are the specific heat, density, volume of the stainless steel piston,

From this lumped heat capacity approximation, the thermal characteristic time scale can be calculated as the following.

$$\begin{aligned} \tau &= c \rho v \Sigma R \\ &= c M \Sigma R \\ &= 460 \times 2 \times 0.34 \\ &= 313 \text{ sec} \end{aligned} \qquad \text{(E.7)}$$

Therefore, the cooling time constant of the displacer assembly is considered as 20 minutes (~ 4τ). Since the pressure of He^3 space drops as the cooling process proceeds, more He^3 gas has to be charged to keep the inside pressure at 40 torr.

By the above zeroth order estimation of cooling time constants, it is concluded that the overall cool-down characteristic time is determined by the magnetic core. There are two ways to make the cool-down period short. First, charging He^3 gas at a high pressure (~ 200 torr) at room temperature so that the onset of natural convection starts earlier. Rayleigh number is increased due to high fluid density. The second method is to move the displacer piston after it is cooled at 4.2 K. In this case, the GGG core can be cooled more effectively by forced convection of cold helium gas , which is cooled at the warm-end heat exchanger by 4.2 K liquid helium.

Appendix F. Instrumentation and system control scheme

F.1 Instrumentation and data acquisition

The instrumentation work can be divided into two parts: sensor installation and data acquisition.

Sensor installation

In order to study the thermal characteristic of the GGG magnetic core, 6 temperature sensors are installed in the core. These are all Allen-Bradley 47 Ω 1/8 W carbon resistors.

The calibration of the temperature sensors was performed before the main experiment and a calibration curve was developed for each sensor (Jeong, 1990). Figure F-1 shows the relative location of the temperature sensors inside the magnetic core tube. In addition to the 6 temperature sensors, the cold-end heater and one magnetic field sensor are installed. The magnetic field sensor is a hall effect generator. For the left magnetic core, a BHA-921 cryogenic axial hall sensor from F.W.Bell is located at the bottom-end of the warm-end heat exchanger inside the liquid helium port. The hall sensor is located outside of the GGG space in order to eliminate its parasitic heating effect and to increase packing density of GGG. The right magnetic core contains the BH-203 hall sensor, which was originally used for the room temperature field measurements. Both sensors are excited by a 100 mA current supply .

The working pressure of He^3 is measured using an Omega Engineering model PX-136 and a model PX-170 piezo-electric pressure transducer. There are three locations in the He^3 space where the pressure is measured: the left magnetic core volume, the right magnetic core volume, and the room temperature step motor volume. Since two core volumes are under liquid helium, the PX-136 absolute pressure transducer and the PX-170 differential pressure transducer are mounted on the top flange and are connected to the He^3 core volume by an outside diameter 3.2 mm stainless steel tube. These pressure transducers have also been calibrated with a Mc-Leod gauge. All calibrated sensors show good linearity and can be useful for measuring transient pressure variation of the system above 5 torr.

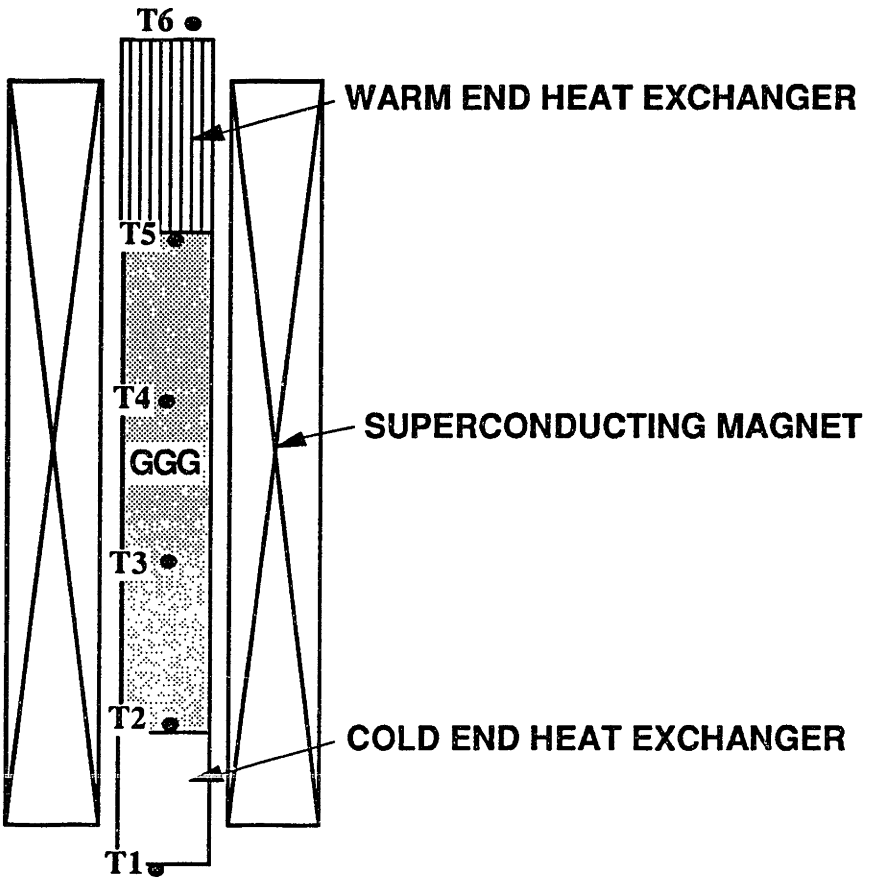

Fig. F-1 Temperature sensor locations in the magnetic core assembly.

For the purpose of monitoring temperature inside the cryostat, 4 temperature sensors (Allen-Bradley 220 Ω carbon resistors) are installed in the cryostat; at the bottom of the 4.2 K part assembly, at the top of the superconducting magnet, and at the top of the displacer. The resistance measurement are performed by applying a constant d.c. current of 10 μA from a Lake Shore 110 current source through the transducers all connected in series, including the temperature sensors inside the magnetic core tube. The voltage across each resistor is amplified and read by the data acquisition system.

Magneto-resistance

In general, a transverse magnetic field increases the electrical resistivity of a carbon resistor. According to the experimental data (Sample, 1974) the relative temperature error caused by the magnetoresistance,

$$\frac{\Delta T}{T_O} \approx \frac{\Delta R / R_O}{[d(lnR_O) / d(lnT)]_{T_o}} \qquad \text{(F.1)}$$

increases as the temperature decreases and the magnetic field increases. In our experimental range, the maximum magnetic field is 3 tesla and the temperature range is above 1.5 K. The temperature measurement error for the 47 Ω resisters is estimated to be below 1 %.

Self-heating

The decision on the values for the Allen-Bradley resistor and the excitation current level is based on the consideration of self-heating effect and data acquisition availability. Figure F-2 is the typical temperature-resistance relation of a 47 Ω resistor.

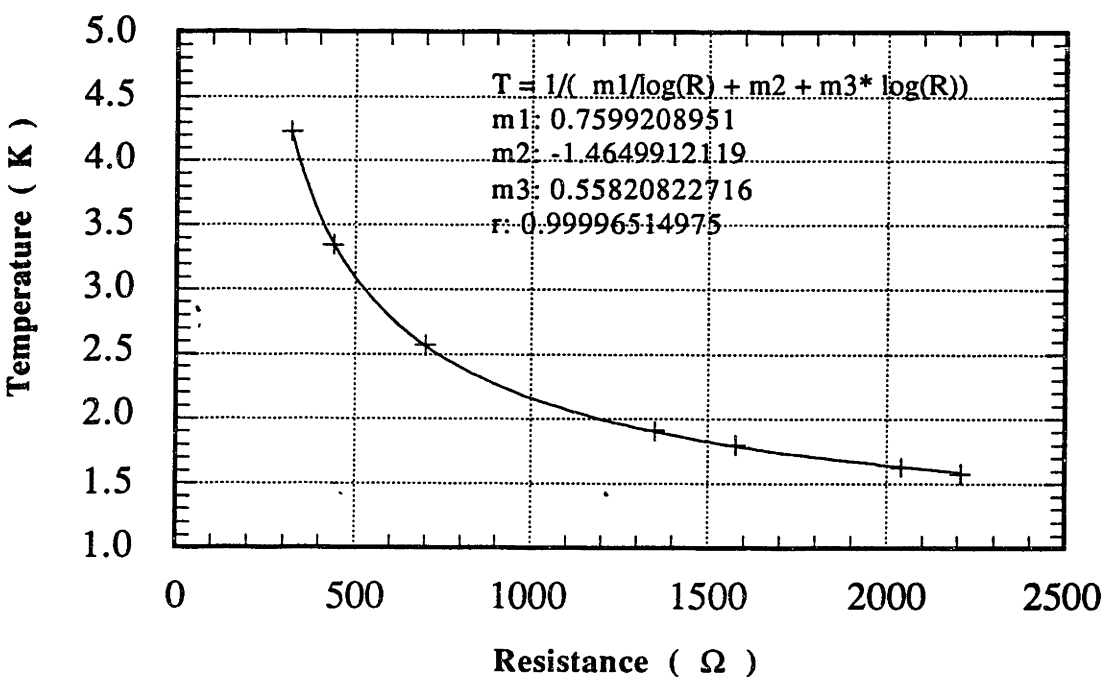

Fig. F-2 Temperature sensor calibration result.

When 10 μA is applied to the resistor with a resistance value of about 2200 Ω at 1.6 K, the Joule heating is,

$$q = i^2R = (10^{-5})^2 \times 2200 = 2.2 \times 10^{-7}\ \text{W}$$
$$= 0.22\ \mu\text{W} \qquad \text{(F.2)}$$

Since this heat generation is negligible, 10 μA is used for exciting all temperature sensors.

Data acquisition

Table F-1 is the summary of experimental data acquisition parameters of the tandem magnetic refrigerator. In order to check the operation of the magnetic refrigerator, some of the important data was processed in real time and displayed selectively on the computer screen while the experiment was progressing.

Table F-1. Data acquisition summary of the tandem magnetic refrigerator.

OBJECTS	MEASURE -MENT	LEGEND	AMPLIFIER (GAIN)	DT2801-A BOARD (GAIN)	ACRO SYSTEM WITH VIR
LEFT CORE	T1(13)	UNDER CHX*	#1 - 92.3		CH.1 (916)-3
	T2(14)	CORE BOTTOM	#2 - 98.0		CH.2 (916)-3
	T3(15)	IN CORE-1/3	#3 - 99.4		CH.3 (916)-3
	T4(17)	IN CORE-2/3	#4 - 98.7		CH.4 (916)-3
	T5(18)	CORE TOP	#5 - 91.2		CH.5 (916)-3
	T6(31)	OVER WHX†	#6 - 92.4		CH.6 (916)-3
	H_L	HALL§	#15 - 109.7	CH.6(2)	
	V	VOLTAGE			CH.8 (916)-2

* Cold-end heat exchanger
† Warm-end heat exchanger
§ Cryogenic hall sensor : 8 mV/tesla

Table F-1. Data acquisition summary of the tandem magnetic refrigerator (continued).

OBJECTS	MEASURE -MENT	LEGEND	AMPLIFIER (GAIN)	DT2801-A BOARD (GAIN)	ACRO SYSTEM WITH VIR
RIGHT CORE	T1(25)	UNDER CHX*	#7 - 98.9	CH.0(4)	
	T2(27)	CORE BOTTOM	#8(#14) - 100.2	CH.1(4)	
	T3(28)	IN CORE-1/3	#9 - 121.7	CH.2(4)	
	T4(29)	IN CORE-2/3	#10 - 116.4	CH.3(4)	
	T5(30)	CORE TOP	#11 - 125.0	CH.4(4)	
	T6(32)	OVER WHX†	#12 - 101.5	CH.5(4)	
	H_R	HALL§			CH.7 (916)-3
	I	CURRENT	#13 - 117.2	CH.7(4)	
PRE-SSURE	P1	R-CORE			CH.1 (911)-4
	P2	IN MOTOR PART			CH.2 (911)-4
	P3	L-CORE			CH.3 (911)-4
POSI-TION	P4	POTENTIO METER			CH.4 (911)-2
DEWAR TEMPE-RATURE	T1	DEWAR BOTTOM			CH.1 (912)-6
	T2	SYSTEM BOTTOM			CH.2 (912)-6
	T3	MAGNET TOP			CH.3 (912)-6
	T4	SYSTEM TOP			CH.4 (912)-6

* Cold-end heat exchanger
† Warm-end heat exchanger
§ Room temperature hali sensor : 107 mV/tesla

Table F-1. Data acquisition summary of the tandem magnetic refrigerator (continued).

OBJECTS	MEASURE -MENT	LEGEND	AMPLIFIER (GAIN)	DT2801-A BOARD (GAIN)	ACRO SYSTEM WITH VIR
LHe LEVEL	Liquid helium				CH.5 (912)-6
MOTOR TEMPE-RATURE	T1	MOTOR BOTTOM			CH.1 (931)-T
	T2	MOTOR CENTER			CH.2 (931)-T
	T3	MOTOR TOP			CH.3 (931)-T

- Left core's temperature data with magnetic field measurement are recorded by the module #916 of Acro-900 data acquisition system. Acro-900 communicates with the Dell-80386 micro-computer via RS-232C cable.

- Right core's temperature and magnetic field data are collected by "Data translation board DT-2801A". Since most temperature data are in millivolt range, they are usually amplified with nominal gain of 100, and then collected by the data acquisition system.

- The pressure measurements are performed by using two absolute type piezo-electric transducers (Omega PX-136) and one differential type one. The absolute type pressure transducers are excited by +15 V d.c. and the differential type pressure transducer is excited by +12 V d.c. The pressure sensor output voltage, which is proportional to the pressure, is directly connected to the ACRO-911 module.

- The displacer position is measured by a 10 kΩ 10-turn potentiometer. This potentiometer has a mechanical connection with the rotating lead screw through a gear ratio of 2:1.

-Dewar temperatures (or cryostat temperatures) are monitored by 220 Ω Allen-Bradley carbon resistors. These sensors are very helpful to understand the inside condition of the cryostat when liquid nitrogen and liquid helium is being charged. For the data collection of

these sensors, a high resolution module of the ACRO-912 is used without intermediate amplifier.

- To measure liquid helium level in the cryostat, a 750 mm long liquid helium level meter from American-Magnetics Inc. is used.

- The step motor temperature data are recorded by using T type thermocouples and an ACRO-931 cold junction compensated thermocouple module.

The data acquisition program which controls the ACRO-900 modules and two DT-2801A data boards are written in Quick Basic and compiled by the Basic compiler. The set of data acquisition programs are listed in Appendix G.

F.2 Displacer motion control

In the section F.1, the details of the data acquisition system is described. This section and the next section discuss the synchronous control method of the overall magnetic refrigerator operation. The system control and the data acquisition control are both directed by a single central processing unit, *i.e.*, Dell 80386 micro-computer synchronously.

To control the displacer motion accurately, a Slo-syn model 250-1002 step motor with a ST250B translator is used. If the translator receives a negative amplitude change of 3 V or more at its input terminal A, the motor shaft advances one step of 1.8°. A triggering voltage at the input terminal B evokes one step backwards. In the tandem magnetic refrigerator operation, when the cycle period is 24 seconds, the displacer motion is completed by the following four processes.

- 5 inch up-stroke for 10 seconds (flow process)
- Pause for 2 seconds (adiabatic process)
- 5 inch down-stroke for 10 seconds (flow process)
- Pause for 2 seconds (adiabatic process)

The triggering voltage signal comes from one of the DT-2801A data boards, which generates sequence of pulse signals as DMA (Direct Memory Access) mode. At the same time, this board produces another analog signal to the magnet power supply for their synchronous operation via DAC0 terminal. Since the analog pulse signal comes from the

computer through one line, this signal has to be physically divided into separate two lines in order to drive the step motor in clockwise and counter-clockwise rotation. This signal splitting action is done by a TTL (Transistor-Transistor Logic) circuit. Figure F.3 shows its schematic diagram.

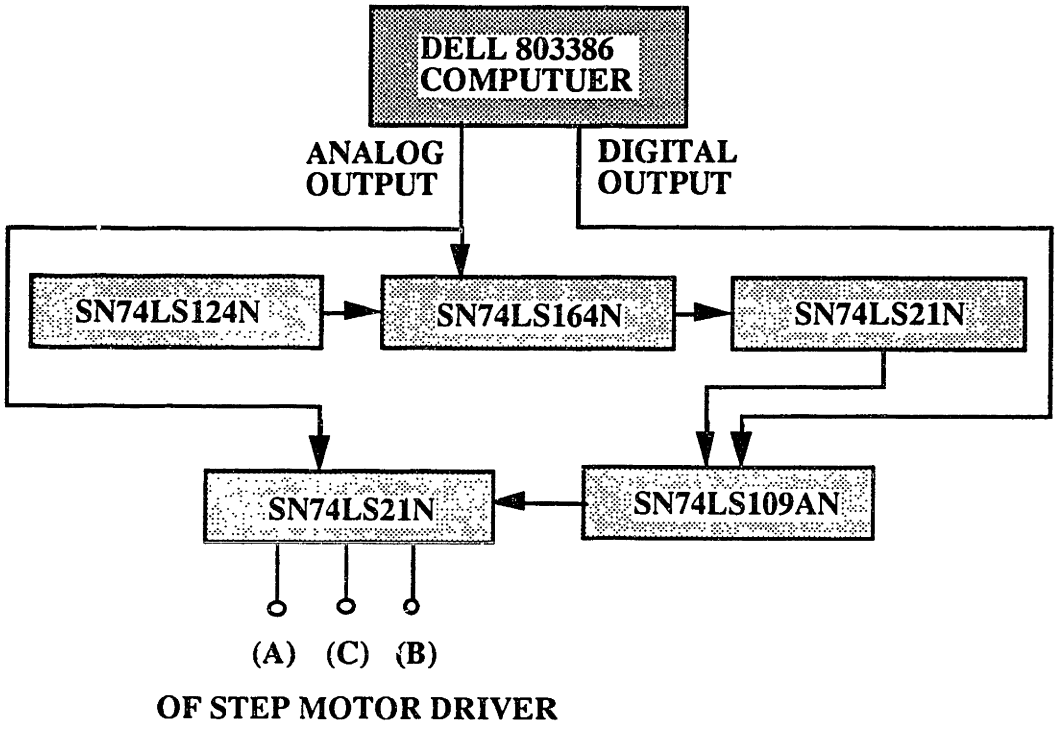

Fig. F-3 Schematic diagram of the TTL circuit for step motor drive.

This TTL circuit is accompanied by several capacitors to eliminate spurious noise signal. The following list summarizes the role of each chip in the circuit.

SN74LS124N : *Dual voltage-controlled oscillator*

- generates pulse signals according to the Resistance-Capacitor connection in port. In this experiment, the output frequency of the oscillator is chosen as 500 Hz which is about 2.5 times more than that of the input signal frequency of step motor driver.
- The output signal of the oscillator is a clock for the next shift register.

SN74LS164N : *8-bit parallel-out serial shift register*

- receives one analog pulse signal from the computer DT2801-A board and + 5 V digital input to give rise to 8 shifted signals according to the clock frequency.
- Four of 8 output signals are connected to the AND gate.
- The shift register and AND gate together detects the duration of null-signal condition of step motor input.

SN74LS21N : *Dual 4 input positive AND gate*
- One AND gate determines whether to supply the analog output for the motor driver or not by receiving 4 inputs from the shift register.
- The other AND gate is used to decide where the computer analog signal goes. If the signal is active in port (A) of the motor drive, the step motor rotates in clockwise direction, and if the signal goes into port (B), the motor does counter-clockwise rotation.

SN74LS109AN: *Dual positive-edge triggered flip-flops with preset and clear*
- supplies two toggle outputs for the Dual AND gate.
- This FIFO switches the direction of motor rotation whenever the computer signal is in low state for more than 4 times of clock periods.

F.3 Power circuit of the tandem superconducting magnets

As mentioned in the last section, the computer sends an analog voltage signal to the bipolar power supply. Then the bipolar power supply provides a necessary output voltage and current to energize the magnet proportional to the input signal.

The tandem superconducting magnet is composed of the persistent mode coil and the variational mode coil. Figure F-4 is the schematic diagram of the power circuit for the tandem magnets. Two persistent coils compose a persistent loop with a persistent switch which is activated by the remotely controlled heater.

In order to dump the magnetic energy of the persistent coils, a 0.8 Ω dump resistor and a diode (1N1188) are connected across the coil leads. The variational mode coil is to be energized by the bipolar power supply. A 2 Ω dump resistor is connected across the variational mode coils in series with a BZW5027 transient suppressor. This transient suppressor only conducts when its terminal voltage exceeds 33 V. When the magnet quenches, the stored magnet energy is to be dumped into this external (at room temperature) dump resistors. The 800 W-1.6 Ω high power resistor was added later to

stabilize the power supply for the highly inductive load. $(R_S)_P$ and $(R_S)_V$, shunt resistors to measure the current, are respectively 0.25 mΩ and 0.2 mΩ.

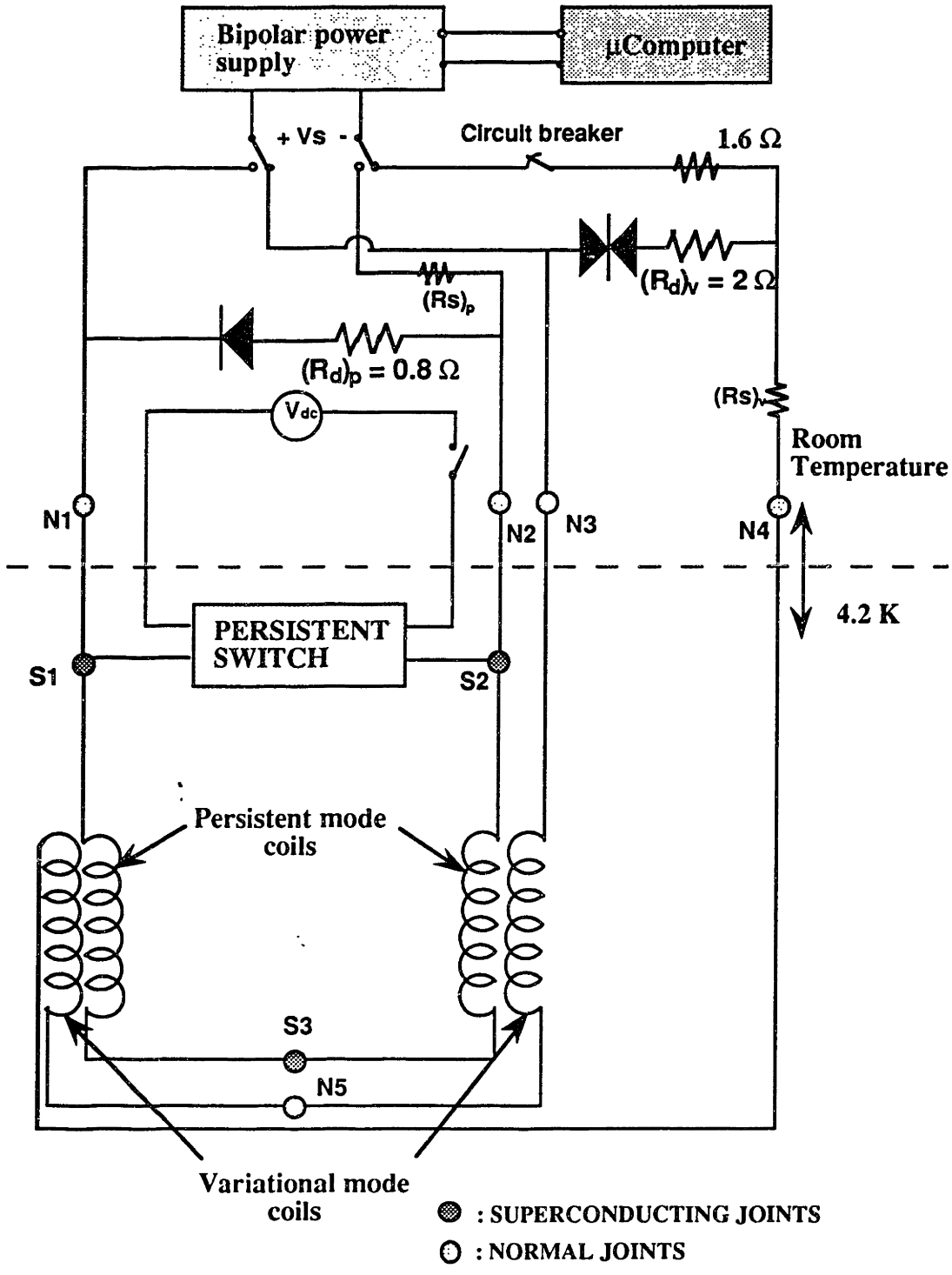

Fig. F-4 Schematic diagram of the power circuit of the tandem magnetic refrigerator.

Appendix G. Computer program lists

G.1 Data acquisition and system control programs

All control programs are written in "Quick Basic" and compiled to execution files.

(1) PRECOOL.BAS (pp.160-161)

- Monitoring 4 temperatures (cryostat bottom, magnet bottom, magnet top, and displacer top) and liquid helium level.
- Used 220 Ω Allen-Bradley carbon resistors for temperature sensors.
- Liquid helium level meter is calibrated for 750 mm long sensor.

(2) MAIN.BAS (pp.162-178)

- Main control program for the magnetic refrigerator.
- Testing displacer operation at 4.2 K is also possible.
- There are voltage controlled charging mode and current controlled charging mode in this program. This is also useful to monitor the system without operating the magnets or the displacer.
- Step motor and power supply are controlled simultaneously by two analog output; DAC0 and DAC1 from DT2801-A board in computer.
- This also utilizes the digital logic circuit to control motor operation.
- The magnets can be energized in ramp or sine wave mode.
- All measurement data are read, but some data (core temperature at the bottom, hall sensor, voltage and current of variational mode coil, displacer position) are only displayed in situ on computer screen.
- This program also has an option to convert raw data to temperature, current, and magnetic field values and store its result to LEFT.DAT, RIGHT.DAT, and PRESS.DAT.

(3) STEPPER.BAS (pp.179-180)

- For initial adjustment of the displacer location.
- Pulse signals from DAC0 of DT2801-A are splitted into two separate terminals of step motor driver by digital logic circuit.
- Usually the initial position of displacer is about 75 mm high from its bottom.

G.2 Simulation program

This is the FORTRAN simulation program lists discussed in Chapter III. The computer program is listed in the following order.

(1) SUPER.FOR (pp.181-192)

- Main simulation program for the tandem magnetic refrigerator.
- Needs input file named SUPER.IN and He^3 data file HE3.DAT.
- Generates the temperature profiles of GGG and helium, refrigeration capacity calculation.

(2) FUNCS.FOR (pp.193-196)

- Set of subroutines for solving energy equations, interpolating He^3 properties, and so on.

(3) GGGPROP.FOR (pp.197-198)

- Calculating thermodynamic properties of GGG.
- Given temperature in Kelvin and $\mu_o H$ in tesla, entropy, s and its derivatives, $ds/d\mu_o H$ (equivalent to vdM/dT) and ds/dT are calculated.

(4) HELIUM.FOR (pp.199-201)

- Thermodynamic property calculation of He^3.
- Generates output data file HE3.DAT which contains density, enthalpy, specific heat , and entropy for a given pressure and at the temperature range between 1 K and 20.8 K. All properties are calculated for superheated state.
- HE3.DAT is an input data file for SUPER.FOR.

```
'   PRECOOL.BAS
'
' This is the program for showing real time data ( 3/10/92 )
'    during Precooling Process.
'
    DEFINT I-J
  OPEN "COM1:9600,N,8,2,CS,DS" FOR RANDOM AS #1
20 IF NOT EOF(1) THEN X$ = INPUT$(1, #1): GOTO 20
    OPEN "PRECOOL.DAT" FOR OUTPUT AS #2
    PRINT #2, " DATE = "; DATE$: PRINT
    PRINT #1, "#2,VIR=-6"
    SCREEN 2
    DIM Style%(10), Y0(10), Y(10)
    VIEW (30, 2)-(630, 172), , 1
    TIMAX = 120: YMAX = 100: YMIN = 0
    WINDOW (0, YMIN)-(TIMAX, YMAX)
    LOCATE 1, 1: PRINT USING "###"; YMAX
    LOCATE 22, 1: PRINT USING "###"; YMIN
    ' LOCATE 11, 2: PRINT USING "###"; 0
    VIEW PRINT 23 TO 25
    FOR J = 1 TO 6
     Y0(J) = 0
    NEXT J
25  INPUT "ENTER TIME IN SECONDS BETWEEN READINGS ( To stop type
0 )", X
28  CLS
    XCOOR = 0
    ' LINE (TIMAX, 0)-(0, 0)
    '   Initializing the 1st coord.
    '
    IF X <= 0 THEN 50
    HOLD = TIMER
30  IF (HOLD >= TIMER - X) GOTO 30
    PRINT " Time  = "; TIME$
    PRINT #2, TIMER;
    HOLD = TIMER
    PRINT #1, "#2,MVIN1,2,3,4,5"
    INPUT #1, V1, V2, V3, V4, V5
    '
    ' Applying 10 micron Amp. to Temp. sensors
    '
    r1 = -V1 * 100
    r2 = -V2 * 100
    r3 = -V3 * 100
    r4 = -V4 * 100
      r = r1
      GOSUB 500
      t1 = t
```

```
        r = r2
        GOSUB 500
        t2 = t
        r = r3
        GOSUB 500
        t3 = t
        r = r4
        GOSUB 500
        t4 = t
      PRINT USING "  ####.#"; v1; v2; v3; v4; V5
      PRINT USING "  ####.#"; t1; t2; t3; t4; V5
      PRINT #2, USING " ####.#"; t1; t2; t3; t4; V5
      Y(1) = 0    ' Nothing
      Y(2) = t1   ' Bottom Temperature - cryostat bottom
      Y(3) = t2   ' Down Temperature - base of magnets and displacer
      Y(4) = t3   ' Up Temperature - top of magnets
      Y(5) = t4   ' Top Temperature - top of displacer
      Y(6) = V5   ' LHe level indicator ( 30" calibrated)
        XCOOR = XCOOR + X
      FOR J = 1 TO 6
        LINE (XCOOR - X, Y0(J))-(XCOOR, Y(J))
        Y0(J) = Y(J)
      NEXT J
      IF XCOOR >= TIMAX THEN 28
      IF INKEY$ <> "" THEN 25
      GOTO 30
50    CLOSE #1
      CLOSE #2
      END

500   '
      '    Calibration for 220 ohm
      '
      wa = 3.64464
      wb = -1.44337
      wc = .142575
      wd = 2.77489
      IF r < .1 THEN 5500
      xl = LOG(r)
      t = (xl - wd) / (wa + wb * xl + wc * xl * xl)
      RETURN
5500  t = 0!
      RETURN
```

```
' ------------------------------------------------
'     MAIN.BAS ( Main-control program for power & motor )
'       4/ 17/92
' ------------------------------------------------
'
'
'
' This is the program to control Power supply and Slo-syn Step Motor
sinchrously
'   while it reads many data.
' This program is also useful for charging magnet in persistent mode.
'
' DAC0 is used for generating pulses for Step motor drive.
' DAC1 is used as a sweeper for Power supply or function generator.
'
'
    DEFINT I-J
    DIM analog.data%(24000),Vref.DATA%(2),Vref.idl%(2)
    DIM ANALOG.B1%(8), VOL.B1(8), SCALED.LSB(8), SCALED.LOW(8),
GAIN%(8), OFFSET(8)
    DIM Style%(10), Y0(10), Y(10)
'
' <---------- DT2801-A A/D conversion in Board 1 ----------
'
'
    CALL select.board(1)
    FOR I = 0 TO 7
        ANALOG.B1%(I) = 0
    NEXT I
'
'   OFFSET OF FILETERED AMPLIFIER 2
'
    OFFSET(0) = 0.006          ' CH#7
    OFFSET(1) = 0.004          ' CH#8+CH#14
    OFFSET(2) = - 0.006        ' CH#9
    OFFSET(3) = - 0.046        ' CH#10
    OFFSET(4) = 0.018          ' CH#11
    OFFSET(5) = 0.045          ' CH#12
    OFFSET(6) = - 0.001        ' CH#15
    OFFSET(7) = 0.001          ' CH#13
'
    HIGH.V! = 10!          ' Highest voltage in range.
    LOW.V! = -10!          ' Lowest voltage in range.
    RANGE! = HIGH.V! - LOW.V!  ' Total voltage range.
    NOC! = 4096!
    LSB! = RANGE! / NOC!       ' Voltage of Least Significant Bit.
    int.clo% = 0       ' Code 0, for internal clock mode.
    FOR I = 0 TO 7
```

```
        ANALOG.B1%(I) = 0
      GAIN%(I) = 4
       SCALED.LSB(I) = LSB! / 4        ' Calculate scaled LSB.
       SCALED.LOW(I) = LOW.V! / 4      ' Calculate scaled low voltage.
    NEXT I
      GAIN%(6) = 2
       SCALED.LSB(6) = LSB! / 2        ' Calculate scaled LSB.
       SCALED.LOW(6) = LOW.V! / 2      ' Calculate scaled low voltage.
' ------------------ DT2801-A A/D conversion in Board 1 ---------------->
'
' ------------------ DT2801-A D/A conversion in Board 2 ----------------
'
    CALL select.board(2)
    cls
    print "* Connect #22 ( DAC0 OUTPUT ) of Board 2 to Synchronizing divider !
" : print
    print "* Connect #23 ( DAC0 GND ) of Board 2 to Synchronizing divider ! " :
print
    print "* Connect #24 ( DAC1 OUTPUT ) of Board 2 to Techron P/S. !" : print
    print "* Connect #27 ( Digital GND ) to #23 in Board 2 ( COMMON ) !" : print
    print "* Connect #28 ( Digital OUT ) of Board 2 to Synchronizing divider ! " :
print
    print "* Turn on the Lake Shore Current Source !" : print
    print "* Turn on the Digital Logic Synchronizing Divider !" : print
    print "* Make sure 5 V P/S. is correctly connected to Synchronizing divider !"
: print
    locate 18,1
    PRINT "      Use 0.5 inch lead screw only !": PRINT
2   PRINT : INPUT " Period [19.2 ~ 36 ( 24 sec recommended )] = "; PERIOD
    cl.div% = (5 / 12 * PERIOD * 1000000) / (1.25 * 200 * 4 * 10) * 2
    CALL SET.CLOCK.divider(cl.div%)
    int.clo% = 0        ' Code 0, for internal clock mode.
    XY.MODE% = -1
    NOC! = 4096
    CALL SETUP.DAC(int.clo%, XY.MODE%)
    Vref.DATA%(1) = (0 + 10!) / 20! * 4096
    Vref.DATA%(2) = (0 + 10!) / 20! * 4096
    CALL DAC.VALUE(XY.MODE%, Vref.DATA%(1))    ' Initialization to 0 V
    number.of.values% = 19200       ' 5.0 in stroke w/ 0.5 in lead screw
'
' -------------find length of buffer for CDD--------------------------
'
   start% = 1
   length% = 0
    CALL xfdl(analog.data%(start%), length%)
   IF length% > number.of.values% GOTO 110
   start% = length% + 2
110  PRINT : PRINT "      start% for DAC control = "; start%
' ------------------ DT2801-A D/A conversion in Board 2 ----------------
```

```
    vmax = 5!
    DMAX% = (vmax + 10!) / 20! * 4096
    vmin = 0!
    DMIN% = (vmin + 10!) / 20! * 4096
    cws = start%
    cwe = cws + 4799
    ccws = cwe + 1601
    ccwe = ccws + 8000
    cw2s = ccwe + 1600
    cw2e = cw2s + 3199
    FOR I = cws TO cw2e + 1
        analog.data%(I) = DMAX%
    NEXT I
    FOR I = cws TO cwe STEP 4
        analog.data%(I) = DMIN%
      NEXT I
    FOR I = ccws TO ccwe STEP 4
        analog.data%(I) = DMIN%
    NEXT I
    FOR I = cw2s TO cw2e STEP 4
        analog.data%(I) = DMIN%
    NEXT I
'
' ---------- DT2801-A Digital Output for presetting FIFO ---------
'                ( MOTOR moves up first. )
'
    CALL ENABLE.FOR.OUTPUT (0)
    CALL OUTPUT.DIGITAL.VALUE (0, 1,&H0)
    CALL OUTPUT.DIGITAL.VALUE (0, 1,&HFFFF)
    '
    ' ------------------------------------
    '  Preparing for Techron Power Supply
    ' ------------------------------------
    '
5   CLS
    LOCATE 5, 1
    PRINT "-------------------< SELECT THE POWER MODE >----------------------"
    LOCATE 7, 1
    PRINT "  FOR CONSTANT CURRENT CALIBRATION MODE ------------------>
TYPE 1 "
    LOCATE 8, 1
    PRINT "  FOR BIPOLAR MAIN CURRENT SWEEP MODE  ------------------->
TYPE 2 "
    LOCATE 9, 1
    PRINT "  FOR JUST MONITORING  ---------------------------------> TYPE 3 "
    LOCATE 10, 1
    PRINT "  FOR CONSTANT VOLTAGE PERSISITENT CURRENT CHARGING
------> TYPE 4 "
    LOCATE 11, 1
```

```
   PRINT "  FOR CONSTANT VOLTAGE MODE MAIN OPERATION ----------
> TYPE 5 "
   LOCATE 16, 1
   PRINT "         You can turn on the POWER SUPPLY !!! "
   PRINT : PRINT " ----------First turn on the constant voltage mode , and "
   PRINT "        if you need, you may switch to the constant current mode !!! "
   INPUT M
   IF M = 1 THEN
       GOTO 10
   ELSEIF M = 2 THEN
       GOTO 20
   ELSEIF M = 3 THEN
       hold = TIMER
     GOTO 30
   ELSEIF M = 4 THEN
       GOTO 70
   ELSEIF M = 5 THEN
       GOTO 80
   ELSE
       GOTO 5
   END IF
   '
   '
10  PRINT " charging time ( sec ) = "; PERIOD/8
   PRINT " idling time ( sec ) = "; PERIOD/8*3
12  INPUT " charging current ( A ) = "; chi
   IF 3.6*chi/(PERIOD/8) > 10 THEN PRINT " Current is too high ! ":goto 12
   PRINT : PRINT " Please wait for a moment to generate pulses ! "
   '
   '   Calibration of Power Supply
   '
   vmax = chi/2
   '
   dch% = 1200
   did% = dch% * 3
   dv = vmax / dch%
   FOR i = start% TO start% + dch% - 1
     v = (i - start% + 1) * dv
     analog.data%(2*i) = (v + 10!) / 20! * 4096
   NEXT i
   FOR i = start% + dch% - 1 TO start% + dch% + did% - 1
     v = vmax
     analog.data%(2*i) = (v + 10!) / 20! * 4096
   NEXT i
   FOR i = start% + dch% + did% - 1 TO start% + 2 * dch% + did% - 1
     v = vmax - (i - start% - dch% - did% + 1) * dv
     analog.data%(2*i) = (v + 10!) / 20! * 4096
   NEXT i
   FOR i = start% + 2 * dch% + did% - 1 TO start% + 2 * (dch% + did%) - 1
```

```
    v = 0!
    analog.data%(2*i) = (v + 10!) / 20! * 4096
  NEXT i
  GOSUB 800
  GOTO 30
20  PRINT : PRINT
  INPUT " Imax = "; Imax
  PRINT " Imin = "; -Imax
  PRINT " PERIOD = "; PERIOD
  dp% = 9600
  number.of.values% = dp% * 2
  vmax = Imax/2
  vmin = -vmax
  dmax% = (vmax + 10!) / 20! * 4096
  dmin% = (vmin + 10!) / 20! * 4096
22  INPUT " RAMP MODE (1)  OR SINE MODE (2) ";RS
  PRINT : PRINT " Please wait for a moment to generate pulses ! "
  IF RS = 1 THEN
     GOTO 50
  ELSEIF RS = 2 THEN
     GOTO 60
  ELSE
     GOTO 22
  END IF
50  dv = vmax / dp% * 4
  FOR i = start% TO start% + dp% / 4 - 1
     v = (i - start% + 1) * dv
     analog.data%(2*i) = (v + 10!) / 20! * 4096
  NEXT i
  FOR i = start% + dp% / 4 - 1 TO start% + dp% * 3 / 4 - 1
     v = vmax - (i - start% - dp% / 4 + 1) * dv
     analog.data%(2*i) = (v + 10!) / 20! * 4096
  NEXT i
  FOR i = start% + dp% * 3 / 4 - 1 TO start% + dp% - 1
     v = vmin + (i - start% - dp% * 3 / 4 + 1) * dv
     analog.data%(2*i) = (v + 10!) / 20! * 4096
  NEXT i
  '
  '  Smoothing kinks at ramp mode in current control energization
  '
  '                -1
  '              -2    0
  '            -3 -------  1
  '          -4 ------------  2
  '        -5 ----------------  3
  '      -6 ------------------------ 4
  '    -7 ------------------------------ 5
  '
```

```
        IF ( N > 2*(start% + dp% / 4 - 6) AND N < 2*(start% + dp% / 4 + 5) ) THEN
analog.data%(N) = analog.data%(2*(start% + dp% / 4 + 5))
        IF ( N > 2*(start% + dp% *3 / 4 - 6) AND N < 2*(start% + dp% * 3 / 4 + 5) )
THEN  analog.data%(N) = analog.data%(2*(start% + dp% * 3 / 4 + 5))

    GOSUB 800
    GOTO 30
60  FOR i = start% TO start% + dp% - 1
      ii = i - start%
        v = vmax * sin( ii*2*3.1415/(dp% - 1) )
        analog.data%(2*i) = (v + 10!) / 20! * 4096
    NEXT i
    GOSUB 800
    GOTO 30
30  GOSUB 1000              ' For just monitoring
    print : INPUT " Do you want to convert data (Y/N) ";A$
    IF A$ = "Y" OR A$ ="y" THEN GOSUB 9000
    END
70  INPUT " charging time ( sec ) = "; chtime
    INPUT " charging voltage ( V ) = "; vol
    INPUT " idling voltage ( V ) = "; vidl
    Dvol% = (Vol/2 + 10!) / 20! * 4096
    Vref.idl%(1) = (vidl/2 + 10!) / 20! * 4096
    Vref.idl%(2) = (vidl/2 + 10!) / 20! * 4096
    dp% = 9600
    FOR i = start% TO start% + dp% - 1
        analog.data%(2*i) = Dvol%
    NEXT i
    number.of.values% = dp% * 2
    GOSUB 900
    GOTO 30
80  INPUT " charging voltage ampiitude ( V ) = "; vol
    vimax = vol / 2 / 1.83 * period / 4
    print "  ----------->  Maximum current flow will be +&- ";vimax
    pvol% = (Vol/2 + 10!) / 20! * 4096
    nvol% = (10! - Vol/2) / 20! * 4096
    dp% = 9600
    FOR i = start% TO start% + dp% - 1
        analog.data%(2*i) = pvol%
    NEXT i
    FOR i = start% + dp% / 4 - 1 TO start% + dp% * 3 / 4 - 1
        analog.data%(2*i) = nvol%
    NEXT i
    number.of.values% = dp% * 2
    '
    '   Smoothing kinks at  voltage control mode energization
    '
    '   + vol -------
    '                 |
```

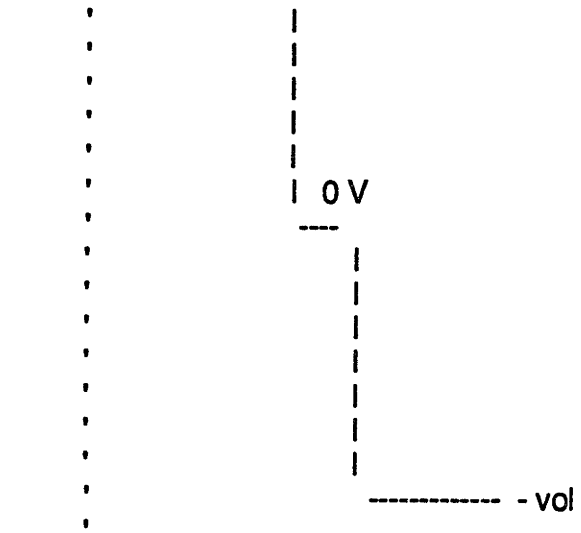


```
        IF ( N > 2*(start% + dp% / 4 - 6) AND N < 2*(start% + dp% / 4 + 5) ) THEN
analog.data%(N) = Vref.DATA%(1)
        IF ( N > 2*(start% + dp% *3 / 4 - 6) AND N < 2*(start% + dp% * 3 / 4 + 5) )
THEN  analog.data%(N) = Vref.DATA%(1)

    GOSUB 800
    GOTO 30
800  '
    ' SUB-PROGRAM FOR DATA ACQUISITION OF ACRO 900 ( current
charging )
    '
   OPEN "COM1:9600,N,8,2,CS,DS" FOR RANDOM AS #1
820  IF NOT EOF(1) THEN X$ = INPUT$(1, #1): GOTO 820
        OPEN "main.dat" FOR OUTPUT AS #2
      PRINT #1, "#3,VIR1,2,3,4,5,6,7=-3"
      PRINT #1, "#3,VIR8=-2"
      PRINT #1, "#1,VIR1,2,3=-4"
      PRINT #1, "#1,VIR4=-2"
        SCREEN 2
        VIEW (30, 2)-(630, 172), , 1
        TIMAX = 120: YMAX = 30: YMIN = -30
        WINDOW (0, YMIN)-(TIMAX, YMAX)
        LOCATE 1, 1: PRINT USING "###"; YMAX
        LOCATE 22, 1: PRINT USING "###"; YMIN
        ' LOCATE 11, 2: PRINT USING "###"; 0
        VIEW PRINT 23 TO 25
        FOR J = 1 TO 7
          Y0(J) = 0
        NEXT J
        ibr = 0
     X=1
828     CLS
        XCOOR = 0
```

```
      LINE (TIMAX, 0)-(0, 0)
    INPUT "PRESS ANY KEY AND RETURN TO START  "; ns
        schtime = TIMER
     CALL CONTINUOUS.DAC.DMA(number.of.values%, analog.data%(start%))
      hold = schtime: GOTO 832
830     CLS : hold = TIMER: XCOOR = 0: LINE (TIMAX, 0)-(0, 0)
832     PRINT #2, USING " ####.#"; TIMER-schtime;
        '
        ' ACRO DATA ACQUISITION
        '
        PRINT #1, "#3,VIN"
        INPUT #1, V1, V2, V3, V4, V5, V6, V7, V8
        PRINT #1, "#1,MVIN1,2,3"
        INPUT #1, V9, V10, V11
        PRINT #1, "#1,VIN4"
      INPUT #1, V12
        '
        ' 15 V excitation for absolute type pressure gage (V9,V10)
        ' 12 V excitation for differential type pressure gage (V11)
        ' 12 V excitation for position sensor (V12)
        '
        GOSUB 500   ' V9 -->P1  ( Pressure of right core )
        GOSUB 510   ' V10-->P2  ( Pressure of motor part )
        GOSUB 520   ' V11-->P3  ( Pressure of left core )
        GOSUB 530   ' V12-->P4  ( Position of displacer )
        GOSUB 540   ' V7 -->HL  ( Hall sensor of Right core )
    CALL select.board(1)
    FOR I = 0 TO 7
      CALL ADC.VALUE (I, GAIN%(I), ANALOG.B1%(I))
    NEXT I
    FOR I = 0 TO 7
        VOL.B1(I) = (ANALOG.B1%(I) * SCALED.LSB(I)) + SCALED.LOW(I) -
OFFSET(I)
    NEXT I
        GOSUB 400   ' V2       -->T2L ( T2 of LEFT CORE )
        GOSUB 410   ' VOL.B1(1) -->T2R ( T2 of RIGHT CORE )
        GOSUB 425   ' VOL.B1(7) -->Civ  ( Current of variational coil )
        GOSUB 430   ' VOL.B1(6) -->HR  ( Hall sensor of Left core )
      '
        PRINT USING "  ##.##"; T2L; T2R; HL; HR; V8; Civ;
      PRINT USING "  ###.#"; P1; P2; P3; P4
        PRINT #2, USING " ###.###"; V1; V2; V3; V4; V5; V6; V7; V8;
VOL.B1(0);VOL.B1(1);VOL.B1(2);VOL.B1(3);VOL.B1(4);VOL.B1(5); VOL.B1(6);
VOL.B1(7); P1; P2; P3; P4
        Y(1) = T2L
        Y(2) = T2R
        Y(3) = HL
        Y(4) = HR
        Y(5) = V8
```

```
        Y(6) = Civ
        Y(7) = P4
          XCOOR = XCOOR + X
        FOR J = 1 TO 7
          LINE (XCOOR - X, Y0(J))-(XCOOR, Y(J))
          Y0(J) = Y(J)
        NEXT J
        IF XCOOR >= TIMAX THEN 830
'
        hold = TIMER
        KeyInput$ = INKEY$
        IF KeyInput$ = "" THEN GOTO 832
850  CALL select.board(2)
    CALL xsdd
    CALL DAC.VALUE(XY.MODE%, Vref.DATA%(1))
    CLOSE #1
    CLOSE #2
    RETURN
900  '
    ' SUB-PROGRAM FOR DATA ACQUISITION OF ACRO 900 ( voltage
charging )
    '
        OPEN "COM1:9600,N,8,2,CS,DS" FOR RANDOM AS #1
920  IF NOT EOF(1) THEN x$ = INPUT$(1, #1): GOTO 920
        OPEN "main.DAT" FOR OUTPUT AS #2
      PRINT #1, "#3,VIR1,2,3,4,5,6,7=-3"
      PRINT #1, "#3,VIR8=-2"
      PRINT #1, "#1,VIR1,2,3=-4"
      PRINT #1, "#1,VIR4=-2"
        SCREEN 2
        VIEW (30, 2)-(630, 172), , 1
        TIMAX = 60: YMAX = 30: YMIN = -30
        WINDOW (0, YMIN)-(TIMAX, YMAX)
        LOCATE 1, 1: PRINT USING "###"; YMAX
        LOCATE 22, 1: PRINT USING "###"; YMIN
        LOCATE 11, 1: PRINT USING "###"; 0
        VIEW PRINT 23 TO 25
        FOR J = 1 TO 7
          Y0(J) = 0
        NEXT J
'
'
        ibr = 0 : x = 0.1
        itime = 0
925     INPUT "ENTER TIME IN SECONDS BETWEEN READINGS ( To stop
type 0 )", x
        IF x <= 0 THEN 950
        IF ibr = 1 THEN 932
928     CLS
```

```
        XCOOR = 0
        LINE (TIMAX, 0)-(0, 0)
        INPUT "PRESS ANY KEY AND RETURN TO START "; ns
        schtime = TIMER
        CALL continuous.DAC.dma(number.of.values%, analog.data%(start%))
        hold = schtime: GOTO 932
930     CLS : hold = TIMER: XCOOR = 0: LINE (TIMAX, 0)-(0, 0)
932     PRINT #2, USING " ####.#"; TIMER-schtime;
        '
        ' ACRO DATA ACQUISITION
        '
        PRINT #1, "#3,VIN"
        INPUT #1, V1, V2, V3, V4, V5, V6, V7, V8
        PRINT #1, "#1,MVIN1,2,3"
        INPUT #1, V9, V10, V11
        PRINT #1, "#1,VIN4"
      INPUT #1, V12
        '
        ' 15 V excitation for absolute type pressure gage (V9,V10)
        ' 12 V excitation for differential type pressure gage (V11)
        ' 12 V excitation for position sensor (V12)
        '
        GOSUB 500   ' V9 -->P1  ( Pressure of right core )
        GOSUB 510   ' V10-->P2  ( Pressure of motor part )
        GOSUB 520   ' V11-->P3  ( Pressure of left core )
        GOSUB 530   ' V12-->P4  ( Position of displacer )
        GOSUB 540   ' V7 -->HL  ( Hall sensor of Right core )
    CALL select.board(1)
    FOR I = 0 TO 7
      CALL ADC.VALUE (I, GAIN%(I), ANALOG.B1%(I))
    NEXT I
    FOR I = 0 TO 7
        VOL.B1(I) = (ANALOG.B1%(I) * SCALED.LSB(I)) + SCALED.LOW(I) -
OFFSET(I)
    NEXT I
        GOSUB 400   ' V2      -->T2L ( T2 of LEFT CORE )
        GOSUB 410   ' VOL.B1(1) -->T2R ( T2 of RIGHT CORE )
        GOSUB 420   ' VOL.B1(7) -->Cip  ( Current of persistent coil )
        GOSUB 430   ' VOL.B1(6) -->HR  ( Hall sensor of Left core )
      '
        PRINT USING "  ##.##"; T2L; T2R; HL; HR; V8; Cip;
      PRINT USING "  ###.#"; P1; P2; P3; P4
        PRINT #2, USING " ###.###"; V1; V2; V3; V4; V5; V6; V7; V8;
VOL.B1(0);VOL.B1(1);VOL.B1(2);VOL.B1(3);VOL.B1(4);VOL.B1(5); VOL.B1(6);
VOL.B1(7); P1; P2; P3; P4
        Y(1) = T2L
        Y(2) = T2R
        Y(3) = HL
        Y(4) = HR
```

```
        Y(5) = V8
        Y(6) = Cip
        Y(7) = P4
          XCOOR = XCOOR + X
        FOR J = 1 TO 7
          LINE (XCOOR - X, Y0(J))-(XCOOR, Y(J))
          Y0(J) = Y(J)
        NEXT J
        IF XCOOR >= TIMAX THEN 930
        IF itime = 1 THEN 940
      IF TIMER - schtime > chtime THEN
        CALL select.board(2)
        CALL xsdd
        CALL DAC.VALUE(XY.MODE%, Vref.idl%(1))
        itime = 1
        END IF
940     IF (hold >= TIMER - x) GOTO 940
        hold = TIMER
        KeyInput$ = INKEY$
        IF KeyInput$ <> "" THEN
          ibr = 1: GOTO 925
        ELSE
          GOTO 932
        END IF
950     CALL select.board(2)
      IF itime = 1 THEN 960
      CALL xsdd
960     CALL DAC.VALUE(XY.MODE%, Vref.DATA%(1))
      CLOSE #1
        CLOSE #2
        RETURN
1000 '
   ' SUB-PROGRAM FOR DATA ACQUISITION OF ACRO 900 ( monitoring )
   '
        OPEN "COM1:9600,N,8,2,CS,DS" FOR RANDOM AS #1
1020  IF NOT EOF(1) THEN x$ = INPUT$(1, #1): GOTO 1020
        OPEN "monitor.DAT" FOR OUTPUT AS #2
      PRINT #1, "#3,VIR1,2,3,4,5,6,7=-3"
      PRINT #1, "#3,VIR8=-2"
      PRINT #1, "#1,VIR1,2,3=-4"
      PRINT #1, "#1,VIR4=-2"
        SCREEN 2
        VIEW (30, 2)-(630, 172), , 1
        TIMAX = 60: YMAX = 30: YMIN = -30
        WINDOW (0, YMIN)-(TIMAX, YMAX)
        LOCATE 1, 1: PRINT USING "###"; YMAX
        LOCATE 22, 1: PRINT USING "###"; YMIN
        LOCATE 11, 1: PRINT USING "###"; 0
        VIEW PRINT 23 TO 25
```

```
        FOR J = 1 TO 7
          Y0(J) = 0
        NEXT J
        ibr = 0 : x = 0.1
1025    IF ibr = 0 THEN 1032
      INPUT "ENTER TIME IN SECONDS BETWEEN READINGS ( To stop type 0
)", x
        IF x <= 0 THEN 1050
        hold = TIMER: GOTO 1032
1030    CLS : hold = TIMER: XCOOR = 0: LINE (TIMAX, 0)-(0, 0)
1032  PRINT #2, USING " #######.#"; TIMER-schtime;
        '
        ' ACRO DATA ACQUISITION
        '
        PRINT #1, "#3,VIN"
        INPUT #1, V1, V2, V3, V4, V5, V6, V7, V8
        PRINT #1, "#1,MVIN1,2,3"
        INPUT #1, V9, V10, V11
        PRINT #1, "#1,VIN4"
      INPUT #1, V12
        '
        ' 15 V excitation for absolute type pressure gage (V9,V10)
        ' 12 V excitation for differential type pressure gage (V11)
        ' 12 V excitation for position sensor (V12)
        '
        GOSUB 500   ' V9 -->P1  ( Pressure of right core )
        GOSUB 510   ' V10-->P2  ( Pressure of motor part )
        GOSUB 520   ' V11-->P3  ( Pressure of left core )
        GOSUB 530   ' V12-->P4  ( Position of displacer )
        GOSUB 540   ' V7 -->HL  ( Hall sensor of Right core )
    CALL select.board(1)
    FOR I = 0 TO 7
      CALL ADC.VALUE (I, GAIN%(I), ANALOG.B1%(I))
    NEXT I
    FOR I = 0 TO 7
        VOL.B1(I) = (ANALOG.B1%(I) * SCALED.LSB(I)) + SCALED.LOW(I) -
OFFSET(I)
    NEXT I
        GOSUB 400   ' V2       -->T2L ( T2 of LEFT CORE )
        GOSUB 410   ' VOL.B1(1) -->T2R ( T2 of RIGHT CORE )
        GOSUB 425   ' VOL.B1(7) -->Civ  ( Current of variational coil )
        GOSUB 430   ' VOL.B1(6) -->HR  ( Hall sensor of Left core )
      '
        PRINT USING "  ##.##"; T2L; T2R; HL; HR; V8; Civ;
      PRINT USING "  ###.#"; P1; P2; P3; P4
        PRINT #2, USING " ###.###"; V1; V2; V3; V4; V5; V6; V7; V8;
VOL.B1(0);VOL.B1(1);VOL.B1(2);VOL.B1(3);VOL.B1(4);VOL.B1(5); VOL.B1(6);
VOL.B1(7); P1; P2; P3; P4
        Y(1) = T2L
```

```
        Y(2) = T2R
        Y(3) = HL
        Y(4) = HR
        Y(5) = V8
        Y(6) = Civ
        Y(7) = P4
          XCOOR = XCOOR + X
        FOR J = 1 TO 7
          LINE (XCOOR - X, Y0(J))-(XCOOR, Y(J))
          Y0(J) = Y(J)
        NEXT J
        IF XCOOR >= TIMAX THEN 1030
'
1040    IF (hold >= TIMER - x) GOTO 1040
        hold = TIMER
        KeyInput$ = INKEY$
        IF KeyInput$ <> "" THEN
          ibr = 1: GOTO 1025
        ELSE
          GOTO 1032
        END IF
1050 SCREEN 0
   LOCATE 5, 1
   PRINT " You have to adjust the displacer position again for next run !"
   PRINT
   PRINT "      Use  prgm. STEPPER to move the piston at center.    "
   CLOSE #1
   CLOSE #2
   RETURN

400  '
   '    Calibration for 48 ohm temp. sensor (#14), AMP 98.0
   '
    T2L = 1 / (-.359 + .02898 * LOG(V2 * 100000/98.0) + .013174 * LOG(V2 *
100000/98.0)^ 2)
   RETURN
410  '
   '    Calibration for 48 ohm temp. sensor (#27), AMP 100.2
   '
    T2R = 1 / (-.285 + .00615 * LOG(VOL.B1(1) * 100000/100.2) + .01481*
LOG(VOL.B1(1)* 100000/100.2)^ 2)
   RETURN
420  '
   '    Rshunt = 0.20 mohm for persistent coil, AMP 117.2
   '
   Cip = VOL.B1(7)/117.2 * 5000
   RETURN
425  '
   '    Rshunt = 0.25 mohm for variational coil, AMP 117.2
```

```
    '
    Civ = VOL.B1(7)/117.2 * 4000
    RETURN
430 '
    '    Calibration for BHA 921 Hall sensor, AMP 118
    '
    HR = VOL.B1(6)/118 / 0.024 * 3
    RETURN
500 '
    '    Calibration for G1 pressure sensor ( Torr )
    '
    P1 = 3.7521 - 5.2433 * V9
    RETURN
510 '
    '    Calibration for G2 pressure sensor ( Torr )
    '
    P2 = 11.862 - 5.2004 * V10
    RETURN
520 '
    '    Calibration for D1 pressure sensor ( Torr )
    '
    P3 = P2 - (-1.14336 - .6404 * V11)
    RETURN
530 '
    '    Calibration for position sensor ( Displacer starts from 6.0 V. )
    '
    P4 = 50 + (V12 - 6) * 25 / 3
    RETURN
540 '
    '    Calibration for BH 203 Hall sensor
    '
    HL = V7/ 0.35 * 3
    RETURN
9000 '
    '   Post-processing of raw data
    '

    OPEN "MAIN.DAT" FOR INPUT AS #3
    OPEN "LEFT.DAT" FOR OUTPUT AS #4
    OPEN "RIGHT.DAT" FOR OUTPUT AS #5
    OPEN "PRESS.DAT" FOR OUTPUT AS #6
    ndc = 0
    PRINT #4, "Lap. Time  TL1   TL2   TL3   TL4   TL5   TL6   HL    V    Ip
Pos."
    PRINT #5, "Lap. Time  TR1   TR2   TR3   TR4   TR5   TR6   Hr    V    Iv
Pos."
    PRINT #6, "Lap. Time  P-RIGHT  P-TOP  P-LEFT  Position"
    DO UNTIL EOF(3)
```

```
      INPUT #3,
TIM,VL1,VL2,VL3,VL4,VL5,VL6,VL7,VL8,VR1,VR2,VR3,VR4,VR5,VR6,VR7,VR8,
P1,P2,P3,P4
      GOSUB 1810 ' ----------+
      GOSUB 1820 '          |
      GOSUB 1830 '    Temp. of left core
      GOSUB 1840 '          |
      GOSUB 1850 '          |
      GOSUB 1860 ' ----------+
      GOSUB 1870 ' -- Hall sensor at left core
      GOSUB 1910 ' ----------+
      GOSUB 1920 '          |
      GOSUB 1930 '    Temp. of right core
      GOSUB 1940 '          |
      GOSUB 1950 '          |
      GOSUB 1960 ' ----------+
      GOSUB 1970 ' -- Hall sensor at right core
      GOSUB 1980 ' -- Persistent Current
      GOSUB 1990 ' -- Variational Current
      PRINT #4, USING " ####.#"; TIM;
      PRINT #4, USING " ###.##"; TL1; TL2; TL3; TL4; TL5; TL6; HL;VL8; Cip; P4
      PRINT #5, USING " ####.#"; TIM;
      PRINT #5, USING " ###.##"; TR1; TR2; TR3; TR4; TR5; TR6; HR;VL8; Civ;
P4
      PRINT #6, USING " ####.#"; TIM;
      PRINT #6, USING "  ####.#"; P1; P2; P3; P4
      ndc = ndc + 1
      LOCATE 20, 1: PRINT " No. of data conversion = "; ndc
   LOOP
   CLOSE #3
   CLOSE #4
   CLOSE #5
   CLOSE #6
   RETURN
1810  '
   '     Calibration for 48 ohm temp. sensor (#13), AMP 92.3
   '
   TL1 = 1 / (-.369 + .06894 * LOG( 472000*VL1/92.3/(5.0-VL1/92.3))/LOG(10)
+ .07053 * (LOG( 472000*VL1/92.3/(5.0-VL1/92.3))/LOG(10))^ 2)
   RETURN
1820  '
   '     Calibration for 48 ohm temp. sensor (#14), AMP 98.0
   '
   TL2 = 1 / (-.359 + .02898 * LOG(VL2 * 100000/98.0) + .013174 * LOG(VL2 *
100000/98.0)^ 2)
   RETURN
1830  '
   '     Calibration for 48 ohm temp. sensor (#15), AMP 99.4
   '
```

```
    TL3 = 1 / (-.367 + .07627 * LOG(VL3 * 100000/99.4)/LOG(10) + .06601 *
(LOG(VL3 * 100000/99.4)/LOG(10))^ 2)
    RETURN
1840  '
    '     Calibration for 48 ohm temp. sensor (#17), AMP 98.7
    '
    TL4 = 1 / (-.4274 + .12075 * LOG(VL4 * 100000/98.7)/LOG(10) + .05772 *
(LOG(VL4 * 100000/98.7)/LOG(10))^ 2)
    RETURN
1850  '
    '     Calibration for 48 ohm temp. sensor (#18), AMP 91.2-->101
    '
    TL5 = 1 / (-.379 + .08243 * LOG(VL5 * 100000/101)/LOG(10) + .06584 *
(LOG(VL5 * 100000/101)/LOG(10))^ 2)
    RETURN
1860  '
    '     Calibration for 48 ohm temp. sensor (#31), AMP 92.4-->95.4
    '
    TL6 = 1 / (-.3399 + .05655 * LOG(VL6 * 100000/95.4)/LOG(10) + .06952 *
(LOG(VL6 * 100000/95.4)/LOG(10))^ 2)
    RETURN
1870  '
     '     Calibration for BH 203 Hall sensor
     '
     HL = VL7/ 0.35 * 3
     RETURN
1910  '
    '     Calibration for 48 ohm temp. sensor (#25), AMP 98.9
    '
    TR1 = 1 / (-.3486 + .06 * LOG( 474000*VR1/98.9/(5.0-VR1/98.9))/LOG(10) +
.07 * (LOG( 474000*VR1/98.9/(5.0-VR1/98.9))/LOG(10))^ 2)
    RETURN
1920  '
    '     Calibration for 48 ohm temp. sensor (#27), AMP 100.2
    '
    TR2 = 1 / (-.285 + .00615 * LOG(VR2 * 100000/100.2) + .01481* LOG(VR2 *
100000/100.2)^ 2)
    RETURN
1930  '
    '     Calibration for 48 ohm temp. sensor (#28), AMP 121.7
    '
    TR3 = 1 / (-.3283 + .04851 * LOG(VR3 * 100000/121.7)/LOG(10) + .07143 *
(LOG(VR3 * 100000/121.7)/LOG(10))^ 2)
    RETURN
1940  '
    '     Calibration for 48 ohm temp. sensor (#29), AMP 116.4
    '
    TR4 = 1 / (-.35376 + .06852 * LOG(VR4 * 100000/116.4)/LOG(10) + .06728 *
(LOG(VR4 * 100000/116.4)/LOG(10))^ 2)
```

```
    RETURN
1950  '
    '     Calibration for 48 ohm temp. sensor (#30), AMP 125.0
    '
    TR5 = 1 / (-.35376 + .06852 * LOG(VR5 * 100000/125.0)/LOG(10) + .06728 *
(LOG(VR5 * 100000/125.0)/LOG(10))^ 2)
    RETURN
1960  '
    '     Calibration for 48 ohm temp. sensor (#32), AMP 101.5
    '
    TR6 = 1 / (-.37468 + .08104 * LOG(VR6 * 100000/101.5)/LOG(10) + .06507 *
(LOG(VR6 * 100000/101.5)/LOG(10))^ 2)
    RETURN
1970  '
    '     Calibration for BHA 921 Hall sensor, AMP 118
    '
    HR = VR7/118 / 0.024 * 3
    RETURN
1980  '
    '     Rshunt = 0.20 mohm for persistent coil, AMP 117.2
    '
    Cip = VR8/117.2 * 5000
    RETURN
1990  '
    '     Rshunt = 0.25 mohm for variational coil, AMP 117.2
    '
    Civ = VR8/117.2 * 4000
    RETURN
```

```
    '   STEPPER.BAS  (12/19/91)  <--- 2ND VERSION (Use only DAC0)
    '
    '   This program lets you move displacer as much as you want.
    '   You need to specify up(0) or down(1), and trasverse inch value.
    '
    CALL SELECT.BOARD(2)       ' Use Board 2 for Motor-control
1220 HIGH.V! = 10!             ' Highest voltage in range.
1230 LOW.V! = -10!             ' Lowest voltage in range.
1240 RANGE! = HIGH.V! - LOW.V!  ' Total voltage range.
1250 '
1260 NOC! = 4096
1280 LSB! = RANGE! / NOC!      ' Voltage of Least Significant Bit.
1290 CPV! = NOC! / RANGE!      ' Counts Per Volt.
    CALL ENABLE.FOR.OUTPUT (0)
1300 '
1310 PRINT
1320 INPUT " Enter 0 FOR UP, 1 FOR DOWN ( -1 terminates) "; DAC.SELECT%
1325 IF DAC.SELECT% < 0 GOTO 1500
1330 IF DAC.SELECT% = 0 OR DAC.SELECT% = 1 GOTO 1350
1340 PRINT " Illegal DAC ": GOTO 1310
1350 DESIRED.VOLTS! = 5!
    REF.VOLTS! = 0!
1360 '
1370 ANALOG.DATA.VALUE% = (DESIRED.VOLTS! - LOW.V!) * CPV!
    REF.DATA.VALUE% = (REF.VOLTS! - LOW.V!) * CPV!

1380 IF ANALOG.DATA.VALUE% > 4095 THEN PRINT " Too high ": GOTO
1350
1390 IF ANALOG.DATA.VALUE% < 0 THEN PRINT " Too low ": GOTO 1350
1400 '
1410 PRINT " Analog Data Value in hexadecimal ";
HEX$(ANALOG.DATA.VALUE%)
1420 '
1430 ACTUAL.VOLTS = (ANALOG.DATA.VALUE% * LSB!) + LOW.V!
1440 PRINT " Actual voltage requested: ". ACTUAL.VOLTS
1450 '
1460 ' This performs the actual data transfer.
1470 '
        INPUT " INCH OF TRAVERSE FOR 0.5 - LEAD SCREW ? "; TR
        NTR = TR / .5 * 200
   if DAC.SELECT% = 0 THEN  1478
      GOTO 1495
1478    CALL OUTPUT.DIGITAL.VALUE (0, 1,&H0)
    FOR NOLOOP = 1 TO NTR
       CALL DAC.VALUE(0, ANALOG.DATA.VALUE%)
       FOR KT = 1 TO 5: NEXT KT
       CALL DAC.VALUE(0, REF.DATA.VALUE%)
```

```
      FOR KT = 1 TO 5: NEXT KT
    NEXT NOLOOP
    GOTO 1310
1495 CALL OUTPUT.DIGITAL.VALUE (0, 1,&H0)
    CALL OUTPUT.DIGITAL.VALUE (0, 1,&HFFFF)  ' Toggle mode
      CALL DAC.VALUE(0, ANALOG.DATA.VALUE%)
      FOR KT = 1 TO 100: NEXT KT
    FOR NOLOOP = 1 TO NTR
      CALL DAC.VALUE(0, ANALOG.DATA.VALUE%)
      FOR KT = 1 TO 5: NEXT KT
      CALL DAC.VALUE(0, REF.DATA.VALUE%)
      FOR KT = 1 TO 5: NEXT KT
    NEXT NOLOOP
    GOTO 1310
1500 PRINT "End of STEPPER.BAS"
```

```
c  SUPER.FOR
c
c     Calculation of transient temperature profiles of magnetic
c     refrigeration  (11/8/1990)
c
c    [ LOOP HIERARCHY ]
c
c     CYCLE LOOP  <---------- # of cycle times
c        itan LOOP  <---------- 1 or 2 for tandem system
c          k LOOP  <---------- 0 to 3 for magnetion process
c            i LOOP  <---------- 2 or 8 steps for each process
c              j LOOP  <---------- # of segments
c                .
c                .
c                .
c              j END
c            i END
c          k END
c        itan END
c     CYCLE END
c
c
c     << Explanation about variables used in the program >>
c
c    [ Helium :   GGG     : Description                  ]
c     ------------------------------------------------------------
c     Ti(1,j)  :  Tg0(1,j)   : initial temp. for 1st core
c     Ti(2,j)  :  Tg0(2,j)   : initial temp. for 2nd core
c     T1(j,i)  :  Tg1(j,i)   : temp. from the former step
c     T2(j)    :  Tg2(j)     : temp. to be calculated
c          nseg ----------->  warm end side
c            1  ----------->  cold end side
c     ------------------------------------------------------------
c
        real m0,mout          ! (g/vol of segment)
        real T1(50,20),T2(50),Ti(2,50),tb(4,10),x(50)
        real m_var(50,0:3),m_error,tot_mass,tot_des   ! (g)
        real m_c(30),m_h(30)                  ! (g)
        real Hfin_c(0:3),Hint_c
        real Hfin_w(0:3),Hint_w,H_c,H_w
        real delt_H_c,delt_H_w,hout_c(10),hout_h(10)
        real Tg2(50),Tg1(50,20),time(0:3),Tg0(2,50),Dc(50)
        real vol         ! (cc) for entire core
        real volseg(0:50)     ! (cc) for a segment
      integer flag,num(0:3)
        common pres
      common jdag
        COMMON hedens(88,5),heenth(88,5),hecp(88,5),other(88,5)
```

```
      OPEN(UNIT=3,FILE='[jeong.heprop]HE3.DAT',TYPE='OLD')
      OPEN(UNIT=1,FILE='[jeong.fortp]super.in',TYPE='OLD')
      OPEN(UNIT=2,FILE='[jeong.fortp]he.t',TYPE='new')
      OPEN(UNIT=4,FILE='[jeong.fortp]ggg.t',TYPE='new')
      OPEN(UNIT=7,FILE='[jeong.fortp]out7.DAT',TYPE='new')
C -----------------------------------------------------------------
C     INPUT ROUNTINE
C -----------------------------------------------------------------
      do j=1,5
       do i=1,88
        READ(3,747) hedens(i,j),heenth(i,j),hecp(i,j),other(i,j)
       enddo
      write(6,747) hedens(1,j),heenth(1,j),hecp(1,j),other(1,j)
      enddo
747   format(f10.3,f10.6,f10.3,f10.5)
     refnet = 0.0
     itan = 0
      vol = 30.4  ! (cc, This is not GGG volume but total core volume.)
     Dcore = 0.0204  ! (m, Normal GGG core diameter )
C
C
C     'Enter 1 for external dead volumes, else enter 0'
      read(1,700) flag
      write(2,700) flag
      if (flag .eq. 1) then
C     'Enter the decay factor'
       read(1,700) fact
      endif
C     'Enter number of complete cycles desired'
      read(1,700) icyl
      write(2,700) icyl
C     'Enter number for temperature input from file'
C     '  enter 0 for input from screen'
      read(1,700) idat
      write(2,700) idat
      if (idat .eq. 0) then
C      write(6,*) 'Enter initial temps, before magnetization,'
C      write(6,*) ' For a linear profile: Tcold_end, Twarm_end'
       read(1,730)  Tcold_end, Twarm_end
       write(2,730)  Tcold_end, Twarm_end
C      write(6,*) 'Enter number of segments in core (less than 51)'
       read(1,700) nseg
       write(2,700) nseg
C      write(6,*) 'Enter 1 for starting from 4.2 K everywhere'
       read(1,700) itrans
       write(2,700) itrans
C
C    Initialize temperature arrays.
C
```

```
      if (itrans.eq.1) then
         do j=1,nseg
        Ti(1,j) = Twarm_end
        Ti(2,j) = Ti(1,j)
        T2(j) =  Ti(1,j)
        T1(j,1) =  Ti(1,j)
        Tg1(j,1) =  Ti(1,j)
        Tg2(j) =  Ti(1,j)
        Tg0(1,j) =  Ti(1,j)
        Tg0(2,j) =  Ti(1,j)
         enddo
      else
       do j=1,nseg
        x(j) = ( j - 0.5 ) / float(nseg)
        Ti(1,j) = Tcold_end + (Twarm_end - Tcold_end) * x(j)
        Ti(2,j) = Ti(1,j)
        T2(j) =  Ti(1,j)
        T1(j,1) =  Ti(1,j)
        Tg1(j,1) =  Ti(1,j)
        Tg2(j) =  Ti(1,j)
        Tg0(1,j) =  Ti(1,j)
        Tg0(2,j) =  Ti(1,j)
         enddo
      endif
       else
         read(idat,16) nseg,itan
c     for He temp. of 1st core
         read(idat,15) (Ti(1,j),j=1,nseg)
c     for GGG temp. of 1st core
         read(idat,15) (Tg0(1,j),j=1,nseg)
c     for He temp. of 2nd core
         read(idat,15) (Ti(2,j),j=1,nseg)
c     for GGG temp. of 2nd core
         read(idat,15) (Tg0(2,j),j=1,nseg)
         do j=1,nseg
           T2(j) = Ti(2,j)
           T1(j,1) = Ti(2,j)
           Tg1(j,1) = Tg0(2,j)
           Tg2(j) = Tg0(2,j)
         enddo
       endif
c      write(6,*) 'Enter the diameter ratio of core'
      read(1,750) dhdc
      AhAc = dhdc * dhdc
      do 500 j=1,nseg
        volseg(j)=vol/nseg*2.0/(AhAc + 1.0) *
     *          (1.0+float(j-1)/float(nseg-1)*(AhAc-1.0))
        Dc(j)=Dcore*sqrt(2.0/(AhAc + 1.0) *
     *          (1.0+float(j-1)/float(nseg-1)*(AhAc-1.0)))
```

```
          write(*,920) j,AhAc,Dc(j),volseg(j)
c       x(j) is used for plotting x - axis
          x(j) = (j-0.5)/float(nseg)
500     continue
        volseg(nseg+1) = volseg(nseg)
        volseg(0) = volseg(1)
          print *,'volseg(1),volseg(nseg)=',volseg(1),volseg(nseg)
           read(1,700) jdag
           write(2,700) jdag
c         write(6,*) 'Enter the operating pressure between 0.02 and 0.06'
          read(1,750) pres
          write(2,750) pres
c         write(6,*) 'Enter the temperature of the warm reservoir'
          read(1,750) Twarm
          write(2,750) Twarm
          if (Twarm .gt. 10) then
            ymax = 20.
          else
            ymax = 10.
          endif
c         write(6,*) 'Enter the temperature of the cold reservoir'
          read(1,750) Tcold
          write(2,750) Tcold
c         write(6,*) 'Enter helium gap around outside of core, (mils)'
          read(1,750) del
          write(2,750) del
          del = del*2.54/1000.
          por = (1.53*2.54 - del/2.) * 3.1415 * del / 11.86
c         write(6,*)'Enter the segment number at which the field divides'
          read(1,700) ndivide
          write(2,700) ndivide
          read(1,700) mfv
          write(2,700) mfv
          read(1,750) slope
          write(2,750) slope
c         write(6,*) 'Enter initial field for the cold and warm ends'
          read(1,730) Hint_c, Hint_w
          write(2,730) Hint_c, Hint_w
c       write(6,*) '    and then for each time step...'
          do k=0,3
c           write(6,*) 'Enter final field for the cold and warm ends'
            read(1,730) Hfin_c(k),Hfin_w(k)
            write(2,730) Hfin_c(k),Hfin_w(k)
c         write(6,*) 'Enter the period during this step'
            read(1,750) time(k)
            write(2,750) time(k)
c         write(6,*) 'Enter number of steps in H (less than 21)'
            read(1,700) num(k)
            write(2,700) num(k)
```

```
c         write(6,*) 'Enter 1 for variable flow'
          read(1,700) idat
          write(2,700) idat
          if (idat .eq. 1) then
c           write(6,*) 'Enter flow in (g) for each time step'
            read(1,760) (m_var(i,k) ,i=1,num(k))
          else
c           write(6,*)'Enter total forced helium flow during process'
            read(1,750) hold
            write(2,750) hold
           do i=1,num(k)
             m_var(i,k) = hold/float(num(k))
            enddo
          endif
        enddo
      read(1,700) iplot
      write(2,700) iplot
c -------------------------------------------------------------------
c       FORMAT ROUTINE
c -------------------------------------------------------------------
700     format(55x,i5)
730     format(50x,2f5.3)
750     format(55x,f5.2)
760     format(55x,f5.3)
890     format(1x,2f10.5)
900     format(//1x,'num = ',i4,' Refrigeration = ',f10.5
     * /1x,'         Net refrigeration = ',f10.5)
910     format(//1x,'num = ',i4,' Heat rejection = ',f10.5
     * /1x,'         Net heat rejection = ',f10.5)
920     format(10x,i4,3f8.5)
15      format(10f6.2)
16      format(2i5)
20      format(' cold end flow',10f7.4)
22      format(' warm end flow',10f7.4)
23      format(f9.2, f6.2, f6.2, f6.2 )
25      format(' tot_mass =',f6.3)
26      format('    itan = ',i2)
c -------------------------------------------------------------------
C       MAGNETIC FIELD INPUT ADJUSTMENT
c -------------------------------------------------------------------
        if (Hfin_c(3) .ne. Hint_c) then
          write(6,*) 'The initial field and final field must match'
          write(6,*) 'Hfin_c(3) is reset to ',Hint_c
          Hfin_c(3) = Hint_c
        endif
        if (Hfin_w(3) .ne. Hint_w) then
          write(6,*) 'The initial field and final field must match'
          write(6,*) 'Hfin_w(3) is reset to ',Hint_w
          Hfin_w(3) = Hint_w
```

```
        endif
c       Save initial temperature array in he.t
        write(2,*) 'Initial temperature of 1st core'
        write(2,15) (Ti(1,j),j=1,nseg)
        write(2,*) 'Initial temperature of 2nd core'
        write(2,15) (Ti(2,j),j=1,nseg)
c ---------------------------------------------------------------
        Tin_w = Twarm
        jcount = 0
c
c ---------------------------------------------------------------
c       TANDEM CORE CALCULATION
c ---------------------------------------------------------------
      if(itan.eq.2) goto 410
      if(jcount.ne.0) goto 410
      k = 1
420     k = k +1
      do jn=1,nseg
        Ti(2,jn) = T2(jn)
        Tg0(2,jn) = Tg2(jn)
      enddo
      if(k.gt.3) goto 410
      goto 400
c
410     dowhile (jcount .lt. icyl)
        jcount = jcount + 1
c
c
      do 430 itan = 1,2
       refnet = 0.0
       refhnet = 0.0
       do 440 jm = 1,nseg
         T1(jm,1) = Ti(itan,jm)
         Tg1(jm,1) = Tg0(itan,jm)
440      continue
c
        write(2,*) ' -'
c
        do k=0,3
c
          H_c = Hfin_c( mod(k+3,4) )
          delt_H_c = (Hfin_c(k) - Hfin_c(mod(k+3,4)))/float(num(k))
          H_w = Hfin_w( mod(k+3,4) )
        delt_H_w = (Hfin_w(k) - Hfin_w(mod(k+3,4)))/float(num(k))
          if (Hfin_c(k) .ge. Hfin_c( mod(k+3,4) ) ) then
c
c
c ---------------------------------------------------------------
c       MAGNETIZING:
```

```
c ---------------------------------------------------------------
c MAGNETIZATION: solve from left to right
c m0 is guessed at left side and then is checked at right side.
c The entire proces is repeted at each time step to get m0 on the
c right end to equal zero.
c
c
        write(6,*) ' '
        tot_mass = 0.
        tot_des = 0.
        m_error = 0.
       delt = time(k)/float(num(k))
c   Iterate over time with i.
      refh = 0.0
        do i=1,num(k)
          m_c(i) = m_var(i,k) - m_error * (.1/(.1 + por))
          icount = 0
100       m0 = m_c(i) / volseg(1)
          h0 = He_HT(Tb(k+2,i))
          do j=1,nseq
             T2(j) = T1(j,i)
           Tg2(j) = Tg1(j,i)
          enddo
c
        T2(0) = Tb(k+2,i)
        T1(0,i) = Tb(k+2,i)
c      Iterate over the segments with j.
          do j=1,nseg
          if (j .gt. ndivide) then
                H1 = H_w
                H2 = H_w + delt_H_w
             else
                H1 = H_c
                H2 = H_c + delt_H_c
             endif
c
            if (mfv.eq.1) then
              hfactor=1.0+(slope-1.0)*float(j-1)/float(nseg-1)
             h1 = h1 * hfactor
             h2 = h2 * hfactor
            endif
c
c       (((( Solving energy balance equation  ))))
c
            f = -.1
            del_T = 0.1
          Tg2(j)  = Tg1(j,i) + 0.1
          T2B = ( T2(j-1)+T1(j-1,i) )/2.0
            dowhile (abs(del_T) .gt. .003 .and. abs(f) .gt. 0.0001)
```

```
            dowhile (del_T*f .lt. 0 .and. abs(f) .gt. 0.0001)
             T2(j) = T2(j) + del_T
c
c       GGG-DAG calculation
c
          if (j.lt.jdag) then
              f = transg(T2(j),T1(j,i),H2,H1,por,m0,h0,havg,mout
     *         ,Tg2(j),Tg1(j,i),delt,T2B,hhh,rmate,re,g,Dc(j))
       if (T2(j).lt.1.1 .or. T1(j,i).lt.1.1) then
       type*,' Magnetizing j,f,T1(j,i),del_T,T2(j)', j,f
       type*,T1(j,i),del_T,T2(j)
      endif
          else
              f = transd(T2(j),T1(j,i),H2,H1,por,m0,h0,havg,mout
     *         ,Tg2(j),Tg1(j,i),delt,T2B)
          endif
            enddo
             del_T = -0.17*del_T
           enddo
           m0 = mout*volseg(j)/volseg(j+1)
           h0 = havg
         enddo ! end of j step
c ---------------------------------------------------------------
c       DENSITY INDUCED NET FLOW ADJUSTMENT
c ---------------------------------------------------------------
c  Decide whether to send back and recalculate with new m_c.
c
         if (icount .eq. 0) tot_des = tot_des + m_var(i,k)
         m_error = (tot_mass+m0*volseg(nseg)) - tot_des
c        if (i .eq. num(k) .and. m_var(i,k) .ge. .0) then
          factor = .2
          if (abs(m_error) .gt. .0001 .and. icount .lt. 6) then
            m_c(i) = m_c(i) - factor*m_error
            icount = icount + 1
            goto 100
          endif
c        endif
c
         m_h(i) = m0 * volseg(nseg)
         tot_mass = tot_mass + m_h(i)

         write(6,23) m_h(i),T2(1),T2(nseg-1),T2(nseg)
         H_c = H_c + delt_H_c
         H_w = H_w + delt_H_w
         do j=1,nseg
            T1(j,i+1) = T2(j)
            Tg1(j,i+1) = Tg2(j)
         enddo
       hout_h(i) = (He_HT(T2(nseg)) - He_HT(Twarm) ) * m_h(i)
```

```
          refh = refh + hout_h(i)
          write(11,890) hout_h(i),T2(nseg)
          enddo          ! end of time step (i)
         refhnet = refhnet + refh
         write(11,910) num(k),refh,refhnet
c----------------------------------------
         if(iplot.ne.1) goto 470
c---------Plotting temperature profiles
           do i=1,num(k)+1
           call set_trace_mg(' ',0,' ',1.)
             call trace_mg(x(1),T1(1,i),nseg)
           enddo
          call ylabel_mg('Temp. of Helium (K)',0.8,'v','TR')
            call xlabel_mg('Distance Along Core',0.8,'h','TR')
            call scale_mg('Y',0.,ymax,2.)
            call fancy_mg
            call grid_mg
            call graph_mg
            call stop_mg
            do i=1,num(k)+1
            call set_trace_mg(' ',0,' ',1.)
              call trace_mg(x(1),Tg1(1,i),nseg)
            enddo
         call ylabel_mg('Temp. of GGG (K)',0.8,'v','TR')
            call xlabel_mg('Distance Along Core',0.8,'h','TR')
            call scale_mg('Y',0.,ymax,2.)
            call fancy_mg
            call grid_mg
            call graph_mg
            call stop_mg
470     continue
c
c
c
      Else

c ---------------------------------------------------------------
c       DEMAGNETIZING:
c ---------------------------------------------------------------
400     H_c = Hfin_c( mod(k+3,4) )
        delt_H_c = (Hfin_c(k) - Hfin_c( mod(k+3,4) ) ) / float(num(k))
        H_w = Hfin_w( mod(k+3,4) )
        delt_H_w = (Hfin_w(k) - Hfin_w( mod(k+3,4) ) ) / float(num(k))
c
        tot_mass = 0.
c   Iterate over time with i.
       ref = 0.0
       delt = time(k)/float(num(k))
c
```

```
      do i=1,num(k)
        m_h(i) = m_var(i,k)
1000    m0 = m_h(i) / volseg(nseg)
        h0 = He_HT(Tin_w)
        do j=1,nseg
          T2(j) = T1(j,i)
        Tg2(j) = Tg1(j,i)
        enddo
      T2(nseg+1) = Tin_w
      T1(nseg+1,i) = Tin_w
c     Iterate over the segments with j.
        do j=nseg,1,-1
            if (j .gt. ndivide) then
              H1 = H_w
              H2 = H_w + delt_H_w
            else
              H1 = H_c
              H2 = H_c + delt_H_c
          endif
c
           if (mfv.eq.1) then
            hfactor=1.0+(slope-1.0)*float(j-1)/float(nseg-1)
           h1 = h1 * hfactor
           h2 = h2 * hfactor
           endif
c
c     (((( Solving energy balance equation ))))
c
          f = .1
          del_T = -0.1
        Tg2(j) = Tg1(j,i) - 0.1
        T2B = ( T1(j+1,i)+T2(j+1) )/2.0
          dowhile (abs(del_T) .gt. .003 .and. abs(f) .gt. 0.0001)
            dowhile (del_T*f .lt. 0 .and. abs(f) .gt. 0.0001)
              T2(j) = T2(j) + del_T
c
c     GGG-DAG calculation
c
          if (j.lt.jdag) then
              f = transg(T2(j),T1(j,i),H2,H1,por,m0,h0,havg,mout
     *          ,Tg2(j),Tg1(j,i),delt,T2B,hhh,rmate,re,g,Dc(j))
   if (T2(j).lt.1.1 .or. T1(j,i).lt.1.1) then
     type*,'deMagnetizing j,f,T1(j,i),del_T,T2(j)', j,f
     type*,T1(j,i),del_T,T2(j)
   endif
          else
              f = transd(ttt2,ttt1,H2,H1,por,m0,h0,havg,mout
     *          ,Tg2(j),Tg1(j,i),delt,T2B)
          endif
```

```
c
                enddo
                del_T = -0.17*del_T
              enddo
                m0 = mout*volseg(j)/volseg(j-1)
                h0 = havg
              if (j.eq.1) type *,'T2(1) = ',T2(1)
              enddo  ! end of j step
c
              m_c(i) = m0 * volseg(1)
              tot_mass = tot_mass + m_c(i)
c
              write(6,23) m_c(i),T2(1),T2(nseg-1),T2(nseg)
              H_c = H_c + delt_H_c
              H_w = H_w + delt_H_w
              do j=1,nseg
                 T1(j,i+1) = T2(j)
                 Tg1(j,i+1) = Tg2(j)
              enddo
            hout_c(i) = (He_HT(T2(1)) - He_HT(Tcold) ) * m_c(i)
            ref = ref + hout_c(i)
            write(11,890) hout_c(i),T2(1)
              Tb(k,i) = T2(1)
              if(Tb(k,i).lt.Tcold) Tb(k,i) = Tcold
            enddo          ! end of time step (i)
c ---------------------------------------------------------------
           refnet = refnet - ref
           write(11,900) num(k),ref,refnet
c ---------------------------------------------------------------
c       PLOTTING ROUTINE
c ---------------------------------------------------------------
           if(iplot.ne.1) goto 480
             do i=1,num(k)+1
             call set_trace_mg(' ',0,' ',1.)
               call trace_mg(x(1),T1(1,i),nseg)
             enddo
            call ylabel_mg('Temp. of Helium (K)',0.8,'v','TR')
              call xlabel_mg('Distance Along Core',0.8,'h','TR')
              call scale_mg('Y',0.,ymax,2.)
              call fancy_mg
              call grid_mg
              call graph_mg
              call stop_mg
              do i=1,num(k)+1
              call set_trace_mg(' ',0,' ',1.)
                call trace_mg(x(1),Tg1(1,i),nseg)
              enddo
           call ylabel_mg('Temp. of GGG (K)',0.8,'v','TR')
              call xlabel_mg('Distance Along Core',0.8,'h','TR')
```

```
          call scale_mg('Y',0.,ymax,2.)
          call fancy_mg
          call grid_mg
          call graph_mg
          call stop_mg
480     continue
c-----------------------------------------
        endif      ! end of warm vrs cold blow

c        save temperature array at end of process
         write(2,26) itan
           write(2,15) (T2(j),j=1,nseg)
           write(2,20) (m_c(i),i=1,num(k))
           write(2,22) (m_h(i),i=1,num(k))
           write(2,25) tot_mass
         write(4,26) itan
           write(4,15) (Tg2(j),j=1,nseg)
           write(4,20) (m_c(i),i=1,num(k))
           write(4,22) (m_h(i),i=1,num(k))
           write(4,25) tot_mass
         do j=1,nseg
              T1(j,1) = T2(j)
              Tg1(j,1) = Tg2(j)
           enddo
         if(jcount.eq.0) goto 420

          enddo          ! end of k iteration
         do j = 1,nseg
          Ti(itan,j) = T2(j)
          Tg0(itan,j) = Tg2(j)
         enddo
430      continue ! end of itan iteration

         enddo          ! end of cycle iteration
c
c
         do itan=1,2
           write(7,16) nseg,itan
         write(7,15) (Ti(itan,j),j=1,nseg)
       enddo
         end
```

```
c      FUNCS.FOR
       FUNCTION TRANSG(T2,T1,H2,H1,por,m0,h0,enthavg,mout
     *  ,Tg2,Tg1,delt,T2B,H,mrate,Re,G) ! (j/g)
c -------------------------------------------------------------
c       GGG CALCULATION
c
c      Date of creation = Nov.18,1989
c -------------------------------------------------------------
        real T2,T1,H2,H1,por,m0,h0
        real enthavg,mout,mrate
       eps = 0.38
         x_g = 1.0 - eps
         x_r = .0 - por
         x_he = eps + por
c
       dp = 0.0007          ! (m, particle diameter)
         rho_g = 7.14                ! (g/cc)
         rho_r = 1.            ! (g/cc)
         Tavg = (T2+T1)/2.  ! (K)
       T2a = (T2B + T2)/2.
       T1a = (T2B + T1)/2.
         enthavg = He_HT(T2) ! (j/g)
         Havg = (H2 + H1)/2.        ! (T)
         mout = m0 + x_he*( He_rho(T1) - He_rho(T2) ) ! (g/cc)
         x3 = x_he*( rhoHe_H(T2) - rhoHe_H(T1) )
       X5 = mout*enthavg - m0*h0
       mrate = (m0 + mout)/2./delt * 0.001 ! (kg/sec)
       dh = 2.*dp/3./(1.-eps)
       dc = 0.018          ! (m, core diameter)
       G = abs(mrate) * 4./(eps*3.14159265*dc*dc)
       Re = dh * G /1.2e-6   ! (viscosity-conductivity 1.2e-6-0.013)
       H = 0.23 * exp(0.7*log(Re) + 1./3.*log(0.7)) * 0.013/dh
       Tg2 = (x3+x5)/(H*Ah*delt*1.0e-6)+T2
         Tgavg = (Tg2+Tg1)/2.      ! (K)
       if (Tgavg.le.1.0) then
        call GGGprop(1.1,Havg,dsdh1,s1,dsdt1)
        call GGGprop(1.0,Havg,dsdh0,s0,dsdt0)
        dSdH = (1.1-Tgavg)/0.1*(dsdh0-dsdh1) + dsdh1
        S = (1.1-Tgavg)/0.1*(s0-s1) + s1
        dSdT = (1.1-Tgavg)/0.1*(dsdt0-dsdt1) + dsdt1
       else
          call GGGPROP(Tgavg,Havg,dSdH,S,dSdT)
       endif
         x1 = x_g*rho_g*Tgavg *( dSdT*(Tg2-Tg1) + dSdH*(H2-H1) )
         x2 = x_r*rho_r*( Rub_HT(T2) - Rub_HT(T1) )
         x4 = - h0*m0 + enthavg * mout
         transg = x1 + x2 + x3 + x4
         if (mout .lt. 0.) then
```

```
        endif
      return
      end

      FUNCTION TRANSd(T2,T1,H2,H1,por,m0,h0,enthavg,mcut) ! (j/g)
c -------------------------------------------------------------
c     POTENTIAL USAGE ROUTINE FOR DAG CALCULATION
c -------------------------------------------------------------
      real T2,T1,H2,H1,por,m0,h0
      real enthavg,mout
      return
      end
      FUNCTION Rub_HT(temp)          ! (J/g-K)
      real temp
         if (temp .lt. 7.045) then
          Rub_HT = 0.
         else
          Rub_HT = (4.4*temp**2 - 62*temp + 250) / 1000.
         endif
      return
      end

      FUNCTION He_rho(Temp)  ! (g/cc)
      real temp
         CALL HEPROP2(temp,dens,enth,CP,COND)
         He_rho = dens
      return
      end

      FUNCTION rhoHe_H(temp)  ! (j/cc)
      real temp
         CALL HEPROP2(temp,dens,enth,CP,COND)
         rhoHe_H = dens * enth   ! (j/cc)
      return
      end

      FUNCTION He_HT(temp)  ! (j/g)
      real temp
         CALL HEPROP2(temp,dens,enth,CP,COND)
         He_HT = enth
      return
      end
c -------------------------------------------------------------
      subroutine HEPROP2(temp,dens,enth,cp,cond)
c -------------------------------------------------------------
c     INTERPOLATING He PROPERTY
c -------------------------------------------------------------
      real temp,dens,enth,cp,cond
      real array(5)
```

```
      common pres
     common jdag
      common hedens(88,5),heenth(88,5),hecp(88,5),other(88,5)
      data array/0.02,0.03,0.04,0.05,0.06/
       j = 1
       dowhile ( pres .gt. array(j+1) )
          j = j+1
       enddo
       pfactor = (pres - array(j)) / (array(j+1) - array(j))

    if (temp .lt. 1.1) then
          type*,temp,'Helium temp less than 1.1'
         hed = (1.1-temp)/0.2*(hedens(1,j)-
     *    hedens(3,j))+hedens(1,j)
         hec = (1.1-temp)/0.2*(hecp(1,j)-
     *    hecp(3,j))+hecp(1,j)
         hee = (1.1-temp)/0.2*(heenth(1,j)-
     *    heenth(3,j))+heenth(1,j)
         heo = (1.1-temp)/0.2*(other(1,j)-
     *    other(3,j))+other(1,j)
         hedd = (1.1-temp)/0.2*(hedens(1,j+1)-
     *    hedens(3,j+1))+hedens(1,j+1)
         hecc = (1.1-temp)/0.2*(hecp(1,j+1)-
     *    hecp(3,j+1))+hecp(1,j+1)
         heee = (1.1-temp)/0.2*(heenth(1,j+1)-
     *    heenth(3,j+1))+heenth(1,j+1)
         heoo = (1.1-temp)/0.2*(other(1,j+1)-
     *    other(3,j+1))+other(1,j+1)
          dens = ( hed + pfactor * ( hedd -
    &          hed) ) / 1000.
          cp = hec + pfactor * ( hecc - hec )
          enth =hee+pfactor*( heee - hee)
          cond = ( heo + pfactor * ( heoo -heo) )/1000.
          return
       elseif (temp .gt. 9.8) then
          type*,temp,'Helium temp greater than 9.8'
        hed = (temp-9.8)/0.1*(hedens(88,j)-
     *    hedens(87,j))+hedens(88,j)
        hec = (temp-9.8)/0.1*(hecp(88,j)-
     *    hecp(87,j))+hecp(88,j)
        hee = (temp-9.8)/0.1*(heenth(88,j)-
     *    heenth(87,j))+heenth(88,j)
        heo = (temp-9.8)/0.1*(other(88,j)-
     *    other(87,j))+other(88,j)
        hedd = (temp-9.8)/0.1*(hedens(88,j+1)-
     *    hedens(87,j+1))+hedens(88,j+1)
        hecc = (temp-9.8)/0.1*(hecp(88,j+1)-
     *    hecp(87,j+1))+hecp(88,j+1)
        heee = (temp-9.8)/0.1*(heenth(88,j+1)-
```

```
*       heenth(87,j+1))+heenth(88,j+1)
        heoo = (temp-9.8)/0.1*(other(88,j+1)-
*       other(87,j+1))+other(88,j+1)
          dens = ( hed + pfactor * ( hedd -
&               hed) ) / 1000.
          cp = hec + pfactor * ( hecc - hec )
          enth =hee+pfactor*( heee - hee)
          cond = ( heo + pfactor * ( heoo -heo) )/1000.
        return
        else
             i = int(10.*temp)
             tfactor = (10.*temp - float(i))
             i = i - 10
        endif

       hold1 = hedens(i,j) + tfactor*(hedens(i+1,j)-hedens(i,j))
      hold2 = hedens(i,j+1)+tfactor*(hedens(i+1,j+1)-
*          hedens(i,j+1))
       dens = ( hold1 + pfactor*(hold2 - hold1) ) / 1000.
       hold1 = heenth(i,j) + tfactor*(heenth(i+1,j)-heenth(i,j))
       hold2 = heenth(i,j+1)+tfactor*(heenth(i+1,j+1)-
*          heenth(i,j+1))
       enth = hold1 + pfactor*(hold2 - hold1)
       hold1 = hecp(i,j) + tfactor*(hecp(i+1,j)-hecp(i,j))
       hold2 = hecp(i,j+1)+tfactor*(hecp(i+1,j+1)-hecp(i,j+1))
       cp = hold1 + pfactor*(hold2 - hold1)
c      hold1 = other(i,j) + tfactor*(other(i+1,j)-other(i,j))
c      hold2 = other(i,j+1)+tfactor*(other(i+1,j+1)-other(i,j+1))
c      cond = (hold1 + pfactor*(hold2 - hold1))/1000.

       return
       end
```

```
c  GGGPROP.FOR
c -----------------------------------------------------------------
      SUBROUTINE GGGPROP(T,uoH,dsduoH,s,dsdT)
c -----------------------------------------------------------------
C
C   Given temperature in Kelvin and uoH in Tesla, entropy s and its
C  derivatives ds/duoH (equivalent to vdM/dT) and ds/dT are calculated.
C  The units are J/(g K) for s, J/(g K T) for ds/duoH, and J/(g K^2)
C  for ds/dT.
C
C   Calculation of ds/duoH is exact from the curvefitted magnetization.
C  Calculation of s and ds/dT is done with the use of Gauss-Legendre
C  Quadrature.
C
C   W and ETA are used in the quadrature method.
C
      DIMENSION W(6),ETA(6)
      DATA ETA/0.1252334085,0.3678314990,0.5873179543,0.7699026742,
     1  0.9041172564,0.9815606342/
      DATA W/0.2491470458,0.2334925365,0.2031674267,0.1600783285,
     1  0.1069393260,0.0471753364/
C
C   Calculation of functions C0,C1,C2,C3, and C4 and their derivatives
C  with respect to temperature:
      C0=13.67388+2.718523*T+0.1278728*T**2-2.5072373E-03*T**3
      C1=-2.980799+0.9144735*T-7.3461875E-02*T**2+1.1088194E-03*
     1  T**3+9.8684995E-06*T**4
      C2=3.166695-0.6364962*T+4.8334930E-02*T**2-1.0840200E-03*
     1  T**3+4.3787923E-06*T**4
      C3=-0.3461423+9.0944469E-02*T-6.9979527E-03*T**2+
     1  1.3868879E-04*T**3
      C4=1.3560383E-02-4.1968897E-03*T+3.3840450E-04*T**2-
     1  6.8436516E-06*T**3
      dC0dT=2.718523+2.*0.1278728*T-3.*2.5072373E-03*T**2
      dC1dT=0.9144735-2.*7.3461875E-02*T+3.*1.1088194E-03*
     1  T**2+4.*9.8684995E-06*T**3
      dC2dT=-0.6364962+2.*4.8334930E-02*T-3.*1.0840200E-03*
     1  T**2+4.*4.3787923E-06*T**3
      dC3dT=9.0944469E-02-2.*6.9979527E-03*T+3.*1.3868879E-04*T**2
      dC4dT=-4.1968897E-03+2.*3.3840450E-04*T-3.*6.8436516E-06*T**2
      d2C0dT2=2.*0.1278728-6.*2.5072373E-03*T
      d2C1dT2=-2.*7.3461875E-02+6.*1.1088194E-03*T+
     1  12.*9.8684995E-06*T**2
      d2C2dT2=2.*4.8334930E-02-6.*1.0840200E-03*T+
     1  12.*4.3787923E-06*T**2
      d2C3dT2=-2.*6.9979527E-03+6.*1.3868879E-04*T
      d2C4dT2=2.*3.3840450E-04-6.*6.8436516E-06*T
C
```

```
C    Calculation of ds/duoH:
       DEN=C0+C1*uoH+C2*uoH**2+C3*uoH**3+C4*uoH**4
       dDENdT=dc0dT+dC1dT*uoH+dC2dT*uoH**2+dC3dT*uoH**3+dC4dT*u
oH**4
       d2DENdT2=d2c0dT2+d2C1dT2*uoH+d2C2dT2*uoH**2+d2C3dT2*uoH*
*3+
     1 d2C4dT2*uoH**4
       dsduoH = -uoH*dDENdT/DEN**2
C
C    Calculation of s and dsdT:  s0 is the entropy at uoH=0, and
C  ds0dT is the derivative of entropy with respect to temperature at
C  uoH=0.  s and dsdT are calculated using Gauss-Legendre Quadrature.
C
       s0=2.3E-07*T**3-6.385E-02/2./T**2+5.096E-02/3./T**3-
     1 (2.3E-07/3.-6.385E-02/2.+5.096E-02/3.)
       ds0dt=3.*2.3E-07*T**2+6.385E-02/T**3-5.096E-02/T**4
       sSUM=0.
       dsdTSUM=0.

       DO 10 I=1,6
       x1=uoH/2.*(1+ETA(I))
       x2=uoH/2.*(1-ETA(I))

        DEN = C0 + C1*x1 + C2*x1**2 + C3*x1**3 + C4*x1**4
        dDENdT = dc0dT +dC1dT*x1+dC2dT*x1**2
+dC3dT*x1**3+dC4dT*x1**4
        d2DENdT2 = d2c0dT2 +d2C1dT2*x1 +d2C2dT2*x1**2
+d2C3dT2*x1**3+
     1  d2C4dT2*x1**4
       vdMdT1 = -x1*dDENdT/DEN**2
       vd2MdT21 = x1*(2.*dDENdT**2-DEN*d2DENdT2)/DEN**3

        DEN = C0 + C1*x2 + C2*x2**2 + C3*x2**3 + C4*x2**4
        dDENdT =dc0dT +dC1dT*x2 +dC2dT*x2**2
+dC3dT*x2**3+dC4dT*x2**4
        d2DENdT2 = d2c0dT2 +d2C1dT2*x2 +d2C2dT2*x2**2
+d2C3dT2*x2**3+
     1  d2C4dT2*x2**4
       vdMdT2 = -x2*dDENdT/DEN**2
       vd2MdT22 = x2*(2.*dDENdT**2-DEN*d2DENdT2)/DEN**3

       sSUM = sSUM + W(I)*(vdMdT1+vdMdT2)
       dsdTSUM = dsdTSUM + W(I)*(vd2MdT21+vd2MdT22)
  10   CONTINUE

       s = s0 + uoH/2.*sSUM
       dsdT=ds0dT+uoH/2.*dsdTSUM
       RETURN
       END
```

```
c HELIUM.FOR
c ------------------------------------------------------------------
c       He3 property calculation ( 9/10/89 )
c ------------------------------------------------------------------
        implicit real*8 (a-h,o-z)
      common p,t,r,p0,t0
      external p0vt,pvt
      dimension pp(5)
        OPEN(7,FILE='he3.dat',status='new')
c ------------------------------------------------------------------
c       Making output data file for input of simulation program.
c ------------------------------------------------------------------
c
c      Universal gas constant (J/mol.K)
c
      r = 8.314d0
      cp0 = 20.8d0
      b1 = 4.942d-6
      b2 = -270.986d-6
      c1 = 2866.0d-12
      t0 = 4.0d0
      p0 = 101325.0d0
        v1 = r*t0/p0
        v2 = v1 + v1/10.0d0
        print *,'v1,v2  = ',v1,v2
        call find(v1,v2,v0,0.000001d0,f0,30,p0vt)
        print *,'v0,f0  = ',v0,f0
c ------------------------------------------------------------------
c       PRESSURE RANGE OF HELIUM PROPERTY
c ------------------------------------------------------------------
      pp(1) = 0.02
      pp(2) = 0.03
      pp(3) = 0.04
      pp(4) = 0.05
      pp(5) = 0.06
c
      do 100 j=1,5
      p = pp(j) *101325.0d0
      do 10 i=0,198
        t = 1.0 + float(i)/10.0d0
        v1 = r*t/p
        v1i = v1*1.0d6
        v2 = v1 + v1/10.0d0
        call find(v1,v2,v,0.000001d0,f0,30,pvt)
        vi = v*1.0d6
        print *,'t,v1,v = ',t,v1i,vi
        den = 0.001d0/v*3.0d0
c
```

```
c     [den] = g/liter
c
c     calculation of enthalpy
c
          h  = -r*t0*(b1/v0 + 2*b2/t0/v0 + 5.0d0/4.0d0*c1/sqrt(t0)
     *         /v0/v0 ) + cp0*(t - t0) + r*t*(b1/v + 2*b2/t/v +
     *         5.0d0/4.0d0*c1/sqrt(t)/v/v)
c
c     calculation of entropy
c
          s = r * (dlog(v/v0) - b1 *(1.0d0/v - 1.0d0/v0) + c1/4.0d0
     *         *(1.0d0/sqrt(t0)/v0/v0 - 1.0d0/sqrt(t)/v/v) ) +
     *         cp0*dlog(t/t0)
          h = h/3.0d0
          s = s/3.0d0

          h2 = h
          cp = (h2-h1)/0.1
c           if (i.eq.1) cp = 0.0d0
          h1 = h
c
c     [h] = J/g   [s] = J/g.K
c
        write(7,600)den,h,cp,s
10      continue
100     continue
600     format(f10.3,f10.6,f10.3,f10.5)
        stop
        end
c-----------------------------------------------------------------------
      subroutine find(x1,x2,x0,e,f0,max,yyy)
c-----------------------------------------------------------------------
c     This subroutine finds a root of yyy.
c----------x1 < x2
        implicit real*8 (a-h,o-z)
        iter = 1
100       call yyy (x1,f1)
      call yyy (x2,f2)
c
      x0 = x1 - f1*(x1-x2)/(f1-f2)
      call yyy (x0,f0)
      if (dabs(f0).le.e) go to 999
      if (iter.gt.max) then
        write(7,777) x1,x2,x0,e,f0,max
        go to 999
      endif
c
      if((x0.gt.x1).and.(x0.lt.x2)) then
        ff = f1*f0
```

```
        if(ff.lt.0.0) x2 = x0
        ff = f2*f0
        if(ff.lt.0.0) x1 = x0
      elseif (x0.le.x1) then
        x2 = x1
        x1 = x0
      elseif (x0.ge.x2) then
        x1 = x2
        x2 = x0
      endif
      iter = iter + 1
c
      go to 100
777   format(//'iteration not converged !!!'//'x1 = ',f9.4/'x2 = ',
     * f9.4/'x0 = ',f9.4/'e = ',f9.4//'f0 = ',f9.4/'max = ',i3)
999   return
      end

c-----------------------------------------------------------------------
      subroutine p0vt(x,y)
c-----------------------------------------------------------------------
       implicit real*8 (a-h,o-z)
       common p,t,r,p0,t0
       b = (4.942d0 - 270.986d0/t0)*1.0d-6
       c = (2866.0d0/sqrt(t0))*1.0d-12
       y = p0*x/(r*t0) - 1.0d0 -b/x -c/x/x
      return
      end
c-----------------------------------------------------------------------
      subroutine pvt(x,y)
c-----------------------------------------------------------------------
       implicit real*8 (a-h,o-z)
       common p,t,r,p0,t0
       b = (4.942d0 - 270.986d0/t)*1.0d-6
       c = (2866.0d0/sqrt(t))*1.0d-12
       y = p*x/(r*t) - 1.0 -b/x -c/x/x
      return
      end
```